Title
Exploring Roles of Notch and Sonic Hedgehog Signaling in the Developing Central Nervous System

Author
Kong, Jennifer Haruko

Publication Date
2015

Peer reviewed|Thesis/dissertation

UNIVERSITY OF CALIFORNIA

Los Angeles

Exploring Roles of Notch and Sonic Hedgehog Signaling in the Developing Central Nervous System

A dissertation submitted in partial satisfaction of the

requirements for the degree Doctor of Philosophy

in Neuroscience

by

Jennifer Haruko Kong

2015

ABSTRACT OF THE DISSERTATION

Exploring Roles of Notch and Sonic Hedgehog Signaling in the Developing Central Nervous System

by

Jennifer Haruko Kong

Doctor of Philosophy in Neuroscience

University of California, Los Angeles, 2015

Professor Bennett G. Novitch, Chair

The central nervous system (CNS) is a very complex and highly organized structure. In the beginning the CNS is a sheet of cells. Over time external cues encourage this sheet to become a tube and from this tube an abundance of cell types are generated. These cells then migrate out, establish contacts with other cells, and form functional circuits. Given the complexity of the CNS, one of the fundamental goals of developmental neurobiology is to understand how this wealth of cellular diversity is generated and organized given the initial guidance of just a few signaling cues. Through the work of many groups, the emerging solution to this unbalanced equation appears to be signaling pathway interactions. To address this we focused our study on the roles and interactions of two major developmental signaling pathways: Notch and Sonic hedgehog (Shh). In the developing CNS, the major role of Notch signaling is progenitor maintenance and the major role of Shh signaling is progenitor patterning. However, when studied together, we observed that Notch signaling was able to modulate a progenitor

cell's response to Shh and in doing so influenced cell fate choices made within the developing spinal cord. Interested in these initial findings, we wanted to study other functions of Notch signaling. In a second study we observed that interactions between Notch and retinoic acid (RA) signaling contributed to neuronal diversity within the caudal hindbrain and rostral spinal cord. Then, in a third study, we observed that Notch signaling maintained apical cell contacts within the developing brain. Collectively, this work illustrates that, within the context of neural development, Notch signaling has multiple functions and this functional diversity is largely facilitated through interactions with other signaling pathways. While the functions of Notch signaling were enriched by pathway interactions, we also took a closer look at the factors that influence Shh signaling activity. In a final study we show that Shh signaling activity can be also be modulated through the protein kinase A (PKA)-direct and PKA-indirect downstream phosphorylation of Gli proteins, bifunctional transcriptional effectors of Shh signaling activity.

This dissertation of Jennifer Haruko Kong is approved.

Alvaro Sagasti

James A. Waschek

Geraldine A. Weinmaster

Bennett G. Novitch, Committee Chair

University of California, Los Angeles

2015

DEDICATION

For my grandfather, Harold Isa, who taught me more than he will ever know.

This was always for you.

For my parents, Diane and Gary, who continue to support and encourage all of my crazy dreams.

TABLE OF CONTENTS

LIST OF FIGURES

ACKNOWLEDGEMENTS

Many of the chapters included in this dissertation are composed of articles that are either published or in preparation for publication.

Chapter 2 is a version of the published article “Notch activity modulates the responsiveness of neural progenitors to Sonic Hedgehog signaling.” Kong JH*, Yang L*, Dessaud E, Chuang K, Moore DM, Rohatgi R, Briscoe J, and Novitch BG. 2015. *Developmental Cell 33(4): 1-15.* In press. *Indicates co-first authors. We thank Samantha Butler, Pawel Niewiadomski, Harley Kornblum, and Gerry Weinmaster for helpful discussions and comments on the manuscript. We thank Tasuku Honjo, Sean Morrison, Charles Murtaugh, and Alessandra Pierani for mice. We thank Tom Jessell, Yasushi Nakagawa, Samuel Pfaff, Keith Phan, L Cheng, and T Sudo for tissue and reagents. Lastly, we would also like to thank Connie Chuy and Scott Nihei for all their cover art submissions.

Chapter 3 is a version of a manuscript in preparation for publication entitled “Notch signaling is required for the maintenance of neural progenitor cell adhesion and polarity within the developing diencephalon.” Kong JH and Novitch BG. We thank Tasuku Honjo, Charles Murtaugh, and Alessandra Pierani for mice and Tamara Caspary for reagents.

Chapter 4 is a version of the published article “Retinoid Acid specifies neuronal identity through graded expression of Ascl1.” 2013. Jacob J, Kong J, Moore S, Milton C, Sasai N, Gonzalez-Quevedo R, Terriente J, Imayoshi I, Kageyama R, Wilkinson DG, Novitch BG, and Briscoe J. *Current Biology 23(5)*: 412-418. DOI: 10.1016/j.cub.2013.01.046

Chapter 5 is a version of the published article “Gli protein activity is controlled by multisite phosphorylation in vertebrate Hedgehog signaling.” 2014. Niewiadomski P, Kong JH, Ahrends R, Ma Y, Humke EW, Khan S, Teruel MN, Novitch BG, Rohatgi R. *Cell Reports 6(1)*: 168-181. DOI: 10.1016/j.celrep.2013.12.003.

I would like to thank my funding sources. The work in this thesis was supported by a grant from the March of Dimes Foundation (6-FY10-296) and a UCLA Graduate Division Dissertation Year Fellowship. Thank you also to the Neuroscience IDP and Neurobiology departments at UCLA for travel funding support. Finally, thank you Dr. Eva Mary Kavan for her generous endowment and the Brain Research Institute at UCLA for their support.

In addition, this work could not have been completed without the help of many people. First and foremost I would like to thank my mentor Dr. Bennett Novitch. Coming into the lab I really didn’t know how to do much, so thank you for taking a chance on me. Thank you for working so hard (yes, I noticed all those 1-2 AM emails), for always pushing me to do interesting experiments, for tirelessly keeping the lab going, for teaching me how to ask good questions, and for fostering a laboratory environment in which I have both learned so much and made so many friends. I would also like to thank all of my thesis committee members: Dr. James Waschek, Dr. Alvaro Sagasti, and Dr. Gerry Weinmaster. I know we didn’t meet as often as we should have, but I really did value all of your inputs. Collectively, you all helped to make our paper so much better.

Next I would really like to thank all the current and past Novitch Lab members (aka. Novitchians). Lin Lin, thank you for being so patient with me during my rotation and initial years in the lab, I know I messed up… a lot. David, thank you for your ceaseless enthusiasm, when I’m tired and beaten down by experiments I try to channel your spirit. Zachary, thank you for patiently teaching me how to electroporate and clone, I know I was a terrible pupil, but thankfully

you were a wonderful teacher. Katrina, thank you for accompanying me on this crazy journey called graduate school, you definitely made the whole process so much better. Caroline, thank you for teaching me all of your ISH secrets, for always injecting a little fun into the lab, for being optimistic when everything seemed terrible, and for being a great sounding board for all my science woes. Destaye, thank you for growing such lovely cells for me, for maintaining all the microscopes on the floor, for making sure all of our orders came through, and for generally just making life in the lab easier. Ken, thank you for fixing all the broken things in lab and for helping me think through many experimental problems. Yoon, thank you for making the late evenings in lab just a little better with your company. Last but not least I really want to thank my smart and talented undergraduate Katherine Chuang who stuck with me for three years. Thank you for all your hard work and I look forward to seeing what a wonderful doctor you will become.

I would also really like to thank Dr. Samantha Butler for all of her guidance and input over the years… and reading through our paper a countless number of times. Life in the Novitch Lab has really been enriched with the addition of the Butler Lab. Thank you also to the many members of the Butler Lab – Sup, Madeline, and Keith. You are all amazing scientists and I have really enjoyed watching your projects develop and grow over the years.

Finally I would like to thank my family for all their love and support over these many years. To my mom and dad, when I see how hard you both work, it inspires me to work harder. Thank you for all the sacrifices you have made and for all the opportunities you have given me. You encouraged me to leave Hawaii and see more of the world, for this I am indebted to you forever. To my mom, thank you for always being there, cheering me on through the laughter and tears, thank you for listening to me rattle on for hours about experiments and results, and thank you for calling every night (regardless of the time) to make sure I got home safely. To my dad, thank you for your continued support and for encouraging me to stick with it these many years. I love you both so much! Thank you also to my wonderful aunties. Aunty Jo, thank you for all the pictures you sent me, they always made me smile and brightened my long days in the lab.

Being away from home has always been hard, but your pictures and updates always made it a little better. Aunty Doreen, I've always enjoyed all our long talks, thank you for checking in with me every time you came down to LA and shipping me so much food. Last but not least, I wanted to thank my wonderful grandparents. In your own ways, you all made sure I received a good education. Thank you especially to Grandma and Grandpa Isa, who not only taught me to love reading and encouraged my many curiosities, but pushed me to be the best I could be. I love you both now and forever.

VITA

EDUCATION AND RESEARCH EXPERIENCE

Willamette University 2003-2007

Bachelor of Arts in Biology (minor in Chemistry)

Graduate with Cum Laude honors

University of Hawaii at Manoa 2007-2008

Research Assistant

Pacific Biosciences Research Center

Bekesy Laboratory of Neurobiology

AWARDS

Dr. Eva Mary Kavan Prize for Excellence in Research on the Brain, UCLA 2015

Dissertation Year Fellowship, UCLA Graduate Division 2013-2014

Distinction in Teaching from UCLA Life Sciences 2009-2010

PUBLICATIONS

Kong JH, Novitch BG. Notch signaling is required for the maintenance of neural progenitor cell adhesion and polarity within the developing diencephalon. In preparation.

Hartline DK and **Kong JH.** The gain and loss of myelin in malacostraca. In preparation.

***Kong JH**, *Yang LL, Dessaud E, Chuang K, Moore DM, Rohatgi R, Briscoe J, Novitch BG. (2015) Notch activity modulates the responsiveness of neural progenitors to Sonic Hedgehog signaling. *Dev Cell 33(4): 1-15*. *indicates shared author publication

Niewiadomski P, **Kong JH**, Ahrends R, Ma Y, Humke EW, Sohini K, Teruel MN, Novitch BG,

Rohatgi R. (2014) Gli protein activity is controlled by multisite phosphorylation in vertebrate hedgehog signaling. *Cell Reports* 6(1): 168-181. DOI: 10.1016/j.celrep.2013.12.003.

Kong JH, Butler SJ, Novitch BG. (2013) My brain told me to do it. *Dev Cell* 25(5): 436-438.

Jacob J, **Kong JH**, Moore S, Milton C, Sasai N, Gonzalez-Quevedo R, Terriente X, Imayoshi I, Kageyama R, Wilkinson DG, Novitch BG, Briscoe J. (2013) Retinoid acid specifies neuronal identity through graded expression of Ascl1. *Current Biology* 23(5): 412-418. DOI: 10.1016/j.cub.2013.01.046.

Hafler BP, Surzenko N, Beier KT, Punzo C, Trimarchi JM, **Kong JH**, Cepko CL. (2012) Transcription factor *Olig2* defines subpopulations of retinal progenitor cells biased toward specific cell fates. *PNAS* 109(20):7882-7887. DOI: 10.1073/pnas.1203138109.

Hartline DK and **Kong JH**. (2009) Development of the giant-axon sheaths in larval lobsters, *Homarus americanus*. The Bulletin of Mount Desert Island Biological Laboratory.

Hartline DK and **Kong JH**. (2009) Axonal sheaths in two reportedly myelinated polychaete nervous systems: *Asychis elongata* and *Capitella sp I*. The Bulletin of Mount Desert Island Biological Laboratory.

PRESENTATIONS AND POSTERS

Hedgehog Meeting: Hedgehog Signaling in Development and Disease. Abstract and Poster (Aug 2014). Ann Arbor, MI.

Broad Stem Cell Research Center Tri-institutional Retreat. Oral Presentation (April 2014). Pacific Grove, CA.

Keystone Symposia on Molecular and Cellular Biology: Neurogenesis. Poster and abstract (Feb 2013). Santa Fe, NM.

UCLA Neuroscience Interdepartmental Retreat. Oral Presentation (May 2011). UCLA.

CHAPTER 1 – Introduction

The development of the vertebrate central nervous system (CNS) depends upon the actions of undifferentiated neural progenitor cells (NPCs) to produce an abundance of unique cell types within a proper place and time of embryogenesis. This strictly choreographed process allows for cellular interactions that are critical for the formation of functional neural networks. Any errors in this process can result in an assortment of devastating neurodevelopmental defects, ranging from major disruptions to the integrity of the CNS to more subtle flaws that can compromise learning, behavior, and motor movement. Remarkably, this cellular diversity largely arises from and is organized by a just a handful of highly conserved signaling cues[1,2]. Thus, understanding how these relatively few cues direct the transition of the CNS from a neural tube to mature brain and spinal cord raises many fundamental developmental neurobiology questions. For example, how does a single signaling cue generate a multitude of cell types, each within a specific duration of development and region of space? While we know a lot about the individual signaling pathways that are initiated by these common signaling cues, what are the molecular mechanisms that determine the responsiveness of a cell to these cues? To account for the dissonance between the cues present and the multitude of cell types they generate, is it possible that the signaling pathways initiated by these cues converge and form complex signaling networks? How is the delicate balance between NPC self-renewal and differentiation maintained so that through the entirety of CNS development all necessary postmitotic cells are generated while an ample population of progenitors are simultaneously preserved? In this thesis, we attempt to address many of these questions.

In the first part of this work we address the issue of cellular diversity and how it is generated from a small pool of signaling cues. Through the efforts of many groups, considerable progress has been made towards understanding how individual extracellular signaling cues

influence cell fate choices in the developing CNS. However, it is becoming increasingly clear that these cues do not influence cell fate choices in isolation, but rather collectively cultivate cellular diversity through complex and highly integrated signaling networks[3,4]. To examine this potential for signaling interactions to produce greater cellular diversity, we looked at interactions between Notch and Sonic hedgehog (Shh) signaling in the ventral spinal cord (Chapter 2) and interactions between Notch and Retinoic Acid (RA) signaling at the hindbrain/spinal cord interface (Chapter 4).

In Chapter Two, we focus on understanding interactions between two vital signaling pathways: Notch and Shh. Previous studies have shown that, within the developing spinal cord, Notch signaling is vital for the maintenance NPCs[5], and Shh signaling plays a major role in the specification and patterning of NPCs[6]. In this chapter we demonstrate that in addition to its progenitor maintenance functions, Notch signaling activity directs NPCs towards more ventral cell identities by potentiating the effects of Shh. In the first part of this chapter, through the use multiple experimental systems (i.e. transgenic mice, chick explants, and cultured cells) we illustrate that Notch signaling activity is necessary for NPCs to respond maximally to Shh and in doing so allows them to adopt ventral-most cell identities. In the second part of this chapter we show that Notch signaling modulates Shh signaling activity through the localization of the Shh receptor Patched1 (Ptch1), which in turn influences the movement of the key Shh effector Smoothened (Smo). Collectively, the data presented in this chapter identify a novel role for Notch signaling in shaping the response of NPCs to the Shh gradient and thereby influencing progenitor cell fate choices within the ventral spinal cord.

In Chapter Four we examine interactions between Notch and RA signaling. Previous studies have shown that, within the developing CNS, RA plays a major role in patterning the hindbrain and spinal cord[7-9]. In this chapter we show that levels of RA signaling activity direct p3 progenitors to become either serotonergic neurons in the caudal hindbrain or V3 interneurons in the rostral spinal cord. Through a variety of experiments we demonstrate that RA signaling acts

through Notch signaling to regulate the expression of Ascl1. We then illustrate that it is this shift in Ascl1 expression that causes a single uniform p3 progenitor population present in both the hindbrain and spinal cord to give rise to two molecularly distinct neuronal cell types (hindbrain serotonergic neurons and V3 spinal interneurons). In this study we illustrate that neuronal diversity is enriched by signaling pathway interactions and that a dramatic divergence of cell fate choices can be produced by a relatively small quantitative difference in the expression of a single transcription factor.

An abundance of signaling pathways have been implicated in progenitor cell maintenance[10-14]. However, the transition towards differentiation requires not only a loss of progenitor identity, but also a loss of the apical attachments that retain the progenitors to the ventricular zone[15]. Throughout the developing CNS, Notch signaling has been shown to be essential for the preservation of neural stem and progenitor cell populations. However, the role of Notch signaling in the maintenance of apical contacts and progenitor cell polarity has been less thoroughly explored. In Chapter Three, we address this and investigate the role of Notch signaling in the maintenance of progenitor cell adhesion and polarity within the neuroepithelial cell layer of the developing diencephalon. In this chapter we show that Notch signaling is essential for the preservation of neuroepithelial integrity within specific regions of the brain. We then illustrate that within the developing diencephalon, an absence of Notch signaling activity results in both premature neurogenesis and a loss of cell adhesion. The loss of neuroepithelial integrity present in the mutant embryos manifests itself as a loss of ependymal cells in postnatal animals, and ultimately becomes hydrocephalus in the adults. In this study we shed light on a previously underappreciated role of Notch signaling as a cell adhesion and cell polarity maintenance factor. In doing so we expand upon the roles of Notch signaling in the developing CNS, recognizing that this signaling pathway does much more than preserve the progenitor cell state.

In Chapter Two we show that Notch signaling modulates the responsiveness of cells to

Shh signaling activity by regulating the movement of Shh signaling components to the primary cilia, a key step in the signal transduction pathway. In Chapter Five we shift our focus to studying other regulators of Shh signaling activity. In this chapter we focus on the downstream processing of Gli proteins, bifunctional transcriptional effectors of Shh signaling activity. In this chapter we examine how the phosphorylation of six serine residues (P1-6) on Gli proteins by protein kinase A (PKA) prevents these transcriptional effectors from becoming transcriptional activators. This occurs in a graded manner, as a loss of phosphates at four of the six residues (P1-4) is sufficient to block the formation of Gli transcriptional repressors (GliR), but a loss of phosphates at all six residues (P1-6) is necessary to generate Gli transcriptional activators (GliA). Within the developing ventral spinal cord, the balance between GliA/GliR directs the differential expression of transcription factors along the dorsoventral axis and in doing so plays a major role in establishing progenitor domain boundaries[16]. Through a final series of experiments, we show that the electroporation of nonphosphorylatable Gli constructs into the chick spinal cord results in an elevations of Shh signaling activity and the ectopic expression of ventral-most progenitor cell types. Thus, collectively, the data presented in this chapter expands upon our understanding of how Shh signaling activity is regulated, and clearly indicates that the phosphorylation of Gli proteins plays a major role in determining whether these transcriptional effectors will become transcriptional activators or repressors in both cell culture and in the developing CNS.

1-1: Spinal cord development

Remarkably, spinal cord development occurs under the guidance of a handful of instructional cues. These cues include, but are not limited to: Sonic Hedgehog (Shh) secreted from the floorplate, Wnt and bone morphogenic proteins (BMPs) from the roofplate, and retinoic acid (RA) from the paraxial mesoderm[6,7,17-21] (**Figure 1-1A**). Early in development, these signals collectively converge onto uncommitted progenitors present within the ventricular zone (VZ) to

regulate the expression of transcription factors along the dorsoventral axis. Over time, cross-repressive interactions between transcription factor pairs sharpen the boundaries between regions of expression, resulting in the generation of at least 11 distinct progenitor domains[22] (**Figure 1-1B**). Initially, each progenitor domain gives rise to a functionally distinct population of postmitotic neurons that migrate out to a specific location of the mantle zone (MZ)[23,24] (**Figure 1-1C-D**). After this period of neurogenesis, there is a wave of gliogenesis, upon which time the progenitor domains stop producing neurons and start generating distinct populations of oligodendrocytes and astrocytes, which similarly migrate out and settle in specific regions of the spinal cord[25] (**Figure 1-1D**).

1-2: Hedgehog signaling

A brief history of Hh signaling

A *Hedgehog (Hh)* mutant was first generated in 1980 through a *Drosophila* mutagenesis screen that targeted embryonic lethal mutants with altered larval segmental patterns[26]. In this original study, spontaneously generated mutant larvae were grouped into three major classes: (I) Gap mutants that lacked multiple continuous segments, (II) Pair-rule mutants that lacked alternating segments, and (III) Segment polarity mutants that had the appropriate number of segments, but lacked proper segmental organization. The *Hh* mutant, classified as a segment polarity mutant, possessed the proper number of segments, but the smooth posterior half of each segment failed to develop leaving only the denticle covered anterior half. The dense presence of hair-like denticles and shortened body length gave the mutant larvae a fuzzy hedgehog-like appearance, a phenotype which ultimately inspired its name. Over a decade later, the *Drosophila Hh* gene was independently isolated by multiple labs[27-30]. Collectively, these studies not only introduced Hh as a diffusible protein that was essential for proper segment formation in the developing *Drosophila*, but lay the groundwork for our current understanding of how signaling pathways have the capacity to organize and pattern tissue in the

early embryo.

Due to genome duplication events in early vertebrates[31], there are three mammalian *Hh* genes: *Sonic hedgehog* (*Shh*); *Indian hedgehog* (*Ihh*); and *Desert hedgehog* (*Dhh*). The three mammalian Hh proteins are remarkably similar. All three proteins are processed by the same mechanisms, have the capacity to bind to the Hh receptors Patched1 and Patched2 (Ptch1 and Ptch2), and ultimately upregulate the expression of known Hh pathway target genes[32,33]. However, each Hh protein has a unique expression pattern in the developing embryo[34]. Shh, the most broadly expressed member of the mammalian Hh family, is present in the brain, spinal cord, limbs, lungs, and gut where it plays an essential role in development and patterning[35-38]. Ihh is present in the pancreas, gut, and bone growth plates where it plays a role in pancreatic, intestinal, and skeletal development[39-41]. Lastly, Dhh expression is primarily restricted to the developing testes and ovaries and is essential for spermatogenesis[42-44].

Hh protein synthesis, lipid modification, and secretion

A newly synthesized Hh protein must undergo multiple posttranslational modifications within the endoplasmic reticulum (ER) to become a functional ligand[45]. In this process, the signal sequence of Hh is first cleaved off to generate a ~45 kDa precursor protein (Hh-FL). The Hh precursor then undergoes an autocatalytic reaction, cleaving itself into two biochemically distinct pieces: (1) a catalytic ~25 kDa carboxy-terminal fragment (Hh-C) and (2) a signaling ~19 kDa amino-terminal fragment (Hh-N). The carboxy-terminal of the Hh precursor facilitates this self-cleavage event through the recruitment of a cholesterol group, which is covalently attached to Hh-N upon the removal of Hh-C[46]. Once the Hh precursor is cleaved, Hh-C is expelled from the ER and degraded. In contrast, the addition of a hydrophobic cholesterol group to Hh-N results in it being tethered to the cell membrane[47]. The attachment of a cholesterol group to the carboxy-terminal of Hh-N is accompanied by the addition of a stable palmitic acid group to the amino-terminal[48]. The palmitoylation of Hh-N is catalyzed by a member of the membrane bound

O-acyltransferase (MBOAT) protein family, which is either skinny hedgehog (ski) in *Drosophila* or Hedgehog acyltransferase (Hhat) in mouse[49,50]. Studies have shown that the addition of both a cholesterol and palmitic acid group to Hh-N facilitates its retention to the plasma membrane and extends its long-range Hh signaling activity[49,51].

In becoming a fully processed Hh protein (Hh-Np) that is capable of activating Hh signaling, a cholesterol and palmitic acid group must be added to Hh-N. These lipid modifications generate a very hydrophobic Hh protein (Hh-Np) that is firmly anchored to the plasma membrane. With a protein so strongly bound to the membrane, the question remains as to how these lipid modifications ultimately help further the range of Hh signaling activity. Thus far there are four proposed mechanisms that address how Hh-Np is spread[18]. (1) Cooperation between Dispatched (Disp) and Scube2. Disp is a twelve-pass transmembrane protein with a sterol sensing domain[38,39]. Hh-Np binds to Disp via a cholesterol-dependent interaction and is removed from the plasma membrane. Disp then passes Hh-Np to the secreted glycoprotein Scube2[52,53], which allows for the release of soluble Hh-Np monomers. (2) Hh-Np monomers self-associate to form large, stable, and highly soluble multimeric complexes[54]. In this configuration, the hydrophobic amino and carboxy-terminals of the Hh-Np monomers are buried deep within the complex to allow for greater solubility and long range signaling[49,55]. (3) Association of Hh-Np to circulating lipoprotein particles, which transport Hh-Np far away from the site of synthesis[56]. (4) Secretion of Hh-Np on exosomes/exovesicles[57,58].

Hh signaling pathway in vertebrates

In the absence of Hh, the twelve-pass transmembrane receptor Patched1 (Ptch1) binds to one of three single-pass transmembrane accessory receptors: cell-adhesion-molecule-related/downregulated by oncogenes (Cdo), brother of Cdo (Boc), and growth arrest-specific 1 (Gas1)[59,60] (**Figure 1-2A1**). Unbound by Hh, intraflagellar transport (IFT) proteins move Ptch1 into the primary cilium, a single nonmotile organelle-like structure present on almost all

vertebrate cells[61,62]. Within the primary cilium, Ptch1 suppresses the activation of the seven-transmembrane protein Smoothened (Smo) and subsequently inhibits its movement into the primary cilium[63] (**Figure 1-2A2**). The exact mechanism through which Ptch1 regulates Smo activity is poorly understood. However, multiple studies have shown that Ptch1 does not directly bind to Smo [63,64], leading many to hypothesize that Ptch1 inhibits Smo activation indirectly, potentially via a suppression of oxysterols[65], oxidized cholesterols that directly bind to and activate Smo[66]. In the absence of Hh, full length Gli proteins (Gli-FL) bind to Sufu in the cytoplasm and the resulting complexes (Gli-FL/Sufu) are recruited to the primary cilia[67] (**Figure 1-2A3**). Gli proteins are a family of zinc finger transcription factors. Vertebrates have a total of three Gli homologs: Gli1, Gli2, and Gli3. Gli1 is only a transcriptional activator[68] and primarily serves as a secondary amplifier of Shh signaling activity. In contrast, Gli2 and Gli3 have the potential to become both transcriptional activators (GliA) and repressors (GliR) because they possess both an activation domain at the carboxy-terminal and a repression domain at the amino-terminal. Despite this bifunctional potential, Gli2 is typically processed into a transcriptional activator (GliA) and Gli3 into a repressor (GliR)[69]. Gli2 and Gli3 have six highly conserved serine residues on the carboxy-terminal of the DNA binding zinc finger domain. In the absence of Smo, these six serine residues are phosphorylated by protein kinase A (PKA), glycogen synthase kinase 3β (GSK3β), and casein kinase 1α (CK1α) (**Figure 1-2A4**). Once phosphorylated, β-transducin repeat containing protein (βTrCP) binds to and ubiquitylates Gli-FL. The carboxy-terminal activation domain is cleaved off, thus generating a Gli transcriptional repressor (GliR) that inhibits downstream gene targets such as *Gli1* and *Ptch1* (**Figure 1-2A5**).

In the presence of Hh, Hh binds to one of three possible Ptch1/Hh co-receptor complexes: Ptch1/Cdo, Ptch1/Boc, or Ptch1/Gas1[46,47] (**Figure 1-2B1**). Upon binding, Ptch1 is internalized via endocytosis and degraded. In the absence of Ptch1, Smo is hyperphosphorylated by two Smo kinases: G protein coupled receptor kinase 2 (GRK2) and casein kinase 1 (CK1α)[70]. Once phosphorylated, β-arrestin 2 (βarr2) and a subunit of the kinesin

2 motor protein complex (Kif3a) bind to Smo and facilitate its translocation into the primary cilia[70,71] (**Figure 1-2B2**). In the presence of Hh, Gli-FL dissociates from Sufu[72] (**Figure 1-2B3**). In the absence of Sufu, Gli-FL is not cleaved and becomes a transcriptional activator (**Figure 1-2B4**).

Shh signaling and its role in patterning the ventral spinal cord

Morphogens are diffusible extracellular signals that have the unique capacity to direct cell fate choices in a concentration dependent manner[73]. Shh is a classic morphogen that has been shown to pattern a variety of tissue types including the developing thalamus, limbs, and spinal cord[17,74,75]. Shh has been extensively studied within the developing ventral spinal cord. Within the developing spinal cord, Shh is initially synthesized and secreted from the notochord and later the floor plate of the neural tube itself[35,76] (**Figure 1-3A**). Over time, Shh diffuses dorsally away from this fixed source, generating a high-to-low Shh concentration gradient along the ventral-to-dorsal axis of the neural tube[77] (**Figure 1-3A**). Through a complex signal transduction pathway, described above, the extracellular Shh concentration a cell is exposed to is translated into a graded intracellular response mediated by Gli proteins. Gli proteins (specifically Gli2 and Gli3) become transcriptional activators (GliA) in the presence of Shh or transcriptional repressors (GliR) in the absence of Shh[69] (**Figure 1-3A**). As the Gli proteins have the same transcriptional targets, it is ultimately the balance between GliA and GliR that determines if a gene target is turned on. Within the spinal cord, the target genes of Shh are divided into two classes of homeodomain transcription factors: the dorsally expressed Class I proteins (Dbx2, Dbx1, Pax6, and Irx3) that are present in the absence of Shh signaling and the ventrally expressed Class II proteins (Nkx6.1, Nkx6.2, Nkx2.2, and Olig2) that are activated by Shh signaling[78] (**Figure 1-3B**). Where the dorsal and ventral-most limits of these protein expression profiles are determined by the Shh gradient, boundaries between domains are established through cross repressive interactions between complementary Class I/II protein

pairs. Ultimately, unique combinations of Class I and Class II proteins subdivide the ventral neural tube into five molecularly distinct progenitor domains (p3, pMN, p2, p1, and p0) (**Figure 1-3C**). Each of these progenitor domains subsequently gives rise to a distinct subset of neurons and glia (**Figure 1-3D**).

Within the developing ventral spinal cord, progenitor domain identities are initially determined by the amount of Shh the cells are exposed to. However, once the cell adopts a progenitor identity, the cell becomes increasingly insensitive to Shh due to Ptch1-mediated negative feedback[79-82]. In the absence of this Shh signaling input, the progenitor domain boundaries are solidified and maintained by gene regulatory networks[83]. Pax6, Olig2, and Nkx2.2 are a prime example of a gene regulatory network. In this network, Pax6 represses the expression of Nkx2.2, Olig2 represses Pax6 and Nkx2.2, and Nkx2.2 represses both Olig2 and Pax6. When one component of this network is removed, the cell identities adjust accordingly. For example, when Olig2 is removed in $Olig2^{-/-}$ embryos, there is an dorsal expansion of Nkx2.2. Then, when Olig2 and Pax6 are both removed in $Olig2^{-/-}$;$Pax6^{-/-}$ double mutant embryos, there is a greater dorsal expansion of Nkx2.2. In both the $Olig2^{-/-}$ and $Olig2^{-/-}$;$Pax6^{-/-}$ embryos, the shifts in Nkx2.2 occurs independently of any changes in Shh signaling activity[83]. Overall, these studies indicate that while the concentration of the morphogen does play a major progenitor patterning role in the ventral spinal cord, it is not the only factor that does this. Gene regulatory networks downstream of Shh signaling also contribute significantly to the final progenitor domain pattern.

Shh signaling activity as a product of concentration and time

Cells were once perceived to be passive recipients of their external surroundings and as such the cell fates they adopted were believed to be solely a product of the morphogen concentration they were exposed to. However, recent studies have revealed that a far more complex and dynamic dialogue exists between morphogens and their cellular targets[84]. This is the case with the morphogen Shh. Within the developing spinal cord, studies have shown that

prolonged exposure to Shh causes NPCs to upregulate Ptch1, both a receptor of Shh and a negative feedback inhibitor, which results in the progressive desensitization of NPCs to Shh over time[81,85]. Taking this desensitization over time into account, the Temporal Adaptation Model proposes that the fate of a NPC is a product of two factors: (1) the quantity of Shh the cell is exposed to and (2) the duration of time over which the cell is exposed to Shh[80,83,85,86]. In Chapter Two we identify Notch signaling as potentially one of the mechanisms underlying this temporal component of Shh signal transduction. Multiple experiments conducted in our lab illustrate that manipulating Notch signaling activity, and thus altering the duration of time a cell is maintained as a Shh-responsive progenitor, shifts the fate of the cell. For example, activation of Notch signaling within the pMN domain produces more ventral p3 cells. Although the shift in ventral spinal cord progenitor identities by manipulating Notch signaling activity is a novel observation, interactions between Notch and Shh signaling have been previously described in a variety of other systems[87-90] and a variety of Shh pathway components have been shown to be direct targets of the Rbpj transcriptional complex[91,92]. However, the precise means through which Notch signaling interacts with Shh signaling remains largely unknown.

1-3: Notch signaling

A brief history of Notch signaling

Notch signaling is a highly conserved signaling pathway that is essential for development in all metazoans. Notch was originally discovered in *Drosophila* in March of 1913, when John S. Dexter noticed and documented a female fly with an unusual wing pattern in one of his stock cultures. Given the shape of the wing, Dexter named this new mutant hypomorph "Perfect Notched." After an extensive series of pairings, Dexter characterized the Notch factor as sex-linked and embryonic lethal when homozygous[93]. In the following few years, the Notch mutant fly was further analyzed by Thomas Hunt Morgan[94] and Otto Mohr[95]. In 1940, the Notch

mutant embryos were analyzed in detail for the first time by Donald F. Poulson. In this study, Poulson observed that in the homozygous null Notch mutant embryos the nervous system was enlarged at the expense of the epidermal tissue[96]. We now know that this phenotype is due to an inappropriate shift in cell fate choices. The immature ectodermal precursors in the developing embryo have the potential to become either neuroblasts or epidermis. In control embryos, about 25% of cells become neuroblasts and 75% become epidermis. However, in Notch mutants the majority of ectodermal precursors become neuroblasts at the expense of epidermis[97,98]. This early example illustrates that Notch signaling plays a major role in development, functioning as a means for progenitor/precursor cells to make critical binary cell fate lineage decisions.

Notch signaling pathway

The Notch signaling pathway is a means through which adjacent cells communicate with each other to coordinate cell fate choices and establish clear boundaries between distinct populations. In the canonical Notch signaling pathway, a transmembrane Notch ligand on one cell binds to a transmembrane Notch receptor on an adjacent cell (**Figure 1-4A**). In mammals, there are four heterodimeric Notch receptors (Notch1, Notch2, Notch3, and Notch4) and five Notch ligands (Delta-like1, Delta-like3, Delta-like4, Jagged1, and Jagged2)[99]. Upon binding to a Notch ligand, the Notch receptor is cleaved twice. The Notch extracellular domain (NECD) is cleaved by an ADAM family metalloproteinase and then subsequently endocytosed with the ligand by the signal sending cell, where the Notch ligand is recycled and the NECD is broken down (**Figure 1-4B**). The Notch intracellular domain (NICD) is cleaved from the cell membrane by γ-secretase, a multi-subunit protease complex. Upon cleavage, NICD translocates to the nucleus and associates with the DNA binding protein Rbpj (recombination signal sequence-binding protein Jκ) (**Figure 1-4C**). In the absence of NICD, Rbpj represses the transcription of downstream genes through the recruitment of a co-repressor complex (Co-Rep) (**Figure 1-4D**).

In the presence of NICD, the co-repressor complex is displaced and replaced with a co-activator complex (Co-Act), thus activating the expression of downstream genes[100]. Mastermind-like proteins (Maml) are transcriptional co-activators that directly bind to NICD and facilitate the generations of a NICD-Rbpj-Maml complex[101]. Notable downstream target genes of the Rbpj transcriptional complex include *Hairy enhancer of split 1/5* (*Hes1/5*), *Hairy enhancer of split with YRPW motif* (*Hey*), *Cyclin D1* (*Ccnd1*), *Myelocytomatosis oncogene* (*Myc*), and *B cell leukemia/lymphoma 2* (*Bcl2*)[102]. *Hes* and *Hey* genes are basic-helix-loop-helix (bHLH) transcription factors that inhibit neuronal differentiation through the repression of proneural genes such as *Mash1* and *Neurogenin2* (*Ngn2*)[103]. Ccnd1 and Myc are regulators of cell cycle progression and Bcl2 regulates apoptosis. Thus, it is through this abundance of gene target variety that Notch signaling is able to regulate differentiation, cellular proliferation, and apoptosis. Recently, through the use of ChIP-Seq technology (chromatin immunoprecipitation in parallel with DNA sequencing), an abundance of new genes (100+) have been identified that are both direct targets of Rbpj and have been shown to be regulated by Notch signaling activity[91,104]. These newly identified Notch target genes are surprisingly diverse. Some of these genes are components of other major signaling pathways, such as Wnt, Shh, and Hippo. Other genes are involved in cellular processes in which the role of Notch signaling has been poorly studied. Overall these new genome-wide studies have rapidly expanded our understanding of the many functions of Notch signaling and support the idea that Notch signaling is one component of a much larger and highly integrated signaling network[3].

Notch signaling patterning mechanisms

At its core, Notch signaling provides a means for cells to communicate with each other to coordinate cell fate decisions. These Notch mediated cell fate decisions can be roughly subdivided into three different categories: lateral inhibition, binary lineage decisions, and inductive signaling[105-107]. (1) Lateral inhibition is a means for a smaller differentiated cell type to

emerge evenly from a homogenous progenitor population. In this process, all the cells that make up the homogenous population initially express equal amounts of Notch ligands and receptors. At some point in development, a subtle change in Notch signaling activity occurs in a small subset of the cells. Notch signaling activity upregulates *Hes* genes, which inhibit the expression of proneural genes (like *Mash1* and *Ngn2*). As proneural genes have the capacity to upregulate the expression of Notch ligands, the inhibition of proneural genes in Notch activated cells results in a loss of ligand expression[108,109]. Thus, through this feedback mechanism, the initial small increase in Notch signaling present in a subset of cells is amplified over time. Notch ligands become enriched in the signal sending cells (which exhibit low levels of Notch signaling activity) and receptors become enriched in the signal receiving cells (which exhibit high levels of Notch signaling activity) (**Figure 1-5A**). (2) Binary lineage decisions are a product of asymmetric cell divisions. In this process, Notch signaling activity is differentially expressed in the two daughter cells, resulting in the generation of two unique cell types from a single precursor. In the context of neural development, one daughter cell is frequently maintained as a progenitor (retaining high levels of Notch signaling activity) and the other daughter cell undergoes either neuronal or glial differentiation (exhibiting low levels of Notch signaling activity). This process ensures that neural progenitors are present throughout development, remaining available for the generation of later born cell types (**Figure 1-5B**). (3) Lastly, inductive signaling results in the establishment of boundaries during development. In this process, Notch signaling is activated in cells at the boundary between two distinct populations. These boundary cells become an organizing center that is involved in coordinating the growth and patterning of the adjacent populations (**Figure 1-5C**).

Notch signaling in vertebrate glial development

Within the developing CNS, Notch signaling plays a major role in both the inhibition of neural differentiation and the maintenance of progenitor populations[110,111]. While Notch signaling

is widely regarded as a permissive signal, that retains cells in a pluripotent progenitor state until the appropriate differentiation cues become present[98], Notch signaling also has the capacity to function as an instructive cue in gliogenesis[112]. Studies have proposed that Notch signaling can actively promote the following glial cell fates: astrocytes in cortical neural stem cell cultures via direct regulation of the astrocyte marker gene, glial fibrillary acidic protein (GFAP)[113]; astrocytes in adult hippocampus-derived multipotent progenitor cultures[114]; Müller glia in the developing retina[115,116]; radial glia in the developing forebrain and cerebellum via direct regulation of the radial glial gene, brain lipid binding protein (BLBP)[117,118]; and Schwann cells in neural crest stem cells[119,120]. Interestingly, while Notch signaling activity has consistently been shown to support astrogliogenesis, its effects on oligodendrogenesis are variable. In optic nerve oligodendrocyte precursor cell cultures, Notch signaling activity inhibited oligodendrocyte differentiation and myelination[121]. On the other hand, in the developing ventral spinal cord, Notch signaling activity promoted the generation of oligodendrocyte precursors at the expense of neurons[122].

The expression of Notch ligands and receptors in the developing spinal cord

Notch receptors and ligands are not uniformly expressed throughout the developing embryo, but are rather present in interesting and frequently complementary patterns. Previous studies have shown that in the developing spinal cord three Notch receptors (Notch1, Notch2, and Notch3) and four Notch ligands (Dll1, Dll4, Jag1, and Jag2) are present, each with their own unique expression pattern. Notch1 is present in all progenitors along the dorsoventral extent[123,124]. Notch2 and Notch3 are restricted to the more ventral progenitors. Dll1 is widely expressed, present in the pd5, p0, p2, pMN, and p3 progenitor domains. The remaining ligands are expressed in a more restricted pattern. Dll4 is present in the p2 progenitor domain, Jag1 in pd6 and p1, and lastly Jag2 is transiently expressed in pMN[123,125-127] (**Figure 1-6**). The homeodomain transcription factor code that establishes the progenitor domains also dictates the expression pattern of the Notch ligands[125].

1-4: Interactions between Shh and Notch signaling

Previous studies have shown that both Notch and Shh signaling are vital for the maintenance of progenitor populations and are involved in the specification of subsequent neural subtypes [69,85,112,128,129]. Although overlapping functions can suggest overlapping pathways, currently relatively little is known about how these two major signals collectively pattern the developing CNS.

Recent studies in the developing zebrafish spinal cord have demonstrated that Notch signaling activity maintains cells as Hh responsive progenitors. Once Notch signaling is lost, the progenitors quickly differentiate into Hh non-responsive interneurons. Thus, by retaining cells as Hh responsive progenitors, Notch signaling is necessary for the generation of later born Shh-induced cell types[87].

Other than development, one area in which Notch and Shh signaling pathway interactions have been more thoroughly studied is in the field of cancer biology. Many developmental signaling pathways, such as Notch and Shh, are frequently upregulated in the same types of cancer. In an effort to develop a cancer treatment, a recent study examined the effects of a Notch inhibitor (a gamma secretase inhibitor called MRK-003) on the rate of tumor cell growth. This studied showed that when a glioblastoma neurosphere line was initially treated with a Notch inhibitor, the cells initially exhibited a decrease in growth. However, over time the cells adapted and, although Hes1 protein levels were still suppressed by the Notch inhibitor, growth returned to normal levels. A closer look revealed that during this period of adaptation, Hedgehog signaling was upregulated. In addition, a ChIP (chromatin immunoprecipitation) experiment found that Hes1 binds to N-boxes (Hes binding sequences) present in the first intro of Gli1[130]. In all, this data suggests that in some tumor lines the Notch pathway target Hes1 may directly bind to and inhibits *Gli1* expression. This data is supported by genomic analyses conducted on *Gli1*. These analyses showed that the genomic sequences of human,

chimpanzee, mouse, and rat *Gli1* are highly conserved. In addition, they revealed that within intron 1 of the mammalian *Gli1* orthologs there is no highly conserved CSL-binding site, but there are two highly conserved N-boxes, DNA sequences Hes/Hey family proteins are known to bind to[131]. Collectively, the findings from these studies suggest Notch signaling modulates Hedgehog signaling through the direct binding of Hes proteins to *Gli1*.

1-5: Cell adhesion and polarity

Role of cell adhesion proteins in neurulation

Neurulation is the process through which the neural plate becomes the neural tube. In vertebrates, the neurulation process can be roughly divided into three steps: neural plate induction, neural plate invagination, and neural tube closure[132]. Initially, the developing embryo is composed of three germ layers. In the process of neural plate induction, extracellular cues secreted from the notochord and axial mesoderm (such as the BMP antagonists Chordin and Noggin) cause the overlying ectoderm to become the neural plate[133]. The neural plate is made up of neuroepithelial cells, which are both morphologically and molecularly distinct from the ectodermal cells they are derived from, as they appear more columnar in shape and express Sox1 (a member of the SoxB1 transcription factor family)[134,135]. After the neural plate is generated, the cells rapidly divide and rise up to form the neural folds that line the neural groove. Lastly, the neural folds fuse at the midline to form the neural tube.

Neurulation is a surprisingly complex process. The transition from a flat two-dimensional neural plate to a three-dimensional neural tube requires forces to physically bend the tissue upward and together[136]. While we still do not completely understand the molecular mechanisms behind these forces, we do know that cell adhesion proteins are essential throughout the neurulation process to hold the neuroepithelial cells together[137]. Cadherins, calcium-dependent cell transmembrane proteins, are a family of cell adhesion proteins that have been shown across species to be essential for proper neurulation[138-140]. These cell adhesion proteins hold

the neuroepithelial cells of the neural plate and neural tube together. While these apical adhesion proteins fulfill an important role in development, allowing the neuroepithellial cells to endure the physical transition from a sheet to a tube, they are still present well into embryogenesis where they maintain the cell polarity of neuroepithelial cells and retain these neural progenitors to the ventricular zone.

Role of adhesion proteins in progenitor maintenance

The neural tube is made up of neuroepithellial cells. These neuroepithelial cells are neural stem/progenitor cells that appear elongated and columnar in shape, thus possessing a clear apical and basal end. The polarity and general integrity of this neuroepithelial cell layer is primarily maintained by the presence of adherens junctions at the apical ends[141-143].

In a process termed interkinetic nuclear migration, the nuclei of the neuroepithelial cells migrate along the apicobasal axis in phase with the cell cycle. Thus, when a cell is in M-phase, the nucleus is present at the apical surface; and when a cell proceeds through S-phase, the nucleus then migrates towards the basal surface[144,145]. Interestingly, when the cell undergoes division, the orientation of the plane of cleavage of the dividing nucleus at the apical surface predicts whether the neuroepithelial cell will undergo proliferative or neurogenic division. If the plane of division is symmetrical, the neuroepithial cell will divide and produce two progenitor cells that will be retained to the ventricular zone (proliferative division). However, if the plane of division is asymmetrical, the neuroepithelial cell will divide and produce one progenitor cell and one cell that will be released from the ventricular zone and undergo differentiation (neurogenic division)[146-148]. Early in development, the neuroepithelial cells undergo multiple rounds of symmetric cell division to increase the overall number of progenitors. However, over time, the neuroepithelial cells begin to undergo rounds of asymmetric cell division to generate neurons and later glia.

The daughter cells produced from a round of asymmetrical cell division are very

different from each other. First, the daughter cells have very different apical/basal contacts. The daughter cell that remains a progenitor retains its apical contacts and is kept in the ventricular zone. However, the daughter cell that undergoes differentiation is released from the ventricular zone through a disassembly of the apical adherens junctions[146]. Second, the daughter cells have very different cell polarity properties and morphologies. The progenitor daughter cell is still highly polarized and retains its columnar shape. However, due to a loss of apical contacts, the cell that undergoes differentiation losses its cellular polarity and becomes round in shape. Lastly, when undergoing cell division, proteins are unequally distributed to the daughter cells. Among the proteins that are unequally distributed to the daughter cells are: Notch1, a Notch receptor; Numb, a Notch antagonist; and Par3, a cell polarity protein[146,149-151].

A role of Notch signaling in asymmetric cell division, cell adhesion, and cell polarity

For a neuroepithelial cell to undergo differentiation it must undergo asymmetrical division, breakdown its apical adhesion contacts to the lumen, and lose its cell polarity. While we currently have a poor understanding of the mechanisms that coordinate these events, previous studies have shown that Notch signaling is involved in all three. The asymmetric inheritance of Notch1, Numb, and Par3 by the two daughter cells results in cells exhibiting different levels of Notch signaling activity[146,149,151]. In the developing *Drosophila*, Notch signaling regulates the expression of various cell adhesion proteins and in doing so plays a major role in organizing the inter-ommatidial cells and primary pigment cells of the eye[152]. Lastly, in regards to cell polarity, an inhibition of Notch signaling activity in mouse ES-derived neural rosette cultures resulted in a loss of cell adhesion, a loss of cell polarity, and a loss of rosette integrity[153]. Similar results were observed in the developing *Drosophila* optic lobe, where a loss of Notch signaling activity resulted in a loss of cell polarity markers and neuroepithelial integrity[154]. None of the studies cited above identify a mechanism through which Notch signaling regulates cell adhesion or cell polarity events. However, a severe loss of neuroepithelial integrity

was also observed when both Hes1 and Hes5 were removed from the developing spinal cord[155]. This additional data suggests that the integrity of cell adhesion and cell polarity may be mediated by Hes genes.

1-6: Retinoic acid signaling

Retinoic acid (RA) signaling is a core developmental signaling pathway. Derived from dietary Vitamin A, the importance of RA in development is perhaps best illustrated through studies on Vitamin A deficiency. When pregnant female rats were maintained on a vitamin A-deficient diet over a short gestational window, the resulting pups exhibited developmental defects to the eyes, skull, trachea, esophagus, limbs, heart, and CNS[156].

Vitamin A (all-trans retinol, at-retinol) is consumed and absorbed into the blood stream via the small intestine. Once in the blood stream, at-retinol binds to retinol binding protein 4 (RBP4). The RBP4 serves as a tag, binding to the membrane receptor STRA6 and allowing for at-retinol to identify and enter into the cytoplasm of target cells. Once in the cytoplasm, at-retinol is converted to biologically functional all-trans retinoic acid (RA) via a two-step oxidation process involving the enzymes retinol or alcohol dehydrogenases (RoDHs or ADHs) and retinaldehyde dehydrogenases (RALDHs)[157]. Once synthesized, RA is shuttled into the nucleus by bind to cellular retinoic acid binding protein 2 (CRABP2). Once in the nucleus, RA binds to two possible receptors: RA receptors (RARs) or retinoid X receptors (RXRs). These RA bound receptors (RA-RAR and RA-RXR) then heterodimerize and bind to retinoic-acid response elements (RAREs) on target genes to activate their transcription[7,158]. Through the use of ChIP-on-chip (chromatin immunoprecipitation combined with microarray hybridization) and ChIP-seq technology, over 300 potential RA-regulated gene targets were recently identified[159]. Among the targets identified were Hox genes and components of the TGFβ (transforming growth factor β) signaling pathway, a pathway known to interact with RA signaling to regulate cell growth and differentiation.

In the developing CNS, RA signaling plays a major role in both anteroposterior and dorsoventral progenitor patterning. Multiple studies have shown that RA signaling drives progenitor cells towards more posterior/rostral cell identities by directly binding to and manipulating the expression of certain Hox genes[159-163]. Additional studies conducted in mouse embryonic cell culture, avian embryos, and chick neural plate explants have also shown that RA drives spinal cord progenitors towards a more dorsal identity[9,164,165]. In addition to its role in patterning, RA signaling also drives progenitors towards neuronal differentiation[166].

In the developing hindbrain, an anteroposterior gradient of RA is produced and maintained by the combined efforts of Raldh2 (an enzyme that catalyzes the conversion of vitamin A to RA) and Cyp26 (a member of the cytochrome P450 enzyme family that metabolizes RA)[8,167-169]. Unlike a typical morphogen gradient, in which the gradient is the product of a soluble factor being secreted from a fixed point, the RA gradient is generated largely by Raldh2 and Cyp26 (a RA-synthesizing enzyme present in the posterior hindbrain and a RA-metabolizing enzyme present in the anterior hindbrain). As the gradient is a product of these two enzymes, when either Raldh2 or Cyp26 are absent, the hindbrain changes dramatically. In Raldh2$^{-/-}$ mutant embryos, the morphology of the posterior-most rhombomeres (r3-r8) are lost and anterior gene expression expands into more posterior regions[8]. In contrast, in Cyp26$^{-/-}$ mutant embryos, the anterior hindbrain takes on a more posterior identity[168].

1-7: Summary

In the beginning there are only a few core signaling pathways present to guide the CNS from sheet of undifferentiated and unorganized cells, to a complex system of interconnected circuits capable of sensing and interacting with the external world. To generate the multitude of cell types required for this transition, these fundamental signaling pathways must interact with each other. In the following work we focus on better understanding two of these signaling pathways: Shh and Notch signaling. In regards to Notch signaling, we describe how Notch

signaling interacts with both Shh and RA signaling to give rise to greater cellular diversity in the developing embryo.

In Chapters 2-4, we focus on portraying Notch signaling as much more than a progenitor maintenance factor. In the context of the developing ventral spinal cord, Notch signaling modulates a progenitor cell's response to extracellular Shh and thus plays a role in progenitor patterning. In the developing hindbrain and rostral spinal cord, Notch signaling works with RA signaling to regulate the expression of the transcription factor Ascl1 and in doing so contributes towards the generation of greater neuronal diversity. Lastly, in the developing diencephalon, Notch signaling is involved in the maintenance of apical adherens junctions and thus preserves the integrity of the neuroepithelial cell layer.

In Chapter 5, we shift our focus from Notch signaling to Shh signaling. Like Notch signaling, Shh signaling acts in conjunction with many other signals and pathways. As a result, the Shh signaling activity a cell experiences is a product of much more than the concentration of extracellular Shh ligand the cell is exposed to. In Chapter 2 we illustrate that Notch signaling modulates a progenitor cell's responsiveness to extracellular Shh by influencing the movement of Ptch1 and Smo to the primary cilia. In Chapter 5 we show that Gli phosphorylation by PKA also plays a significant role in regulating Shh signaling activity, by inhibiting these transcriptional effectors from becoming transcriptional activators in a graded manner.

Lastly, in Chapter 6 we discuss the implications of our findings in the context of cancer. Both Notch and Shh signaling activity are elevated in an assortment of cancers. Some evidence indicates that, just as Notch signaling is able to amplify a progenitor cell's response to Shh signaling in the context of the developing CNS, Notch signaling may also be elevate Shh signaling activity in the context of cancer. Thus, a greater understanding of how these pathways interact appropriately in the context of development may help us to understand how these pathways go awry in the context of cancer.

FIGURES

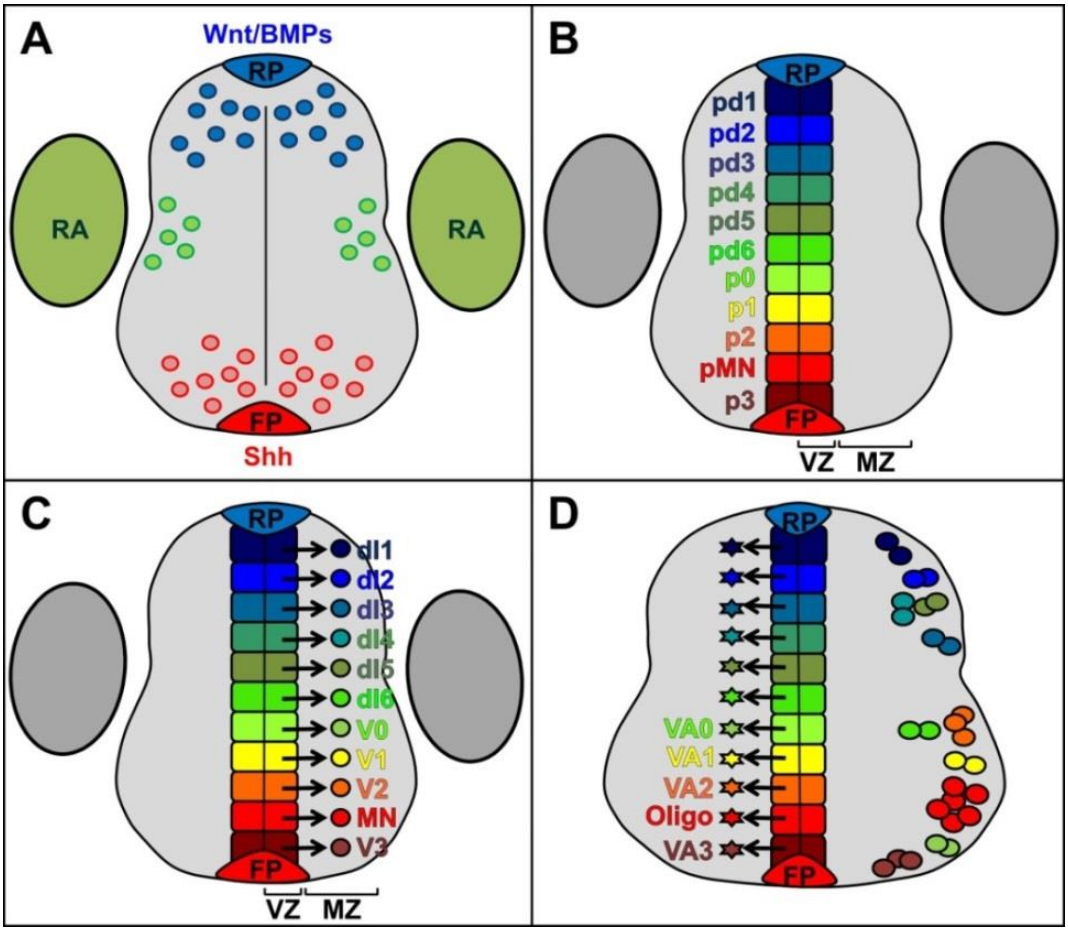

Figure 1-1: Spinal cord development

(A) The developing neural tube is exposed to sonic hedgehog (Shh) secreted from the floorplate (FP), Wnt and bone morphogenic proteins (BMPs) from the roofplate (RP), and retinoic acid (RA) from the paraxial mesoderm.

(B) These external signaling cues converge upon uncommitted neural progenitors present within the ventricular zone (VZ), resulting in the generation of 11 distinct progenitor domains along the dorsoventral axis.

(C) Each progenitor domains gives rise to a unique population of neurons.

(D) Over time, the postmitotic neurons migrate out and settle in a specific location of the mantle

zone (MZ). After a period of neurogenesis (C), the progenitor domains stop generating neurons and begin generating glial cells.

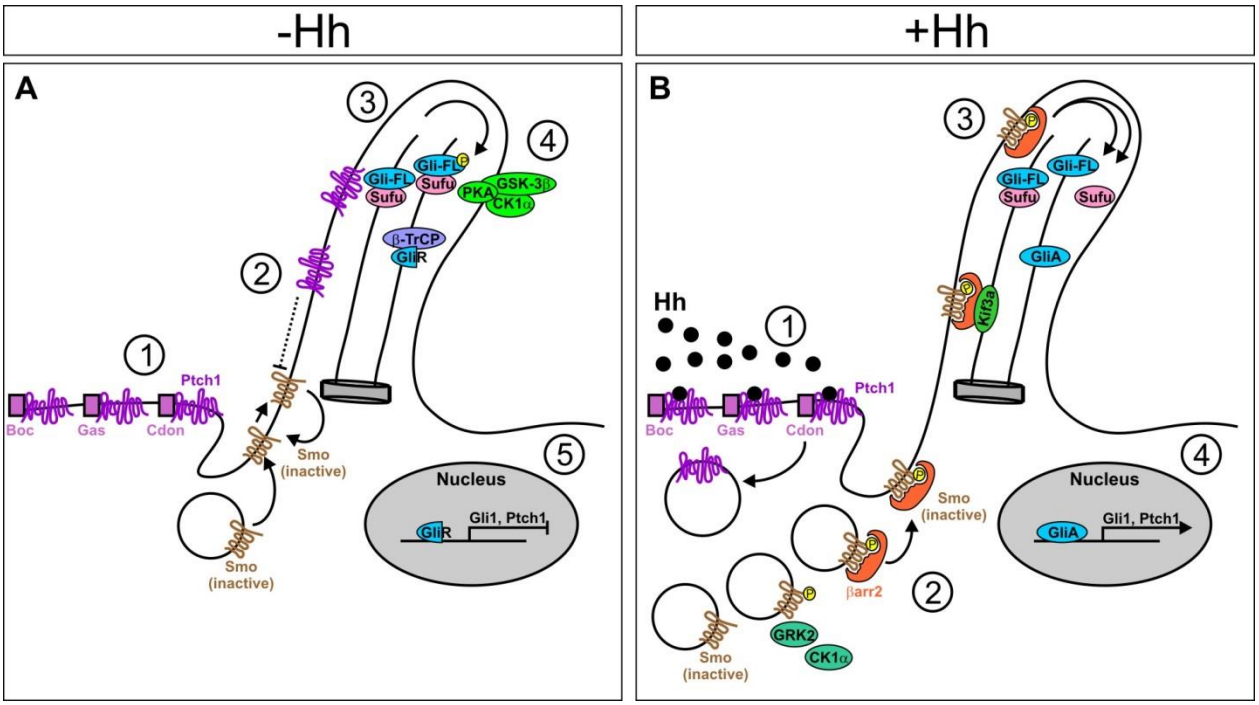

Figure 1-2: Hedgehog signaling pathway

(A) (A1) In the absence of Hedgehog (Hh) ligand, the twelve-pass Hh transmembrane receptor Patched1 (Ptch1) accumulates at the base of and within the primary cilium. **(A2)** Through an indirect mechanism, the presence of Ptch1 represses the activation and movement of the seven-pass transmembrane protein Smoothened (Smo) into the primary cilium. **(A3/A4)** In the absence of Smo, full length Gli proteins (Gli-FL) remain bound to Sufu and are phosphorylated by protein kinase A (PKA), glycogen synthase kinase 3β (GSK3β), and casein kinase 1α (CK1α). Once phosphorylated, the Gli proteins are ubiquitylated by β-transducin repeat containing protein (βTrCP). **(A5)** Gli proteins are then cleaved to process these proteins into transcriptional repressors (GliR), which then translocate to the nucleus and repress downstream gene targets that include *Gli1* and *Ptch1*.

(B) (B1) In the presence of Hh, the Hh ligand binds to Ptch1 or one of three single-pass Hh transmembrane accessory receptors: cell adhesion molecule related/downregulated by oncogenes (Cdo), brother of Cdo (Boc) and growth arrest specific 1 (Gas1). Upon binding to the

Hh ligand, Ptch1 is endocytosed and degraded. **(B2)** In the absence of Ptch1, Smo is phosphorylated by G protein coupled receptor kinase 2 (GRK2) and casein kinase 1α (CK1α), which then allows Smo to bind to β-arrestin 2 (βarr2) and a subunit of the kinesin motor protein complex (Kif3a), allowing for the movement of Smo into the primary cilium. **(B3)** In the presence of Smo, Gli-FL dissociates from Sufu, an event which inhibits its phosphorylation. In the absence phosphorylation, full length Gli proteins (Gli-FL) are not cleaved and are processed into transcriptional activators (GliA). **(B4)** GliA translocate into the nucleus and activate downstream genes like Gli1 and Ptch1. Adapted from Briscoe and Therond, 2013.

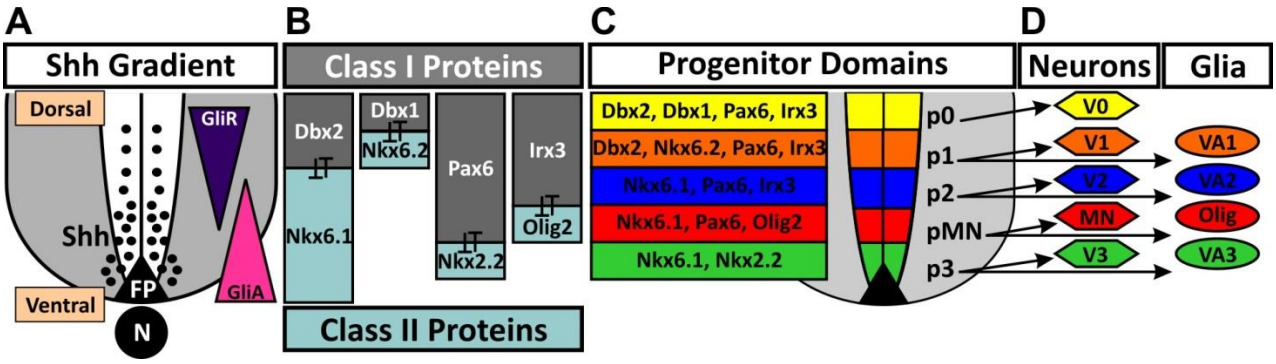

Figure 1-3: The role of Shh signaling in ventral spinal cord patterning

(A) Shh ligand is secreted by the notochord (N) and the floor plate (FP) of the neural tube. Shh acts in a dose-dependent manner to alter the processing of Gli proteins from transcriptional repressors (GliR) to transcriptional activators (GliA). **(B)** The net balance between GliR and GliA influences the expression of various homeodomain transcription factors along the dorsoventral axis. These transcription factors can be grouped into two classes: Class I proteins (Dbx2, Dbx1, Pax6, and Irx3) that are present in the absence of Shh and Class II proteins (Nkx6.1, Nkx6.2, Nkx2.2, and Olig2) that require Shh for their activation. **(C)** Ultimately, unique combinations of Class I and Class II transcription factors subdivide the ventral spinal cord into five molecularly distinct progenitor domains (p0, p1, p2, pMN, and p3). **(D)** Over time, each of these progenitor domains give rise to distinct types of neurons and then glia.

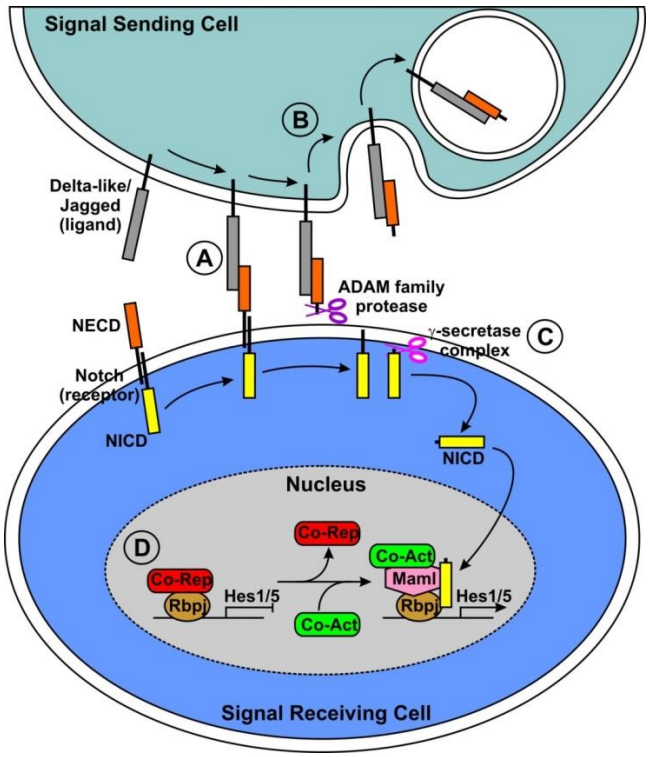

Figure 1-4: Notch signaling pathway

(A) One of five Notch ligands (Dll1, Dll3, Dll4, Jag1, and Jag2) on the signal sending cell binds to one of four Notch receptors (Notch1-4) on the signal receiving cell. Upon binding, the Notch receptor is cleaved twice: the Notch extracellular domain (NECD) is cleaved by an ADAM family protease and the Notch intracellular domain (NICD) is cleaved by a λ-secretase protease complex. **(B)** Attached to the Notch ligand, NECD is endocytosed by the signal sending cell. **(C)** NICD translocates to the nucleus and associates with the DNA binding protein Rbpj (recombination signal sequence binding protein Jκ). **(D)** In the absence of NICD, Rbpj associates with a co-repressor complex (Co-Rep). In the presence of NICD, the co-repressor complex is broken up and replaced with a co-activator complex (Co-Act). The generation of a co-activator complex is facilitated by mastermind-like (Maml) transcriptional co-activators. Downstream Notch gene targets include *Hes1* and *Hes5*, members of the Hairy enhancer of split family that inhibit neurogenesis. Adapted from Amsen, et al., 2009 and Ranganathan, et al., 2011.

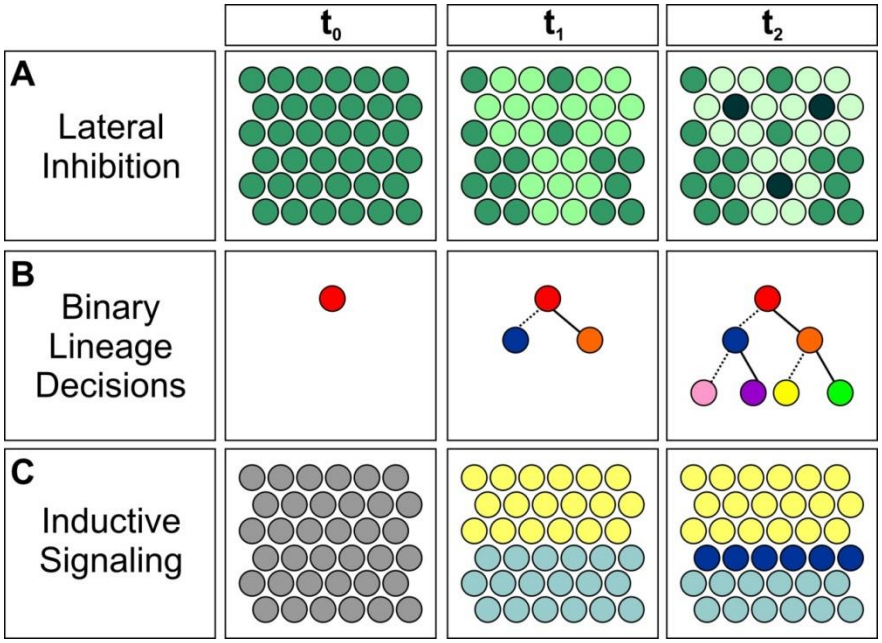

Figure 1-5: Notch signaling patterning mechanisms

(A) Lateral inhibition. Initially (t_0), all the cells are homogenous (green cells). Over time (t_1) an imbalance in Notch signaling activity occurs. Due to signaling feedback, the small imbalance in in Notch signaling activity is amplified over time (t_2), resulting in cells with an abundance of Notch ligands (dark green cells, low Notch signaling activity) and cells with an abundance of Notch receptors (light green cells, high Notch signaling activity)

(B) Binary lineage decisions. A single precursor cells gives rise to two unique daughter cells. Notch signaling is activated in one daughter cell (solid line) and Notch signaling is not activated in the other daughter cell (dashed line). The different colors represent that various cell types that can be generated from a single cell.

(C) Inductive signaling to establish boundaries between cell populations. One population of cells (yellow) signals to a neighboring group of cells (blue) and a new cell population (dark blue) is created at the boundary. Notch signaling is elevated in these boundary cells and becomes an organizing center, coordinating growth in the adjacent populations. Adapted from Haines and Irvine, 2003.

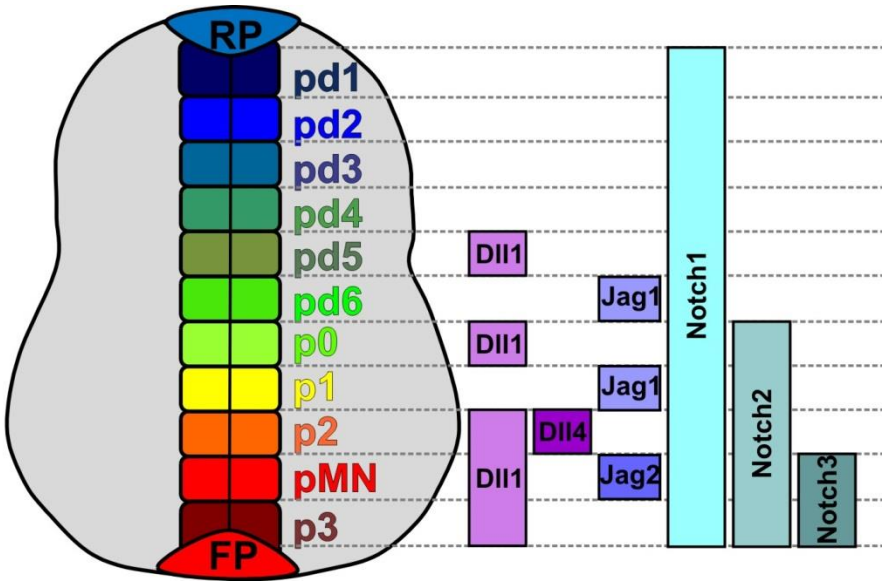

Figure 1-6: The expression of Notch ligands and receptors in the developing spinal cord

Notch receptors (Notch1, Notch2, and Notch3) and ligands (Dll1, Dll4, Jag1, and Jag2) are expressed in complementary patterns along the dorsoventral axis of the developing spinal cord. While the progenitor domain expression of the Notch ligands is accurate, the expression of the Notch receptors are estimates based on published data. Generated from Lindsell, et al., 1996; Mitsiadis, et al., 2001; Marklund, et al., 2010; Skaggs, et al., 2011; and Rabadan, et al., 2012.

REFERENCES

1 Barolo, S. & Posakony, J. W. Three habits of highly effective signaling pathways: principles of transcriptional control by developmental cell signaling. *Genes & development* **16**, 1167-1181, doi:10.1101/gad.976502 (2002).

2 Pires-daSilva, A. & Sommer, R. J. The evolution of signalling pathways in animal development. *Nature reviews. Genetics* **4**, 39-49, doi:10.1038/nrg977 (2003).

3 Hurlbut, G. D., Kankel, M. W., Lake, R. J. & Artavanis-Tsakonas, S. Crossing paths with Notch in the hyper-network. *Current opinion in cell biology* **19**, 166-175, doi:10.1016/j.ceb.2007.02.012 (2007).

4 Guruharsha, K. G., Kankel, M. W. & Artavanis-Tsakonas, S. The Notch signalling system: recent insights into the complexity of a conserved pathway. *Nature reviews. Genetics* **13**, 654-666, doi:10.1038/nrg3272 (2012).

5 Yoon, K. & Gaiano, N. Notch signaling in the mammalian central nervous system: insights from mouse mutants. *Nature neuroscience* **8**, 709-715, doi:10.1038/nn1475 (2005).

6 Briscoe, J. & Novitch, B. G. Regulatory pathways linking progenitor patterning, cell fates and neurogenesis in the ventral neural tube. *Philosophical transactions of the Royal Society of London. Series B, Biological sciences* **363**, 57-70, doi:10.1098/rstb.2006.2012 (2008).

7 Maden, M. Retinoic acid in the development, regeneration and maintenance of the nervous system. *Nature reviews. Neuroscience* **8**, 755-765, doi:10.1038/nrn2212 (2007).

8 Niederreither, K., Vermot, J., Schuhbaur, B., Chambon, P. & Dolle, P. Retinoic acid synthesis and hindbrain patterning in the mouse embryo. *Development* **127**, 75-85 (2000).

9 Novitch, B. G., Wichterle, H., Jessell, T. M. & Sockanathan, S. A requirement for retinoic acid-mediated transcriptional activation in ventral neural patterning and motor neuron specification. *Neuron* **40**, 81-95 (2003).

10 Machold, R. *et al.* Sonic hedgehog is required for progenitor cell maintenance in telencephalic stem cell niches. *Neuron* **39**, 937-950 (2003).

11 Hitoshi, S. *et al.* Notch pathway molecules are essential for the maintenance, but not the generation, of mammalian neural stem cells. *Genes & development* **16**, 846-858, doi:10.1101/gad.975202 (2002).

12 Pevny, L. & Placzek, M. SOX genes and neural progenitor identity. *Current opinion in neurobiology* **15**, 7-13, doi:10.1016/j.conb.2005.01.016 (2005).

13 Graham, V., Khudyakov, J., Ellis, P. & Pevny, L. SOX2 functions to maintain neural progenitor identity. *Neuron* **39**, 749-765 (2003).

14 Zechner, D. *et al.* beta-Catenin signals regulate cell growth and the balance between progenitor cell expansion and differentiation in the nervous system. *Developmental biology* **258**, 406-418 (2003).

15 Rousso, D. L. *et al.* Foxp-mediated suppression of N-cadherin regulates neuroepithelial character and progenitor maintenance in the CNS. *Neuron* **74**, 314-330, doi:10.1016/j.neuron.2012.02.024 (2012).

16 Stamataki, D., Ulloa, F., Tsoni, S. V., Mynett, A. & Briscoe, J. A gradient of Gli activity mediates graded Sonic Hedgehog signaling in the neural tube. *Genes & development* **19**, 626-641, doi:10.1101/gad.325905 (2005).

17 Jessell, T. M. Neuronal specification in the spinal cord: inductive signals and transcriptional codes. *Nature reviews. Genetics* **1**, 20-29, doi:10.1038/35049541 (2000).

18 Briscoe, J. & Therond, P. P. The mechanisms of Hedgehog signalling and its roles in development and disease. *Nature reviews. Molecular cell biology* **14**, 416-429, doi:10.1038/nrm3598 (2013).

19 Le Dreau, G. & Marti, E. The multiple activities of BMPs during spinal cord development. *Cellular and molecular life sciences : CMLS* **70**, 4293-4305, doi:10.1007/s00018-013-1354-9 (2013).

20 Helms, A. W. & Johnson, J. E. Specification of dorsal spinal cord interneurons. *Current opinion in neurobiology* **13**, 42-49 (2003).

21 Muroyama, Y., Fujihara, M., Ikeya, M., Kondoh, H. & Takada, S. Wnt signaling plays an essential role in neuronal specification of the dorsal spinal cord. *Genes & development* **16**, 548-553, doi:10.1101/gad.937102 (2002).

22 Alaynick, W. A., Jessell, T. M. & Pfaff, S. L. SnapShot: spinal cord development. *Cell* **146**, 178-178 e171, doi:10.1016/j.cell.2011.06.038 (2011).

23 Gomez-Skarmeta, J. L., Campuzano, S. & Modolell, J. Half a century of neural prepatterning: the story of a few bristles and many genes. *Nature reviews. Neuroscience* **4**, 587-598, doi:10.1038/nrn1142 (2003).

24 Lee, S. K. & Pfaff, S. L. Transcriptional networks regulating neuronal identity in the developing spinal cord. *Nature neuroscience* **4 Suppl**, 1183-1191, doi:10.1038/nn750 (2001).

25 Hochstim, C., Deneen, B., Lukaszewicz, A., Zhou, Q. & Anderson, D. J. Identification of positionally distinct astrocyte subtypes whose identities are specified by a homeodomain code. *Cell* **133**, 510-522, doi:S0092-8674(08)00396-6 [pii] 10.1016/j.cell.2008.02.046 (2008).

26 Nusslein-Volhard, C. & Wieschaus, E. Mutations affecting segment number and polarity in Drosophila. *Nature* **287**, 795-801 (1980).

27 Lee, J. J., von Kessler, D. P., Parks, S. & Beachy, P. A. Secretion and localized transcription suggest a role in positional signaling for products of the segmentation gene hedgehog. *Cell* **71**, 33-50 (1992).

28 Mohler, J. & Vani, K. Molecular organization and embryonic expression of the hedgehog gene involved in cell-cell communication in segmental patterning of Drosophila. *Development* **115**, 957-971 (1992).

29 Tabata, T., Eaton, S. & Kornberg, T. B. The Drosophila hedgehog gene is expressed specifically in posterior compartment cells and is a target of engrailed regulation. *Genes & development* **6**, 2635-2645 (1992).

30 Tashiro, S. *et al.* Structure and expression of hedgehog, a Drosophila segment-polarity gene required for cell-cell communication. *Gene* **124**, 183-189 (1993).

31 Wada, H. & Makabe, K. Genome duplications of early vertebrates as a possible chronicle of the evolutionary history of the neural crest. *International journal of biological sciences* **2**, 133-141 (2006).

32 Pathi, S. *et al.* Comparative biological responses to human Sonic, Indian, and Desert hedgehog. *Mechanisms of development* **106**, 107-117 (2001).

33 Carpenter, D. *et al.* Characterization of two patched receptors for the vertebrate hedgehog protein family. *Proc Natl Acad Sci U S A* **95**, 13630-13634 (1998).

34 Varjosalo, M. & Taipale, J. Hedgehog: functions and mechanisms. *Genes & development* **22**, 2454-2472, doi:10.1101/gad.1693608 (2008).

35 Echelard, Y. *et al.* Sonic hedgehog, a member of a family of putative signaling molecules, is implicated in the regulation of CNS polarity. *Cell* **75**, 1417-1430 (1993).

36 Bellusci, S. *et al.* Involvement of Sonic hedgehog (Shh) in mouse embryonic lung growth and morphogenesis. *Development* **124**, 53-63 (1997).

37 Ramalho-Santos, M., Melton, D. A. & McMahon, A. P. Hedgehog signals regulate multiple aspects of gastrointestinal development. *Development* **127**, 2763-2772 (2000).

38 Litingtung, Y., Lei, L., Westphal, H. & Chiang, C. Sonic hedgehog is essential to foregut development. *Nature genetics* **20**, 58-61, doi:10.1038/1717 (1998).

39 St-Jacques, B., Hammerschmidt, M. & McMahon, A. P. Indian hedgehog signaling regulates proliferation and differentiation of chondrocytes and is essential for bone formation. *Genes & development* **13**, 2072-2086 (1999).

40 Lanske, B. *et al.* PTH/PTHrP receptor in early development and Indian hedgehog-regulated bone growth. *Science* **273**, 663-666 (1996).

41 Hebrok, M., Kim, S. K., St Jacques, B., McMahon, A. P. & Melton, D. A. Regulation of pancreas development by hedgehog signaling. *Development* **127**, 4905-4913 (2000).

42 Bitgood, M. J., Shen, L. & McMahon, A. P. Sertoli cell signaling by Desert hedgehog regulates the male germline. *Current biology : CB* **6**, 298-304 (1996).

43 Yao, H. H., Whoriskey, W. & Capel, B. Desert Hedgehog/Patched 1 signaling specifies fetal Leydig cell fate in testis organogenesis. *Genes & development* **16**, 1433-1440, doi:10.1101/gad.981202 (2002).

44 Wijgerde, M., Ooms, M., Hoogerbrugge, J. W. & Grootegoed, J. A. Hedgehog signaling in mouse ovary: Indian hedgehog and desert hedgehog from granulosa cells induce target gene expression in developing theca cells. *Endocrinology* **146**, 3558-3566, doi:10.1210/en.2005-0311 (2005).

45 Chen, X. *et al.* Processing and turnover of the Hedgehog protein in the endoplasmic reticulum. *The Journal of cell biology* **192**, 825-838, doi:10.1083/jcb.201008090 (2011).

46 Porter, J. A. *et al.* Hedgehog patterning activity: role of a lipophilic modification mediated by the carboxy-terminal autoprocessing domain. *Cell* **86**, 21-34 (1996).

47 Porter, J. A., Young, K. E. & Beachy, P. A. Cholesterol modification of hedgehog signaling proteins in animal development. *Science* **274**, 255-259 (1996).

48 Chamoun, Z. *et al.* Skinny hedgehog, an acyltransferase required for palmitoylation and activity of the hedgehog signal. *Science* **293**, 2080-2084, doi:10.1126/science.1064437 (2001).

49 Chen, M. H., Li, Y. J., Kawakami, T., Xu, S. M. & Chuang, P. T. Palmitoylation is required for the production of a soluble multimeric Hedgehog protein complex and long-range signaling in vertebrates. *Genes & development* **18**, 641-659, doi:10.1101/gad.1185804 (2004).

50 Buglino, J. A. & Resh, M. D. Hhat is a palmitoylacyltransferase with specificity for N-palmitoylation of Sonic Hedgehog. *The Journal of biological chemistry* **283**, 22076-22088, doi:10.1074/jbc.M803901200 (2008).

51 Lewis, P. M. *et al.* Cholesterol modification of sonic hedgehog is required for long-range signaling activity and effective modulation of signaling by Ptc1. *Cell* **105**, 599-612 (2001).

52 Tukachinsky, H., Kuzmickas, R. P., Jao, C. Y., Liu, J. & Salic, A. Dispatched and scube mediate the efficient secretion of the cholesterol-modified hedgehog ligand. *Cell reports* **2**, 308-320, doi:10.1016/j.celrep.2012.07.010 (2012).

53 Creanga, A. *et al.* Scube/You activity mediates release of dually lipid-modified Hedgehog signal in soluble form. *Genes & development* **26**, 1312-1325, doi:10.1101/gad.191866.112 (2012).

54 Zeng, X. *et al.* A freely diffusible form of Sonic hedgehog mediates long-range signalling. *Nature* **411**, 716-720, doi:10.1038/35079648 (2001).

55 Ho, K. S. & Scott, M. P. Sonic hedgehog in the nervous system: functions, modifications and mechanisms. *Current opinion in neurobiology* **12**, 57-63 (2002).

56 Panakova, D., Sprong, H., Marois, E., Thiele, C. & Eaton, S. Lipoprotein particles are required for Hedgehog and Wingless signalling. *Nature* **435**, 58-65, doi:10.1038/nature03504 (2005).

57 Vyas, N. *et al.* Vertebrate Hedgehog is secreted on two types of extracellular vesicles with different signaling properties. *Scientific reports* **4**, 7357, doi:10.1038/srep07357 (2014).

58 Gradilla, A. C. *et al.* Exosomes as Hedgehog carriers in cytoneme-mediated transport and secretion. *Nature communications* **5**, 5649, doi:10.1038/ncomms6649 (2014).

59 Izzi, L. *et al.* Boc and Gas1 each form distinct Shh receptor complexes with Ptch1 and are required for Shh-mediated cell proliferation. *Developmental cell* **20**, 788-801, doi:10.1016/j.devcel.2011.04.017 (2011).

60 Allen, B. L. *et al.* Overlapping roles and collective requirement for the coreceptors GAS1, CDO, and BOC in SHH pathway function. *Developmental cell* **20**, 775-787, doi:10.1016/j.devcel.2011.04.018 (2011).

61 Pazour, G. J. & Witman, G. B. The vertebrate primary cilium is a sensory organelle. *Current opinion in cell biology* **15**, 105-110 (2003).

62 Keady, B. T. *et al.* IFT25 links the signal-dependent movement of Hedgehog components to intraflagellar transport. *Developmental cell* **22**, 940-951, doi:10.1016/j.devcel.2012.04.009 (2012).

63 Taipale, J., Cooper, M. K., Maiti, T. & Beachy, P. A. Patched acts catalytically to suppress the activity of Smoothened. *Nature* **418**, 892-897, doi:10.1038/nature00989 (2002).

64 Denef, N., Neubuser, D., Perez, L. & Cohen, S. M. Hedgehog induces opposite changes in turnover and subcellular localization of patched and smoothened. *Cell* **102**, 521-531 (2000).

65 Rohatgi, R. & Scott, M. P. Patching the gaps in Hedgehog signalling. *Nature cell biology* **9**, 1005-1009, doi:10.1038/ncb435 (2007).

66 Nachtergaele, S. *et al.* Oxysterols are allosteric activators of the oncoprotein Smoothened. *Nature chemical biology* **8**, 211-220, doi:10.1038/nchembio.765 (2012).

67 Humke, E. W., Dorn, K. V., Milenkovic, L., Scott, M. P. & Rohatgi, R. The output of Hedgehog signaling is controlled by the dynamic association between Suppressor of

Fused and the Gli proteins. *Genes & development* **24**, 670-682, doi:10.1101/gad.1902910 (2010).

68 Ruiz i Altaba, A. Combinatorial Gli gene function in floor plate and neuronal inductions by Sonic hedgehog. *Development* **125**, 2203-2212 (1998).

69 Hui, C. C. & Angers, S. Gli proteins in development and disease. *Annu Rev Cell Dev Biol* **27**, 513-537, doi:10.1146/annurev-cellbio-092910-154048 (2011).

70 Chen, Y. *et al.* Sonic Hedgehog dependent phosphorylation by CK1alpha and GRK2 is required for ciliary accumulation and activation of smoothened. *PLoS Biol* **9**, e1001083, doi:10.1371/journal.pbio.1001083 (2011).

71 Kovacs, J. J. *et al.* Beta-arrestin-mediated localization of smoothened to the primary cilium. *Science* **320**, 1777-1781, doi:10.1126/science.1157983 (2008).

72 Tukachinsky, H., Lopez, L. V. & Salic, A. A mechanism for vertebrate Hedgehog signaling: recruitment to cilia and dissociation of SuFu-Gli protein complexes. *The Journal of cell biology* **191**, 415-428, doi:10.1083/jcb.201004108 (2010).

73 Rogers, K. W. & Schier, A. F. Morphogen gradients: from generation to interpretation. *Annu Rev Cell Dev Biol* **27**, 377-407, doi:10.1146/annurev-cellbio-092910-154148 (2011).

74 Vue, T. Y. *et al.* Sonic hedgehog signaling controls thalamic progenitor identity and nuclei specification in mice. *J Neurosci* **29**, 4484-4497, doi:10.1523/JNEUROSCI.0656-09.2009 (2009).

75 Chang, D. T. *et al.* Products, genetic linkage and limb patterning activity of a murine hedgehog gene. *Development* **120**, 3339-3353 (1994).

76 Placzek, M. & Briscoe, J. The floor plate: multiple cells, multiple signals. *Nature reviews. Neuroscience* **6**, 230-240, doi:10.1038/nrn1628 (2005).

77 Chamberlain, C. E., Jeong, J., Guo, C., Allen, B. L. & McMahon, A. P. Notochord-derived Shh concentrates in close association with the apically positioned basal body in

neural target cells and forms a dynamic gradient during neural patterning. *Development* **135**, 1097-1106, doi:10.1242/dev.013086 (2008).

78 Briscoe, J., Pierani, A., Jessell, T. M. & Ericson, J. A homeodomain protein code specifies progenitor cell identity and neuronal fate in the ventral neural tube. *Cell* **101**, 435-445 (2000).

79 Ribes, V. *et al.* Distinct Sonic Hedgehog signaling dynamics specify floor plate and ventral neuronal progenitors in the vertebrate neural tube. *Genes & development* **24**, 1186-1200, doi:10.1101/gad.559910 (2010).

80 Dessaud, E., McMahon, A. P. & Briscoe, J. Pattern formation in the vertebrate neural tube: a sonic hedgehog morphogen-regulated transcriptional network. *Development* **135**, 2489-2503, doi:10.1242/dev.009324 (2008).

81 Jeong, J. & McMahon, A. P. Growth and pattern of the mammalian neural tube are governed by partially overlapping feedback activities of the hedgehog antagonists patched 1 and Hhip1. *Development* **132**, 143-154, doi:10.1242/dev.01566 (2005).

82 Holtz, A. M. *et al.* Essential role for ligand-dependent feedback antagonism of vertebrate hedgehog signaling by PTCH1, PTCH2 and HHIP1 during neural patterning. *Development* **140**, 3423-3434, doi:10.1242/dev.095083 (2013).

83 Balaskas, N. *et al.* Gene regulatory logic for reading the Sonic Hedgehog signaling gradient in the vertebrate neural tube. *Cell* **148**, 273-284, doi:10.1016/j.cell.2011.10.047 (2012).

84 Kerszberg, M. & Wolpert, L. Specifying positional information in the embryo: looking beyond morphogens. *Cell* **130**, 205-209, doi:10.1016/j.cell.2007.06.038 (2007).

85 Dessaud, E. *et al.* Interpretation of the sonic hedgehog morphogen gradient by a temporal adaptation mechanism. *Nature* **450**, 717-720, doi:10.1038/nature06347 (2007).

86 Dessaud, E. *et al.* Dynamic assignment and maintenance of positional identity in the ventral neural tube by the morphogen sonic hedgehog. *PLoS Biol* **8**, e1000382, doi:10.1371/journal.pbio.1000382 (2010).

87 Huang, P., Xiong, F., Megason, S. G. & Schier, A. F. Attenuation of Notch and Hedgehog signaling is required for fate specification in the spinal cord. *PLoS genetics* **8**, e1002762, doi:10.1371/journal.pgen.1002762 (2012).

88 Hallahan, A. R. *et al.* The SmoA1 mouse model reveals that notch signaling is critical for the growth and survival of sonic hedgehog-induced medulloblastomas. *Cancer research* **64**, 7794-7800, doi:10.1158/0008-5472.CAN-04-1813 (2004).

89 Casso, D. J., Biehs, B. & Kornberg, T. B. A novel interaction between hedgehog and Notch promotes proliferation at the anterior-posterior organizer of the Drosophila wing. *Genetics* **187**, 485-499, doi:10.1534/genetics.110.125138 (2011).

90 Lopez, S. L. *et al.* Notch activates sonic hedgehog and both are involved in the specification of dorsal midline cell-fates in Xenopus. *Development* **130**, 2225-2238 (2003).

91 Li, Y., Hibbs, M. A., Gard, A. L., Shylo, N. A. & Yun, K. Genome-wide analysis of N1ICD/RBPJ targets in vivo reveals direct transcriptional regulation of Wnt, SHH, and hippo pathway effectors by Notch1. *Stem cells* **30**, 741-752, doi:10.1002/stem.1030 (2012).

92 Hamidi, H., Gustafason, D., Pellegrini, M. & Gasson, J. Identification of novel targets of CSL-dependent Notch signaling in hematopoiesis. *PloS one* **6**, e20022, doi:10.1371/journal.pone.0020022 (2011).

93 Dexter, J. S. The analysis of a case of continuous variation in Drosophila by a study of its linkage relations. *The American Naturalist* **48**, 712-758 (1914).

94 Morgan, T. H., Bridges, C.B. Sex-linked inheritance in Drosophila. *Carnegie Institution of Washington* **237**, 1-86 (1916).

95 Mohr, O. L. Character Changes Caused by Mutation of an Entire Region of a Chromosome in Drosophila. *Genetics* **4**, 275-282 (1919).

96 Poulson, D. F. The effects of certain X-chromosome deficiencies on the embryonic development of Drosophila Melanogaster. *Journal of Experimental Zoology* **83**, 271-325 (1940).

97 Fortini, M. E. Notch signaling: the core pathway and its posttranslational regulation. *Developmental cell* **16**, 633-647, doi:10.1016/j.devcel.2009.03.010 (2009).

98 Louvi, A. & Artavanis-Tsakonas, S. Notch signalling in vertebrate neural development. *Nature reviews. Neuroscience* **7**, 93-102, doi:10.1038/nrn1847 (2006).

99 Andersson, E. R., Sandberg, R. & Lendahl, U. Notch signaling: simplicity in design, versatility in function. *Development* **138**, 3593-3612, doi:10.1242/dev.063610 (2011).

100 Kopan, R. & Ilagan, M. X. The canonical Notch signaling pathway: unfolding the activation mechanism. *Cell* **137**, 216-233, doi:10.1016/j.cell.2009.03.045 (2009).

101 Wu, L. *et al.* MAML1, a human homologue of Drosophila mastermind, is a transcriptional co-activator for NOTCH receptors. *Nature genetics* **26**, 484-489, doi:10.1038/82644 (2000).

102 Ranganathan, P., Weaver, K. L. & Capobianco, A. J. Notch signalling in solid tumours: a little bit of everything but not all the time. *Nature reviews. Cancer* **11**, 338-351, doi:10.1038/nrc3035 (2011).

103 Kageyama, R., Ohtsuka, T. & Kobayashi, T. The Hes gene family: repressors and oscillators that orchestrate embryogenesis. *Development* **134**, 1243-1251, doi:10.1242/dev.000786 (2007).

104 Castel, D. *et al.* Dynamic binding of RBPJ is determined by Notch signaling status. *Genes & development* **27**, 1059-1071, doi:10.1101/gad.211912.112 (2013).

105 Bray, S. Notch signalling in Drosophila: three ways to use a pathway. *Seminars in cell & developmental biology* **9**, 591-597, doi:10.1006/scdb.1998.0262 (1998).

106 Haines, N. & Irvine, K. D. Glycosylation regulates Notch signalling. *Nature reviews. Molecular cell biology* **4**, 786-797, doi:10.1038/nrm1228 (2003).

107 Bray, S. J. Notch signalling: a simple pathway becomes complex. *Nature reviews. Molecular cell biology* **7**, 678-689, doi:10.1038/nrm2009 (2006).

108 Castro, D. S. *et al.* Proneural bHLH and Brn proteins coregulate a neurogenic program through cooperative binding to a conserved DNA motif. *Developmental cell* **11**, 831-844, doi:10.1016/j.devcel.2006.10.006 (2006).

109 Kageyama, R., Ohtsuka, T., Shimojo, H. & Imayoshi, I. Dynamic Notch signaling in neural progenitor cells and a revised view of lateral inhibition. *Nature neuroscience* **11**, 1247-1251 (2008).

110 Lewis, J. Neurogenic genes and vertebrate neurogenesis. *Current opinion in neurobiology* **6**, 3-10 (1996).

111 Henrique, D. *et al.* Maintenance of neuroepithelial progenitor cells by Delta-Notch signalling in the embryonic chick retina. *Current biology : CB* **7**, 661-670 (1997).

112 Gaiano, N. & Fishell, G. The role of notch in promoting glial and neural stem cell fates. *Annual review of neuroscience* **25**, 471-490, doi:10.1146/annurev.neuro.25.030702.130823 (2002).

113 Ge, W. *et al.* Notch signaling promotes astrogliogenesis via direct CSL-mediated glial gene activation. *Journal of neuroscience research* **69**, 848-860, doi:10.1002/jnr.10364 (2002).

114 Tanigaki, K. *et al.* Notch1 and Notch3 instructively restrict bFGF-responsive multipotent neural progenitor cells to an astroglial fate. *Neuron* **29**, 45-55 (2001).

115 Scheer, N., Groth, A., Hans, S. & Campos-Ortega, J. A. An instructive function for Notch in promoting gliogenesis in the zebrafish retina. *Development* **128**, 1099-1107 (2001).

116 Bernardos, R. L., Lentz, S. I., Wolfe, M. S. & Raymond, P. A. Notch-Delta signaling is required for spatial patterning and Muller glia differentiation in the zebrafish retina. *Developmental biology* **278**, 381-395, doi:10.1016/j.ydbio.2004.11.018 (2005).

117 Gaiano, N., Nye, J. S. & Fishell, G. Radial glial identity is promoted by Notch1 signaling in the murine forebrain. *Neuron* **26**, 395-404 (2000).

118 Anthony, T. E., Mason, H. A., Gridley, T., Fishell, G. & Heintz, N. Brain lipid-binding protein is a direct target of Notch signaling in radial glial cells. *Genes & development* **19**, 1028-1033, doi:10.1101/gad.1302105 (2005).

119 Morrison, S. J. *et al.* Transient Notch activation initiates an irreversible switch from neurogenesis to gliogenesis by neural crest stem cells. *Cell* **101**, 499-510 (2000).

120 Woodhoo, A. *et al.* Notch controls embryonic Schwann cell differentiation, postnatal myelination and adult plasticity. *Nature neuroscience* **12**, 839-847, doi:10.1038/nn.2323 (2009).

121 Wang, S. *et al.* Notch receptor activation inhibits oligodendrocyte differentiation. *Neuron* **21**, 63-75 (1998).

122 Park, H. C. & Appel, B. Delta-Notch signaling regulates oligodendrocyte specification. *Development* **130**, 3747-3755 (2003).

123 Lindsell, C. E., Boulter, J., diSibio, G., Gossler, A. & Weinmaster, G. Expression patterns of Jagged, Delta1, Notch1, Notch2, and Notch3 genes identify ligand-receptor pairs that may function in neural development. *Mol Cell Neurosci* **8**, 14-27, doi:10.1006/mcne.1996.0040 (1996).

124 Mitsiadis, T. A., Gayet, O., Zhang, N. & Carroll, P. Expression of Deltex1 during mouse embryogenesis: comparison with Notch1, 2 and 3 expression. *Mechanisms of development* **109**, 399-403 (2001).

125 Marklund, U. *et al.* Domain-specific control of neurogenesis achieved through patterned regulation of Notch ligand expression. *Development* **137**, 437-445, doi:10.1242/dev.036806 (2010).

126 Skaggs, K., Martin, D. M. & Novitch, B. G. Regulation of spinal interneuron development by the Olig-related protein Bhlhb5 and Notch signaling. *Development* **138**, 3199-3211, doi:10.1242/dev.057281 (2011).

127 Rabadan, M. A. *et al.* Jagged2 controls the generation of motor neuron and oligodendrocyte progenitors in the ventral spinal cord. *Cell death and differentiation* **19**, 209-219, doi:10.1038/cdd.2011.84 (2012).

128 Dave, R. K. *et al.* Sonic hedgehog and notch signaling can cooperate to regulate neurogenic divisions of neocortical progenitors. *PloS one* **6**, e14680, doi:10.1371/journal.pone.0014680 (2011).

129 Yang, X. *et al.* Notch1 signaling influences v2 interneuron and motor neuron development in the spinal cord. *Developmental neuroscience* **28**, 102-117, doi:10.1159/000090757 (2006).

130 Schreck, K. C. *et al.* The Notch target Hes1 directly modulates Gli1 expression and Hedgehog signaling: a potential mechanism of therapeutic resistance. *Clinical cancer research : an official journal of the American Association for Cancer Research* **16**, 6060-6070, doi:10.1158/1078-0432.CCR-10-1624 (2010).

131 Katoh, Y. & Katoh, M. Integrative genomic analyses on GLI1: positive regulation of GLI1 by Hedgehog-GLI, TGFbeta-Smads, and RTK-PI3K-AKT signals, and negative regulation of GLI1 by Notch-CSL-HES/HEY, and GPCR-Gs-PKA signals. *International journal of oncology* **35**, 187-192 (2009).

132 Colas, J. F. & Schoenwolf, G. C. Towards a cellular and molecular understanding of neurulation. *Developmental dynamics : an official publication of the American Association of Anatomists* **221**, 117-145, doi:10.1002/dvdy.1144 (2001).

133 Bachiller, D. *et al.* The organizer factors Chordin and Noggin are required for mouse forebrain development. *Nature* **403**, 658-661, doi:10.1038/35001072 (2000).

134 Lowery, L. A. & Sive, H. Strategies of vertebrate neurulation and a re-evaluation of teleost neural tube formation. *Mechanisms of development* **121**, 1189-1197, doi:10.1016/j.mod.2004.04.022 (2004).

135 Suter, D. M., Tirefort, D., Julien, S. & Krause, K. H. A Sox1 to Pax6 switch drives neuroectoderm to radial glia progression during differentiation of mouse embryonic stem cells. *Stem cells* **27**, 49-58, doi:10.1634/stemcells.2008-0319 (2009).

136 Schoenwolf, G. C. & Smith, J. L. Mechanisms of neurulation: traditional viewpoint and recent advances. *Development* **109**, 243-270 (1990).

137 Halbleib, J. M. & Nelson, W. J. Cadherins in development: cell adhesion, sorting, and tissue morphogenesis. *Genes & development* **20**, 3199-3214, doi:10.1101/gad.1486806 (2006).

138 Detrick, R. J., Dickey, D. & Kintner, C. R. The effects of N-cadherin misexpression on morphogenesis in Xenopus embryos. *Neuron* **4**, 493-506 (1990).

139 Fujimori, T., Miyatani, S. & Takeichi, M. Ectopic expression of N-cadherin perturbs histogenesis in Xenopus embryos. *Development* **110**, 97-104 (1990).

140 Dady, A., Blavet, C. & Duband, J. L. Timing and kinetics of E- to N-cadherin switch during neurulation in the avian embryo. *Developmental dynamics : an official publication of the American Association of Anatomists* **241**, 1333-1349, doi:10.1002/dvdy.23813 (2012).

141 Chenn, A., Zhang, Y. A., Chang, B. T. & McConnell, S. K. Intrinsic polarity of mammalian neuroepithelial cells. *Mol Cell Neurosci* **11**, 183-193, doi:10.1006/mcne.1998.0680 (1998).

142 Imai, F. *et al.* Inactivation of aPKClambda results in the loss of adherens junctions in neuroepithelial cells without affecting neurogenesis in mouse neocortex. *Development* **133**, 1735-1744, doi:10.1242/dev.02330 (2006).

143 Kadowaki, M. *et al.* N-cadherin mediates cortical organization in the mouse brain. *Developmental biology* **304**, 22-33, doi:10.1016/j.ydbio.2006.12.014 (2007).

144 Willardsen, M. I. & Link, B. A. Cell biological regulation of division fate in vertebrate neuroepithelial cells. *Developmental dynamics : an official publication of the American Association of Anatomists* **240**, 1865-1879, doi:10.1002/dvdy.22684 (2011).

145 Baye, L. M. & Link, B. A. Interkinetic nuclear migration and the selection of neurogenic cell divisions during vertebrate retinogenesis. *J Neurosci* **27**, 10143-10152, doi:10.1523/JNEUROSCI.2754-07.2007 (2007).

146 Chenn, A. & McConnell, S. K. Cleavage orientation and the asymmetric inheritance of Notch1 immunoreactivity in mammalian neurogenesis. *Cell* **82**, 631-641 (1995).

147 Martin, A. H. Significance of mitotic spindle fibre orientation in the neural tube. *Nature* **216**, 1133-1134 (1967).

148 Gotz, M. & Huttner, W. B. The cell biology of neurogenesis. *Nature reviews. Molecular cell biology* **6**, 777-788, doi:10.1038/nrm1739 (2005).

149 Zhong, W., Feder, J. N., Jiang, M. M., Jan, L. Y. & Jan, Y. N. Asymmetric localization of a mammalian numb homolog during mouse cortical neurogenesis. *Neuron* **17**, 43-53 (1996).

150 Cayouette, M., Whitmore, A. V., Jeffery, G. & Raff, M. Asymmetric segregation of Numb in retinal development and the influence of the pigmented epithelium. *J Neurosci* **21**, 5643-5651 (2001).

151 Bultje, R. S. *et al.* Mammalian Par3 regulates progenitor cell asymmetric division via notch signaling in the developing neocortex. *Neuron* **63**, 189-202, doi:10.1016/j.neuron.2009.07.004 (2009).

152 Bao, S. Notch controls cell adhesion in the Drosophila eye. *PLoS genetics* **10**, e1004087, doi:10.1371/journal.pgen.1004087 (2014).

153 Main, H., Radenkovic, J., Jin, S. B., Lendahl, U. & Andersson, E. R. Notch signaling maintains neural rosette polarity. *PloS one* **8**, e62959, doi:10.1371/journal.pone.0062959 (2013).

154 Wang, W. *et al.* Notch signaling regulates neuroepithelial stem cell maintenance and neuroblast formation in Drosophila optic lobe development. *Developmental biology* **350**, 414-428, doi:10.1016/j.ydbio.2010.12.002 (2011).

155 Hatakeyama, J. *et al.* Hes genes regulate size, shape and histogenesis of the nervous system by control of the timing of neural stem cell differentiation. *Development* **131**, 5539-5550 (2004).

156 Dickman, E. D., Thaller, C. & Smith, S. M. Temporally-regulated retinoic acid depletion produces specific neural crest, ocular and nervous system defects. *Development* **124**, 3111-3121 (1997).

157 Maden, M. Retinoid signalling in the development of the central nervous system. *Nature reviews. Neuroscience* **3**, 843-853, doi:10.1038/nrn963 (2002).

158 Kam, R. K., Deng, Y., Chen, Y. & Zhao, H. Retinoic acid synthesis and functions in early embryonic development. *Cell & bioscience* **2**, 11, doi:10.1186/2045-3701-2-11 (2012).

159 Delacroix, L. *et al.* Cell-specific interaction of retinoic acid receptors with target genes in mouse embryonic fibroblasts and embryonic stem cells. *Molecular and cellular biology* **30**, 231-244, doi:10.1128/MCB.00756-09 (2010).

160 Durston, A. J. *et al.* Retinoic acid causes an anteroposterior transformation in the developing central nervous system. *Nature* **340**, 140-144, doi:10.1038/340140a0 (1989).

161 Conlon, R. A. & Rossant, J. Exogenous retinoic acid rapidly induces anterior ectopic expression of murine Hox-2 genes in vivo. *Development* **116**, 357-368 (1992).

162 Koop, D. *et al.* Retinoic acid signaling targets Hox genes during the amphioxus gastrula stage: insights into early anterior-posterior patterning of the chordate body plan. *Developmental biology* **338**, 98-106, doi:10.1016/j.ydbio.2009.11.016 (2010).

163 Huang, D., Chen, S. W. & Gudas, L. J. Analysis of two distinct retinoic acid response elements in the homeobox gene Hoxb1 in transgenic mice. *Developmental dynamics : an official publication of the American Association of Anatomists* **223**, 353-370, doi:10.1002/dvdy.10057 (2002).

164 Okada, Y., Shimazaki, T., Sobue, G. & Okano, H. Retinoic-acid-concentration-dependent acquisition of neural cell identity during in vitro differentiation of mouse embryonic stem cells. *Developmental biology* **275**, 124-142, doi:10.1016/j.ydbio.2004.07.038 (2004).

165 Wilson, L., Gale, E., Chambers, D. & Maden, M. Retinoic acid and the control of dorsoventral patterning in the avian spinal cord. *Developmental biology* **269**, 433-446, doi:10.1016/j.ydbio.2004.01.034 (2004).

166 Sharpe, C. R. & Goldstone, K. Retinoid receptors promote primary neurogenesis in Xenopus. *Development* **124**, 515-523 (1997).

167 Hernandez, R. E., Putzke, A. P., Myers, J. P., Margaretha, L. & Moens, C. B. Cyp26 enzymes generate the retinoic acid response pattern necessary for hindbrain development. *Development* **134**, 177-187, doi:10.1242/dev.02706 (2007).

168 Abu-Abed, S. *et al.* The retinoic acid-metabolizing enzyme, CYP26A1, is essential for normal hindbrain patterning, vertebral identity, and development of posterior structures. *Genes & development* **15**, 226-240 (2001).

169 Swindell, E. C. *et al.* Complementary domains of retinoic acid production and degradation in the early chick embryo. *Developmental biology* **216**, 282-296, doi:10.1006/dbio.1999.9487 (1999).

CHAPTER 2 – Notch Activity Modulates the Responsiveness of Neural Progenitors to Sonic Hedgehog Signaling

ABSTRACT

Throughout the developing nervous system, neural stem and progenitor cells give rise to diverse classes of neurons and glia in a spatially and temporally coordinated manner. In the ventral spinal cord, much of this diversity emerges through the morphogen actions of Sonic hedgehog (Shh). Interpretation of the Shh gradient depends on both the amount of ligand and duration of exposure, but the mechanisms permitting prolonged responses to Shh are not well understood. We demonstrate that Notch signaling plays an essential role in this process, enabling neural progenitors to attain sufficiently high levels of Shh pathway activity needed to direct the ventral-most cell fates. Notch activity regulates subcellular localization of the Shh receptor Patched1, gating the translocation of the key effector Smoothened to primary cilia and its downstream signaling activities. These data reveal an unexpected role for Notch shaping the interpretation of the Shh morphogen gradient and influencing cell fate determination.

This chapter is modified from:

Kong JH*, Yang L*, Dessaud E, Chuang K, Moore DM, Rohatgi R, Briscoe J, and Novitch BG. (2015). Notch activity modulates the responsiveness of neural progenitors to Sonic Hedgehog signaling. *Developmental Cell 33(4): 1-15. In press.* *Indicated co-first authors.

JHK. LY, JB, and BGN designed the experiments and wrote the manuscript. JHK, LY, and KC performed a majority of the experiments. ED prepared and analyzed all chick spinal cord explant experiments. DMM generated the human neural progenitors. RR contributed vital reagents and cell lines.

INTRODUCTION

Neuronal and glial diversity in the central nervous system emerges in large part through the concomitant and combinatorial actions of morphogen signals such as Sonic hedgehog (Shh), Bone Morphogenetic Proteins (BMPs), Wnts, and retinoids that organize neural progenitor cells (NPCs) into discrete domains along the dorsoventral and rostrocaudal axes[1-3]. Each of these domains is defined by their expression of unique combinations of transcription factors and ability to generate specific classes of neurons and glia[1-4]. The prevailing model for morphogen signaling posits that differential cellular responses arise due to the signal concentrations that cells encounter[5]; yet, the duration of exposure to a fixed amount of signal can also elicit graded domain responses and influence fate decisions[6]. These results suggest that an important aspect of morphogen interpretation is the ability of cells to maintain their responsiveness to these cues as development proceeds. However, the mechanisms that permit this competence over time are not well understood.

One of the best-studied examples of morphogen signaling is the patterning response of NPCs in the ventral spinal cord to Shh. Shh acts on NPCs in a dose-dependent manner, binding to its primary receptors Patched1 and 2 (Ptch1/2) to initiate a cascade of intracellular signaling events centered on the translocation of the G protein-coupled receptor Smoothened (Smo) to primary cilia[7-9]. The presence of Smo in cilia modulates the proteolysis and activity of the Gli family of Zn-finger transcription factors, which in turn regulate the expression of many NPC fate determinants that subdivide the ventral spinal cord into three distinct ventral NPC domains: p3, pMN, and p2[2,8,9]. These domains are distinguished by their shared expression of the transcription factor Nkx6.1 and differential expression of Nkx2.2, Olig2, and Irx3, respectively[2,8,10,11]. The pMN gives rise to motor neurons (MNs) while the p3 and p2 domains produce distinct classes of spinal interneurons that modulate MN activities. Later in development, Olig2^{+} NPCs form a domain of oligodendrocyte precursors (pOL) that disperse and migrate throughout the spinal cord before differentiating into myelinating oligodendrocytes[4].

The p3 and p2 domains similarly transform into astroglial progenitor groups (pVA3 and pVA2) producing astrocytes that colonize distinct regions of the ventral spinal cord[12,13].

While these fates can be specified through the administration of different concentrations of Shh ligand in vitro[8,9], NPCs also acquire their ventral identities through time-dependent mechanisms. NPCs treated with moderate doses of Shh initially express the pMN determinant Olig2; however, if Shh/Gli signaling is sustained, they subsequently express Nkx2.2 and adopt the more ventral p3 fate[14-16]. Recent studies in the zebrafish spinal cord have further demonstrated that progenitor maintenance mediated by the Notch signaling pathway plays an important role enabling later born Shh-induced cell types to emerge[17]. Together, these findings indicate that cells must remain in an undifferentiated state to properly interpret the Shh morphogen gradient, but do not resolve the mechanism by which the maintenance of NPC characteristics influences Shh responsiveness, and whether retaining cells in a progenitor state influences spatial patterning.

The Notch signaling pathway serves as a major regulator of NPC maintenance and both neuronal and glial development[18,19]. Notch receptors are broadly expressed by NPCs and activated by the Delta-like and Jagged families of transmembrane ligands presented by neighboring cells[19,20]. Activated Notch receptors are cleaved by the Presenilin γ-secretase complex, liberating Notch intracellular domain (NICD) fragments. NICD subsequently forms transcriptional activating complexes with the DNA binding protein Rbpj and members of the mastermind-like (MAML) coactivator family[19,20]. Rbpj-NICD-MAML complexes regulate a number of targets most notably Hes genes, bHLH transcription factors that repress proneural genes, inhibit neuronal differentiation, and promote NPC maintenance[19-21]. Through these actions, Notch signaling suppresses neuronal differentiation and endows cells with gliogenic potential. NICD misexpression can further promote specific glial cell fates, such as radial glia in the forebrain, Müller glia in the retina, and astrocytes in neural stem cell cultures[22-25] while inhibiting oligodendrocyte differentiation[26]. These data implicate a role for Notch in glial fate

selection, though the mechanisms underlying these effects remain unclear.

Here, we test the contributions of Notch signaling on both the establishment of NPC identities and glial fate determination. We show that activation and inactivation of the Notch pathway modify the responses of NPCs to Shh, altering both their dorsoventral register and ability to generate distinct classes of neurons and glial cells. Notch activity strikingly acts at the most proximal steps in the Shh transduction pathway, affecting the trafficking of Smo and Ptch1 to primary cilia. Together, these findings reveal a novel role for Notch signaling shaping the interpretation of the Shh morphogen gradient and assignment of cell fates.

MATERIALS AND METHODS

Animal preparation and tissue analysis: *Olig2*^{Cre} and *Dbx1*^{Cre} mice were generated as previously described[15,27]. Cre mice were crossed with *R26R*^{GFP} transgenic reporter mice (B6;129-*Gt(ROSA)26Sor*^{tm2Sho}/J; Jackson Labs Stock #004077)[28]; *R26R*$^{NICD\text{-}nGFP}$ transgenic floxed mice (*Gt(ROSA)26Sor*$^{tm1(Notch1)Dam}$/J; Jackson Labs Stock #008159)[29], or *Rbpj*^{CKO} mice[30]. *Olig2*$^{-/-}$, *Nkx2.2*$^{-/-}$ and *Pax6*$^{Sey/Sey}$ mutant mice were generated as previously described[11,31]. All mice were maintained and tissue collected in accordance with guidelines set forth by the UCLA Institutional Animal Care and Use Committee. Chick neural plate explants were generated as previously described[15]. All spinal cord tissues were fixed, cryoprotected, sectioned, and processed for immunohistochemistry or in situ hybridization as previously described[11,32].

Cell Culture and primary cilia analysis: NIH-3T3 fibroblasts (CRL-1658) and C2C12 myoblasts (CRL-1772) were purchased from ATCC. Shh-LIGHT2 cells were used as previously described[33]. *Ptch1*$^{-/-}$ and *Ptch1*$^{-/-}$; Ptch1-YFP MEFs were generated as previously described[34,35]. Primitive human neuroepithelial progenitors were generated from embryonic stem cells as previously described[36]. For cilia analysis in fibroblasts, cells were plated onto glass coverslips, grown to 80-100% confluency in DMEM containing 10% bovine calf serum (BCS) and then changed to low serum media (0.5% BCS) at the beginning of experiments. Cells were fixed in 4% paraformaldehyde, incubated with indicated primary and secondary antibodies, and

mounted in Prolong Gold (Invitrogen).

Statistical Analyses: Unless otherwise stated, cell counts, luciferase assays, and qPCR analyses are presented as mean values ± SEM. For Figures 1Q, 2M-2N, 3M-3N, 5I, 6K-L, 7S, S3J-S3K, S4G, S4AF-S4AI, S7Q, S7R, and S8I experimental conditions were compared to the control and a one-way analysis of variance (ANOVA) with a Dunnett's post-hoc test was performed. For the data shown in Figures 4G-4H, 5C, 5L, 5N, S5D, S5I, S5J-S5K, and S8H-S8J unpaired, two-tailed t-test were performed. All ciliary Smo fluorescence data sets did not pass the Shapiro-Wilk normality test. Thus, for all ciliary Smo analyses between two groups (Figures 5M, 7E, 7J, S8B, S8D, S8F) two-tailed nonparametric Mann-Whitney tests were performed. For analyses between three or more groups (Figures 5J-5K, 7O, S5A, S6D, S6H, S6L) nonparametric Kruskal-Wallis tests were used along with Dunnett's post-hoc tests. All statistical analyses were calculated using Graphpad Prism 6 software. Significance was assumed when $p < 0.05$.

In ovo electroporation and tissue preparation: Fertilized chicken eggs were purchased from McIntyre Poultry and Fertile Eggs (Lakeside, CA) and maintained in a cabinet incubator at 38ºC with 60% humidity. All embryos were electroporated at e2 (HH stages 12-14) and collected 48 hours later at e4 (HH stages 20-22), as previously described[11,37]. Embryos were fixed in 4% PFA for 1 hour, rinsed in PBS, cryoprotected in 30% sucrose overnight, cryosectioned into 12 µm thick sections, and then processed for immunohistochemistry or in situ hybridization as previously described[11,38]. List of constructs used in our electroporations: pCIG (pCAGGS-ires-GFP), pCIG-NICD, Shh (rat Shh cDNA driven by a CMV promoter)[39], SmoM2 (a constitutively activated form of Smo that is resistant to Ptc inhibition via a mutation of Trp535 to a Leu, driven by the En-2 promoter/enhancer)[40,41], and GliA (pCAGGS-Gli3A, a dominant active form of human Gli3 generated through the deletion of the Gli3 repressor domain, driven by a CMV enhancer/chicken α-actin promoter)[42]. Plotted data represents the mean ± SEM from at least 8 well electroporated spinal cords for each condition.

Antibodies and in situ hybridization probes: Primary antibodies used for immunohistochemistry were as follows: mouse anti-Arl13b (NeuroMab 75-287), 1:100; mouse anti-Ascl1[43], 1:200; rabbit anti-BLBP (Chemicon/Millipore AB9558), 1:2,000; rabbit anti-β-Catenin (Sigma C2206), 1:1,000; guinea pig anti-Chx10 (Vsx2)[44], 1:5,000; mouse anti-Cre (Covance MMS-106P), 1:2,000; rabbit anti-Dbx1[45], 1:1,000; rabbit anti-Dbx2 (Abcam ab25554), 1:4,000; mouse anti-Foxa2 (Developmental Studies Hybridoma Bank 4C7), 1:200; rabbit anti-Foxa2[46], 1:4,000; guinea pig anti-Foxp1[47], 1:16,000; goat anti-Gata3 (Santa Cruz Biotechnology sc-1236), 1:200; chicken anti-GFP (Aves Labs GFP-1020), 1:1,000; rabbit anti-GFP (Invitrogen A6455), 1:4000; sheep anti-GFP (AbD Serotec 4745-1051), 1:800; rabbit anti-Hb9 (Mnx1)[48], 1:8000; rabbit anti-Hes1[49], 1:2,000; rabbit anti-Irx3[37], 1:8,000; goat anti-Islet1 (R&D Systems AF1837), 1:8,000; rabbit anti-Islet1/2[50], 1:20,000; rabbit anti-Lhx3[51], 1:4,000; rat anti-N-cadherin (Developmental Studies Hybridoma Bank MNCD2), 1:50; rabbit anti-N-cadherin (Abcam ab12221), 1:1,000; mouse anti-NeuN (Millipore MAB377B), 1:2,000; goat anti-Neurog2 (Santa Cruz Biotechnology sc-19233), 1:1,000; rabbit anti-Nf1a[52], 1:3,000; mouse anti-Nkx2.2 (Developmental Studies Hybridoma Bank 74.5A5), 1:25; rabbit anti-Nkx2.2[53], 1:10,000; guinea pig anti-Nkx6.1[54], 1:4,000; mouse anti-Nkx6.1 (Developmental Studies Hybridoma Bank F55A10), 1:25; rabbit anti-nNos (Immunostar 24287), 1:10,000; rabbit anti-Cleaved-Notch1 (Cell Signaling Technology 2421), 1:500; rabbit anti-Numb (Abcam ab14140), 1:4,000; rabbit anti-Olig2 (chick)[11], 1:8,000; guinea pig anti-Olig2 (mouse)[37], 1:20,000; rabbit anti-Olig2 (mouse) (Millipore AB9610), 1:5,000; rabbit anti-Par3 (Millipore 07-330), 1:100; mouse anti-Pax6 (Developmental Studies Hybridoma Bank), 1:100; rabbit anti-Pax6, (Covance), 1:4,000; rat anti-Pdgfrα (eBiosciences 14-1401), 1:1,000; rabbit anti-aPKC (PKCζ), (Santa Cruz Biotechnology SC-216), 1:1600; rabbit anti-Ptch1[35], 1:500; rat anti-Rbpj (Active Motif 61506), 1:100; mouse anti-Shh (Developmental Studies Hybridoma Bank 5E1), 1:100; rabbit anti-Smo (Abcam ab38686), 1:3,000; rabbit anti-Smo[35], 1:500; goat anti-Sox2 (Santa Cruz Biotechnology sc-17320), 1:2,000; goat anti-Sox10 (R&D Systems AF2864), 1:300; mouse anti-αTubulin (Sigma

T6793), 1:1,000; rabbit anti-βIII-Tubulin (TUJ1) (Covance MRB-435P), 1:5,000. Alexa^{488}-, FITC-, Cy3-, Cy5-, and Dylight^{649}-conjugated secondary antibodies were obtained from Jackson Immunoresearch Laboratories, Inc. (West Grove, PA). RNA probes were generated by in vitro transcription of PCR products amplified from mouse spinal cord cDNA. Primers against the following genes were designed using the program Primer3 (http://bioinfo.ut.ee/primer3/). *Hes5*, forward 5'-GGATGAGCTCGTTCCTCTGG-3' and reverse 5'-GAGATTAACCCTCACTAAAGGGAGCAGGCTGAGTGCTTTCCTA-3' and *Neurog3*, forward 5'-AGGCTTCTCATCGGTACCCT-3' and reverse 5'-GAGATTAACCCTCACTAAAGGGCATAGGCTAGGGCTTTCCGG-3'. The underlined text denotes a T3 polymerase binding site incorporated into the reverse primer. Probes for *Fgfr3*[32], *Slit1*[12], *Gli1* and *Ptch1*[55] were used as previously described. All probes were generated using a Digoxigenin (DIG) RNA Labeling Kit (Roche) and visualized using a combination of Anti-DIG-alkaline phosphatase (AP) Fab fragments (Roche) and NBT/BCIP (Roche).

Chick neural explant culture: Neural tissue was isolated from chick embryos (HH stage 10) and cultured as previously described[15,56]. Two types of explants were prepared: intermediate spinal cord explants (i) and ventral neural plate plus floor plate explants (vf). Shh was generated as previously described[57] and the concentration of each new batch determined by comparison with previous batches. NKX2.2 and OLIG2 quantifications consist of data collected from 7-10 explants per condition. Plotted data represents the mean ± SEM.

Fluorescence activated cell sorting (FACS): *Olig2^{Cre}* mice were crossed with *R26R^{GFP}* transgenic reporter mice, *R26R$^{NICD-GFP}$* transgenic mice, and *Rbpj^{CKO}*mice. Mouse embryos were collected at E11.5, the spinal cords were dissected out, and the cells were dissociated using papain (Papain Dissociation Kit, Worthington). To separate out aggregates, the dissociated cells were resuspended into sorting buffer (Hanks Buffered Saline Solution with 1% Horse Serum) and passed through a 0.45 µm filter. To selectively sort out live cells, the cell viability stain 7-Amino Actinomycin-D (7AAD) was added to the sorted cells immediately prior to

FACS. GFP+/7AAD- cells were isolated using a Becton Dickinson Aria-II High Speed Cell Sorter and collected directly into 200-400 µl Buffer RLT for RNA extraction (RNeasy Mini Kit, Qiagen).

Quantitative PCR: qPCR was carried out as previously described[31]. Briefly, total RNA was extracted using the RNeasy Mini Kit (Qiagen). For each sample, ~500-1000 ng of total RNA was used to synthesize cDNA by reverse transcription using the SuperScript III First-Strand Synthesis System (Invitrogen). In each qPCR reaction, cDNA was combined with LightCycler 480 SYBR Green I Master Mix (Roche) and the following exon-spanning primer pairs: mouse *Gli1*, forward 5'-CACCGTGGGAGTAAACAGGCCTTCC-3' and reverse 5'-CCAGAGCGTTACACACCTGCCCTTC-3'[58]; mouse *Gli1*, forward 5'-ATCTCTCTTTCCTCCTCCTCC-3' and reverse 5'-CGAGGCTGGCATCAGAA-3'[59]; mouse *Patched1*, forward 5'-CTGCCTGTCCTCTTATCCTTC-3' and reverse 5'-AGACCCATTGTTCGTGTGAC-3'; mouse *Sox2*, forward 5'-CACATGGCCCAGCACTAC-3' and reverse 5'-CCCTCCCAATTCCCTTGTATC-3'; mouse *Gapdh*, forward 5′–GGCCTTCCGTGTTCCTAC–3′ and reverse 5′–TGTCATCATACTTGGCAGGTT–3'[59]; mouse *Hes1*, forward 5'-GGCGAAGGGCAAGAATAAATG-3' and reverse 5'-GTGCTTCACAGTCATTTCCAG-3'. The 18 to 20-mer primers were either chosen from papers as cited or designed using the IDT Primer Quest Program (http://www.idtdna.com/primerquest/Home/Index). All primer pairs were experimentally validated using E10.5 whole spinal cord cDNA. In this validation process each pair was shown to have amplification efficiency between 1.8-2.2 and possess a single gene-specific product using melting curve analysis. All samples were run using a Roche LightCycler 480 real-time PCR system in duplicates or triplicates, and relative mRNA expression levels determined by normalizing the crossing points of each gene of interest to *Gapdh*. Unless otherwise indicated relative gene expression profiles were plotted by comparison to the average value of control samples, set to 1.0.

Cell Culture:

Reagents: Shh (Akron Biotech) was reconstituted in 0.1% BSA, DAPT and Purmorphamine (Calbiochem) in DMSO, and SAG (Calbiochem) in water. To account for these different vehicles, all control samples were treated with equivalent volumes of DMSO and BSA to experimental samples. The concentrations of Shh, Pur, SAG, and DAPT used were empirically determined by exposing fibroblast cells to a range of doses and assessing Shh and Notch signaling activity using qPCR and luciferase assays. Across batches, Shh (50 nM), Pur (5 μM), and SAG (1 μM) consistently activated Shh signaling. However, there were some potency differences between batches of DAPT (5-25 μM). To account for these differences, we optimized the concentration of each lot of DAPT using qPCR measurement of *Hes1* mRNA to readout Notch signaling activity. In each experiment, the amount of DAPT used was found to reduce *Hes1* expression by at least 50%.

NIH-3T3 cells and primary MEFs: NIH-3T3 cells were cultured in high glucose (4.5 g/L glucose) Dulbecco's modified Eagle's medium (DMEM) with 110 mg/L sodium pyruvate (Gibco), 10% bovine calf serum (BCS, Gibco), 1x glutamax (Gibco), 1% Penicillin:Streptomycin (Gibco), and 0.2% Primocin (InvivoGen). Shh-LIGHT2 cells were cultured in high glucose (4.5 g/L glucose) DMEM with 110 mg/L sodium pyruvate (Gibco), 10% BCS (Gibco), 0.15 mg/ml zeocin (Invitrogen), and 0.4 mg/ml geneticin (Gibco), as previously described[33]. Wild-type, *Ptch1*$^{-/-}$*, and* *Ptch1*$^{-/-}$;Ptch1-YFP mouse embryo fibroblasts were cultured as previously described[35]. For Shh induction experiments, cells were plated onto 8 mm coverslips in 24-well plates (40,000 cells/well) in regular (10% BCS) growth media. Upon reaching 80-100% confluency, cells were moved into low serum media (0.5% BCS) supplemented with one or more of the following: Shh ligand (50 nM, Akron Biotech), Purmorphamine (5 μM, Calbiochem), SAG (1 μM, Calbiochem), DAPT (18.75 μM, Calbiochem), SAHM (20 μM, Calbiochem), and JLK6 (20 μM, Calbiochem).

C2C12 myoblasts: C2C12 cells were plated directly onto 8 mm coverslips in a 24-well plate (40,000 cells/well) in DMEM with L-glutamine (Gibco) supplemented with 10% FBS. Upon

reaching 80-100% confluency, the cells were switched to a low serum media (0.5% FBS) and treated with Shh ± DAPT for 12 hr.

Human neural progenitors: Primitive human neuroepithelial progenitors were generated from embryonic stem cells as previously described[60]. After 10 days of culture in vitro, neural rosettes were manually picked and plated onto poly-ornithine/laminin coated coverslips in DMEM/F12 (Hyclone), 1x N2 (Life Technologies), 0.1 mM NEAA (Life Technologies), 1 mg/mL heparin (Sigma), and 10% FBS (Hyclone), and allowed to attach for 24 hr. The following day, FBS was removed and the neural rosettes were exposed to Shh ± DAPT for 12 hr.

Transient transfection of NIH-3T3 cells: NIH-3T3 cells were transiently transfected with either pCIG, pCIG-NICD,pCIG-Hes1, EF.CMV.RFP (Addgene plasmid # 17619), or EF.mHes1.CMV.GFP (Addgene plasmid # 17622) constructs[61-63] using the transfection reagent FuGENE6 (Roche) at a DNA:FuGENE6 ratio of 1:3.

Luciferase assays:

In chick explants: Gli activity was measured in chick neural explants as previously described[15]. Briefly, chick embryos (HH stage 10) were co-electroporated with a Gli-binding site firefly luciferase reporter and a cytomegalovirus promoter::renilla luciferase plasmid (Promega) to normalize for transfection efficiency, returned to the incubator for 2 hr, and then collected for explant culture. Upon isolation, neural explants were exposed to Shh ± DAPT for 12 or 24 hr. Tissue was then homogenized on ice in Passive Lysis Buffer and processed using a Dual-Luciferase Reporter Assay System (Promega). Each data point represents the mean ± SEM from 7-10 explants.

In cells: All luciferase assays were conducted using Shh-LIGHT2 cells, NIH-3T3 cells that have been stably cotransfected with Gli-binding site::firefly luciferase and herpes simplex virus thymidine kinase (HSV TK) promoter::renilla luciferase plasmids[33]. Shh-LIGHT2 cells were cultured in 96-well plates (30,000 cells/well) in regular serum media (10% BCS). Upon reaching 80-100% confluency, the cells were moved into a low serum media (0.5% BCS) containing Shh

ligand (0-50 nM, Akron Biotech) ± DAPT (0-50 µM, Calbiochem). After 24 hr, cells were rinsed in PBS and then lysed in Passive Lysis Buffer (100 µl/well, Promega Dual-Luciferase Reporter Assay System). Luciferase activities were measured in a Tecan M1000 microplate reader equipped with an automatic injector. For each sample, Gli-dependent firefly luciferase activity was normalized to HSV TK::renilla luciferase activity and the resulting ratio reported in relative luciferase units (RLU). All luciferase conditions were run as duplicate or triplicate samples. Each data point represents the mean ± SEM.

Tissue image analysis: Fluorescence and DIC images were collected using either a Zeiss LSM5 Exciter or LSM780 confocal imaging system or a Zeiss AxioImager M2 fluorescence microscope equipped with Apotome attachment and motorized stage. Images were collected and processed using LSM Exciter, Zeiss AxioVision, Zeiss Efficient Navigation (ZEN), and Adobe Photoshop software. Fluorescence intensity quantifications and cell number counts were performed using the NIH developed image processing program ImageJ with an Image-based Tool for Counting Nuclei (ITCN) plugin. Composite images were assembled using CorelDRAW X7 software.

Analysis of Smo and Ptch1 presence in primary cilia: Fixed cells were imaged on an inverted Zeiss LSM 780 laser scanning confocal microscope or an upright Zeiss AxioImager M2 fluorescence microscope equipped with Apotome attachment and motorized stage. Images were taken with 20x, 40x oil, and 63x oil immersion objectives. For each experiment, coverslips from each condition were processed side by side to ensure that the cells were fixed and stained for the same duration of time. To ensure uniformity in imaging, the gain, offset, and laser power settings on the microscope were held constant for Smo and Ptch1. Quantification of relative ciliary Smo and Ptch1 fluorescence levels were performed as previously described[64,65], with minor modifications. Briefly, using the program ImageJ, an outline was first drawn around each cilium (labeled by α-acetylated tubulin or Arl13b staining), and the corresponding intensity of Smo or Ptch1 fluorescence within and adjacent to the cilium measured. From these

measurements, a ratio of the intensity was then calculated for each cilium (ratio = intensity of fluorescence within the cilium ÷ fluorescence adjacent to the cilium). When this ratio (i.e. relative ciliary Smo or Ptch1 fluorescence) is close to 1, the intensity of Smo or Ptch1 fluorescence within the cilium is not above background levels. The relative fluorescence values within a primary cilium that visually appeared to be Smo or Ptch1 positive varied widely based on cell type. In NIH-3T3 cells, the relative Smo or Ptch1 fluorescence within a positive primary cilium was at least 1.3-1.5. In human neural progenitors, the relative Smo fluorescence within a positive primary cilium was at least 3. Smo and Ptch1 were measured in approximately 100-800 primary cilia per each experimental group. These 100-800 relative ciliary fluorescence values were then represented in a box and whisker graph. In each graph, the upper and lower limits of the box represent the 25^{th} to 75^{th} percentiles, the line in the center is the median, and the whiskers encompass the 5^{th} to the 95^{th} percentiles. In each graph, the black numbers present above or below the box plots are the number of primary cilia analyzed for each group and the red numbers are the percentage of Smo or Ptch1 positive cilia. Although all statistical evaluations were done using the relative ciliary fluorescence values, Smo or Ptch1 positive cilia percentages were included on each plot to distill the data into binary “positive” or “negative” cilia values. To determine if a primary cilium was Smo or Ptch1 positive, we established a “cut-off” ciliary fluorescence value unique to each experiment, as there was frequently variance in background staining values. We then grouped all cilia above the cut-off as positive and those below as negative. In most experiments, the cut-off was determined to be the value at which there were 5% Smo^{+} or $Ptch1^{+}$ primary cilia in the negative control group (i.e. the group that possessed the fewest Smo or Ptch1-positive cilia). The negative control for Smo was the No Shh group and the negative control for Ptch1 was the Shh-only treated group. In some experiments, no true negative control group was present and in these cases the cut-off value was set to 1.5 for NIH-3T3 cells and 3.0 for human neural progenitors, based on the background staining values in surrounding regions away from the cilia.

Analysis of primary cilia lengths: Primary cilia of fixed cells were labeled using α-acetylated tubulin and Arl13b antibodies, and imaged on an inverted Zeiss LSM 780 laser scanning confocal microscope equipped with either a 63x or 100x oil immersion objective. To ensure the full length of each cilium was accurately measured, thin z-stacks were acquired and 3D surface reconstructions of the primary cilia generated using ZEN software (Carl Zeiss, Germany). All experimental cilia measurements were normalized against control cilia measurements. The values reported thus represent the mean changes in the percentage of cilia length ± SEM. For each condition, the lengths of over 100 cilia were individually analyzed. The reduction in primary cilia length observed with DAPT addition and extension with NICD transfection was observed with both α-acetylated tubulin and Arl13b labeled cilia. Data was analyzed using an unpaired, two-tailed t-test. Significance was assumed when $p < 0.05$.

Immunoblotting: Cell cultures were scaled up to 100 mm plates and grown as described above. Cells were manually scraped, rinsed once in PBS, lysed in a modified RIPA buffer (1% NP40, 1% sodium deoxycholate, 0.3% SDS, 150 mM NaCl, 1 mM EDTA, 50 mM Tris pH6.8, 1 mM PMSF, 1x complete protease cocktail (Roche)) for 2 hr on ice with vortexing every 10 min, and clarified by centrifugation for 30 min at 14,000 RPM at 4ºC. Protein lysates were resolved on an 8-10% polyacrylamide gel and processed for immunoblotting with the following antibodies: Rabbit anti-Notch1 (Val1744, Cell Signaling Technologies), 1:1000; rabbit anti-Ptch1 (Rohatgi Lab), 1:1000; mouse anti-actin (Millipore), 1:1000, followed by HRP-conjugated anti-mouse and anti-rabbit secondary antibodies (Jackson Immunoresearch), 1:50,000. Membranes were processed using ECL 2 Western Blotting Substrates (Thermo Scientific) and bands detected using a Typhoon FLA 7000 imaging system (GE Healthcare Life Sciences).

RESULTS

Manipulation of Notch signaling alters the dorsoventral register of NPCs

We first used *Olig2^{Cre}* mice[15] to selectively activate or inactivate Notch signaling in the p3 and pMN domains between embryonic day (E) 9.5-10.5 (**Figures 2-S1A-W**). This strategy was accomplished by crossing *Olig2^{Cre}* to mice harboring: 1) a Cre-inducible *R26R^{GFP}* transgenic reporter[28] (control condition), 2) a *R26R$^{NICD\text{-}GFP}$* transgene and reporter[29] ("Notch-On" condition), or 3) a Cre-inactivatable Rbpj allele[30] along with the *R26R^{GFP}* transgenic reporter ("Notch-Off" condition) (**Figure 2-1A**). The impact of these Notch pathway manipulations was evident by E11.5, as Notch-On mice displayed elevated expression of the Notch effectors Hes1 and *Hes5,* which are normally very low in the pMN, and reduced expression of proneural transcription factors including Neurog2*,* Ascl1*,* and *Neurog3* (**Figures 2-S2A-N**). Conversely, Notch-Off mice displayed reductions in Hes1 and *Hes5* expression, and increased levels of Neurog2, Ascl1, and *Neurog3* (**Figures 2-S2O-U**). While the ventral ventricular zone (VZ) narrowed in Notch-Off mice, a contiguous band of Sox2^{+} NPCs was maintained throughout development, and both the neuroepithelial architecture and apicobasal polarity of progenitors were preserved (**Figures 2-S2V-AI**). This phenotype contrasts with mutations in other members of the Notch pathway such as *Hes1* and *Hes5* whose combined loss disrupts the neuroepithelium[66]. The persistence of NPCs and neuroepithelial organization in *Olig2^{Cre}*; Notch-Off mutants may be explained by the lasting presence of Hes1 in ventral progenitors despite the loss of *Rbpj* (**Figures 2-S2Q-R**), most likely due to Notch-independent activation of Hes1 by Shh, as has been described in other tissues[67,68].

We next examined the impact of these Notch manipulations on dorsoventral patterning. Remarkably, activating Notch signaling led to a notable reduction in Olig2^{+} pMN cells by ~E11.5 and a nearly complete loss of Olig2^{+} NPCs throughout the rest of embryonic development (**Figures 2-1B-K and 2-1Q**). Notch-Off mice exhibited the reciprocal phenotype, with a ~1.5 to ~2.5-fold increase in the number of Olig2^{+} progenitors from E11.5 to postnatal day (P)0.5

(**Figures 2-1L-P, and 2-1Q**). While Olig2^{+} cells were reduced in Notch-On mice, the overall number of ventral NPCs expressing Nkx6.1 increased by ~50% (**Figure 2-2M**). The loss of Olig2 from Nkx6.1^{+} NPCs coincided with the increased expression of the p3 determinant Nkx2.2 (**Figures 2-2A-H and 2-2N**). Given that Nkx2.2 can repress Olig2[10,11,69], the loss of pMN cells in Notch-On mice is likely due to their transformation towards the more ventral p3 fate. This conclusion was supported by the reduced percentage of Nkx6.1^{+} progenitors expressing Nkx2.2 and corresponding increase in Olig2^{+} cells seen in Notch-Off spinal cords (**Figures 2-2I-L and 2-2N**). Collectively, these data demonstrate that Notch signaling plays a critical role enhancing the ventral character of NPCs and influencing their partitioning between pMN and p3 identities.

Notch-mediated changes in ventral NPCs alter neuronal and glial fates

We next used *R26R^{GFP}* lineage tracing to assess the fate of the Notch-manipulated cells. Consistent with the loss of Olig2, Notch-On spinal cords exhibited a ~35% reduction in MN formation (**Figures 2-S3A-F and 2-S3J-L**). Most of this deficit resulted from the selective loss of Foxp1^{+} lateral motor column (LMC) MNs at limb levels and preganglionic column (PGC) MNs at thoracic levels, with little change to Foxp1^{-} medial and hypaxial motor column (MMC and HMC) MNs (Figure S3K)[47]. LMC and PGC MNs are amongst the last MN subtypes to be formed[50], suggesting that Notch activity must be silenced for the generation of these later-born cell types. Nevertheless, Notch-Off spinal cords did not exhibit any obvious defects in either MN formation or segregation into different columnar subgroups (**Figures 2-S3G-L**).

Olig2^{Cre}-mediated Notch manipulations produced much more striking changes in glial fate selection. In E18.5 control embryos, *Olig2^{Cre}* derivatives include both Sox10^{+} Pdgfrα^{+} oligodendrocyte progenitors scattered throughout the spinal cord and BLBP^{+} Nf1A^{+} Nkx6.1^{+} Fgfr3^{+} Slit1^{+} VA3 astrocyte precursors and differentiated astrocytes located in the ventral-most white matter (**Figures 2-3 and 2-S3M-U**)[12]. Notch-On spinal cords exhibited a nearly complete loss of oligodendrocyte precursors and corresponding increase in VA3-like astrocyte precursors

(**Figures 2-3A-H, 2-3M-O and 2-S3M-R**)[12]. Conversely, Notch-Off spinal cords produced more oligodendrocyte precursors and fewer astrocyte precursors and differentiated VA3 astrocytes (**Figures 2-3I-O and 2-S3S-U**). Together, these data show that early changes in NPC fates following Notch pathway manipulation lead to corresponding alterations in neuronal and, more strikingly, glial identities.

Notch signaling is only able to shift NPC identities within the ventral spinal cord

Previous studies observed that glial fates could be altered by deleting *Rbpj* function from all spinal NPCs[70], raising the question of whether our results stemmed from direct effects of Notch activity on glial fate selection or were a secondary consequence of altered dorsoventral patterning. To distinguish between these possibilities we examined the consequences of manipulating Notch activity in the p0 domain of the intermediate spinal cord using a *Dbx1*^{Cre} driver[14,27]. *Dbx1*^{Cre}-mediated Notch activation expanded the numbers of Dbx1^{+} and Dbx2^{+} progenitors (**Figures 2-S4A-D' and 2-S4G**), while Notch inactivation disrupted neuroepithelial organization and depleted these cells (**Figures 2-S4E-S**). Despite these effects, we observed no changes in the dorsoventral register of NPCs or shifts in glial identities as seen with *Olig2*^{Cre}-based manipulations (**Figures 2-S4T-AI**). Thus, while manipulation of the Notch pathway can change the balance between NPC maintenance and differentiation within the intermediate spinal cord, it appears insufficient to evoke changes in dorsoventral patterning and associated neuronal and glial fates.

Notch signaling alters ventral progenitor identities by modulating responses to Shh

Progenitor identities within the ventral spinal cord are primarily influenced by their exposure to extracellular Shh emanating from the notochord and floor plate at the midline[8,71]. The selective effects of Notch activity on cell fate assignment in the ventral versus intermediate spinal cord led us to consider that Notch could be acting on the former by altering the

responsiveness of neural progenitors to Shh. Within the ventral spinal cord, Shh signaling activity is thought to peak at ~E8-9[16,55]. After E9, neural progenitors become increasingly insensitive to Shh due to negative feedback regulation[55,72-74]. In the absence of additional Shh signaling, progenitor domain boundaries then become fully realized and maintained by cross-repressive gene transcription networks[16]. Due to these adaptations, Shh signaling activity within the ventral-most progenitors is expected to be very low as the cells become refractory to Shh ligand. We confirmed that this was indeed the case at the E11.5 time point when changes in neural progenitor identities were evident. The absence of *Gli1* and *Ptch1* mRNA from the floor plate and low levels in the p3 domain at this time point thus serves as an indicator that these cells had previously experienced high levels of Shh signaling (**Figures 2-S5A-C**)[16]. The highest levels of *Gli1* and *Ptch1* mRNA expression are in turn associated with the pMN-p1 progenitor groups, which have been exposed to lower doses of Shh. (**Figures 2-S5A-C**). This spatial pattern of *Gli1* and *Ptch1* expression was markedly changed in the spinal cords in which Notch activity had been changed. NICD misexpression reduced the expression of both genes within the presumptive pMN such that they appeared comparable to the low levels normally seen in the p3 domain (**Figures 2-S5D-F**). In contrast, *Rbpj* deletion increased *Gli1* and *Ptch1* expression within the presumptive p3 domain to a level closer to that normally seen in the pMN (**Figures 2-S5G-I**). We further quantified these changes using qPCR, normalizing the expression of each gene relative to *Sox2* to account for the overall changes in progenitor numbers following Notch manipulations. Consistent with the in situ analysis, *Gli1* and *Ptch1* expression were reduced by ~60% following NICD misexpression and increased by more than 50% by Rbpj deletion (**Figures 2-S5J-K**). Shh expression was not obviously altered in these mutant mice (data not shown), suggesting that these manipulations of Notch signaling are most likely due to changes in the ability of neural progenitors to respond to the endogenous Shh gradient.

The selective effects of Notch activity on cell fate assignment in the ventral versus

intermediate spinal cord suggests that Notch modulates the responsiveness of NPCs to Shh ligand produced at the ventral midline. To test this possibility, we used the classic chick intermediate [i] neural plate explant system to examine the fates of NPCs exposed to moderate (1 nM) or high (4 nM) amounts of Shh and varying amounts of the γ-secretase inhibitor DAPT (N-[N-(3,5-Difluorophenacetyl)-L-alanyl]-S-phenylglycine t-butyl ester) to reduce Notch receptor cleavage and downstream signaling[15,75,76]. High amounts of Shh produced numerous Nkx2.2$^+$ p3 cells and a small number of Olig2$^+$ pMN cells (**Figure 2-4D**) as previously described[15]. However, when Notch activity was reduced using DAPT, the number of Nkx2.2$^+$ progenitors was reduced while Olig2$^+$ cells increased (**Figures 2-4E-F**), recapitulating the phenotype seen in Notch-Off mice (**Figures 2-2I-J and 2-2N**). Interestingly, the effects of DAPT up to 25 μM appeared selective: they blunted the Nkx2.2-inducing activity of high doses of Shh but did not block the Olig2-inducing activity of lower doses of Shh (**Figures 2-4A-C**). These results suggest Notch is required for NPCs to experience high but not low levels of Shh signaling.

To verify that these NPC identity shifts were due to effects of Notch on Shh pathway activity, [i] explants were isolated from chick embryos electroporated with a Gli binding site-Luciferase (GBS-Luciferase) reporter to measure Gli function after Shh administration[15,77]. DAPT addition led to a >50% decrease in GBS-Luciferase activity over that seen with Shh alone (**Figure 2-4G**). Similar results were obtained with measurement of GBS-Luciferase activity in ventral neural plate plus floor plate [vf] explants, in which Gli activity is driven by the endogenous Shh produced by floor plate cells (**Figure 2-4H**). Collectively, these data demonstrate that Notch signaling is required for NPCs to attain the highest levels of Gli activity and assume the ventral-most fates.

Notch signaling facilitates the accumulation of Smo within primary cilia

We next sought to determine a mechanism that could explain the modulatory effects of Notch signaling on Shh responsiveness. Given that the requirement of Notch for Shh responses

appears to be conserved in NPCs across species, we tested whether it was also conserved across cell types. NIH-3T3 mouse fibroblasts are a cell line shown to be Notch responsive[78] and in which the cellular and molecular details of Shh signaling are well established[33,35,79]. We first validated the system by exposing Shh-Light2 cells, a NIH-3T3 derivative stably transfected with a GBS-Luciferase reporter, to increasing concentrations of Shh and observed dose-dependent increases in Luciferase activity (**Figure 2-5A**). Strikingly, the addition of DAPT to these cultures reduced Shh-induced GBS-Luciferase activity (**Figure 2-5B**), recapitulating the effects seen with neural plate explants (**Figures 2-4D-H**). Quantitative polymerase chain reaction (qPCR) analysis showed that DAPT similarly impacted endogenous Shh response genes such as *Gli1* and *Ptch1* (**Figure 2-5C**).

We then used the NIH-3T3 fibroblast system to pinpoint where Notch activity acts in the Shh transduction cascade. One of the first steps is the translocation of Smo to primary cilia, which initiates the conversion of Gli proteins into transcriptional activators[35,80]. DAPT dramatically reduced Shh-induced Smo accumulation within primary cilia, acting in a dose-dependent manner (**Figures 2-5D-F, 25I-K, and 2-S6A**). This change occurred without any obvious impact on *Smo* mRNA, alterations in cell polarity, or presence of primary cilia, though DAPT addition alone reduced average cilia length by 12.6% ± 1.3%; $p < 0.001$ (**Figures 2-5C and S6B-I**). To confirm that reductions in ciliary Smo were due to changes in Notch pathway activity, we repeated these experiments using two additional small molecule inhibitors: SAHM1, a peptide that prevents assembly of the NICD-Rbpj-MAML1 transcriptional activator complex[81] and JLK6 (7-Amino-4-chloro-3-methoxyisocoumarin; also referred to as γ-secretase inhibitor XI), a molecule that blocks activation of some γ-secretase targets such as beta-amyloid precursor proteins while sparing others, including the Notch receptors[82]. Verifying these activities, we found that both DAPT and SAHM1 reduced *Hes1* gene expression in NIH-3T3 cells by ~65-75%, whereas JLK6 had no discernible effect (**Figure 2-5I**). Importantly, SAHM1 reduced Shh-induced ciliary accumulation of Smo in a manner similar to DAPT (**Figures 2-5G**

and 2-5J). JLK6 in contrast had no effect on Smo localization (**Figures 2-5H and 2-5K**).

We further tested whether the impact of Notch activity on Shh-induced Smo localization was limited to NIH-3T3 cells or more broadly applicable to other cell types including human NPCs, primary mouse embryonic fibroblasts (MEFs), and C2C12 mouse myoblasts. In all cases, DAPT reduced Shh-induced Smo accumulation within primary cilia (**Figures 2-S7A-M**), suggesting that the crosstalk between the Notch and Shh pathways is conserved across germ layers and species.

Since Notch inhibition reduced both the presence of Smo within primary cilia and Shh pathway activity, we tested whether the converse was also true. NIH-3T3 cells were transiently transfected with a vector expressing *NICD* and an IRES-*nEGFP* reporter cassette to activate Notch signaling, and both Smo localization and the expression of Shh-target genes evaluated. *NICD*-transfected cells exhibited a ~40 fold increase in *Hes1* expression irrespective of Shh stimulation (**Figure 2-5L**). Primary cilia were also slightly longer (17.5% ± 3.9%, $p < 0.001$) in *NICD*-transfected cells compared to *nEGFP*-only transfection controls, consistent with the reduced cilia lengths seen with DAPT addition. Upon Shh treatment, *NICD*-transfected cells exhibited an increase in the level of Smo within primary cilia and ~2 to 3-fold higher levels of *Gli1* expression (**Figures 2-5M-N**). These effects were only seen after the addition of Shh. Together, these results illustrate that Notch activity is not only required for Shh responsiveness, but can also potentiate its signaling function.

Given that *Hes1* was notably changed in all of our Notch manipulations, we tested whether direct elevation of *Hes1* could similarly increase cellular responses to Shh ligand. Interestingly, in a manner similar to *NICD* misexpression, *Hes1* misexpression was sufficient to increase Shh-evoked movement of Smo to the primary cilia and resulted in increased activation of *Gli1* ~1.8-fold (**Figures 2-S6J-L**). Collectively, these results suggest that the potentiating effects of Notch on Shh signaling result from activation of Hes genes and potentially other downstream effectors.

Given the ability of Notch signaling to promote localization of Smo to cilia in cultured cells, we examined whether this effect could also be seen in the developing spinal cord. In E10.5 control embryos, high amounts of Smo were present in the cilia of both floor plate and Nkx2.2^{+} p3 cells and lower levels present in Olig2^{+} pMN cells (**Figures 2-6A-B"**). In Notch-Off spinal cords, most *Olig2^{Cre}*-derived NPCs exhibited lower levels of ciliary Smo, and this change preceded shifts in Olig2 and Nkx2.2 expression (**Figures 2-6C-D" and 2-6K**). By E11.5, the extent of Smo localization within cilia along the dorsoventral axis of Notch-Off mutants was reduced by ~60% compared to littermate controls (**Figures 2-6E-F' and 2-6I-L**). Notch-On mutants by contrast showed a dorsal expansion in the extent of Smo localization within primary cilia (**Figures 2-6G-H' and 2-6L**).

Changes in the ciliary accumulation of Smo following Notch manipulations could stem from either direct effects of Notch on Smo trafficking or indirect effects related to Notch having altered NPC identities. To distinguish between these possibilities, we examined Smo staining in the spinal cords of *Nkx2.2*, *Olig2*, and *Pax6* mutant mice, where dorsoventral patterning is known to be severely disrupted[8]. Remarkably, the dorsal limits of ciliary Smo in all mutants were similar to control littermates, despite clear changes in NPC fates (**Figures 2-S8A-R**). In *Nkx2.2* mutants, this alteration permitted the unusual presence of Olig2 in cells exhibiting high amounts of Smo in their cilia (**Figures 2-S8J and 2-S8N**), a phenotype that was never seen in control embryos or those in which Notch activity had been manipulated (**Figures 2-6E-L**). Collectively, these data show that Notch activity influences Smo accumulation within primary cilia in multiple cell types in vitro and spinal cord NPCs in vivo, and acts upstream of the transcription factor network controlling dorsoventral fates.

Notch activity sets the levels of Ptch1 present in primary cilia, thereby gating Smo entry

We next sought to identify a mechanism that could account for the observed effects of Notch signaling on Smo localization and Shh pathway activity. Our observations that DAPT

reduces Smo protein levels in primary cilia suggested that early steps in the Shh transduction could be involved. To explore this possibility further, we used the 3T3 cell system to test whether DAPT-associated reduction in Smo translocation could be bypassed by the addition of small molecule agonists of Smo, Purmorphamine and Smoothened Agonist (SAG), as both molecules can drive Smo into primary cilia in a ligand independent manner[83-85]. Both Pur and SAG potently induced Smo translocation to primary cilia as expected, but unlike Shh ligand, their activities were not impeded by DAPT addition (**Figures 2-7A-E**), suggesting that the DAPT blockade most likely lies at the steps between Shh ligand binding and Smo activation. To test this further, we examined when Notch activity could boost the activity of different components of the Shh signaling pathway when electroporated into the chick spinal cord. For these experiments, Notch signaling was elevated through transfection of an NICD expression vector and Shh signaling increased using one of three constructs: (i) Shh, an expression construct encoding full length rat Shh[39]; (ii) SmoM2, a ligand-independent activated form of Smo[40]; and (iii) Gli3A, a ligand-independent activated form of Gli3[77]. Plasmids encoding NICD and these Shh pathway components were co-electroporated at e2 and embryos collected two days later for immunohistochemical analysis focusing on changes in the expression of ventral markers including NKX2.2 and OLIG2. To help reveal the potentiating effects of NICD, we used minimal amounts of each Shh pathway component that were empirically determined to produce mild ventralizing effects on their own (**Figures 2-S9A, 2-S9C, 2-S9E, 2-S9G, and 2-S9I**). Electroporation with the NICD alone led to a ~25% increase in the number of Nkx2.2+ cells (**Figures 2-S9A-B, and 2-S9I**), recapitulating the p3 expansion seen in Notch activated transgenic mice (**Figure 2-2**). When combined with NICD, only co-electroporation with Shh displayed any increase in ventralizing activity (**Figure 2-S9C-I**). This result supports the SAG/Pur/DAPT experiments conducted in NIH-3T3 cells (**Figures 2-7A-E**), further suggesting that Notch activity acts at the most proximal steps in Shh signal transduction.

We thus focused our attention on the actions of Notch on the Shh receptor Ptch1. In the

absence of ligand, Ptch1 localizes around the base and within primary cilia, where it inhibits Smo entry and Gli activation[35]. Shh binding to Ptch1 promotes its exit from primary cilia and concomitant Smo accumulation[35]. Since endogenous Ptch1 protein was difficult to detect in NIH-3T3 cells by antibody staining, we utilized Ptch1-YFP MEFs generated by infection of *Ptch1*$^{LacZ/LacZ}$ mutant cells with a retrovirus expressing a Ptch1-YFP fusion protein[35]. In the absence of Shh, ~75% of primary cilia contained Ptch1 (**Figures 2-7F and 2-7J**). When DAPT was added for 12 hr, the number of Ptch1^{+} primary cilia increased to ~90% (**Figures 2-7G and 2-7J**). This ~15% elevation is notable in that its magnitude is consistent with the ~15-20% decrease in Smo^{+} cilia upon Shh and DAPT co-administration (**Figures 2-5J-K**). DAPT was also able to impede the clearance of Ptch1 from primary cilia upon Shh stimulation (**Figure 2-7H-J**). Remarkably, the effects of DAPT on Ptch1 localization occurred without any change in either *Ptch1* mRNA or protein levels in both Ptch1-YFP MEFs and NIH-3T3 cells (**Figures 2-S10G-I**).

These results prompted us to examine whether the effects of DAPT on Smo trafficking to primary cilia occurs immediately after its addition, or rather requires more time to enable Ptch1 to increase and thereby block Smo entry. Smo normally accumulates in primary cilia within 4 hr of Shh addition[35] (**Figures 2-S10A-B**). When Shh and DAPT were coadministered, there was no decrease in Smo presence within primary cilia at either the 4 or 6 hr time points; rather, Smo reduction only became evident after ~12 hr (**Figures 2-S10A-B**). In contrast, when cells were pre-treated with DAPT for 8 hr and then exposed to Shh plus DAPT for an additional 4 hr, significant reductions in Smo ciliary accumulation were observed (**Figures 2-S10C-D**). These data indicate that the suppressive actions of DAPT on Smo localization follow the time course of Ptch1 accumulation within primary cilia. We further found that the actions of DAPT required new transcription, as changes in Smo localization were partially blocked by coadministration of DAPT and the RNA polymerase inhibitor α-amanitin (**Figures 2-S10E-F**). These results suggest that Notch modulates Ptch1 and Smo levels in and around primary cilia through a transcriptional mechanism.

To test whether Ptch1 mediates the inhibitory effects of DAPT on Smo, we measured the impact of DAPT addition to *Ptch1*$^{LacZ/LacZ}$ mutant MEFs. Whereas DAPT potently inhibited Smo accumulation in the cilia of Shh-treated control MEFs, it was unable to do so in *Ptch1* null cells (**Figures 2-7K-O and 2-S10J**). Collectively, these data show that Notch signaling influences Smo accumulation by regulating the ciliary presence of Ptch1.

Finally, we tested whether altered localization or abundance of Ptch1 protein was observed after manipulations of the Notch pathway in the ventral spinal cord. In Notch-On mutants, Ptch1 protein staining in and around the primary cilia was notably reduced, fitting with the observed increase in Smo presence (**Figures 2-6E-H', 2-7P-Q and 2-7S**). By contrast, Notch-Off mutants showed elevated Ptch1 at the apical membrane and cilia in accordance with the reductions in Smo staining (**Figures 2-6I-J' and 2-7R-S**). Together, these in vitro and in vivo experiments demonstrate that Notch signaling plays an integral role modulating Ptch1 localization to gate Smo entry into primary cilia. Through these actions, Notch can regulate the downstream activation of the Shh transduction pathway and assignment of NPC fates.

DISCUSSION

It is well established that the dorsoventral identity of NPCs in the spinal cord and other regions of the CNS is influenced by the concentration of Shh ligand that they are exposed to[8,9,86]. However, Shh concentration is only part of the means though which graded signaling responses are achieved. Other important factors include: (1) the duration of time over which cells are exposed to Shh, (2) the ability of cells to modulate their responsiveness to Shh through changes in the expression and/or subcellular distribution of key signal transduction components such as Ptch1 and Smo, (3) changes in the expression of proteins that modulate Shh-Ptch1 interactions or modify Shh itself, and (4) cross-regulatory interactions between Shh-regulated transcription factors that assign specific cell fates[8,9,87]. Our studies show that Notch signaling plays a crucial role in these first two processes, serving to sustain NPCs in an undifferentiated,

Shh-responsive state while also influencing the ciliary trafficking of Ptch1 and Smo and downstream activation of Gli transcription factors (**Figure 2-8**). Together, these data provide important insights into the mechanisms through which NPCs interpret the Shh gradient and reveal a novel, and potentially general mechanism by which the Notch and Shh signaling pathways collaborate to direct cell fate decisions.

Notch-mediated changes in Shh transduction influence the selection of NPC fates

Our data show that manipulating the Notch pathway modulates the dorsoventral register of NPCs, with Notch activation and inactivation respectively increasing or decreasing the formation of the ventral-most cell types reflected by alterations in Nkx2.2 and Olig2 expression and shifts in specific classes of neurons and glia. Importantly, multiple lines of evidence indicate that these changes are due to the ability of Notch to modulate how NPCs interpret the endogenous Shh signaling gradient rather than more direct effects on cell fate determination. First, all changes in NPC fates occurred within the context of Nkx6.1^{+} progenitors, which reflect the limit of endogenous Shh signaling in spinal cord [54]. Second, Notch manipulation in the intermediate spinal cord impacted NPC maintenance, without any change in dorsoventral patterning or shift in glial cell types. Third, in fibroblasts, Notch activation and inactivation were unable to modulate Smo trafficking to primary cilia or Gli transcriptional activity without the coadministration of Shh ligand. Collectively these data indicate that in the context of tissue patterning, Notch plays a supporting role tuning the response of cells to Shh present in the developing embryo or culture media.

It has long been appreciated that the influences of Shh on neural fate selection are generally restricted to dividing cells[57]. Recent studies have provided molecular explanations for this relationship showing that most Shh/Gli-regulated genes are coregulated by SoxB1 transcription factors such as Sox2 that are broadly expressed by NPCs[88-90]. Some of the positive effects of Notch on Shh signaling could thus be accounted for by its ability to elevate

SoxB1 levels as it maintains NPCs in an undifferentiated state. However, our data indicate that Notch can also act at a more proximal level, regulating the ciliary localization of at least two key components of the Shh transduction pathway, Ptch1 and Smo. Ptch1 appears to be the most directly impacted by Notch, as the addition of DAPT alone to fibroblasts promotes Ptch1 accumulation within primary cilia (**Figure 2-7F-G and 2-7J**), and Ptch1 is known to block Smo entry and downstream signaling events[35]. Moreover, DAPT was unable to reduce Smo accumulation within cilia in the absence of Ptch1 or in the presence of Pur and SAG, small molecules that bypass Ptch1 function (**Figures 2-7A-E and 2-7K-O**). These observations in fibroblasts also hold true for spinal cord NPCs, as *Rbpj* deletion increased Ptch1 protein in and around primary cilia whereas NICD misexpression reduced it, with corresponding changes in ciliary Smo and ultimately expression of specific NPC fate determinants (**Figures 2-7P-S**).

Notch as a modulator of ciliary trafficking

How might Notch signaling alter Ptch1 and Smo trafficking? In epidermal cells, Notch receptors and processing enzymes are located in and adjacent to primary cilia, and ciliary transport is required for Notch pathway activity[91]. Based on this proximity, Notch signaling components could conceivably impact the interactions of ciliary transport proteins with Shh signaling components. However, our results point to Notch acting through a transcriptional mechanism. First, changes in NPC fates and Gli transcriptional activity were seen with either removal of Rbpj function or increased expression of NICD, components whose main sites of action are known to be in the nucleus. Second, the Shh-potentiating activities seen with NICD misexpression were partially recapitulated by the forced expression of Hes1, one of the best-known downstream transcriptional effectors of the Notch pathway. Third, the effects of DAPT administration on Ptch1 and Smo trafficking were not immediate, but rather required at least 8 hr of exposure, which is more than sufficient time for a transcriptionally mediated response. Lastly, DAPT effects on Smo trafficking were blocked by the addition of the transcriptional

inhibitor α-amanitin. Together, these results lead us to propose that Notch and Hes genes modulate Shh signaling by regulating the expression of genes whose products impact the trafficking of Ptch1, Smo, and potentially other Shh signaling components to primary cilia, designated as 'X' for direct Notch effectors and 'Y' for Hes-suppressed effectors (**Figure 2-8**).

While a great deal is known about the transcriptional control of *Ptch1* in response to Shh pathway activation, relatively little is known about the regulation of Ptch1 protein trafficking. Some insights into this process have been recently made by observations that Ptch1 exit from primary cilia requires the function of the intraflagellar transport (IFT) protein Ift25[92], and endocytic turnover mediated by the ubiquitin E3 ligases Smurf1 and Smurf2[93]. Loss of these components results in Ptch1 accumulation within primary cilia and reduced cellular responses to Shh[92,93], reminiscent of the effects seen with the loss of Notch signaling. However, none of these genes were changed by our Notch manipulations (JHK. and BGN, unpublished data). A better understanding of the downstream targets of Notch and Hes1 should yield important new insights into how the localization and function of Ptch1 and other Shh signaling components may be controlled.

A role for Notch gating responses to other developmental signals dependent on cilia?

The primary cilium is a nonmotile organelle that is present on almost all vertebrate cells[94]. Although primary cilia were first observed over a century ago[95], their function as an antenna-like organelle that allows cells to detect extracellular environmental stimuli and modulate an appropriate intracellular response has only recently been realized. In addition to Shh signaling, primary cilia are thought to be essential for Hippo, mTor, Notch, Pdgfrα, and Wnt signaling[91,96-99]. The importance of primary cilia is perhaps best illustrated through ciliopathies, a group of genetic disorders that are due to defects in the generation or function of cilia, that collectively affect nearly every major organ in the human body[100]. As no protein synthesis occurs within the cilium, the formation of the cilium and the accumulation of signaling pathway

components within the cilium are entirely dependent on the IFT system to shuttle proteins to their proper areas[101].

While our study focused on the impact of Notch on Shh signaling by altering the localization of Ptch1 and Smo, the mechanisms used to achieve this result are likely to have a broader impact on other signaling pathways that depend upon the IFT system. Consistent with this hypothesis we have carried out a series of preliminary expression profiling experiments in NIH-3T3 cells which indicate that DAPT addition reduces the expression of several proteins known to be associated with primary cilia[102] including components of the Pdgfrα and Wnt signaling pathways, and various extracellular matrix proteins (JHK. and BGN, unpublished data). In this regard, the mechanism through which Notch gates the responsiveness of cells to Shh might signify a more general role for Notch modulating ciliary transport that could impact multiple signaling pathways involved in both development and disease.

FIGURES

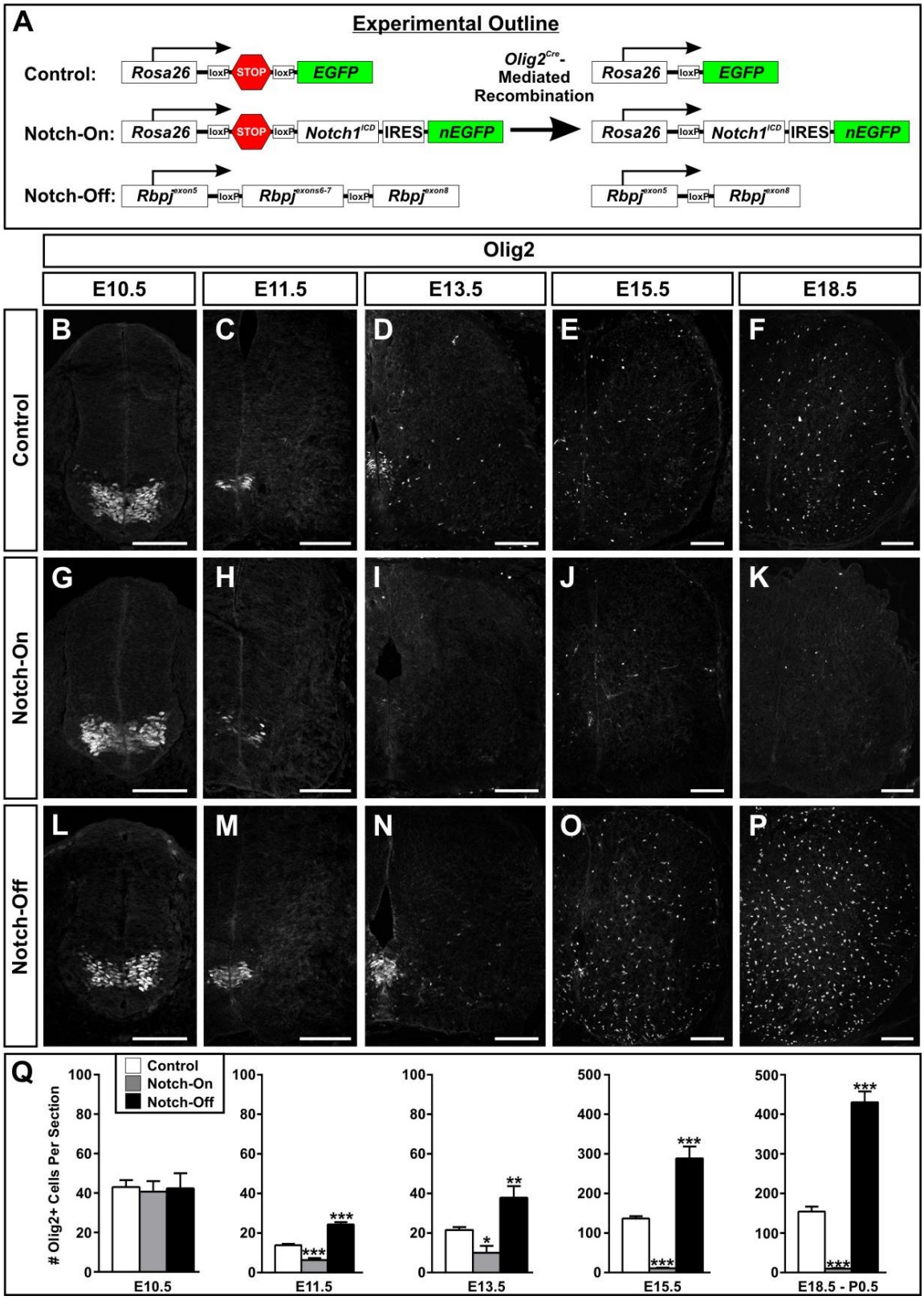

Figure 2-1: Manipulation of Notch signaling alters Olig2 expression

(A) Schematic of *Olig2*^{Cre}-mediated manipulations used to activate or inactivate Notch signaling. Notch-On indicates NICD misexpression and Notch-Off indicates *Rbpj* deletion. Control conditions include crosses to mice carrying a *R26R*^{GFP} reporter.

(B-F) At E10.5-E11.5, Olig2 is initially expressed by MN progenitors and later oligodendrocyte progenitors.

(G-P) In Notch-On mice, Olig2$^+$ cells decline from E11.5 onward. In Notch-Off mice, Olig2$^+$ cells increase. Scale bars = 100 μm.

(Q) Quantification of Olig2$^+$ cells per spinal cord half at the indicated time points. Plots show the mean ± SEM from multiple sections collected from 4-25 embryos from each group. *$p < 0.05$, **$p < 0.01$, ***$p < 0.001$

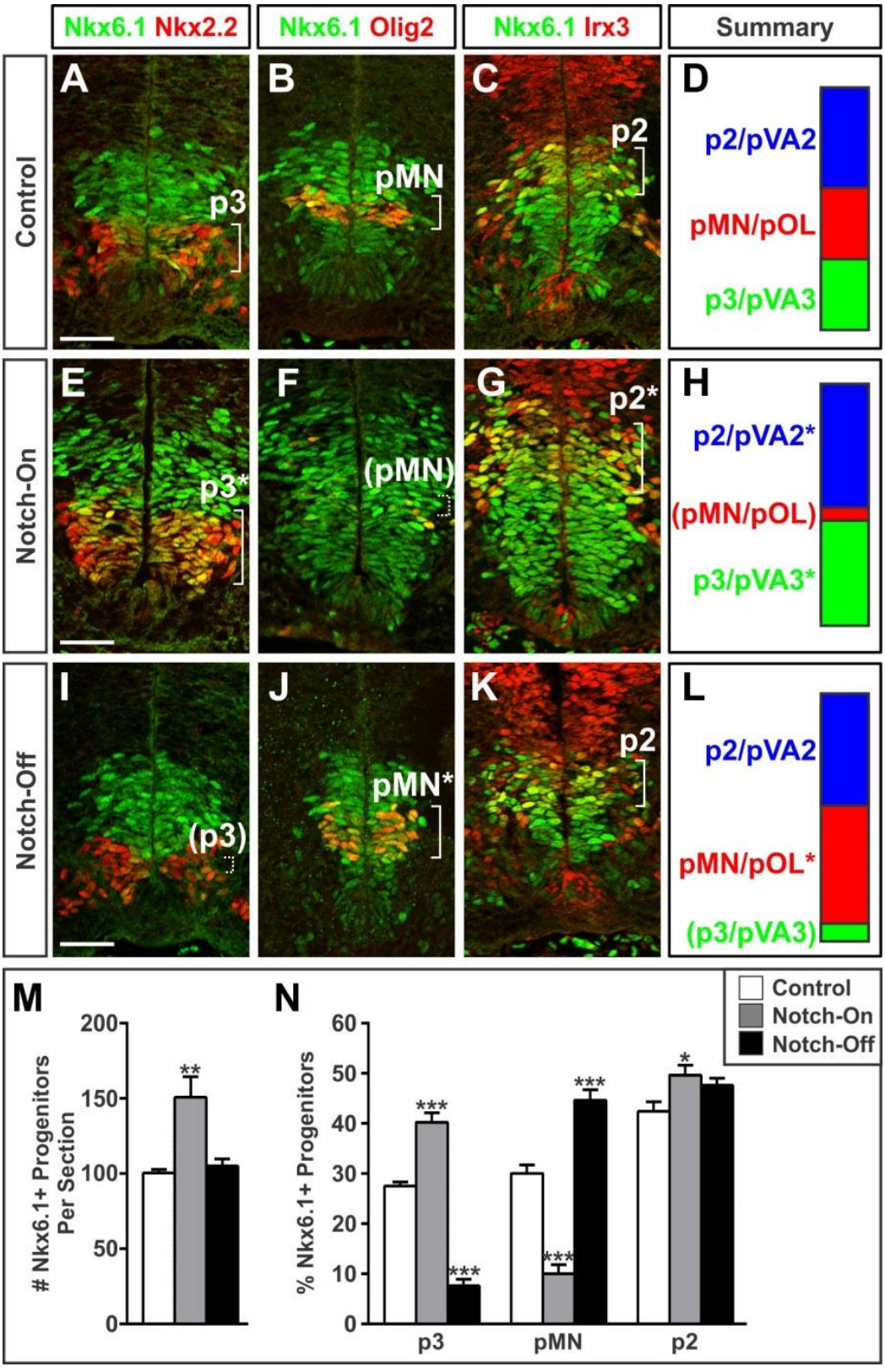
Nkx6.1 Nkx2.2
Nkx6.1 Olig2
Nkx6.1 Irx3
Summary
Control
Notch-On
Notch-Off
A
B
C
D
E
F
G
H
I
J
K
L
p3
pMN
p2
p2/pVA2
pMN/pOL
p3/pVA3
p3*
(pMN)
p2*
p2/pVA2*
(pMN/pOL)
p3/pVA3*
(p3)
pMN*
p2
p2/pVA2
pMN/pOL*
(p3/pVA3)
M
Nkx6.1+ Progenitors Per Section
200
150
100
50
0
**
N
% Nkx6.1+ Progenitors
60
50
40
30
20
10
0
***
***
***
***
*
p3
pMN
p2
Control
Notch-On
Notch-Off

Figure 2-2: Changes in Notch signaling alter the dorsoventral identities of ventral spinal cord progenitors.

(A-D) In E11.5 control spinal cords, ventral progenitors are distinguishable by coexpression of Nkx6.1 and Nkx2.2 (p3), Nkx6.1 and Olig2 (pMN), and Nkx6.1 and Irx3 (p2).

(E-H) More Nkx6.1^{+} progenitors are present in Notch-On mutants. Within this population, the percentage expressing Nkx2.2 increased while the percentage expressing Olig2 decreased.

(I-L) Notch-Off mutants contain a reduced percentage of Nkx6.1^{+} progenitors expressing Nkx2.2 and reciprocal increase in Olig2. Scale bars = 50 μm.

(M-N) Quantification of the total number of Nkx6.1^{+} progenitors present and their subdivision into p3, pMN, and p2. Plots show the mean ± SEM from multiple sections collected from 7-9 embryos for each group. *$p < 0.05$, **$p < 0.01$, ***$p < 0.001$.

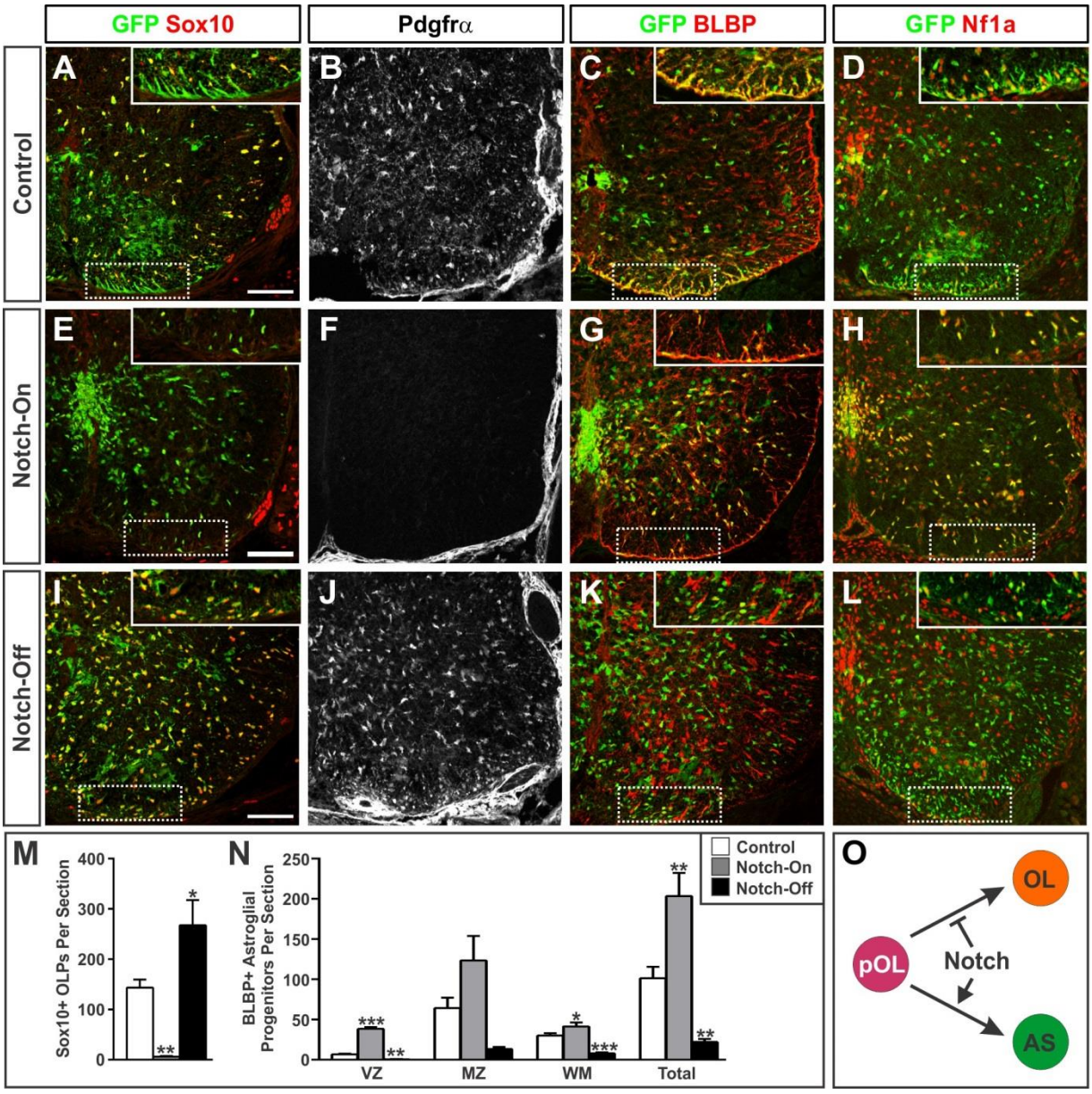
GFP Sox10
Pdgfrα
GFP BLBP
GFP Nf1a
Control
Notch-On
Notch-Off
A
B
C
D
E
F
G
H
I
J
K
L
M
Sox10+ OLPs Per Section
400
300
200
100
0
*
**
N
BLBP+ Astroglial Progenitors Per Section
250
200
150
100
50
0
***
**
*
**
***
**
VZ
MZ
WM
Total
Control
Notch-On
Notch-Off
O
OL
pOL
Notch
AS

Figure 2-3: Manipulation of Notch signaling alters glial fates.

(A-D) In E18.5 control spinal cords, *Olig2*^{Cre}; *R26R*^{GFP}-labeled descendants include Sox10^{+}/PDGFRα^{+} oligodendrocyte precursors (OLPs), BLBP^{+}/NF1a^{+} pVA3 astrocyte progenitors.

(E-H) Notch activation suppresses OLP formation and expands pVA3 progenitors.

(I-L) Notch inactivation expands OLP production at the expense of pVA3 progenitors. Scale bars = 100 µm.

(M-N) Quantification of total OLP (GFP+/Sox10^{+}) and pVA3 astrocyte progenitors (GFP+/BLBP^{+}) per spinal cord half. pVA3 counts are divided based on localization within the ventricular zone (VZ), marginal zone (MZ), or white matter (WM). Plots show the mean ± SEM from multiple sections collected from 3-7 embryos for each group. *$p < 0.05$, **$p < 0.01$, ***$p < 0.001$.

(O) Summary of the role of Notch signaling in directing glial fate choices.

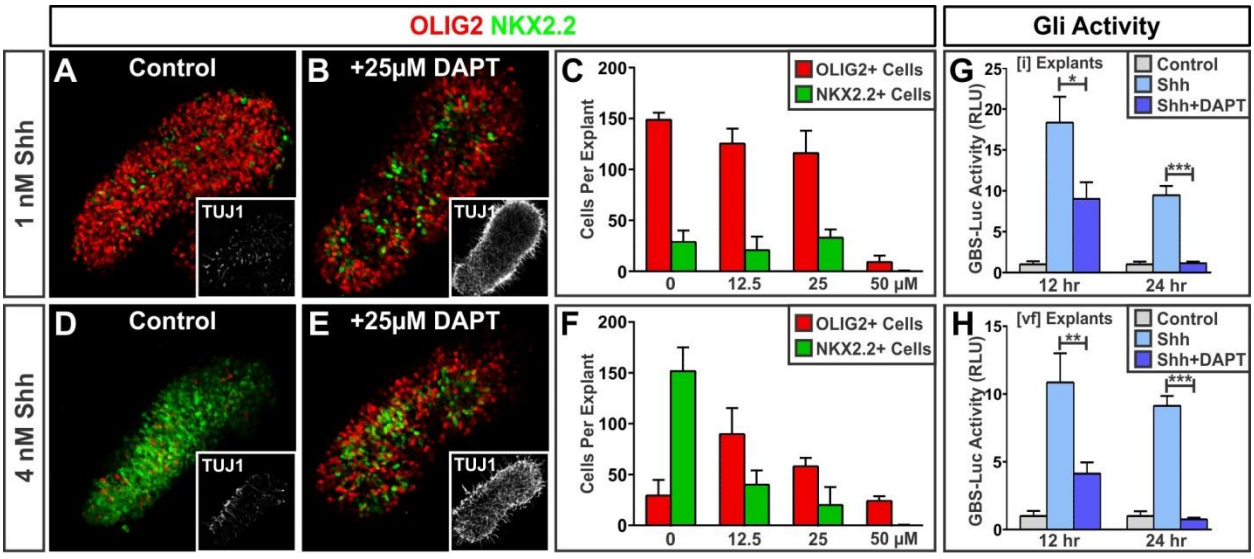

Figure 2-4: Inhibition of Notch reduces Gli activity and assignment of the p3 fate.

(A-B, D-E) Representative images of HH stage 10 chick intermediate neural plate [i] explants cultured for 24 hr in 1 or 4 nM Shh ± 25 μM DAPT. Explants were stained with Nkx2.2 and Olig2 antibodies to identify p3 and pMN cells. Insets show DAPT addition increases Tuj1^{+} neurons, as expected for a Notch inhibitor.

(C, F) Quantification of p3 and pMN cells present in [i] explants cultured in either 1 or 4 nM Shh and varying amounts of DAPT (0-50 μM). n ≥ 5 explants per condition and plots display cells/explant ± SEM.

(G) Gli activity measurements of [i] explants isolated from chick embryos electroporated with a GBS-Luciferase reporter construct and cultured with or without 4 nM Shh ± 25 μM DAPT. n ≥ 5 explants per condition were collected; plots display relative GBS-Luciferase activity (Relative Light Units) ± SEM.

(H) Gli activity measurements in [vf] explants isolated from embryos electroporated with the GBS-luciferase reporter and cultured in the presence or absence of 25 μM DAPT. n ≥ 5 explants per condition; relative GBS-Luciferase activity ± SEM. *p < 0.05, **p < 0.01, ***p < 0.001.

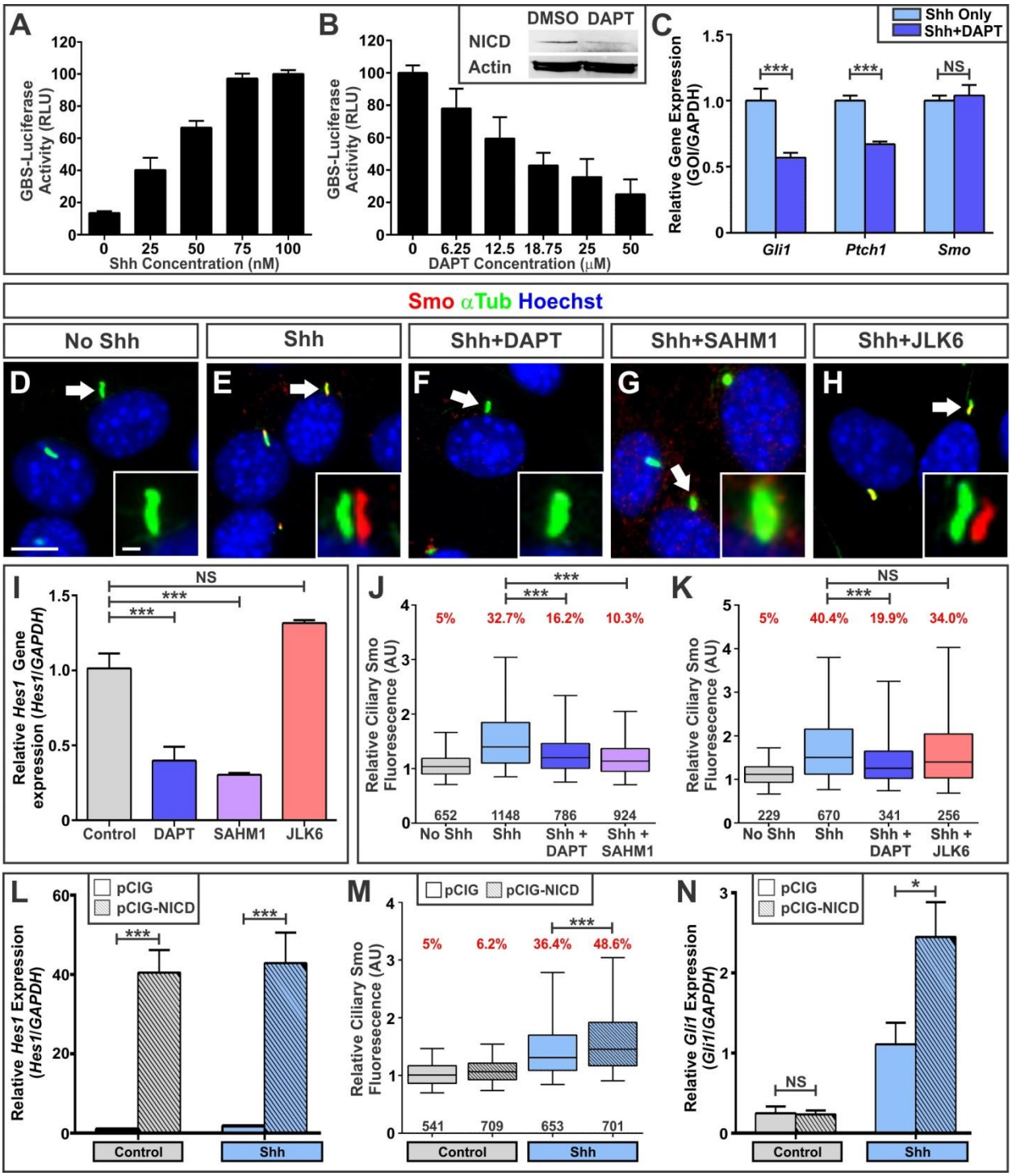
A
GBS-Luciferase Activity (RLU)
Shh Concentration (nM)
B
DMSO DAPT
NICD
Actin
DAPT Concentration (μM)
C
Shh Only
Shh+DAPT
Relative Gene Expression (GOI/GAPDH)
Gli1
Ptch1
Smo
Smo αTub Hoechst
No Shh
Shh
Shh+DAPT
Shh+SAHM1
Shh+JLK6
D
E
F
G
H
I
Relative Hes1 Gene expression (Hes1/GAPDH)
Control
DAPT
SAHM1
JLK6
J
Relative Ciliary Smo Fluorescence (AU)
5%
32.7%
16.2%
10.3%
652
1148
786
924
No Shh
Shh
Shh + DAPT
Shh + SAHM1
K
5%
40.4%
19.9%
34.0%
229
670
341
256
No Shh
Shh
Shh + DAPT
Shh + JLK6
L
pCIG
pCIG-NICD
Relative Hes1 Expression (Hes1/GAPDH)
Control
Shh
M
pCIG
pCIG-NICD
Relative Ciliary Smo Fluorescence (AU)
5%
6.2%
36.4%
48.6%
541
709
653
701
Control
Shh
N
pCIG
pCIG-NICD
Relative Gli1 Expression (Gli1/GAPDH)
NS
Control
Shh

Figure 2-5: Notch signaling regulates the ciliary location of Smo and Shh pathway activity in fibroblasts.

(A-B) GBS-luciferase reporter activity in 3T3 Shh-LIGHT2 cells cultured in either Shh (0-100 nM) or a range of DAPT (0-50 μM) in the presence of a single concentration of Shh (50 nM). Points represent mean GBS-luciferase activity (Relative Light Units) ± SEM from 4-6 independent samples. Inset shows immunoblotting for cleaved NICD and Actin.

(C) qPCR analysis of *Gli1*, *Ptch1*, and *Smo* expression in NIH-3T3 cells cultured in Shh (50 nM) ± DAPT (18.75 μM). Plot shows mean *Gapdh*-normalized gene expression levels ± SEM from 6 samples. Not significant (NS), $p > 0.05$; ***$p < 0.001$.

(D-H) Changes in the localization of Smo to primary cilia of NIH-3T3 cells treated with Shh and Notch inhibitors (DAPT, 18.75 μM and SAHM1, 20 μM) or a γ-secretase inhibitor that spares Notch function (JLK6, 20 μM). Cells were immunostained for αTubulin (αTub) (green), Smo (red), and Hoechst (blue, nuclei). Arrows denote cilia in the insets where Smo and αTub channels are offset to show colocalization. Low and High mag scale bars = 10 and 1 μm.

(I) qPCR analysis of *Hes1* in NIH-3T3 cells exposed to DAPT (18.75 μM), SAHM1 (20 μM), or JLK6 (20 μM). Plots show mean *Gapdh*-normalized mRNA expression levels relative to unstimulated controls ± SEM from 3-5 samples. *$p < 0.05$, **$p < 0.01$, ***$p < 0.001$.

(J-K) Box and whisker plots of ciliary Smo fluorescence in NIH-3T3 cells treated as indicated. The number of cilia analyzed in each group is indicated in black. The percentage of cilia with Smo is indicated in red. NS, $p > 0.05$, ***$p < 0.001$.

(L, N) qPCR analysis of *Hes1* and *Gli1* in NIH-3T3 cells transiently transfected with pCIG or pCIG-NICD vectors and then cultured in the presence or absence of Shh (50 nM). Plots show mean *Gapdh*-normalized expression levels relative to pCIG controls ± SEM from 5-6 samples for each condition. **(M)** Box and whisker plots of the ciliary Smo fluorescence in transfected cells. NS, $p > 0.05$, *$p < 0.05$, ***$p < 0.001$.

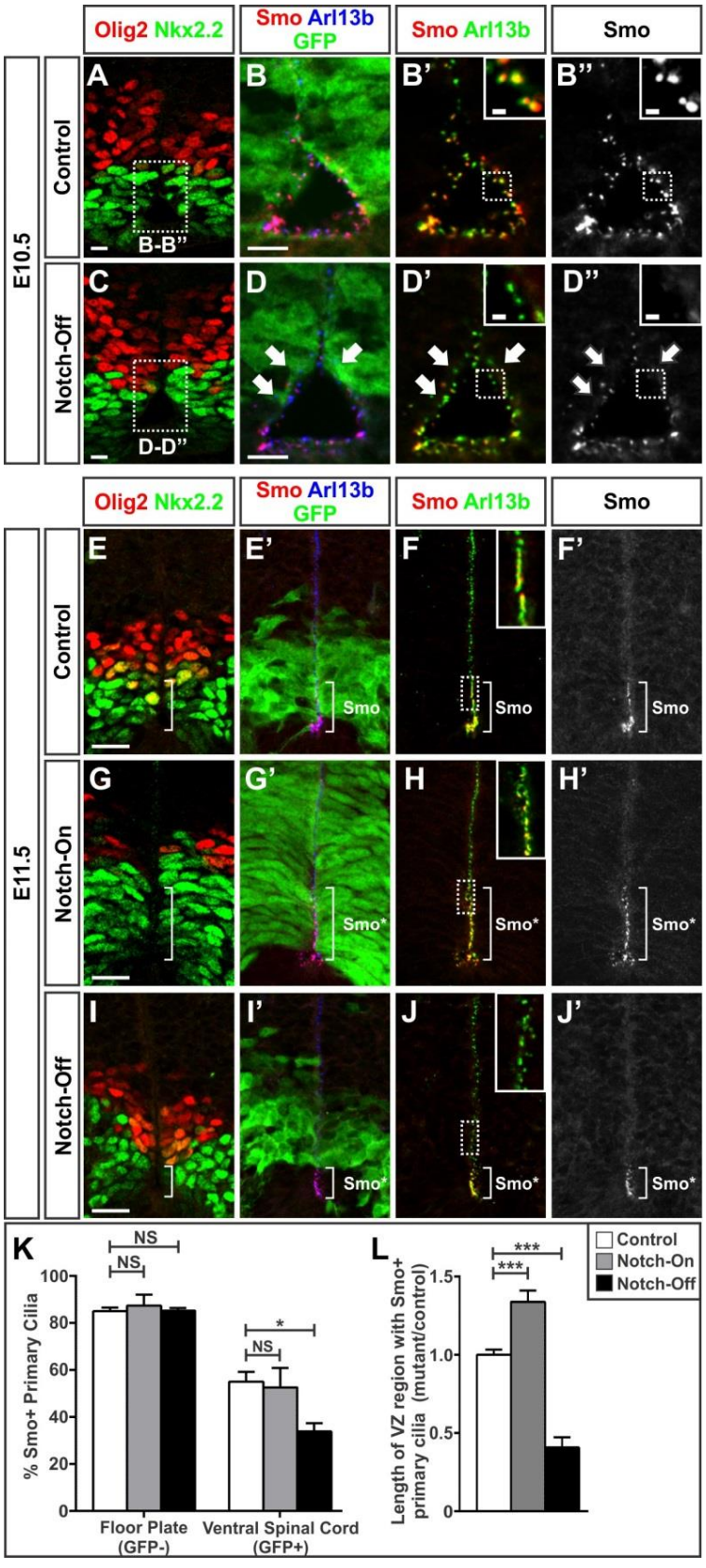
Olig2 Nkx2.2
Smo Arl13b GFP
Smo Arl13b
Smo
E10.5
Control
Notch-Off
A
B
B'
B''
B-B''
C
D
D'
D''
D-D''
E11.5
Notch-On
E
E'
F
F'
G
G'
H
H'
I
I'
J
J'
Smo
Smo*
K
% Smo+ Primary Cilia
NS
NS
*
NS
Floor Plate (GFP-)
Ventral Spinal Cord (GFP+)
L
Length of VZ region with Smo+ primary cilia (mutant/control)
***
***
Control
Notch-On
Notch-Off

Figure 2-6: Notch signaling influences the ciliary accumulation of Smo in ventral spinal cord NPCs.

(A-D) Analysis of Smo^+ primary cilia present on ventral progenitors in E10.5 embryos. Arrows in (D) indicate regions of Cre recombination. In Notch-Off embryos, ciliary Smo is absent in recombined regions. Low (A, C) and high (B, D) mag scale bars = 10 μm and 2 μm.

(E-J) Analysis of primary cilia in E11.5 embryos. Brackets illustrate the dorsoventral extent of Smo^+ primary cilia, a region where $Nkx2.2^+$ p3 cells are present. Scale bars = 20 μm.

(K) Quantification of Smo^+ primary cilia at E10.5 counted from the GFP- floor plate and GFP^+ ventral progenitors. Plots show the mean percentage of Smo^+ primary cilia ± SEM from multiple sections collected from 3-4 embryos from each group. NS, $p > 0.05$ and $*p < 0.05$.

(L) Quantification of the dorsoventral limits of Smo^+ primary cilia at E11.5. Plots show mean lengths of the ventricular zone lined with Smo^+ cilia ± SEM. All measured lengths were normalized to littermate controls. Analysis was conducted on multiple sections collected from 3-9 embryos from each experimental group. $*p < 0.05$, $**p < 0.01$, $***p < 0.001$.

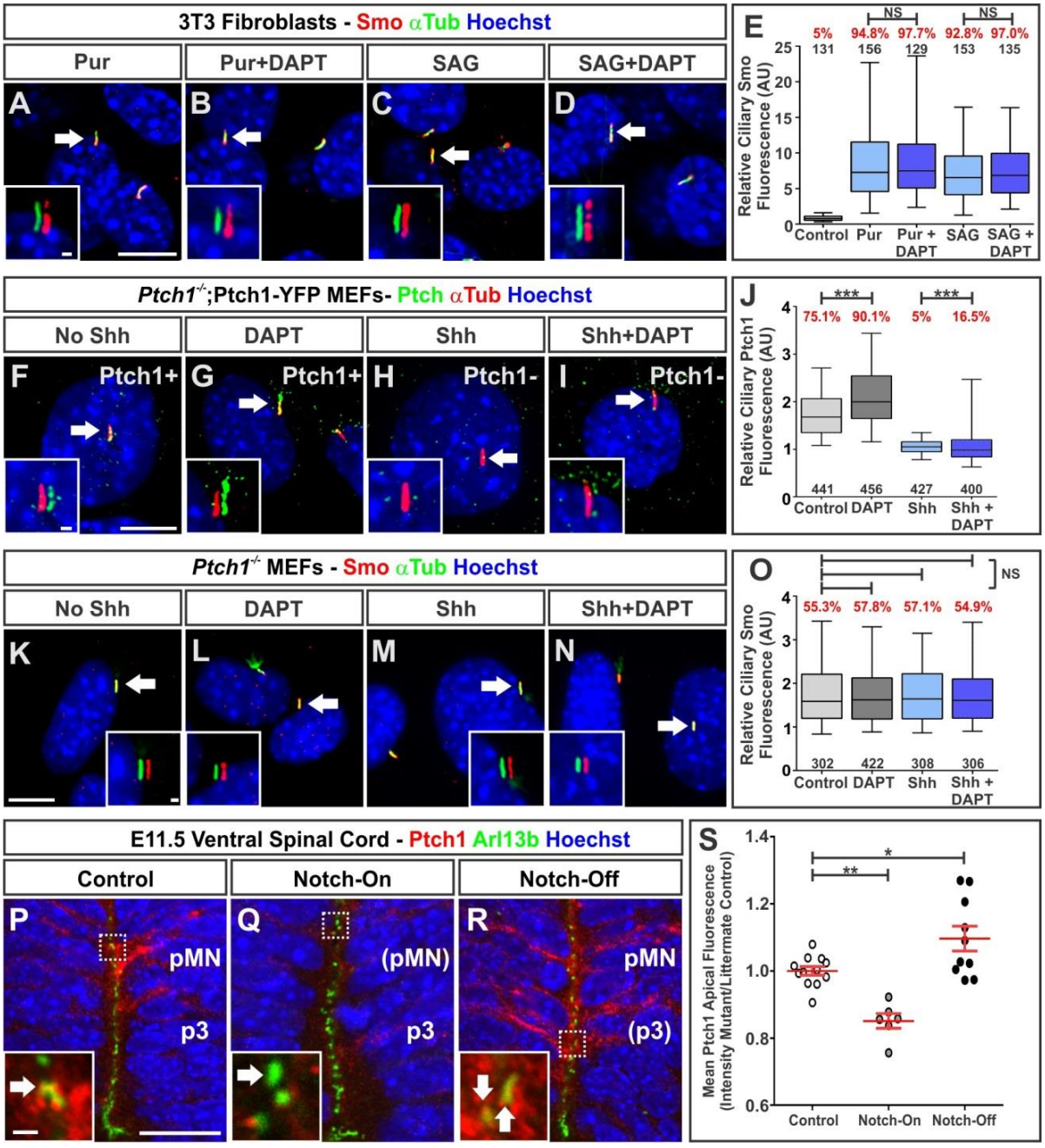
3T3 Fibroblasts - Smo αTub Hoechst
Pur
Pur+DAPT
SAG
SAG+DAPT
A
B
C
D
E
NS
NS
5%
94.8%
97.7%
92.8%
97.0%
131
156
129
153
135
Relative Ciliary Smo Fluorescence (AU)
Control
Pur
Pur + DAPT
SAG
SAG + DAPT
Ptch1-/-;Ptch1-YFP MEFs- Ptch αTub Hoechst
No Shh
DAPT
Shh
Shh+DAPT
F
Ptch1+
G
Ptch1+
H
Ptch1-
I
Ptch1-
J
***
***
75.1%
90.1%
5%
16.5%
441
456
427
400
Relative Ciliary Ptch1 Fluorescence (AU)
Control
DAPT
Shh
Shh + DAPT
Ptch1-/- MEFs - Smo αTub Hoechst
No Shh
DAPT
Shh
Shh+DAPT
K
L
M
N
O
NS
55.3%
57.8%
57.1%
54.9%
302
422
308
306
Relative Ciliary Smo Fluorescence (AU)
Control
DAPT
Shh
Shh + DAPT
E11.5 Ventral Spinal Cord - Ptch1 Arl13b Hoechst
Control
Notch-On
Notch-Off
P
pMN
p3
Q
(pMN)
p3
R
pMN
(p3)
S
*
**
Mean Ptch1 Apical Fluorescence (Intensity Mutant/Littermate Control)
Control
Notch-On
Notch-Off

Figure 2-7: Notch signaling regulates Ptch1 presence in and around primary cilia.

(A-D) Analysis of Smo enrichment in primary cilia of NIH-3T3 cells treated with Pur (5 μM) or SAG (1 μM) ± DAPT (18.75 μM). Arrows denote cilia shown in the insets, in which Smo and αTub are offset to show colocalization. Low and high mag scale bars = 10 μm and 1 μm.

(E) Box and whisker plots of ciliary Smo fluorescence in NIH-3T3 cells treated with Pur or SAG ± DAPT. The black numbers indicate the number of cilia analyzed. The red numbers indicate the percentage of cilia with Smo. NS, $p > 0.05$.

(F-I) Ciliary enrichment of Ptch1 in *Ptch1*$^{-/-}$*;Ptch1-YFP* MEFs after exposure to DAPT (18.75 μM) with or without Shh (50 nM). Low and high mag scale bars = 10 μm and 1 μm.

(J) Box and whisker plots of ciliary Ptch1 fluorescence in *Ptch1*$^{-/-}$*;Ptch1-YFP* MEFs. ***$p < 0.001$.

(K-N) Analysis of Smo localization in *Ptch1-/-* MEFs treated with or without Shh (50 nM) ± DAPT (18.75 μM). Arrows denote cilia shown in the insets, in which Smo and αTub channels are offset to show colocalization. Scale bars = 10 μm and 1 μm (insets).

(O) Box and whisker plots of ciliary Smo fluorescence in *Ptch1-/-* MEFs treated with or without Shh (50 nM) ± DAPT (18.75 μM). NS, $p > 0.05$.

(P-R) Apical Ptch1 staining in the ventral spinal cord of E11.5 embryos. The pMN and p3 labels were determined by serial section staining for Olig2 and Nkx2.2 (not shown). Insets show Ptch1 presence in Arl13b-stained primary cilia. Scale bars = 20 μm and 1 μm (insets).

(S) Scatterplot of the mean intensity of apical Ptch1 staining in a 250 μm^2 area ± SEM. Each point represents the mean intensity from multiple sections collected from single embryo. Each group is comprised of data from 6-12 embryos. The intensity of Ptch1 was normalized to littermate controls. *$p < 0.05$, **$p < 0.01$.

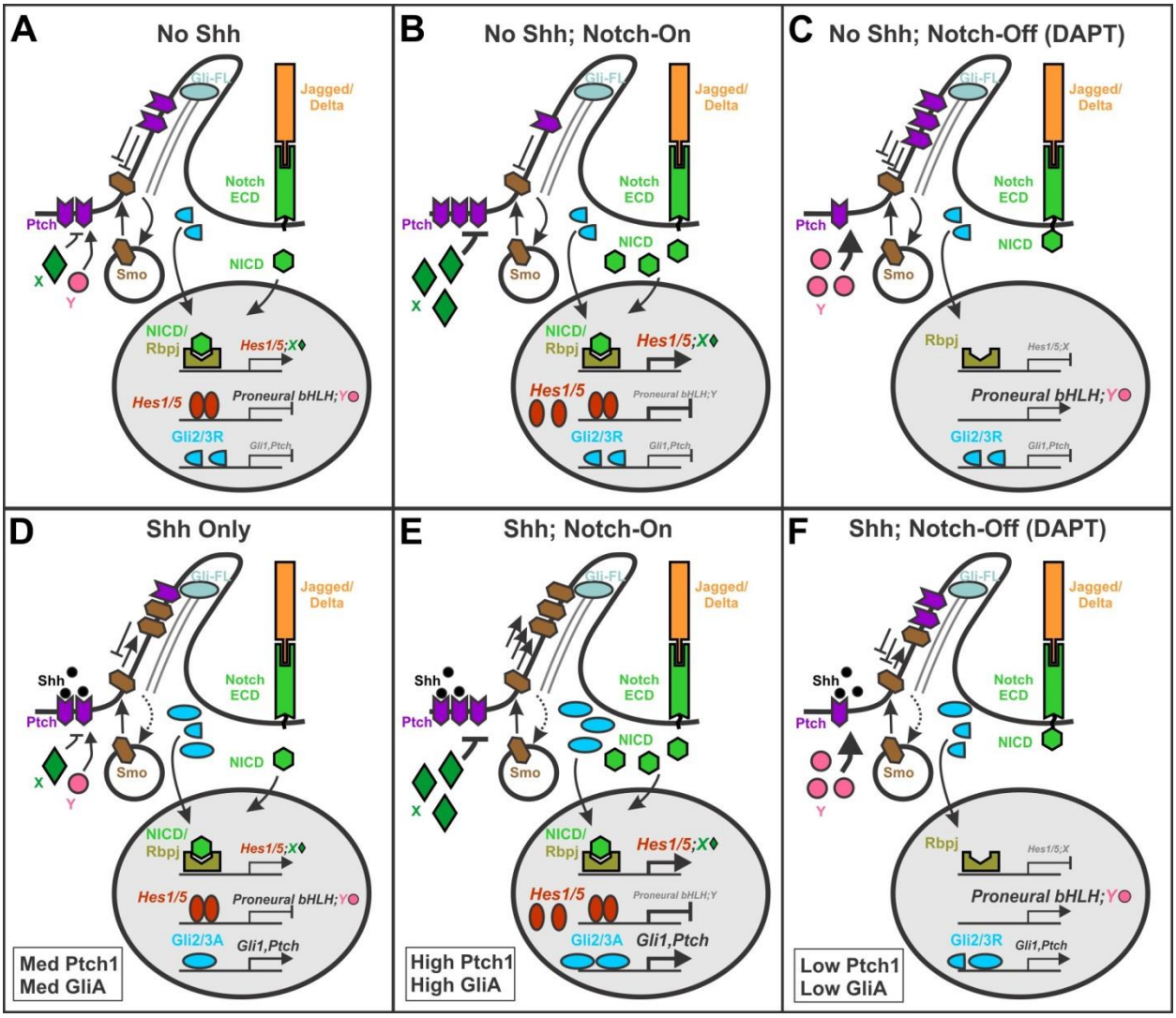
A
No Shh
Gli-FL
Jagged/
Delta
Notch
ECD
Ptch
Smo
NICD
X
Y
NICD/
Rbpj
Hes1/5;X
Hes1/5
Proneural bHLH;Y
Gli2/3R
Gli1,Ptch
B
No Shh; Notch-On
C
No Shh; Notch-Off (DAPT)
Rbpj
D
Shh Only
Shh
Gli2/3A
Med Ptch1
Med GliA
E
Shh; Notch-On
High Ptch1
High GliA
F
Shh; Notch-Off (DAPT)
Low Ptch1
Low GliA

Figure 2-8: Models for interactions between Notch and Shh signaling

Models depicting how Notch signaling modulates cellular responses to Shh by regulating the movement of Ptch1 to the primary cilia.

(A, D) In the absence of Shh, Ptch1 is present within and adjacent to primary cilia. Shh ligand binds to Ptch1, permitting Smo entry into the cilia where it stimulates Gli transcriptional activities. Direct downstream effectors of Notch signaling that promote Ptch1 clearance from primary cilia (X) and indirect effectors suppressed by Hes genes (Y) that increase Ptch1 ciliary accumulation are depicted.

(B, E) Notch activation via the ectopic expression of NICD reduces Ptch1 presence within primary cilia facilitating Smo entry and activation of Gli proteins.

(C, F) Notch inhibition, via the addition of DAPT or removal of Rbpj, elevates the presence of Ptch1 within primary cilia. Smo entry is impeded and Gli activities correspondingly reduced.

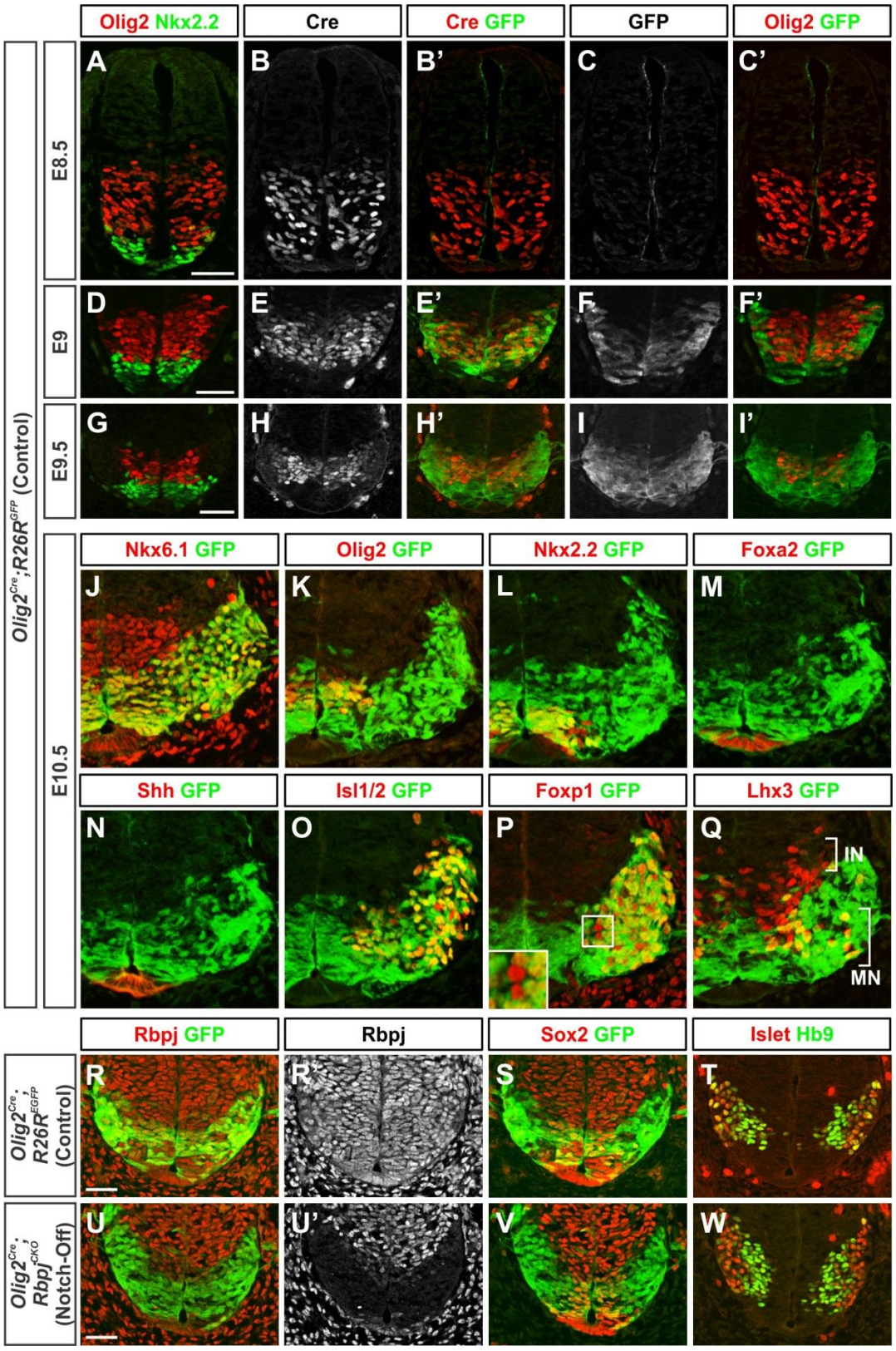
Olig2 Nkx2.2
Cre
Cre GFP
GFP
Olig2 GFP
A
B
B'
C
C'
E8.5
D
E
E'
F
F'
E9
G
H
H'
I
I'
E9.5
Olig2Cre;R26RGFP (Control)
Nkx6.1 GFP
Olig2 GFP
Nkx2.2 GFP
Foxa2 GFP
J
K
L
M
E10.5
Shh GFP
Isl1/2 GFP
Foxp1 GFP
Lhx3 GFP
N
O
P
Q
IN
MN
Rbpj GFP
Rbpj
Sox2 GFP
Islet Hb9
Olig2Cre; R26REGFP (Control)
R
R'
S
T
Olig2Cre; RbpjcKO (Notch-Off)
U
U'
V
W

Supplementary Figure 2-S1: Temporal and spatial documentation of *Olig2^{Cre}* mediated recombination

(A-I) Serial transverse spinal cord sections from E8.5-E9.5 Control (*Olig2^{Cre}; R26R^{GFP}*) embryos. Tissue was immunostained with Nkx2.2, Olig2, Cre, and GFP antibodies to assess where and when recombination occurred. Scale bars = 50 μm.

(J-Q) Analysis of E10.5 *Olig2^{Cre}; R26R^{GFP}* Control embryos shows that Cre recombination takes place in both the pMN (Nkx6.1^{+}/Olig2^{+}) and p3 (Nkx6.1^{+}/Nxk2.2^{+}) domains, but not in the floor plate (Foxa2^{+} or Shh^{+}). At this time point, Cre recombination had occurred in nearly all MNs (Isl1/2^{+}), including both LMC (FoxP1^{+}) and MMC (Lhx3^{+}) subgroups. Inset in (P) reveals a small population of non-recombined MNs. Note that Lhx3 is also prominently expressed by newborn V2 interneurons that form above the motor columns.

(R-W) Notch-Off embryos display an absence of Rbpj protein from pMN, p3 progenitors, and differentiated (Islet^{+}/Hb9^{+}) MNs starting around E9.5. Note that Sox2 is maintained in pMN/p3 cells despite the loss of Rbpj. Scale bars = 50 μm.

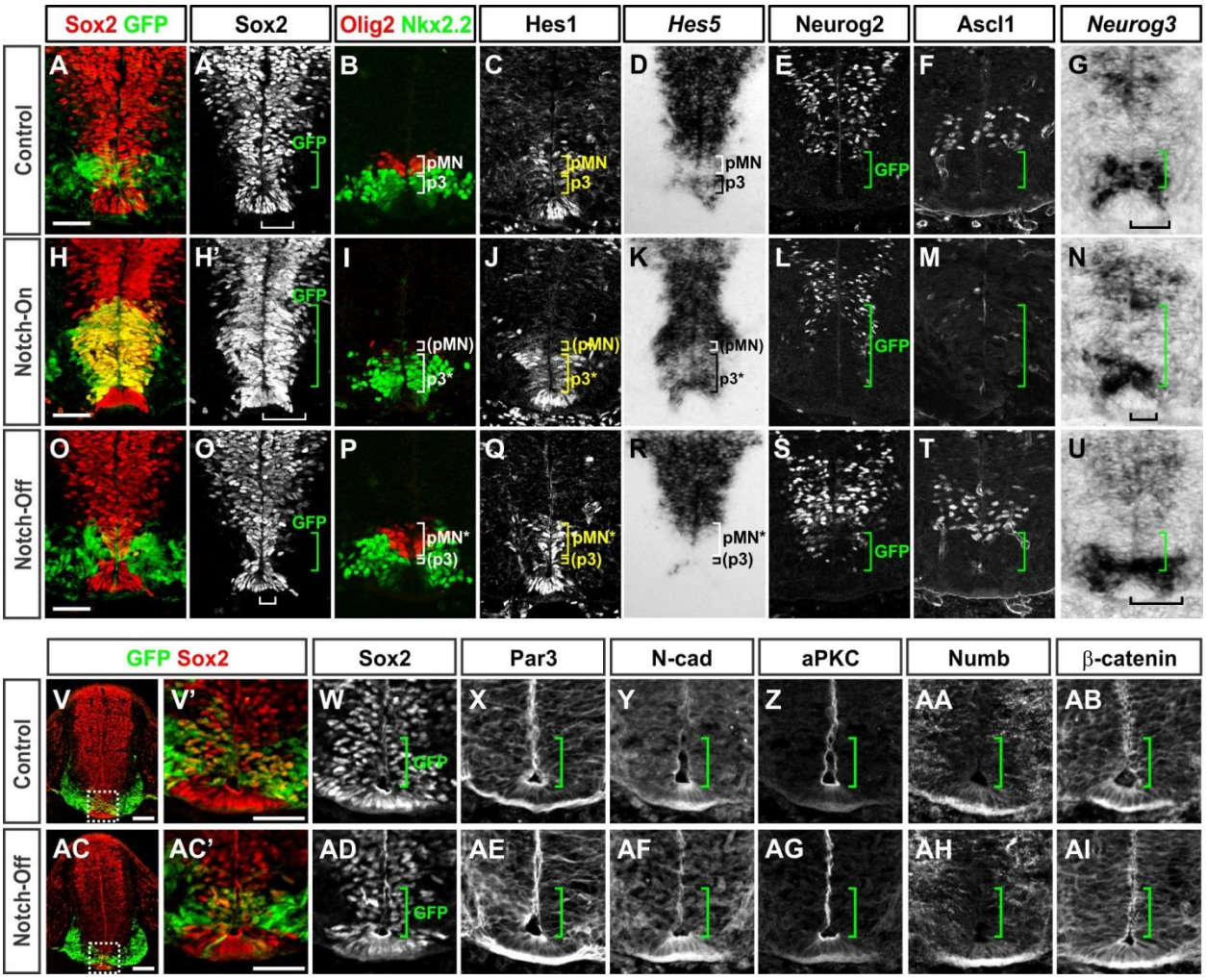
Sox2 GFP
Sox2
Olig2 Nkx2.2
Hes1
Hes5
Neurog2
Ascl1
Neurog3
Control
Notch-On
Notch-Off
A
A'
B
C
D
E
F
G
H
H'
I
J
K
L
M
N
O
O'
P
Q
R
S
T
U
GFP
pMN
p3
(pMN)
p3*
pMN*
(p3)
GFP Sox2
Par3
N-cad
aPKC
Numb
β-catenin
V
V'
W
X
Y
Z
AA
AB
AC
AC'
AD
AE
AF
AG
AH
AI

Supplementary Figure 2-S2: Notch signaling is activated in Notch-On embryos and reduced in Notch-Off embryos without any major disruptions to the neuroepithelial organization

(A-U) Analysis of Notch signaling activity in Control (A-G), Notch-On (H-N), and Notch-Off (O-U) E11.5 embryos. (A, H, O) Green brackets demarcate the dorsoventral extent of the GFP^+ region of recombination and white brackets indicate the thickness of the $Sox2^+$ ventricular zone (VZ) within this same region. As predicted, NICD misexpression (Notch-On) expands the thickness of the $Sox2^+$ VZ, increases expression of canonical downstream Notch effectors (Hes1 and *Hes5*), and reduces expression of proneural transcription factors (Neurog2, Ascl1, and *Neurog3*). Conversely, Rbpj deletion (Notch-Off) has the opposite effect. Note, however, that Sox2 and Hes1 expression are maintained in the ventral spinal cord despite the removal of Rbpj (panels O and Q). Scale bars = 50 μm.

(V-AI) The neuroepithelial architecture and apicobasal polarity of neural progenitors is preserved in the ventral spinal cord of Notch-Off (AC-AI) E11.5 embryos. Within the region of recombination (marked by the green brackets), the lasting integrity of the ventricular zone is apparent through the maintenance of $Sox2^+$ progenitors and the continued presence of various cell polarity components (Par3, aPKC, and Numb) and cell adhesion molecules (N-cadherin and β-catenin). Scale bars = 100 μm.

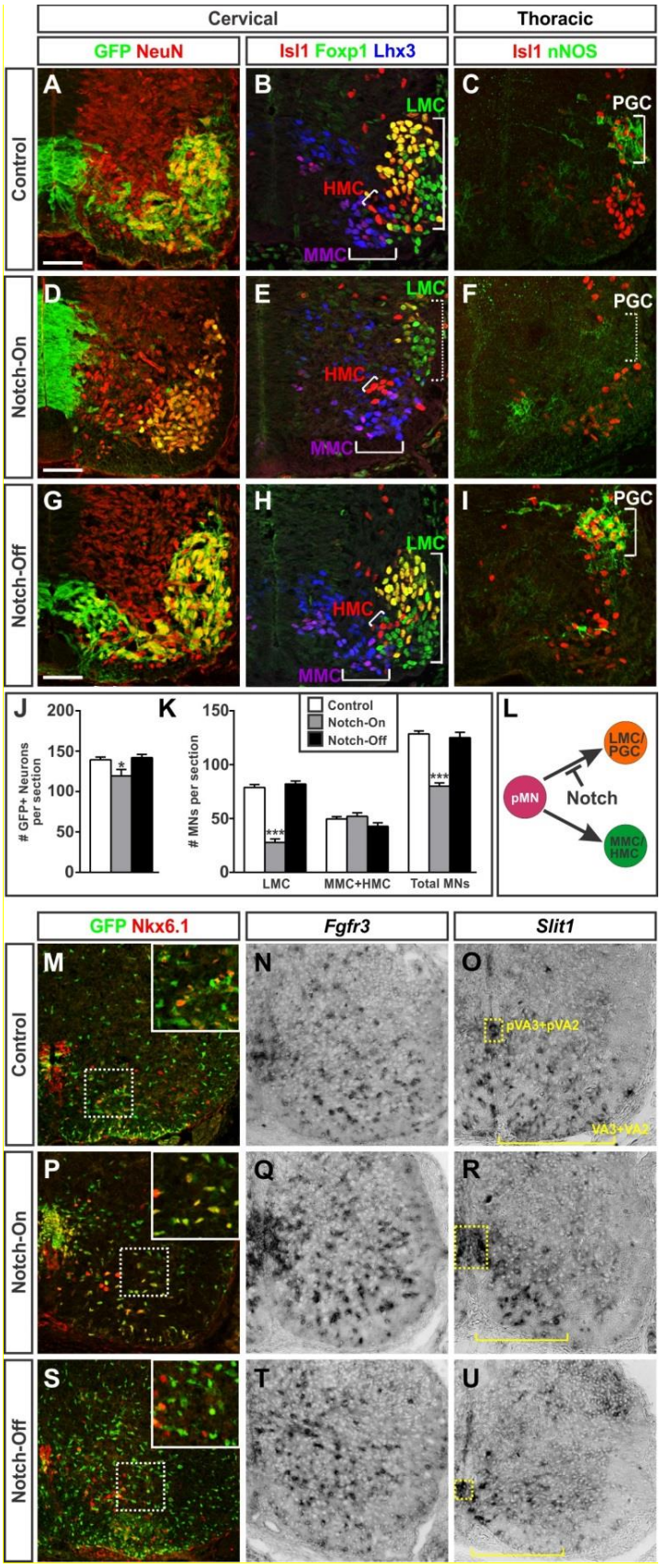
Cervical
Thoracic
GFP NeuN
Isl1 Foxp1 Lhx3
Isl1 nNOS
Control
Notch-On
Notch-Off
A
B
C
D
E
F
G
H
I
LMC
HMC
MMC
PGC
J
K
L
GFP+ Neurons per section
MNs per section
Control
Notch-On
Notch-Off
LMC
MMC+HMC
Total MNs
pMN
Notch
LMC/ PGC
MMC/ HMC
GFP Nkx6.1
Fgfr3
Slit1
M
N
O
P
Q
R
S
T
U
pVA3+pVA2
VA3+VA2

Supplementary Figure 2-S3: The effect of Notch signaling manipulations on MN and glial cell fates

(A-I) In E11.5 embryos, *Olig2*^{Cre}-derived neurons (GFP$^+$/NeuN$^+$) include LMC (FoxP1$^+$), HMC (Isl1$^+$/FoxP1$^-$/Lhx3$^-$), MMC (Isl1$^+$/FoxP1$^-$/Lhx3$^+$), and PGC (Isl1$^+$/nNOS$^+$) MNs. Scale bars = 50 µm.

(J) Quantification of the total number of recombined neurons (GFP$^+$/NeuN$^+$) per spinal cord half. Plots show the mean ± SEM from multiple sections collected from 11-13 embryos from each experimental condition. NS, $p > 0.05$ and $^*p < 0.05$.

(K) Quantification of the total number of MNs (Isl1$^+$ and/or Hb9$^+$), LMC MNs (FoxP1$^+$), and MMC plus HMC MNs (Foxp1$^-$ Isl1$^+$ Lhx3$^+$ and Foxp1$^-$ Isl1$^+$ Lhx3$^-$) per spinal cord half. In this analysis, all MNs were counted regardless of their GFP expression. Plots show the mean ± SEM from multiple sections collected from 8-30 embryos from each experimental condition. NS, $p > 0.05$ and $^{***}p < 0.001$.

(L) Summary of the role of Notch signaling in directing MN cell fates.

(M-U) Analysis of the impact of Notch manipulations on glial cell fates at E18.5.

(M-O) In Control embryos, *Olig2*^{Cre}-derivatives marked by GFP expression include pVA3 astrocyte progenitors and differentiated VA3 astrocytes that express Nkx6.1 (Hochstim et al, 2008). Serial section analysis reveals the presence of *Fgfr3*, which is expressed by multiple groups of astrocyte progenitors, and *Slit1*, which is selectively expressed by VA3 progenitors and differentiated astrocytes (Hochstim et al, 2008).

(P-U) Notch activation increases while Notch inactivation decreases the production of cells expressing the pVA3 and VA3 markers Nkx6.1, *Fgfr3*, and *Slit1*.

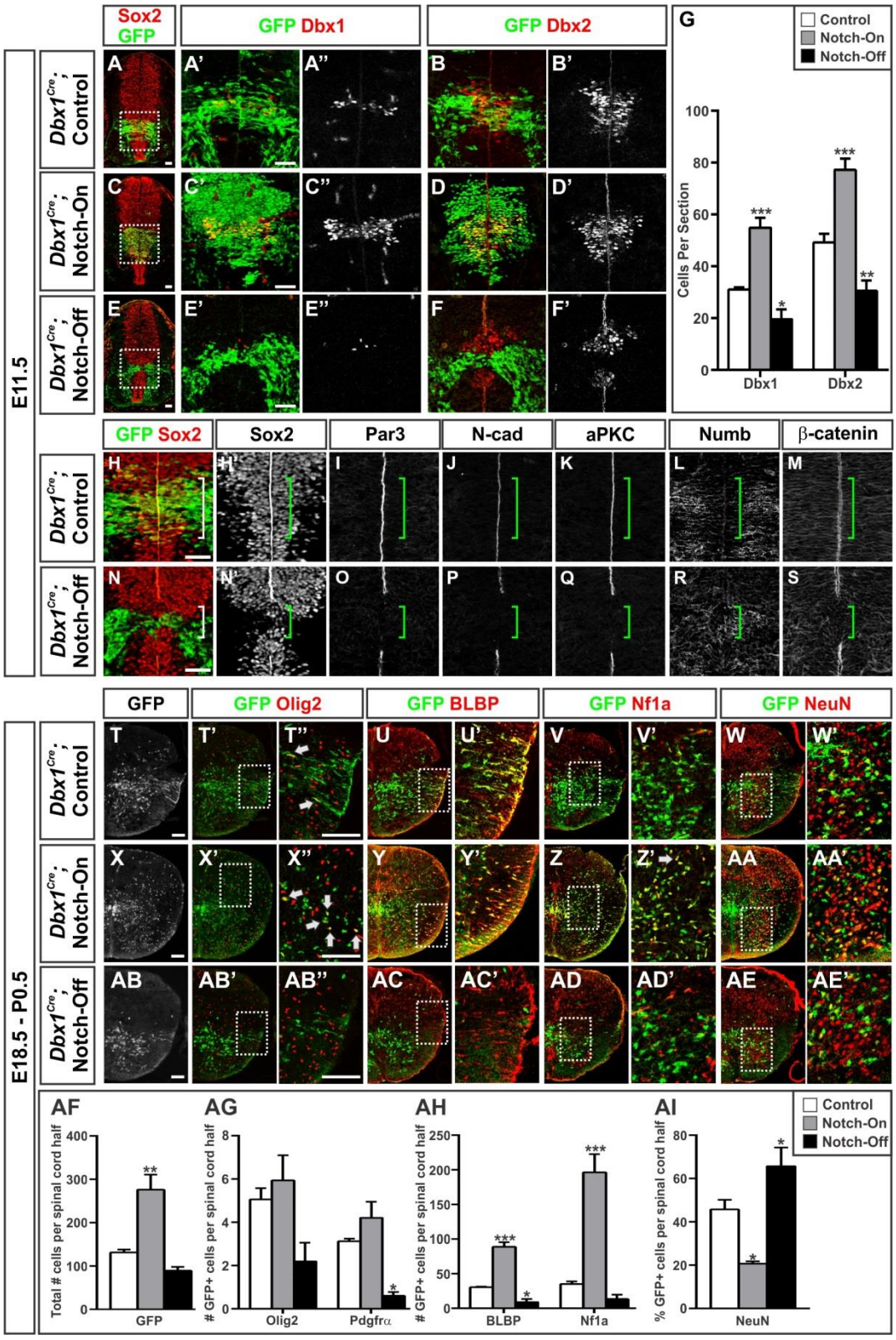
E11.5
E18.5 - P0.5
Dbx1Cre; Control
Dbx1Cre; Notch-On
Dbx1Cre; Notch-Off
Sox2 GFP
GFP Dbx1
GFP Dbx2
G
Control
Notch-On
Notch-Off
Cells Per Section
Dbx1
Dbx2
GFP Sox2
Sox2
Par3
N-cad
aPKC
Numb
β-catenin
GFP
GFP Olig2
GFP BLBP
GFP Nf1a
GFP NeuN
AF
AG
AH
AI
Total # cells per spinal cord half
GFP+ cells per spinal cord half
% GFP+ cells per spinal cord half
GFP
Olig2
Pdgfrα
BLBP
Nf1a
NeuN

Supplementary Figure 2-S4: Manipulation of Notch signaling alters neuronal differentiation and progenitor maintenance in the intermediate spinal cord without overt changes in dorsoventral patterning or glial identities

(A-F) In E11.5 control embryos, *Dbx1*^{Cre}-mediated recombination occurs within p0 (Dbx1^{+} Dbx2^{+}) and p1 (Dbx1^{-} Dbx2^{+}) progenitors. Notch activation increases while Notch inactivation decreases the formation of these cells. Scale bars = 50 µm. **(G)** Quantification of the total number of Dbx1^{+} and Dbx2^{+} progenitors present in E11.5 Control, Notch-On, and Notch-Off embryos. For this analysis, progenitors were counted regardless of their GFP expression. Plots represent mean cell counts ± SEM from multiple sections collected from 6-8 embryos from each transgenic line. *p < 0.05, **p < 0.01, ***p < 0.001. **(H-S)** The neuroepithelial architecture and apicobasal polarity of neural progenitors is greatly disrupted in the intermediate spinal cord of E11.5 *Dbx1*^{Cre}; Notch-Off embryos (N-S). Within the region of recombination, this disruption can be observed through the complete loss of Sox2^{+} progenitors, cell polarity components (Par3 and aPKC), and cell-to-cell adhesion molecules (N-cadherin and β-catenin). Green brackets demarcate recombination. Scale bars = 100 µm. **(T-AE)** In E18.5 Control embryos and P0.5 neonates, GFP^{+} Dbx1^{Cre}-derivatives include astrocyte precursors and astrocytes (BLBP^{+}/Nf1a^{+}), differentiated neurons (NeuN^{+}), but only a small number of oligodendrocyte precursors (OLPs) (Olig2^{+} or Pdgfrα^{+}). Notch activation increases the formation of astrocyte progenitors and astrocytes while reducing neurogenesis. Notch inactivation has the opposite effect. In contrast to *Olig2*^{Cre}-mediated manipulations, *Dbx1*^{Cre}-mediated Notch activation does not show any suppressive effect on oligodendrocyte formation. Likewise, *Dbx1*^{Cre}-mediated Notch inactivation does not lead to the formation of ectopic oligodendrocyte progenitors. Scale bars = 100 µm. **(AF-AI)** Quantification of the total number of GFP^{+} cells per spinal cord half, GFP^{+} OLPs (GFP^{+}/Olig2^{+} and GFP^{+}/Pdgfrα^{+}), astrocyte precursors and astrocytes (GFP^{+}/BLBP^{+} and

$GFP^+/Nf1a^+$), and neurons ($GFP^+/NeuN^+$). Plots display the mean ± SEM from multiple sections collected from 4-5 embryos for each experimental condition. *$p < 0.05$, **$p < 0.01$, ***$p < 0.001$.

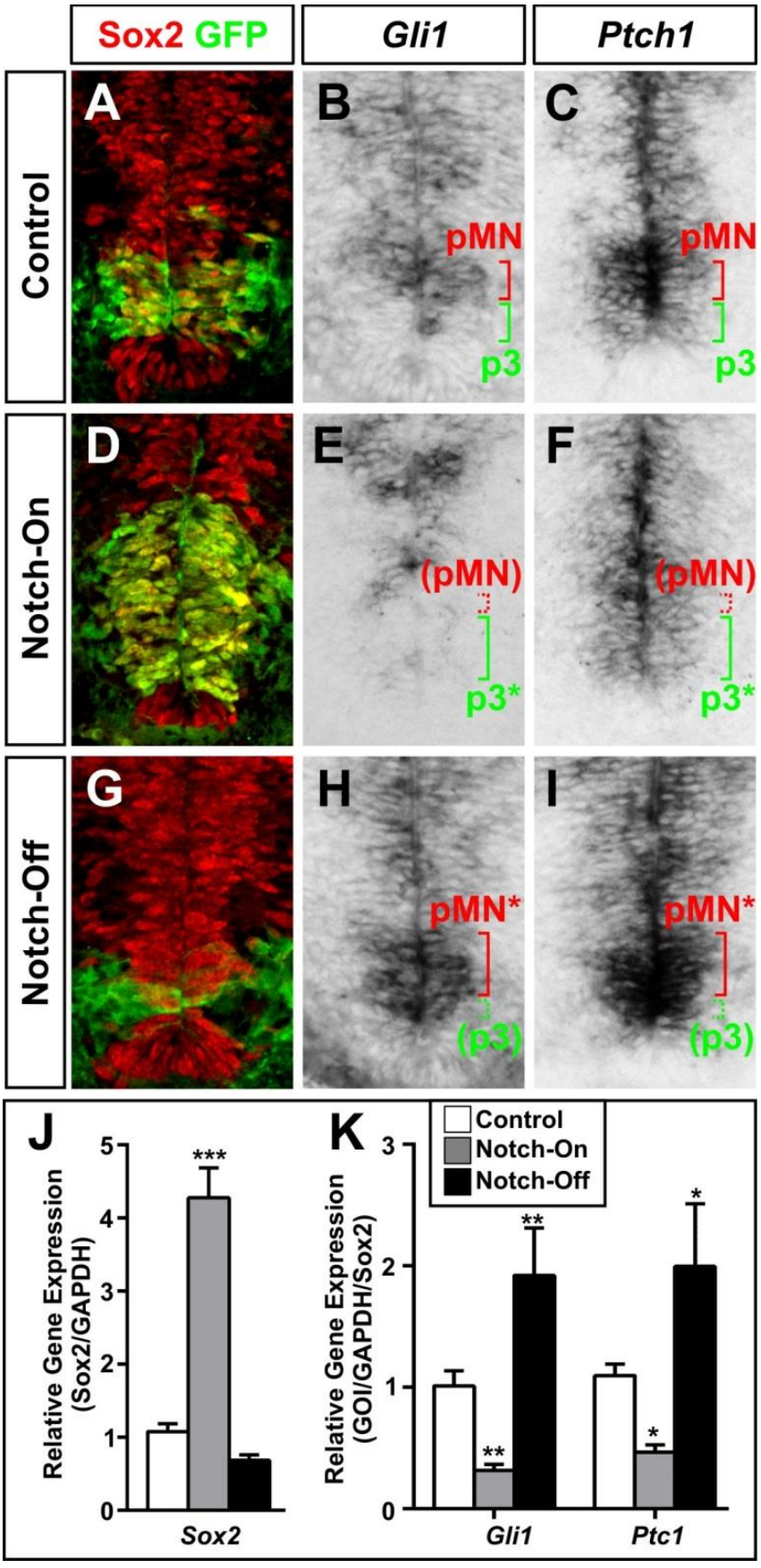
Sox2 GFP
Gli1
Ptch1
Control
Notch-On
Notch-Off
A
B
C
D
E
F
G
H
I
pMN
p3
(pMN)
p3*
pMN*
(p3)
J
Relative Gene Expression (Sox2/GAPDH)
Sox2
K
Control
Notch-On
Notch-Off
Relative Gene Expression (GOI/GAPDH/Sox2)
Gli1
Ptc1

Supplementary Figure 2-S5: Notch signaling manipulations modulate how progenitor cells respond to Shh within the ventral spinal cord

(A-I) Transverse spinal cord sections from Control, Notch-On, and Notch-Off E11.5 embryos immunostained with Sox2 and GFP to see the region of recombination and RNA in situ hybridization for *Gli1* and *Ptch1* to assess Shh signaling activity. The dorsoventral extent of the pMN and p3 domains, as denoted by the red and green brackets, was determined by staining serial sections (not shown).

(A-C) In Control ($Olig2^{Cre}$; $R26R^{EGFP}$) E11.5 embryos, $Olig2^{Cre}$-mediated recombination occurs predominantly with the pMN and p3 domains. At this age, *Gli1* and *Ptch1* mRNA expression is elevated in the pMN domain and reduced in the p3.

(D-I) Notch signaling activation (Notch-On) reduces the expression of *Gli1* and *Ptch1*, whereas Notch inhibition (Notch-Off) elevates these genes.

(J-K) Quantitative PCR analysis of FACS sorted GFP+ cells from E11.5 Control, Notch-On, and Notch-Off embryos. Gene expression was normalized against *Gapdh*. To account for the variability of Sox2+ progenitors across transgenic lines, *Gli1* and *Ptch1* expression was further normalized against *Sox2*. Plots represent the mean ± SEM from cells sorted from 5-10 embryos from each transgenic line.

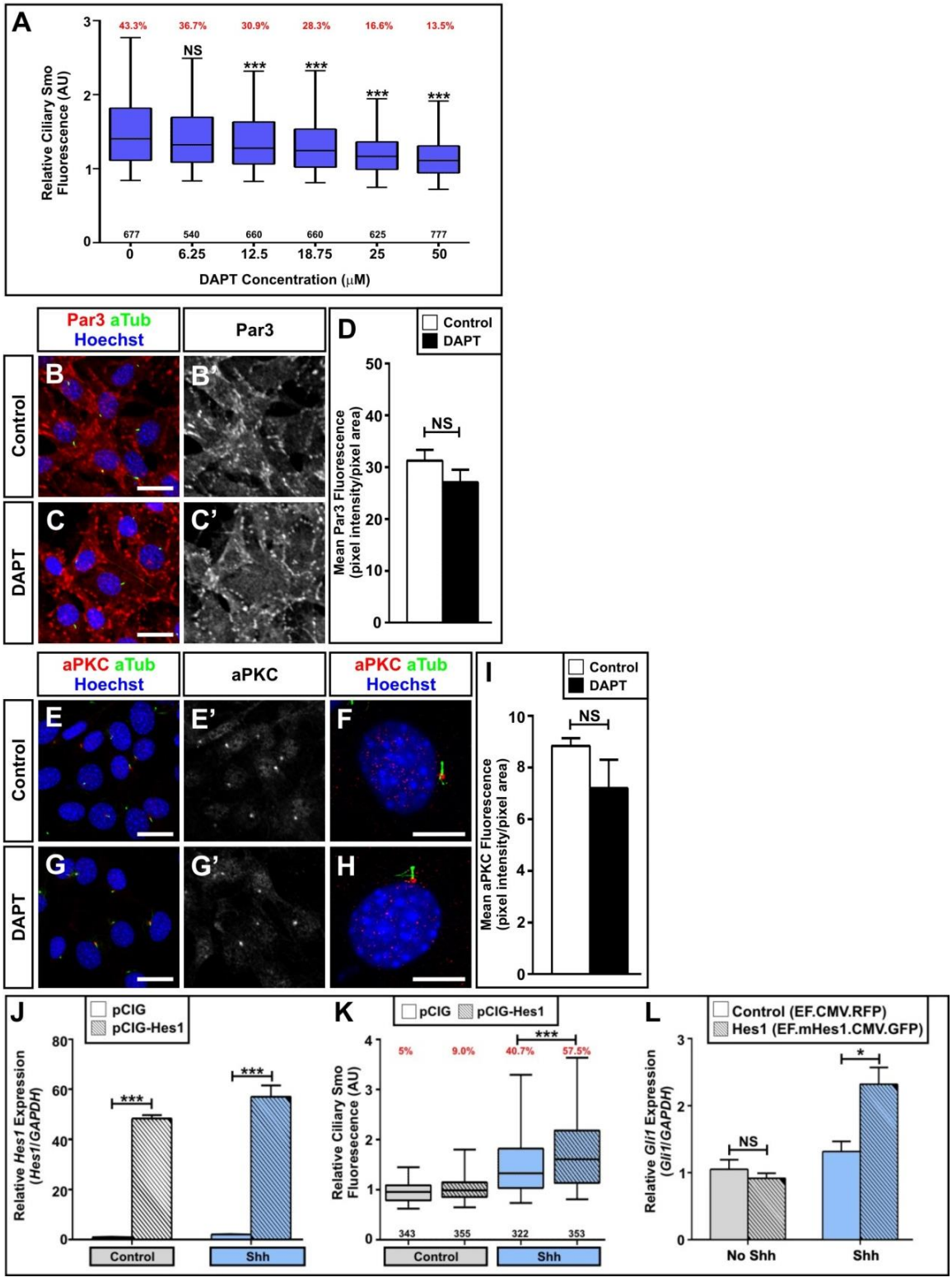
A
Relative Ciliary Smo Fluorescence (AU)
43.3%
36.7%
30.9%
28.3%
16.6%
13.5%
NS
***
***
***
***
677
540
660
660
625
777
0
6.25
12.5
18.75
25
50
DAPT Concentration (μM)
Par3 aTub Hoechst
Par3
Control
DAPT
B
B'
C
C'
D
Control
DAPT
Mean Par3 Fluorescence (pixel intensity/pixel area)
NS
aPKC aTub Hoechst
aPKC
aPKC aTub Hoechst
E
E'
F
G
G'
H
I
Control
DAPT
Mean aPKC Fluorescence (pixel intensity/pixel area)
NS
J
pCIG
pCIG-Hes1
Relative Hes1 Expression (Hes1/GAPDH)
***
***
Control
Shh
K
pCIG
pCIG-Hes1
Relative Ciliary Smo Fluorescence (AU)
5%
9.0%
40.7%
57.5%
***
343
355
322
353
Control
Shh
L
Control (EF.CMV.RFP)
Hes1 (EF.mHes1.CMV.GFP)
Relative Gli1 Expression (Gli1/GAPDH)
NS
*
No Shh
Shh

Supplementary Figure 2-S6: Inhibition of Notch signaling reduces Smo trafficking to the primary cilia of NIH-3T3 fibroblasts with no disruption to apicobasal polarity

(A) Box and whisker plots of Smo fluorescence in the cilia of NIH-3T3 cells cultured in the presence of 50 nM Shh and various doses of DAPT (0-50 μM). The box extends from the 25th to 75th percentile, the line through the box represents the median, and the whiskers encompass the 5th to 95th percentile. The number of cilia analyzed is indicated in black below the box plots and the percentage of Smo^{+} cilia indicated in red above the box plots. DAPT reduces Smo presence within the primary cilia in a dose-dependent manner. For statistical analyses, all DAPT doses were compared to the Control (DMSO) group. NS, $p > 0.05$ and *** $p < 0.001$.

(B-C) Par3 immunofluorescence analysis of Control (DMSO) and DAPT (18.75 μM) treated NIH-3T3 cells. Scale bars = 20 μm.

(D) Quantification of the mean intensity ± SEM of Par3 fluorescence in a 320 μm x 320 μm area.

(E-H) aPKC immunofluorescence analysis of Control (DMSO) and DAPT (18.75 μM) treated NIH-3T3 cells. Low mag scale bars = 20 μm. High mag scale bars = 10 μm.

(I) Quantification of the mean intensity ± SEM of aPKC fluorescence in a 320 μm x 320 μm area.

(J, L) qPCR analysis of *Hes1* and *Gli1* in NIH-3T3 cells transiently transfected with pCIG, pCIG-mHes1, EF.CMV.RFP, or EF.mHes1.CMV.GFP expression vectors and then cultured in the presence or absence of Shh for 12 hr. Plots show mean *Gapdh*-normalized expression levels relative to pCIG or EF.CMV.RFP controls ± SEM from 3-6 samples for each condition.

(K) Box and whisker plots of the ciliary Smo fluorescence in transfected cells. NS, $p > 0.05$, *$p < 0.05$, ***$p < 0.001$.

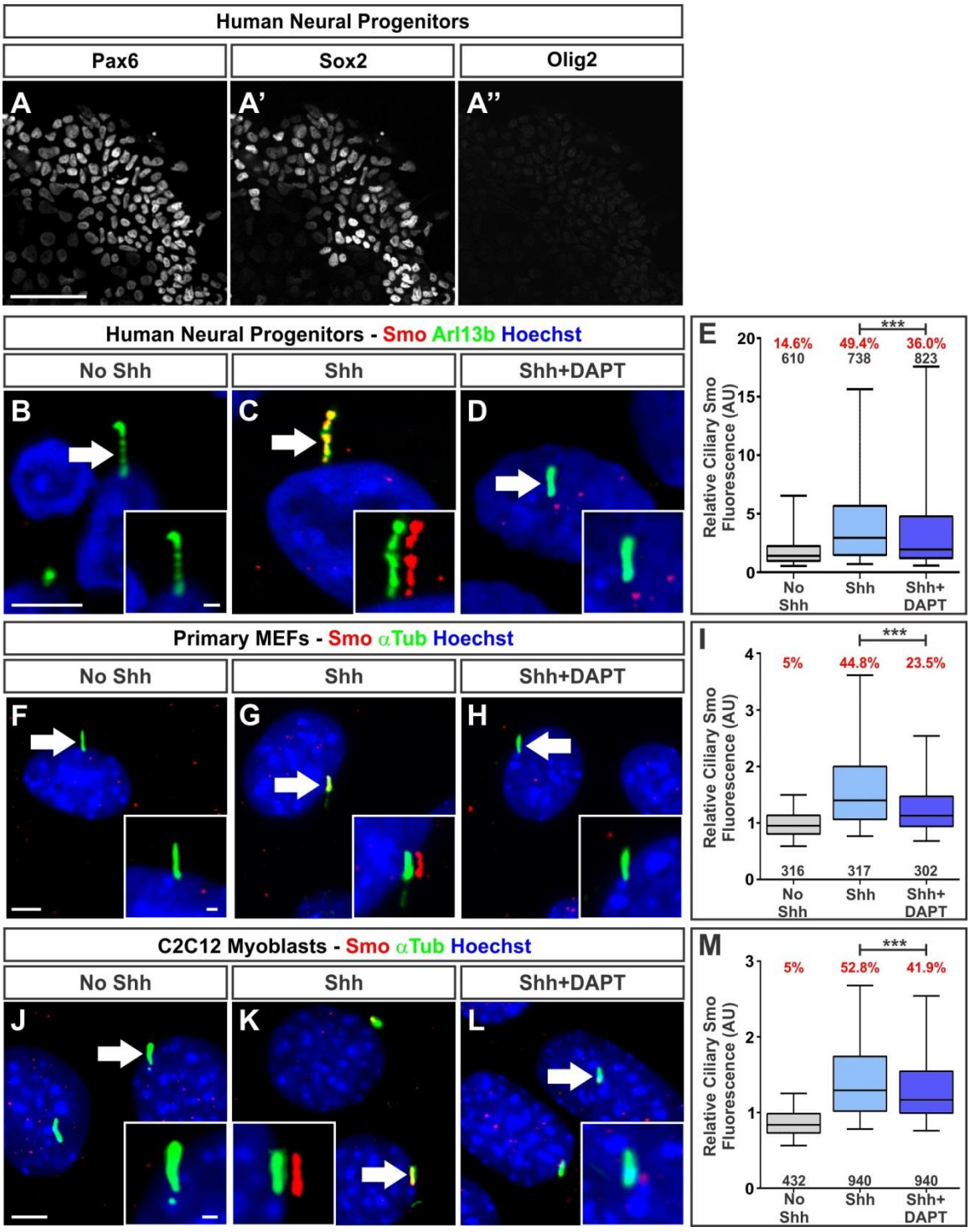
Human Neural Progenitors
Pax6
Sox2
Olig2
A
A'
A''
Human Neural Progenitors - Smo Arl13b Hoechst
No Shh
Shh
Shh+DAPT
B
C
D
E
14.6%
610
49.4%
738
36.0%
823
***
Relative Ciliary Smo Fluorescence (AU)
No Shh
Shh
Shh+ DAPT
Primary MEFs - Smo αTub Hoechst
F
G
H
I
5%
44.8%
23.5%
316
317
302
C2C12 Myoblasts - Smo αTub Hoechst
J
K
L
M
5%
52.8%
41.9%
432
940
940

Supplementary Figure 2-S7: Inhibition of Notch signaling reduces Smo trafficking to primary cilia in a range of cell types

(A-A'') Immunofluorescence analysis of day 11 human spinal neural progenitors generated from the directed differentiation of H9 human embryonic stem cells. The majority of these cells express canonical neural progenitor markers such as SOX2 and PAX6, but not OLIG2 prior to the addition of Shh. Scale bars = 100 μm.

(B-M) Human neural progenitors (B-D), primary mouse embryonic fibroblasts (MEFs) (F-H), and mouse C2C12 skeletal myoblasts (J-L) exposed to 50 nM Shh with or without DAPT for 12 hr. Plated cells were immunostained for Smo (red), Arl13b or αTubulin (green, primary cilia), and Hoechst (blue). Arrows denote cilia shown in the insets, in which Smo and Arl13b/αTubulin channels are offset to better show colocalization. Low mag scale bars = 5 μm. High mag scale bars in insets = 1 μm.

(E, I, M) Box and whisker plots of Smo fluorescence in the cilia of various cell types. The box represents the 25^{th} to 75^{th} percentile, the line through the box represents the median, and the whiskers encompass the 5^{th} to 95^{th} percentile. The number of cilia analyzed is indicated in black and the percentage of Smo^{+} cilia indicated in red. ***$p < 0.001$.

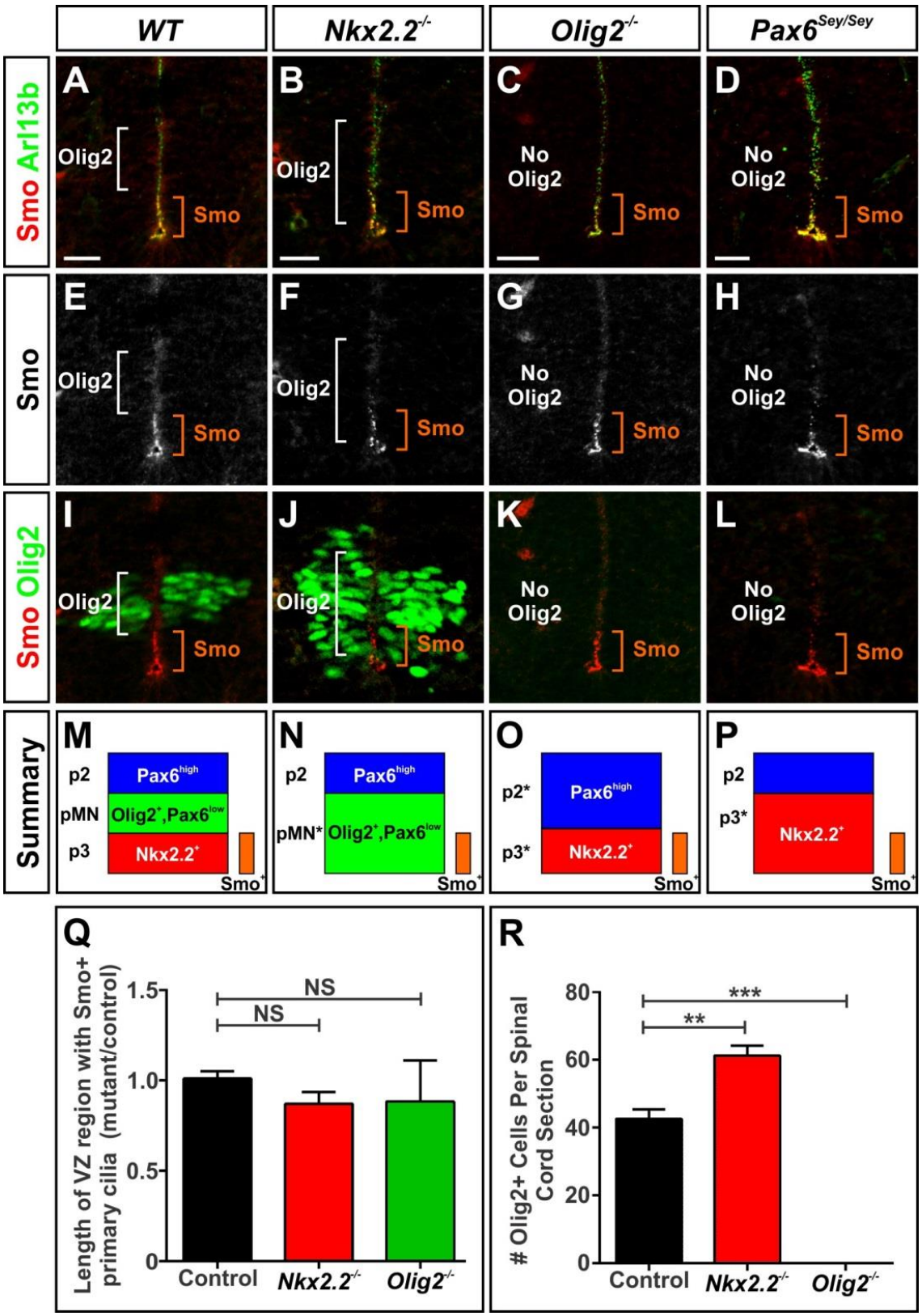
WT
Nkx2.2-/-
Olig2-/-
Pax6Sey/Sey
Smo Arl13b
Smo
Smo Olig2
Summary
A
B
C
D
E
F
G
H
I
J
K
L
M
N
O
P
Olig2
No Olig2
Smo
p2
pMN
p3
p2*
pMN*
p3*
Pax6high
Olig2+,Pax6low
Nkx2.2+
Smo+
Q
R
Length of VZ region with Smo+ primary cilia (mutant/control)
Olig2+ Cells Per Spinal Cord Section
NS
***
**
Control
Nkx2.2-/-
Olig2-/-

Supplementary Figure 2-S8: Manipulating neural progenitor identities in a manner independent of Notch signaling does not alter Smo accumulation within primary cilia

(A-L) Analysis of Smo^{+} primary cilia present on ventral spinal cord progenitors in E11.5 *WT* (A, E, I), *Nkx2.2*$^{-/-}$ (B, F, J), *Olig2*$^{-/-}$ (C, G, K), and *Pax6*$^{Sey/Sey}$ (D, H, L) mutants. Tissues were stained with antibodies against Smo, Arl13b, and Olig2. White brackets denote the limits of the $Olig2^{+}$/pMN progenitor domain and the orange brackets illustrate the dorsoventral extent of progenitor cells with Smo^{+} primary cilia. All scale bars = 20 µm.

(M-P) Summary of the mutant spinal cord data.

(Q) Quantification of the dorsoventral limits of Smo^{+} primary cilia in *WT*, *Nkx2.2*$^{-/-}$, and *Olig2*$^{-/-}$ mutants. Plots represent the mean length ± SEM of Smo^{+} cilia normalized against littermate controls. For this analysis, multiple sections were imaged from at least 3 embryos from each experimental group. NS, $p > 0.05$.

(R) Quantification of the number of $Olig2^{+}$ cells per spinal cord. Plots represent the mean ± SEM from multiple sections collected from 3-4 embryos from each group. $^{**}p < 0.01$ and $^{***}p < 0.001$.

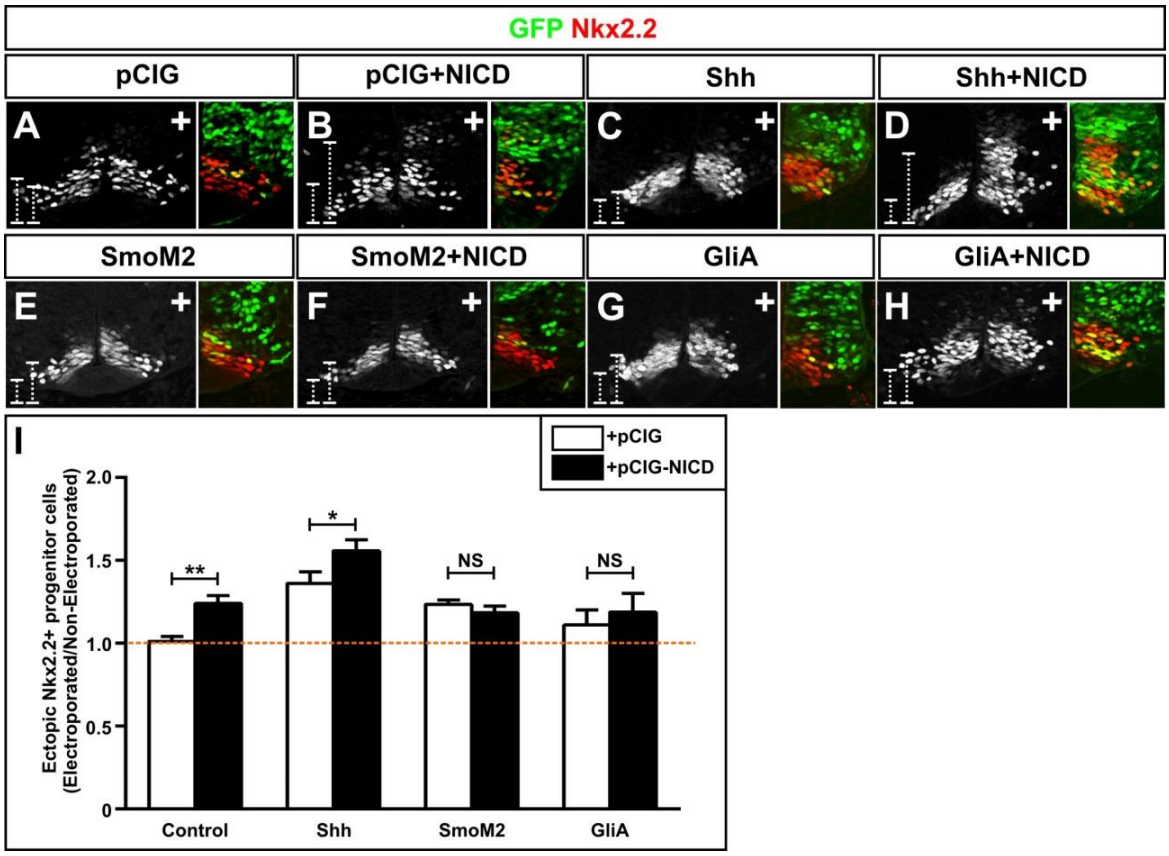

Supplementary Figure 2-S9: Notch signaling activation amplifies a cell's response to Shh

(A-I) Analysis of chick spinal cords co-electroporated with a minimal concentration of a Shh signaling activator (0.05 □g/□l Shh, 0.01 □g/□l SmoM2, or 0.025 □g/□l GliA) and a Notch signaling activator (0.1 □g/□l pCIG-NICD). As a measure of Shh signaling activity, the dorsoventral length of the p3 domain (Nkx2.2+ cells) was measured and a ratio generated by comparing the electroporated side to the non-electroporated side. **(A-H)** The "+" marks the electroporated side. The dotted lines represent the length of the p3 domain, where the left and right lines represent the non-electroporated and electroporated sides, respectively. **(I)** Quantification of the length of the p3 domain, represented as a mean ratio of the electroporated side compared to the non-electroporated side ± SEM. Data was collected from multiple sections from 8-30 embryos for each condition.

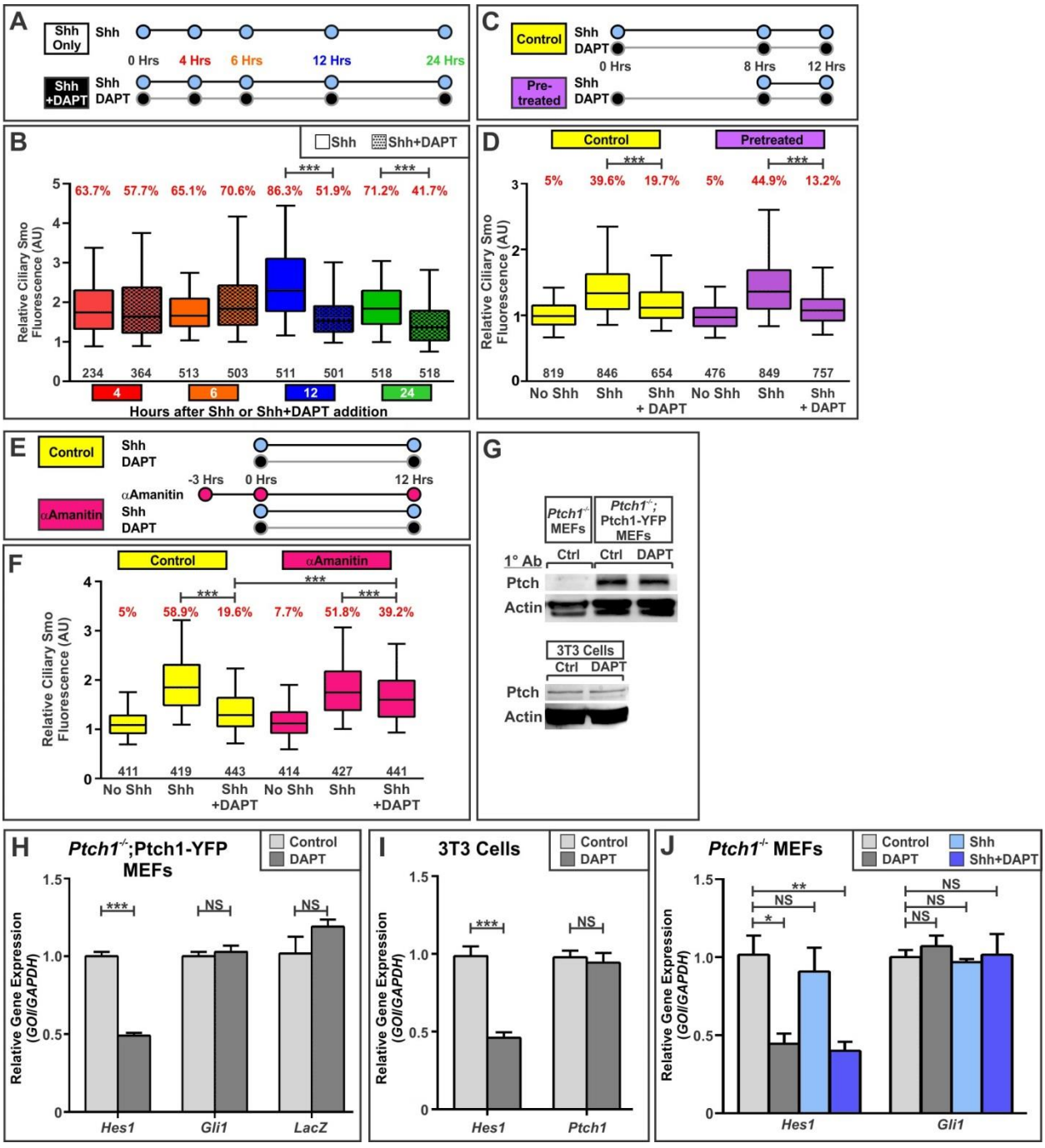
A
Shh Only
Shh
0 Hrs
4 Hrs
6 Hrs
12 Hrs
24 Hrs
Shh +DAPT
Shh
DAPT
B
Shh
Shh+DAPT
***
***
63.7%
57.7%
65.1%
70.6%
86.3%
51.9%
71.2%
41.7%
Relative Ciliary Smo Fluorescence (AU)
234
364
513
503
511
501
518
518
4
6
12
24
Hours after Shh or Shh+DAPT addition
C
Control
Shh
DAPT
0 Hrs
8 Hrs
12 Hrs
Pre-treated
Shh
DAPT
D
Control
Pretreated
***
***
5%
39.6%
19.7%
5%
44.9%
13.2%
Relative Ciliary Smo Fluorescence (AU)
819
846
654
476
849
757
No Shh
Shh
Shh + DAPT
No Shh
Shh
Shh + DAPT
E
Control
Shh
DAPT
-3 Hrs
0 Hrs
12 Hrs
αAmanitin
αAmanitin
Shh
DAPT
F
Control
αAmanitin
***
***
***
5%
58.9%
19.6%
7.7%
51.8%
39.2%
Relative Ciliary Smo Fluorescence (AU)
411
419
443
414
427
441
No Shh
Shh
Shh +DAPT
No Shh
Shh
Shh +DAPT
G
Ptch1-/- MEFs
Ptch1-/-; Ptch1-YFP MEFs
1° Ab
Ctrl
Ctrl
DAPT
Ptch
Actin
3T3 Cells
Ctrl
DAPT
Ptch
Actin
H
Ptch1-/-;Ptch1-YFP MEFs
Control
DAPT
***
NS
NS
Relative Gene Expression (GOI/GAPDH)
Hes1
Gli1
LacZ
I
3T3 Cells
Control
DAPT
***
NS
Relative Gene Expression (GOI/GAPDH)
Hes1
Ptch1
J
Ptch1-/- MEFs
Control
DAPT
Shh
Shh+DAPT
**
NS
*
NS
NS
NS
Relative Gene Expression (GOI/GAPDH)
Hes1
Gli1

Supplementary Figure 2-S10: Manipulating neural progenitor identities in a manner independent of Notch signaling does not alter Smo accumulation within primary cilia

(A) Outline of the time course experiments in which NIH-3T3 cells were exposed to 50 nM Shh alone or in the presence of 18.75 μM DAPT for 4, 6, 12, and 24 hr.

(B) Box and whisker plots of Smo fluorescence in the cilia of cells treated with Shh ± DAPT for 4, 6, 12, and 24 hr. The box represents the 25^{th} to 75^{th} percentile, the line through the box represents the median, and the whiskers encompass the 5^{th} to 95^{th} percentile. The number of cilia analyzed is indicated in black below the box plots, and percentage of Smo^{+} cilia indicated in red above the box plots. Reductions in Smo^{+} primary cilia were first observed at 12 hr. ***$p < 0.001$.

(C) Outline of the pretreatment experiment, in which NIH-3T3 cells were exposed to either Shh+DAPT for 12 hr (Control) or exposed to DAPT alone for 8 hr and then Shh+DAPT for an additional 4 hr (Pretreatment).

(D) Box and whisker plots of ciliary Smo fluorescence under Control and DAPT Pretreated conditions. ***$p < 0.001$.

(E) Outline of the α-amanitin experiment. NIH-3T3 cells were exposed to the transcriptional inhibitor α-amanitin 3 hr prior to the addition of Shh with or without DAPT.

(F) Box and whisker plots of ciliary Smo fluorescence in the presence or absence of α-amanitin. ***$p < 0.001$.

(G) Immunoblotting for Ptch1 and Actin in cell lysates of *Ptch1*$^{-/-}$ MEFs*, Ptch1*$^{-/-}$*; Ptch1-YFP* MEFs, and NIH-3T3 cells treated with either DMSO (Control) or DAPT for 24 hr.

(H) qPCR analysis of *Ptch1*$^{-/-}$*;Ptch1-YFP* MEFs treated with either DMSO (Control) or DAPT for 12 hr. Plot shows mean *Gapdh*-normalized gene expression levels relative to the Control group ± SEM from 4 samples. NS, $p > 0.05$, ***$p < 0.001$, unpaired t-test.

(I) qPCR analysis of NIH-3T3 cells treated with DMSO (Control) or DAPT for 24 hr. Plot represents mean *Gapdh*-normalized gene expression levels relative to the control group ± SEM

from 3 samples. NS, $p > 0.05$, *$p < 0.05$, **$p < 0.01$, ***$p < 0.001$.

(J) qPCR analysis of *Ptch1*$^{-/-}$ MEFs treated with DMSO (Control), DAPT, Shh, or Shh+DAPT for 24 hr. Plot represents mean *Gapdh*-normalized gene expression levels relative to the Control group ± SEM from 3 samples. NS, $p > 0.05$, *$p < 0.05$, **$p < 0.01$, ***$p < 0.001$.

ACKNOWLEDGEMENTS

We thank S. Butler, P. Niewiadomski, H. Kornblum, and G. Weinmaster for helpful discussions and comments on the manuscript; T. Honjo, S. Morrison, C. Murtaugh, and A. Pierani for mice; L. Cheng, T. Jessell, Y. Nakagawa, K. Phan, S. Pfaff, and T. Sudo for reagents. We also thank K. Dale for communications before submission of the manuscript. This work was supported by the UCLA Broad Center for Regenerative Medicine and Stem Cell Research, the Rose Hills Foundation, and grants to BGN from the March of Dimes Foundation (6-FY10-296) and the NINDS (NS053976 and NS072804). JHK was also supported by a UCLA Dissertation Year Fellowship. RR was supported by grants from the NIGMS (DP2GM10544) and the March of Dimes Foundation (6-FY13-104). ED and JB were supported by the Medical Research Council (UK) (U117560541) and the Wellcome Trust (WT098326MA).

REFERENCES

1 Le Dreau, G. & Marti, E. The multiple activities of BMPs during spinal cord development. *Cellular and molecular life sciences : CMLS* **70**, 4293-4305, doi:10.1007/s00018-013-1354-9 (2013).

2 Briscoe, J. & Novitch, B. G. Regulatory pathways linking progenitor patterning, cell fates and neurogenesis in the ventral neural tube. *Philosophical transactions of the Royal Society of London. Series B, Biological sciences* **363**, 57-70, doi:10.1098/rstb.2006.2012 (2008).

3 Butler, S. J. & Bronner, M. E. From classical to current: Analyzing peripheral nervous system and spinal cord lineage and fate. *Developmental biology* **398**, 135-146, doi:10.1016/j.ydbio.2014.09.033 (2015).

4 Rowitch, D. H. & Kriegstein, A. R. Developmental genetics of vertebrate glial-cell specification. *Nature* **468**, 214-222, doi:10.1038/nature09611 (2010).

5 Rogers, K. W. & Schier, A. F. Morphogen gradients: from generation to interpretation. *Annu Rev Cell Dev Biol* **27**, 377-407, doi:10.1146/annurev-cellbio-092910-154148 (2011).

6 Kutejova, E., Briscoe, J. & Kicheva, A. Temporal dynamics of patterning by morphogen gradients. *Current opinion in genetics & development* **19**, 315-322, doi:10.1016/j.gde.2009.05.004 (2009).

7 Eggenschwiler, J. T. & Anderson, K. V. Cilia and developmental signaling. *Annu Rev Cell Dev Biol* **23**, 345-373, doi:10.1146/annurev.cellbio.23.090506.123249 (2007).

8 Dessaud, E., McMahon, A. P. & Briscoe, J. Pattern formation in the vertebrate neural tube: a sonic hedgehog morphogen-regulated transcriptional network. *Development* **135**, 2489-2503, doi:10.1242/dev.009324 (2008).

9 Ribes, V. & Briscoe, J. Establishing and interpreting graded Sonic Hedgehog signaling during vertebrate neural tube patterning: the role of negative feedback. *Cold Spring Harbor perspectives in biology* **1**, a002014, doi:10.1101/cshperspect.a002014 (2009).

10 Mizuguchi, R. *et al.* Combinatorial roles of olig2 and neurogenin2 in the coordinated induction of pan-neuronal and subtype-specific properties of motoneurons. *Neuron* **31**, 757-771. (2001).

11 Novitch, B. G., Chen, A. I. & Jessell, T. M. Coordinate regulation of motor neuron subtype identity and pan-neuronal properties by the bHLH repressor Olig2. *Neuron* **31**, 773-789 (2001).

12 Hochstim, C., Deneen, B., Lukaszewicz, A., Zhou, Q. & Anderson, D. J. Identification of positionally distinct astrocyte subtypes whose identities are specified by a homeodomain code. *Cell* **133**, 510-522, doi:S0092-8674(08)00396-6 [pii] 10.1016/j.cell.2008.02.046 (2008).

13 Muroyama, Y., Fujiwara, Y., Orkin, S. H. & Rowitch, D. H. Specification of astrocytes by bHLH protein SCL in a restricted region of the neural tube. *Nature* **438**, 360-363, doi:10.1038/nature04139 (2005).

14 Dessaud, E. *et al.* Dynamic assignment and maintenance of positional identity in the ventral neural tube by the morphogen sonic hedgehog. *PLoS biology* **8**, e1000382, doi:10.1371/journal.pbio.1000382 (2010).

15 Dessaud, E. *et al.* Interpretation of the sonic hedgehog morphogen gradient by a temporal adaptation mechanism. *Nature* **450**, 717-720, doi:10.1038/nature06347 (2007).

16 Balaskas, N. *et al.* Gene regulatory logic for reading the Sonic Hedgehog signaling gradient in the vertebrate neural tube. *Cell* **148**, 273-284, doi:10.1016/j.cell.2011.10.047 (2012).

17 Huang, P., Xiong, F., Megason, S. G. & Schier, A. F. Attenuation of Notch and Hedgehog signaling is required for fate specification in the spinal cord. *PLoS genetics* **8**, e1002762, doi:10.1371/journal.pgen.1002762 (2012).

18 Gaiano, N. & Fishell, G. The role of notch in promoting glial and neural stem cell fates. *Annual review of neuroscience* **25**, 471-490, doi:10.1146/annurev.neuro.25.030702.130823 (2002).

19 Pierfelice, T., Alberi, L. & Gaiano, N. Notch in the vertebrate nervous system: an old dog with new tricks. *Neuron* **69**, 840-855, doi:10.1016/j.neuron.2011.02.031 (2011).

20 Kageyama, R., Ohtsuka, T., Shimojo, H. & Imayoshi, I. Dynamic regulation of Notch signaling in neural progenitor cells. *Current opinion in cell biology* **21**, 733-740, doi:10.1016/j.ceb.2009.08.009 (2009).

21 Kageyama, R., Ohtsuka, T. & Kobayashi, T. The Hes gene family: repressors and oscillators that orchestrate embryogenesis. *Development* **134**, 1243-1251, doi:10.1242/dev.000786 (2007).

22 Furukawa, T., Mukherjee, S., Bao, Z. Z., Morrow, E. M. & Cepko, C. L. rax, Hes1, and notch1 promote the formation of Muller glia by postnatal retinal progenitor cells. *Neuron* **26**, 383-394 (2000).

23 Gaiano, N., Nye, J. S. & Fishell, G. Radial glial identity is promoted by Notch1 signaling in the murine forebrain. *Neuron* **26**, 395-404 (2000).

24 Scheer, N., Groth, A., Hans, S. & Campos-Ortega, J. A. An instructive function for Notch in promoting gliogenesis in the zebrafish retina. *Development* **128**, 1099-1107 (2001).

25 Ge, W. *et al.* Notch signaling promotes astrogliogenesis via direct CSL-mediated glial gene activation. *Journal of neuroscience research* **69**, 848-860, doi:10.1002/jnr.10364 (2002).

26 Wang, S. *et al.* Notch receptor activation inhibits oligodendrocyte differentiation. *Neuron* **21**, 63-75 (1998).

27 Bielle, F. *et al.* Multiple origins of Cajal-Retzius cells at the borders of the developing pallium. *Nature neuroscience* **8**, 1002-1012, doi:10.1038/nn1511 (2005).

28 Mao, X., Fujiwara, Y., Chapdelaine, A., Yang, H. & Orkin, S. H. Activation of EGFP expression by Cre-mediated excision in a new ROSA26 reporter mouse strain. *Blood* **97**, 324-326 (2001).

29 Murtaugh, L. C., Stanger, B. Z., Kwan, K. M. & Melton, D. A. Notch signaling controls multiple steps of pancreatic differentiation. *Proc Natl Acad Sci U S A* **100**, 14920-14925 (2003).

30 Han, H. *et al.* Inducible gene knockout of transcription factor recombination signal binding protein-J reveals its essential role in T versus B lineage decision. *International immunology* **14**, 637-645 (2002).

31 Rousso, D. L. *et al.* Foxp-mediated suppression of N-cadherin regulates neuroepithelial character and progenitor maintenance in the CNS. *Neuron* **74**, 314-330, doi:10.1016/j.neuron.2012.02.024 (2012).

32 Gaber, Z. B., Butler, S. J. & Novitch, B. G. PLZF regulates fibroblast growth factor responsiveness and maintenance of neural progenitors. *PLoS Biol* **11**, e1001676, doi:10.1371/journal.pbio.1001676 (2013).

33 Taipale, J. *et al.* Effects of oncogenic mutations in Smoothened and Patched can be reversed by cyclopamine. *Nature* **406**, 1005-1009, doi:10.1038/35023008 (2000).

34 Rohatgi, R., Milenkovic, L., Corcoran, R. B. & Scott, M. P. Hedgehog signal transduction by Smoothened: pharmacologic evidence for a 2-step activation process. *Proc Natl Acad Sci U S A* **106**, 3196-3201, doi:10.1073/pnas.0813373106 (2009).

35 Rohatgi, R., Milenkovic, L. & Scott, M. P. Patched1 regulates hedgehog signaling at the primary cilium. *Science* **317**, 372-376, doi:10.1126/science.1139740 (2007).

36 Hu, B. Y., Du, Z. W. & Zhang, S. C. Differentiation of human oligodendrocytes from pluripotent stem cells. *Nature protocols* **4**, 1614-1622, doi:10.1038/nprot.2009.186 (2009).

37 Novitch, B. G., Wichterle, H., Jessell, T. M. & Sockanathan, S. A requirement for retinoic acid-mediated transcriptional activation in ventral neural patterning and motor neuron specification. *Neuron* **40**, 81-95 (2003).

38 Pearson, C. A. *et al.* FGF-dependent midline-derived progenitor cells in hypothalamic infundibular development. *Development* **138**, 2613-2624, doi:10.1242/dev.062794 (2011).

39 Roelink, H. *et al.* Floor plate and motor neuron induction by vhh-1, a vertebrate homolog of hedgehog expressed by the notochord. *Cell* **76**, 761-775 (1994).

40 Xie, J. *et al.* Activating Smoothened mutations in sporadic basal-cell carcinoma. *Nature* **391**, 90-92, doi:10.1038/34201 (1998).

41 Hynes, M. *et al.* The seven-transmembrane receptor smoothened cell-autonomously induces multiple ventral cell types. *Nature neuroscience* **3**, 41-46, doi:10.1038/71114 (2000).

42 Stamataki, D., Ulloa, F., Tsoni, S. V., Mynett, A. & Briscoe, J. A gradient of Gli activity mediates graded Sonic Hedgehog signaling in the neural tube. *Genes & development* **19**, 626-641, doi:10.1101/gad.325905 (2005).

43 Lo, L. C., Johnson, J. E., Wuenschell, C. W., Saito, T. & Anderson, D. J. Mammalian achaete-scute homolog 1 is transiently expressed by spatially restricted subsets of early neuroepithelial and neural crest cells. *Genes & development* **5**, 1524-1537 (1991).

44 Thaler, J. *et al.* Active suppression of interneuron programs within developing motor neurons revealed by analysis of homeodomain factor HB9. *Neuron* **23**, 675-687 (1999).

45 Vue, T. Y. *et al.* Characterization of progenitor domains in the developing mouse thalamus. *J Comp Neurol* **505**, 73-91, doi:10.1002/cne.21467 (2007).

46 Weinstein, D. C. *et al.* The winged-helix transcription factor HNF-3 beta is required for notochord development in the mouse embryo. *Cell* **78**, 575-588 (1994).

47 Rousso, D. L., Gaber, Z. B., Wellik, D., Morrisey, E. E. & Novitch, B. G. Coordinated actions of the forkhead protein Foxp1 and Hox proteins in the columnar organization of spinal motor neurons. *Neuron* **59**, 226-240, doi:10.1016/j.neuron.2008.06.025 (2008).

48 Arber, S. *et al.* Requirement for the homeobox gene Hb9 in the consolidation of motor neuron identity. *Neuron* **23**, 659-674. (1999).

49 Ito, T. *et al.* Basic helix-loop-helix transcription factors regulate the neuroendocrine differentiation of fetal mouse pulmonary epithelium. *Development* **127**, 3913-3921 (2000).

50 Tsuchida, T. *et al.* Topographic organization of embryonic motor neurons defined by expression of LIM homeobox genes. *Cell* **79**, 957-970 (1994).

51 Ericson, J. *et al.* Pax6 controls progenitor cell identity and neuronal fate in response to graded Shh signaling. *Cell* **90**, 169-180 (1997).

52 Kang, P. *et al.* Sox9 and NFIA coordinate a transcriptional regulatory cascade during the initiation of gliogenesis. *Neuron* **74**, 79-94, doi:10.1016/j.neuron.2012.01.024 (2012).

53 Briscoe, J. *et al.* Homeobox gene Nkx2.2 and specification of neuronal identity by graded Sonic hedgehog signalling. *Nature* **398**, 622-627, doi:10.1038/19315 (1999).

54 Briscoe, J., Pierani, A., Jessell, T. M. & Ericson, J. A homeodomain protein code specifies progenitor cell identity and neuronal fate in the ventral neural tube. *Cell* **101**, 435-445 (2000).

55 Ribes, V. *et al.* Distinct Sonic Hedgehog signaling dynamics specify floor plate and ventral neuronal progenitors in the vertebrate neural tube. *Genes & development* **24**, 1186-1200, doi:10.1101/gad.559910 (2010).

56 Yamada, T., Pfaff, S. L., Edlund, T. & Jessell, T. M. Control of cell pattern in the neural tube: motor neuron induction by diffusible factors from notochord and floor plate. *Cell* **73**, 673-686 (1993).

57 Ericson, J., Morton, S., Kawakami, A., Roelink, H. & Jessell, T. M. Two critical periods of Sonic Hedgehog signaling required for the specification of motor neuron identity. *Cell* **87**, 661-673 (1996).

58 Regl, G. *et al.* Human GLI2 and GLI1 are part of a positive feedback mechanism in Basal Cell Carcinoma. *Oncogene* **21**, 5529-5539, doi:10.1038/sj.onc.1205748 (2002).

59 Lelievre, V. *et al.* Disruption of the PACAP gene promotes medulloblastoma in ptc1 mutant mice. *Developmental biology* **313**, 359-370, doi:10.1016/j.ydbio.2007.10.031 (2008).

60 Hu, B. Y. & Zhang, S. C. Differentiation of spinal motor neurons from pluripotent human stem cells. *Nature protocols* **4**, 1295-1304, doi:10.1038/nprot.2009.127 (2009).

61 Megason, S. G. & McMahon, A. P. A mitogen gradient of dorsal midline Wnts organizes growth in the CNS. *Development* **129**, 2087-2098 (2002).

62 Yu, X. *et al.* HES1 inhibits cycling of hematopoietic progenitor cells via DNA binding. *Stem cells* **24**, 876-888, doi:10.1634/stemcells.2005-0598 (2006).

63 Yu, X. *et al.* Lentiviral vectors with two independent internal promoters transfer high-level expression of multiple transgenes to human hematopoietic stem-progenitor cells. *Molecular therapy : the journal of the American Society of Gene Therapy* **7**, 827-838 (2003).

64 Mukhopadhyay, S. *et al.* The ciliary G-protein-coupled receptor Gpr161 negatively regulates the Sonic hedgehog pathway via cAMP signaling. *Cell* **152**, 210-223, doi:10.1016/j.cell.2012.12.026 (2013).

65 Nachtergaele, S. *et al.* Structure and function of the Smoothened extracellular domain in vertebrate Hedgehog signaling. *eLife* **2**, e01340, doi:10.7554/eLife.01340 (2013).

66 Hatakeyama, J. *et al.* Hes genes regulate size, shape and histogenesis of the nervous system by control of the timing of neural stem cell differentiation. *Development* **131**, 5539-5550 (2004).

67 Ingram, W. J., McCue, K. I., Tran, T. H., Hallahan, A. R. & Wainwright, B. J. Sonic Hedgehog regulates Hes1 through a novel mechanism that is independent of canonical Notch pathway signalling. *Oncogene* **27**, 1489-1500, doi:10.1038/sj.onc.1210767 (2008).

68 Wall, D. S. *et al.* Progenitor cell proliferation in the retina is dependent on Notch-independent Sonic hedgehog/Hes1 activity. *The Journal of cell biology* **184**, 101-112 (2009).

69 Sun, T. *et al.* Cross-repressive interaction of the Olig2 and Nkx2.2 transcription factors in developing neural tube associated with formation of a specific physical complex. *J Neurosci* **23**, 9547-9556 (2003).

70 Taylor, M. K., Yeager, K. & Morrison, S. J. Physiological Notch signaling promotes gliogenesis in the developing peripheral and central nervous systems. *Development* **134**, 2435-2447, doi:10.1242/dev.005520 (2007).

71 Briscoe, J. & Ericson, J. The specification of neuronal identity by graded Sonic Hedgehog signalling. *Seminars in cell & developmental biology* **10**, 353-362, doi:10.1006/scdb.1999.0295 (1999).

72 Dessaud, E. *et al.* Dynamic assignment and maintenance of positional identity in the ventral neural tube by the morphogen sonic hedgehog. *PLoS Biol* **8**, e1000382, doi:10.1371/journal.pbio.1000382 (2010).

73 Jeong, J. & McMahon, A. P. Growth and pattern of the mammalian neural tube are governed by partially overlapping feedback activities of the hedgehog antagonists patched 1 and Hhip1. *Development* **132**, 143-154, doi:10.1242/dev.01566 (2005).

74 Holtz, A. M. *et al.* Essential role for ligand-dependent feedback antagonism of vertebrate hedgehog signaling by PTCH1, PTCH2 and HHIP1 during neural patterning. *Development* **140**, 3423-3434, doi:10.1242/dev.095083 (2013).

75 Dovey, H. F. *et al.* Functional gamma-secretase inhibitors reduce beta-amyloid peptide levels in brain. *J Neurochem* **76**, 173-181 (2001).

76 Geling, A., Steiner, H., Willem, M., Bally-Cuif, L. & Haass, C. A gamma-secretase inhibitor blocks Notch signaling in vivo and causes a severe neurogenic phenotype in zebrafish. *EMBO reports* **3**, 688-694, doi:10.1093/embo-reports/kvf124 (2002).

77 Stamataki, D., Ulloa, F., Tsoni, S. V., Mynett, A. & Briscoe, J. A gradient of Gli activity mediates graded Sonic Hedgehog signaling in the neural tube. *Genes & development* **19**, 626-641, doi:10.1101/gad.325905 (2005).

78 Small, D. *et al.* Notch activation suppresses fibroblast growth factor-dependent cellular transformation. *The Journal of biological chemistry* **278**, 16405-16413, doi:10.1074/jbc.M300464200 (2003).

79 Tukachinsky, H., Lopez, L. V. & Salic, A. A mechanism for vertebrate Hedgehog signaling: recruitment to cilia and dissociation of SuFu-Gli protein complexes. *The Journal of cell biology* **191**, 415-428, doi:10.1083/jcb.201004108 (2010).

80 Corbit, K. C. *et al.* Vertebrate Smoothened functions at the primary cilium. *Nature* **437**, 1018-1021, doi:10.1038/nature04117 (2005).

81 Moellering, R. E. *et al.* Direct inhibition of the NOTCH transcription factor complex. *Nature* **462**, 182-188, doi:10.1038/nature08543 (2009).

82 Petit, A. *et al.* New protease inhibitors prevent gamma-secretase-mediated production of Abeta40/42 without affecting Notch cleavage. *Nature cell biology* **3**, 507-511, doi:10.1038/35074581 (2001).

83 Sinha, S. & Chen, J. K. Purmorphamine activates the Hedgehog pathway by targeting Smoothened. *Nat Chem Biol* **2**, 29-30, doi:10.1038/nchembio753 (2006).

84 Chen, J. K., Taipale, J., Young, K. E., Maiti, T. & Beachy, P. A. Small molecule modulation of Smoothened activity. *Proc Natl Acad Sci U S A* **99**, 14071-14076, doi:10.1073/pnas.182542899 (2002).

85 Wang, Y., Zhou, Z., Walsh, C. T. & McMahon, A. P. Selective translocation of intracellular Smoothened to the primary cilium in response to Hedgehog pathway modulation. *Proceedings of the National Academy of Sciences of the United States of America* **106**, 2623-2628, doi:10.1073/pnas.0812110106 (2009).

86 Fuccillo, M., Joyner, A. L. & Fishell, G. Morphogen to mitogen: the multiple roles of hedgehog signalling in vertebrate neural development. *Nature reviews. Neuroscience* **7**, 772-783, doi:10.1038/nrn1990 (2006).

87 Briscoe, J. & Therond, P. P. The mechanisms of Hedgehog signalling and its roles in development and disease. *Nature reviews. Molecular cell biology* **14**, 416-429, doi:10.1038/nrm3598 (2013).

88 Oosterveen, T. *et al.* Mechanistic differences in the transcriptional interpretation of local and long-range Shh morphogen signaling. *Developmental cell* **23**, 1006-1019, doi:10.1016/j.devcel.2012.09.015 (2012).

89 Oosterveen, T. *et al.* SoxB1-driven transcriptional network underlies neural-specific interpretation of morphogen signals. *Proc Natl Acad Sci U S A* **110**, 7330-7335, doi:10.1073/pnas.1220010110 (2013).

90 Peterson, K. A. *et al.* Neural-specific Sox2 input and differential Gli-binding affinity provide context and positional information in Shh-directed neural patterning. *Genes & development* **26**, 2802-2816, doi:10.1101/gad.207142.112 (2012).

91 Ezratty, E. J. *et al.* A role for the primary cilium in Notch signaling and epidermal differentiation during skin development. *Cell* **145**, 1129-1141, doi:10.1016/j.cell.2011.05.030 (2011).

92 Keady, B. T. *et al.* IFT25 links the signal-dependent movement of Hedgehog components to intraflagellar transport. *Developmental cell* **22**, 940-951, doi:10.1016/j.devcel.2012.04.009 (2012).

93 Yue, S. *et al.* Requirement of Smurf-mediated endocytosis of Patched1 in Sonic Hedgehog signal reception. *eLife*, e02555, doi:10.7554/eLife.02555 (2014).

94 Pazour, G. J. & Witman, G. B. The vertebrate primary cilium is a sensory organelle. *Current opinion in cell biology* **15**, 105-110 (2003).

95 Zimmermann, K. W. Beiträge zur Kenntniss einiger Drüsen und Epithelien [English translation: Contributions to knowledge of some glands and epithelium]. *Archiv für mikroskopische Anatomie* **52**, 552-706 (1898).

96 Habbig, S. *et al.* NPHP4, a cilia-associated protein, negatively regulates the Hippo pathway. *The Journal of cell biology* **193**, 633-642, doi:10.1083/jcb.201009069 (2011).

97 Boehlke, C. *et al.* Primary cilia regulate mTORC1 activity and cell size through Lkb1. *Nature cell biology* **12**, 1115-1122, doi:10.1038/ncb2117 (2010).

98 Lancaster, M. A., Schroth, J. & Gleeson, J. G. Subcellular spatial regulation of canonical Wnt signalling at the primary cilium. *Nature cell biology* **13**, 700-707, doi:10.1038/ncb2259 (2011).

99 Schneider, L. *et al.* PDGFRalphaalpha signaling is regulated through the primary cilium in fibroblasts. *Current biology : CB* **15**, 1861-1866, doi:10.1016/j.cub.2005.09.012 (2005).

100 Novarino, G., Akizu, N. & Gleeson, J. G. Modeling human disease in humans: the ciliopathies. *Cell* **147**, 70-79, doi:10.1016/j.cell.2011.09.014 (2011).

101 Pedersen, L. B. & Rosenbaum, J. L. Intraflagellar transport (IFT) role in ciliary assembly, resorption and signalling. *Current topics in developmental biology* **85**, 23-61, doi:10.1016/S0070-2153(08)00802-8 (2008).

102 Ishikawa, H., Thompson, J., Yates, J. R., 3rd & Marshall, W. F. Proteomic analysis of mammalian primary cilia. *Current biology : CB* **22**, 414-419, doi:10.1016/j.cub.2012.01.031 (2012).

CHAPTER 3 - Notch signaling is required for the maintenance of cell adhesion and cell polarity of neural progenitors within the developing diencephalon

ABSTRACT

In the developing central nervous system (CNS), the transition of neuroepithelial cells from progenitors to neurons requires both a shift in molecular identity and a disassembly of apical cell adhesion proteins. While much is known about the mechanisms that molecularly maintain cells as progenitors and inhibit neuronal differentiation, far less is known about how these same mechanisms regulate the maintenance and disassembly of the apical contacts that retain these cells to the ventricular zone. This is the case with Notch signaling. Notch signaling plays a major role in the maintenance of neural progenitors, but very little is known about its role in the maintenance of apical adherens junctions. In this study we examined the role of Notch signaling in the maintenance of cell adhesion and polarity in neuroepithelial progenitor cells. Using a Cre-*loxP* mediated gene targeting approach we selectively ablated Notch signaling activity within regions of the developing brain. We observed that a loss of Notch signaling activity specifically within the developing diencephalon resulted in premature neurogenesis, a degradation of apical adhesion junctions, and a loss cell polarity. Over time, this loss of neuroepithelial integrity in the embryo manifested itself as a loss of ependymal integrity in the adult, ultimately resulting in obstructive hydrocephalus. Collectively, these data illustrate that the maintenance of cells as progenitors by Notch signaling extends beyond the suppression of proneural genes. Our findings indicate that Notch signaling also plays an active role in the maintenance of apical attachments that retain progenitors to the proliferative ventricular zone.

This chapter is modified from:

Kong JH and Novitch BG. (2015) Notch signaling is required for the maintenance of neural progenitor cell adhesion and polarity within the developing diencephalon. *In preparation for publication.*

JHK performed the experiments and wrote the manuscript under the guidance of BGN.

INTRODUCTION

The development of the central nervous system (CNS) relies on a relatively small population of neural progenitor cells (NPCs) to generate an abundance of different types of neurons and glia. In this highly regulated process, each type of cell must be generated within a specific region of space and time to facilitate interactions that produce functional motor and sensory circuits. As existing NPCs are depleted due to differentiation, progenitor reserves must be simultaneously replenished through a process of self-renewal. Thus, the proper growth and organization of the CNS relies heavily upon the dynamic balance between NPC maintenance and differentiation. A perturbation of this balance can be detrimental, resulting in profound structural defects and impaired cognitive function[1-3].

The CNS begins as a pseudostratified epithelial cell layer made up of NPCs. These neuroepithelial cells are highly polarized and this polarity is maintained largely by adherens junctions at the apical surface[4-6]. As the NPCs progress through the cell cycle, their nuclei migrate along the apicobasal axis. In this process, called interkinetic nuclear migration, cell nuclei in M-phase are present at the apical surface and as the cells transition into G1/S-phase the nuclei migrate towards the basal surface[7,8]. At the apical surface, the orientation of the cleavage plane predicts the fate of the daughter cells. In this process, NPCs with either divide symmetrically to produce two daughter progenitors (proliferative division) or asymmetrically to produce one progenitor and one differentiated cell (neurogenic division)[9-11]. Initially in

development, NPCs undergo multiple rounds of symmetric cell division to expand the progenitor population and over time, when neurogenesis is initiated, the NPCs begin to undergo asymmetric cell division. Upon asymmetric division, the daughter cell that remains a progenitor retains its adherens junction while the cell that undergoes differentiation detaches from the apical membrane[9]. Asymmetric cell division also results in the unequal distribution of proteins to the daughter cells. Of the proteins that are unequally distributed are Notch1 and Numb, a Notch receptor and Notch antagonist, respectively[9,12,13].

The relationship between neuronal differentiation, asymmetric cell division, the loss of apical cell adhesion, and the loss of apicobasal polarity remains poorly understood. However, Notch signaling has been implicated in all four of these events. Notch signaling is a highly conserved signaling pathway that has been shown to play a critical role in both promoting progenitor maintenance[14] and suppressing neurogenesis[15-17]. Notch signaling ligands, receptors, and effectors are expressed in complex spatial-temporal patterns throughout the developing brain and spinal cord[18-20]. Upon ligand binding, the Notch receptor is cleaved and the Notch intracellular domain (NICD) translocates to the nucleus where it binds to the Rbpj complex. In the absence of NICD, Rbpj is bound to co-repressors and functions as a transcriptional repressor complex. In the presence of NICD, NICD binds to the Rbpj co-repressor complex and converts it into a co-activator complex. The Rbpj-NICD co-activator complex upregulates downstream targets, most notable of these are the *Hes* genes which are bHLH transcriptional regulators that repress proneural gene expression[16,21]. The role of Notch signaling in repressing neuronal differentiation is well established. However, Notch signaling has also been shown to regulate asymmetric cell division[22,23], apical cell adhesion[24,25], and cell polarity[26] within specific cell types. While much is known, the details of the interaction between Notch signaling and the integrity of the neuroepithelial cell layer has not been thoroughly studied in the vertebrate CNS.

In this study, we address the interactions between Notch signaling and neuroepithelial integrity. Using transgenic mice, we show that the conditional deletion of Notch signaling activity within specific regions of the developing diencephalon results in both precocious neuronal differentiation and a loss of neuroepithelial cell adhesion and polarity. Unable to recover from this loss, the disrupted neuroepithelial cells became disorganized ependymal cells, the ventricular system became obstructed, and the mutant mice developed hydrocephalus in postnatal life. Collectively, our data suggests that Notch signaling not only plays a role in neural progenitor maintenance, but is also essential for the maintenance of neuroepithelial and ependymal cell integrity within specific regions of the developing brain.

MATERIALS AND METHODS

Animal preparation and tissue analysis: *Olig2*^{Cre} and *Dbx1*^{Cre} mice were generated as previously described[27,28]. Cre mice were crossed with *R26R*^{GFP} transgenic reporter mice (B6;129-*Gt(ROSA)26Sor*^{tm2Sho}/J; Jackson Labs Stock #004077) [29] and *Rbpj*^{CKO} mice [30]. All mice were maintained and tissue collected in accordance with guidelines set forth by the UCLA Institutional Animal Care and Use Committee. Mouse brain and spinal cord tissues were collected and fixed in chilled 4% paraformaldehype (PFA, Ted Pella) for the following durations of time: E10.5-E11.5 (1 Hour), E12.5 (2 Hours), E13.5 (3 Hours), E14.5 (4 Hours), E15.5-E16.5 (5 Hours), E17.5-P3 (Overnight). After fixation the tissue was cryoprotected in 30% sucrose, mounted in optimal cutting temperature (OCT), cryosectioned into 12 µm thick sections, and processed for immunohistochemistry or in situ hybridization as previously described[27,31-33].

Antibodies and in situ hybridization probes: Primary antibodies used for immunohistochemistry were as follows: chicken anti-GFP (Aves Labs, GFP-1020), 1:1,000; rabbit anti-Hes1[34], 1:2,000; mouse anti-Mash1[35], 1:200; goat anti-Neurog2 (Santa Cruz Biotechnology sc-19233), 1:1,000; rabbit anti-Nkx2.2[36], 1:10,000; guinea pig anti-Olig2[37] (1:20,000); rabbit anti-Olig2 (Millipore AB9610), 1:5,000; rat anti-Rbpj (Active Motif 61506),

1:100; anti-Shh (Developmental Studies Hybridoma Bank 5E1), 1:100; goat anti-Sox2 (Santa Cruz Biotechnology sc-17320), 1:2,000. All antibodies were diluted to a working concentration in AB Block solution (Block = 1% Heat inactivated Horse Serum in PBS with 0.1% Triton X-100). Alexa488-, FITC-, Cy3-, Cy5-, and Dylight649-conjugated secondary antibodies were obtained from Jackson Immunoresearch Laboratories, Inc. (West Grove, PA). RNA probes were generated by in vitro transcription of PCR products amplified from mouse spinal cord cDNA. Primers against the following genes were designed using the program Primer3 (http://bioinfo.ut.ee/primer3/). *Hes5*, forward 5'-GGATGAGCTCGTTCCTCTGG-3' and reverse 5'-GAGATTAACCCTCACTAAAGGGAGCAGGCTGAGTGCTTTCCTA-3' and *Neurog3*, forward 5'-AGGCTTCTCATCGGTACCCT-3' and reverse 5'-GAGATTAACCCTCACTAAAGGGCATAGGCTAGGGCTTTCCGG-3'. The underlined text denotes a T3 polymerase binding site incorporated into the reverse primer.

Evans blue dye injections: P0-5.5 neonatal mice were euthanized in accordance with guidelines set forth by the UCLA Institutional Animal Care and Use Committee. The skin was removed from the skull and, with the skull still intact, a glass capillary needle was used to slowly inject 5-10 µl of Evans blue dye (4% diluted in sterile PBS) into the lateral ventricles to visualize the pathway of the cerebral spinal fluid (CSF) through the ventricular system[38,39]. After Evans blue dye addition, the brain was removed from the skull, briefly rinsed in PBS, and then fixed overnight in 4% PFA. After fixation, the brains were rinsed thoroughly in PBS and then assessed for obstructive hydrocephalus. Brains were then scored as either "asymptomatic" or "hydrocephalus" based on the distance the dye traveled.

Vibratome sections: The brains were sectioned to better assess where the obstruction occurred in the P0-5.5 neonatal mutant mice. After Evans blue dye injection into the lateral ventricles, the brains were fixed, thoroughly rinsed in PBS, mounted in 4% low melting agarose (prepared in PBS), and then 300 µm serial coronal sections were cut on a Leica VT1000S vibratome.

Tissue clearing: To better see where the obstruction occurred in the P5.5 neonatal mutant mouse brains, after Evans blue dye was injected into the lateral ventricles the brains were made transparent as previously described[40]. The protocol was modified slightly from what was reported. Briefly, the tissue was fixed in 4% PFA overnight at 4ºC, rinsed thoroughly in PBS, bleached overnight in a solution of 33.3% H_2O_2/13.3% DMSO/53.4% MeOH at 4ºC, dehydrated in a series of MeOH washes, post-fixed overnight in a solution of 20% DMSO/80% MeOH at 4ºC, rinsed in MeOH, and then cleared in BABB (33.3% benzyl alchohol/66.6% benzyl benzoate).

Statistical Analysis: In Figure 3-4, the mouse masses are represented as mean values ± SEM. For the data shown in Figures 3-4C and 3-4F an unpaired, two-tailed t-test was performed. Significance was assumed when $p < 0.05$. *$p < 0.05$, **$p < 0.01$, ***$p < 0.001$.

RESULTS

Olig2 expression within the developing forebrain

Notch signaling is a highly conserved signaling pathway that plays a major role in the proper development and patterning of multiple structures including the brain, spinal cord, heart, pancreas, intestines, bone, and somites[16,41-47]. The importance of Notch signaling in development is perhaps best illustrated in the homozygous *Rbpj*$^{-/-}$ embryos, where a complete loss of the Notch transcriptional effector Rbpj results in delayed growth and ultimately embryonic death at e8.5-e10.5[48]. Given the early lethality of the *Rbpj*$^{-/-}$ mutants, to study the role of Notch signaling in the maintenance of neural progenitors that give rise to the ependymal cell layer, we used a Cre-*loxP* mediated gene targeting approach to selectively inhibit Notch signaling in specific regions of the embryonic brain. Knowing the confined expression of Olig2 in the developing forebrain, we chose to cross Olig2^{Cre} mice[27] with mice harboring either a *R26R*^{GFP} transgenic reporter[29] (Control condition) or a Cre-inactivatable Rbpj allele[30] and a *R26R*^{GFP} transgenic reporter[29] (Rbpj^{CKO} condition). Consistent with previous studies, in control

embryos Olig2 was weakly expressed within the lateral ganglionic eminence (LGE) and strongly expressed within the medial ganglionic eminence (MGE), anterior entopeduncular/preoptic area (AEP/POA), ventral thalamus, and prethalamus (**Figures 3-1D-H and 3-S1A-L**)[49-54]. In our manipulations, GFP highly overlapped with Olig2 (**Figures 3-1D-H**), indicating to us that we could confidently use GFP to identify cells that had undergone $Olig2^{Cre}$ mediated recombination.

To assess for changes in Notch signaling activity we examined the expression of *Hes5*, a well-established and faithful Notch effector[55,56]. Unexpectedly, the loss of Rbpj had widely varying effects on both *Hes5* expression and neural progenitor maintenance. In the rostral telencephalon (Plane 1), a loss of Rbpj from the MGE resulted in no reduction in *Hes5* or Sox2+ neural progenitors (**Figure 3-2A-B**). In the rostral diencephalon (Plane 2), the loss of Rbpj within the POA resulted in a robust loss of *Hes5* and thinning of the neural progenitors (**Figure 3-2C-D**). Lastly, within the caudal diencephalon (Plane 5), the loss of Rbpj within the prethalamus resulted in an expansive loss of *Hes5* and neural progenitors (**Figure 3-2E-F**). One explanation for this varied response could be due to a regulation of *Hes1* and *Hes5* that is independent of canonical Notch signaling[57,58]. A prime candidate would be Shh signaling. Previous studies have shown that Shh signaling has the ability to activate Hes1 and Hes5 in the absence of Notch signaling[57]. In a previous study we were able to show that, when Rbpj was removed from progenitors within the developing ventral spinal cord, the presence of Shh elevated the expression of Hes1 in a Notch-independent manner, thus preserving the adherens junctions in the manipulated cells[59]. As Shh is highly present in regions near both the MGE and POA, it is possible that Hes1 is similarly compensating for a loss of Hes5 in these regions[60]

Loss of cell polarity and cell adhesion in the neuroepithelium of $Rbpj^{CKO}$ mutants

The ventricular zone is composed of neuroepithelial cells, highly polarized neural progenitors that are maintained by junctional adhesion proteins[4,61]. In the caudal diencephalon of $Rbpj^{CKO}$ mutants, in addition to a loss of neural progenitors, the apical edges of the

recombined regions appeared ragged and disorganized suggesting the integrity of the neuroepithalial cell layer was compromised (**Figure 3-2E-F**). To examine this further we used various antibodies to evaluate changes in cell identity, polarity, and adhesion. As expected, Notch signaling inhibition resulted in both a reduction in Sox2+ neural progenitors and an increase in Tuj1+ neurons (**Figure 3-3A-F and 3-3K-L**). However, to our surprise, this massive increase in neurogenesis tore apart the neuroepithelial cell layer. Multiple lines of evidence point towards a loss of neuroepithelial integrity. First, we observed a loss of apically localized primary cilia and wedge-shaped morphology (**Figure 3-3G-J**), both features of neuroepithelial cells[62,63]. Second, we observed a loss of multiple apically enriched proteins that are known to maintain the integrity of the neuroepithelial layer; including the cell polarity marker atypical protein kinase C (aPKC) and the cell adhesion markers N-cadherin (Ncad) and β-catenin (βCat) (**Figure 3-3M-R**). Lastly, in this region the Notch ligand Jagged1 is enriched in the membrane of the neural progenitors. The presence of this Notch ligand was also loss in the RBP^{CKO} tissue (**Figure 3-3S-T**). Further analysis of control and $Rbpj^{CKO}$ embryos at e10.5 indicated that the neuroepithelial cells initially developed normally in the mutants (**Figure 3-S2A-L**) and only began to degrade at e11.5 (**data not shown and Table 3-2**). Collectively, this data indicates that within the caudal diencephalon Notch signaling is necessary for the maintenance of the integrity of the neuroepithelial cell layer.

Disruption of the neuroepithelial cell layer within the developing diencephalon of $Rbpj^{CKO}$ mutants results in severe obstructive hydrocephalus

Due to the selective loss of Notch signaling activity in $Olig2^{+}$ progenitors, $Rbpj^{CKO}$ mice were viable. At birth, the $Rbpj^{CKO}$ pups were indistinguishable from control littermates. However, at P5, the $Rbpj^{CKO}$ mutants were slightly smaller (~15%) and in a portion of these mutants we began observe a domed head which is characteristic of hydrocephalus (**Figure 3-4A-C**). The distinction between control and mutant mice grew over time and at P20-26 the $Rbpj^{CKO}$ mice

were noticeably smaller than controls (~55%). Although all the mutant mice were smaller than littermate controls, at P20-26 only ~50% of the mutants developed severe hydrocephalus and had to be euthanized (**Figure 3-4D-G**). Rbpj^{CKO} mutants that did not develop a severely domed head were classified as asymptomatic. A closer inspection of the asymptomatic Rbpj^{CKO} brains revealed that the ventricles were slightly dilated, indicating the flow of cerebral spinal fluid (CSF) through the ventricular system was initially blocked, but then relieved in these mutants.

The underlying cause of hydrocephalus can be due to many factors including: developmental defects that obstruct a portion of the ventricular system, a loss of CSF flow due to ciliary defects, or an overproduction of CSF by the choroid plexus. In fact, a brief literature search revealed over 50 genetic mutant mouse models that exhibit hydrocephalus with a varying degree of penetrance (**Table 3-1**). Thus, to determine if the loss of neuroepithelial cell integrity observed in the embryonic mutants was the source of the hydrocephalus in the postnatal mice, we first needed to determine the cause of the hydrocephalus. In this assessment, we first decided to determine if the hydrocephalus was obstructive or communicating. To do this, we injected ~5-10 µl of Evans blue dye into the lateral ventricles of P5.5 brains. In control brains, the Evans blue dye filled the lateral ventricles, then passively flowed through the Foramen of Monro, the third ventricle, the Aqueduct of Sylvius, the fourth ventricle, and then out via the central canal (**Figure 3-5A-B**). In Rbpj^{CKO} brains, the Evans blue dye accumulated in the enlarged lateral ventricles and went no further, indicating that the hydrocephalus was obstructive (**Figure 3-5C-D**). Interestingly, although only 50% of the Rbpj^{CKO} mutants exhibited severely domed heads at P20-26 (**Figure 3-5D-G**), using this Evans blue assay we observed that the ventricular system of all mutant brains at P5.5 were obstructed and had enlarged lateral ventricles (n = 39 control, 10 Rbpj^{CKO}). Next we wanted to determine where the obstruction occurred. The absence of Evans blue dye beyond the lateral ventricles suggested the closure was located somewhere in the Foramen of Monro or the third ventricle. A closer inspection via vibratome sections revealed the obstruction was present along the rostral

third ventricle. Further analysis of this region via immunohistochemical analysis revealed that the cells lining the third ventricle in this obstructed region were severely disrupted (**Figure 3-5A-B, inset**). Collectively, the data indicates that the hydrocephalus exhibited by the Rbpj^{CKO} mutant is due to a loss of the integrity of the inner cell layer lining the third ventricle.

In Rbpj^{CKO} mutants, a loss of neuroepithelial integrity in the embryo results in a loss of ependymal integrity in the adult

The ependyma is comprised of a single layer of ciliated cells that line the entire ventricular system[64]. Ependymal cells have multiple roles including the propulsion of CSF through the ventricles, the secretion and absorption of water to and from the CSF, and functions as a physical barrier to prevent neurotoxic substances from entering the brain[64-67]. The ependymal cells are derived from neuroepithelial radial glial cells and do not become mature multiciliated cells until later in postnatal life[68]. As a derivative of the neuroepithelium, we wanted to determine if the loss of neuroepithelial integrity we observed in the embryonic Rbpj^{CKO} brains (**Figure 3-6A-B, 3-S4A-D**) resulted in a loss of ependymal cell layer integrity in the adult brains. As the increased pressure produced by the accumulation of CSF can itself alter the morphology of the ependymal cells[69], we restricted our analysis of ependymal cells to asymptomatic Rbpj^{CKO} mutants, mutants that lacked a clearly domed head but upon dissection did still present with slightly enlarged lateral ventricles. In control adult brains, the ependymal cell layer lining the third ventricle was intact and clearly identified by the expression of the intermediate filament marker Vimentin and a secretory protein S100β[67,70] (**Figure 3-6C-D**). In contrast, the ependymal cells lining the third ventricle were disorganized and expressed little to no Vimentin or S100β (**Figure 3-6E-F**). Collectively, this data suggests that Notch signaling maintains the integrity of the neuroepithelial cell layer. In the absence of Notch signaling activity, the neuroepithelial cells become disorganized, this results in a loss of ependymal cell integrity and ultimately obstructive hydrocephalus.

DISCUSSION

Notch signaling is essential for the maintenance of neuroepithelial integrity in the developing diencephalon

The transition of neuroepithelial cells from progenitors to neurons requires both a change in molecular identity and a disassembly of the apical contacts that bind the cells to the ventricular zone. Thus, in regards to balancing progenitor maintenance and differentiation, it is clear that differentiation must occur in moderation to not only guarantee a sufficient progenitor population is maintained to give rise to later born cell types, but to also ensure an adequate number of apical adhesion proteins are present to maintain the integrity of the neuroepithelial cell layer. While much is known about the mechanisms that regulate progenitor maintenance, relatively little is known about the mechanisms that maintain apical adherens junctions or the means through which a loss of progenitor character triggers the release of the cell from the ventricular zone. In our study we implicate Notch signaling in both of these processes. Our studies revealed that, in a specific region of the developing brain, Notch signaling is necessary for both the maintenance of neural progenitors and the maintenance of cell adhesion complexes. A loss of Notch signaling in this region not only results in premature neurogenesis, but also an acute loss of cell adhesion and cell polarity. The consequences of this loss is severe, resulting in a loss of neuroepithelial cell layer integrity in the embryo, a loss of ependymal cell layer integrity in the adults, and ultimately the occurrence of obstructive hydrocephalus. Collectively, our data provide important insights into the mechanisms that maintain the balance between proliferation and differentiation, by illustrating that Notch signaling not only maintains cells as progenitors through the inhibition of proneural gene expression, but also through the maintenance of cell adhesion proteins.

The loss of neuroepithlial integrity in the Rbpj^{CKO} mutants was limited to a critical region of the developing brain

The Cre-*loxP* mediated gene targeting approach we used allowed us to selectively inhibit Notch signaling in three distinct regions of the developing brain: MGE, POA, and thalamus/prethalamus (**Figure 3-1**). However, we only observed a loss of cell adhesion and neuroepithelial integrity in the prethalamus of the caudal diencephalon. A closer look revealed that the effects of our manipulations on Notch signaling and progenitor maintenance varied greatly throughout the brain. In the MGE, a loss of Rbpj had no effect on the expression of *Hes5* (**Figure 3-2A-B**). In the POA, a loss of Rbpj resulted in an acute loss of *Hes5*, but only a thinning of Sox2+ progenitors (**Figure 3-2C-D**). Lastly, in the prethalamus of the caudal diencephalon, a loss of Rbpj resulted in an acute loss of *Hes5*, a depletion of Sox2+ progenitors, and a disruption of the neuroepithelial cell layer due to a loss of apical adhesion proteins (**Figure 3-2E-F**). What could account for such a diverse difference in response?

Among the Hes genes expressed in the developing CNS, Hes5 is typically regarded as the most reliable readout of Notch signaling activity[71]. Thus, in the Rbpj^{CKO} tissue, we were surprised to see no change in *Hes5* expression in the MGE. However, other members of the Hes/Hey gene family can be activated by Notch-independent pathways. For example, Hes1 is activated by Shh signaling and Hey2 is activated by FGF signaling[57,58,72]. Thus, it is very possible that the sustained expression of Hes5 in the MGE is a product of input from a Notch-independent pathway. This possibility is supported by other studies, which similarly observed no change in Hes5 expression in the developing hindbrain and retina upon conditional Rbpj deletion[73,74].

In the Rbpj^{CKO} mutants, a severe loss of *Hes5* was observed in the POA. However, where a loss of Notch signaling activity results in a disruption of neuroepithelial integrity in the thalamus/prethalamus, only a moderate loss of Sox2+ progenitors were observed in the POA.

This discrepancy could be due to the lasting presence of other Hes genes in the region. We previously observed this compensatory effect mediated by other members of the Hes family, in the spinal cord. In a previous study we removed Notch signaling in both the intermediate and ventral spinal cord. Although we observed premature neurogenesis in both regions, the neuroepithelial integrity was only disrupted in the intermediate spinal cord[59]. Further analysis revealed that the integrity of the ventricular zone was preserved due to the continued presence of Hes1 in the ventral spinal cord, which was activated by Shh in a Notch-independent manner. As is observed in the ventral spinal cord, the POA is located very closely to a source of Shh[75,76]. Thus, the maintenance of neuroepithelial organization in the POA could similarly be due to the lasting presence of Hes1 in this region.

Collectively, our data reveal that the loss of Notch signaling activity had a very different effect on progenitors depending on the region it was removed from. The differences in the severity of the response are interesting because they indicate that the maintenance of neuroepithelial integrity is the product of multiple factors. Notch signaling is merely one of these maintenance factors. As other factors must be present in the MGE and POA to prevent the neuroepithelium from dismantling in the absence of Notch signaling activity, it suddenly becomes clear that the caudal diencephalon (specifically the region lining the third ventricle) lacks these extra safety factors. As the third ventricle is very thin, it is naturally a weak point in the ventricular system that is susceptible to closure. This is evident in our mouse model, where a small loss of ependymal cell integrity lining the third ventricle was sufficient to generate severe hydrocephalus.

Is this loss of neuroepithelial integrity in Rbpj^{CKO} mutants mediated by Hes genes or another Notch target gene?

The loss of neuroepithelial integrity we observed in the diencephalon of the Rbpj^{CKO} mutants strongly resembled the disorganization of the ventral spinal cord observed in *Hes1*$^{-/-}$

/Hes5$^{-/-}$ double mutants[77]. Most notable, both mutant models exhibit premature neurogenesis and a loss of apical adherens junctions. These similarities suggest that the loss of neuroepithelial integrity we observed in the Rbpj^{CKO} mutants is similarly due to a loss of Hes1 and Hes5 expression in this region. However, it is also possible that integrity of the ventricular zone is mediated through other Notch target genes. Recently, using ChIP-Seq technology, multiple labs have identified numerous novel Rbpj target genes. Of these newly identified genes, multiple have known cell adhesion functions[78-80]. Thus, it is possible that in our manipulations Rbpj is directly targeting a gene involved in the maintenance of cell adhesion and/or cell polarity.

Disorganization of neuroepithelium, due to a loss of cell adhesion and polarity, is a causal factor in obstructive hydrocephalus in Rbpj^{CKO} mice

Hydrocephalus is a medical condition that is characterized by the accumulation of cerebral spinal fluid (CSF) in the ventricles of the brain. While no official statistics exist, the National Hydrocephalus Foundation estimates that hydrocephalus occurs in one out of every 500 live births and is the leading cause of pediatric brain surgery in the United States. As there is no cure for hydrocephalus, cerebral shunts are the most commonly used method to treat the symptoms, reducing intercranial pressure by transporting excess CSF to the abdomen. Although hydrocephalus is relatively common, the genetics and molecular pathogenesis of this condition are complex and poorly understood[81]. Hydrocephalus has been studied in numerous mouse models to better understand the factors that give rise to this condition. Through these genetic mouse models it now clear that hydrocephalus can be the product of cell adhesion defects, craniofacial defects, ciliary defects, structural brain defects, and mutations that result in the overproduction of CSF or the inability to regulate its presence within the brain ventricles (**Table 3-2**).

The root cause of the hydrocephalus in the Rbpj^{CKO} mice is a loss of cell adhesion and

cell polarity in the caudal diencephalon. This loss of cell adhesion results in a disorganization of neuroepithelial cells in the embryonic brain and a disruption of ependymal cells in the adult brain. The size and placement of the disruption is sufficient to obstruct the third ventricle. Unable to pass, the CSF quickly accumulates in the lateral ventricles and results in hydrocephalus. The hydrocephalus observed in the $Rbpj^{CKO}$ mutants, strongly resembles the hydrocephalus observed in the following knockout mice: $Dlg5^{-/-}$[82], $L1cam^{-/-}$[83], $Lgl1^{-/-}$[84], and $Myh10^{-/-}$[85]. A disruption of adherens junctions and loss of cell polarity are the primary defects responsible for the hydrocephalus observed in the $Dlg5^{-/-}$, $L1cam^{-/-}$, $Lgl1^{-/-}$, and $Myh10^{-/-}$ knockouts. Thus, this further supports our observation that the hydrocephalus exhibited in the $Rbpj^{CKO}$ mutants is due to a loss of cell adhesion and polarity.

In summary, we report that in the developing CNS, Notch signaling plays a vital role in progenitor and cell adhesion maintenance. While it is well known that Notch signaling preserves the progenitor cell state through an inhibition of proneural gene expression, we illustrate that Notch signaling plays an equally important role in the maintenance of apical adhesion contacts and cell polarity. By maintaining the integrity of the neuroepithelial cell layer, Notch signaling is vital for the development of an intact ventricular system. In the absence of Notch signaling activity, the ependymal cells lining the third ventricle are disrupted, resulting in severe obstructive hydrocephalus.

FIGURES

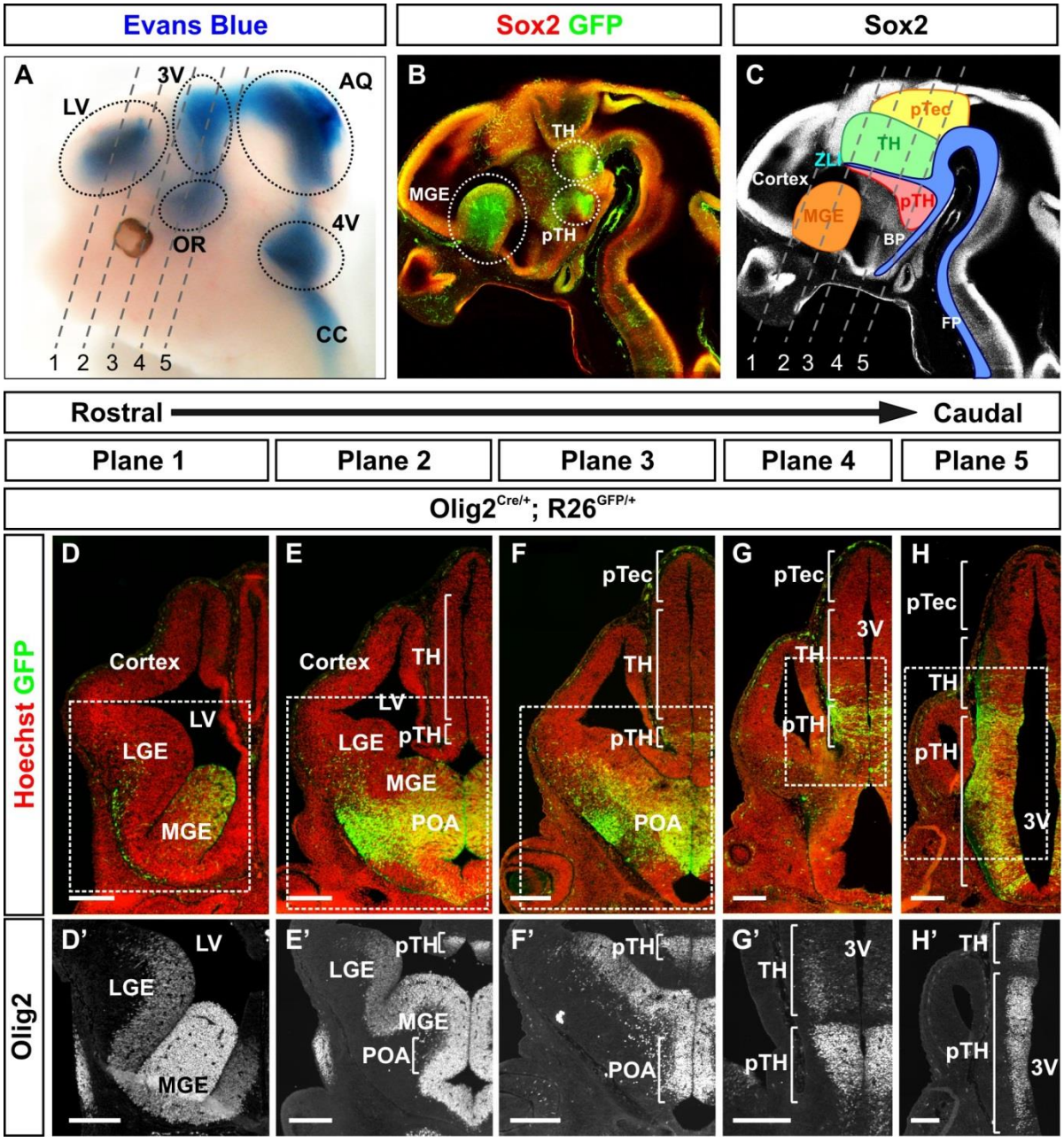
Evans Blue
Sox2 GFP
Sox2
A
3V
AQ
LV
4V
OR
CC
1 2 3 4 5
B
TH
MGE
pTH
C
pTec
TH
ZLI
Cortex
pTH
MGE
BP
FP
1 2 3 4 5
Rostral
Caudal
Plane 1
Plane 2
Plane 3
Plane 4
Plane 5
Olig2Cre/+; R26GFP/+
Hoechst GFP
D
Cortex
LV
LGE
MGE
E
Cortex
TH
LV
LGE
pTH
MGE
POA
F
pTec
TH
pTH
POA
G
pTec
3V
TH
pTH
H
pTec
TH
pTH
3V
Olig2
D'
LV
LGE
MGE
E'
pTH
LGE
MGE
POA
F'
pTH
POA
G'
3V
TH
pTH
H'
TH
pTH
3V

Figure 3-1: Spatial analysis of Olig2^{Cre} mediated recombination in the developing brain

(A-C) Lateral view of the head of a control e12.5 mouse embryo (Olig2$^{Cre/+}$; R26$^{GFP/+}$). Dashed black and grey lines (1-5) represent the planes of coronal sections captured in images D-H. **(A)** Evans blue dye injected into the lateral ventricles (LV) to illustrate the location of the optic recess (OR), third ventricle (3V), Sylvian Aqueduct (Aq), Fourth ventricle (4V), and central canal (CC). **(B)** Wholemount immunofluorescence. Dotted white circles identify two major GFP+ populations within the brain, one within the telencephalon and the other in the diencephalon. **(C)** A schematic to illustrate the location of the basal plate (BP), floor plate (FP), medial ganglionic eminence (MGE), pretectum (pTec), prethalamus (pTH), thalamus (TH), and zona limitans intrathalamica (ZLI). The basal plate, ZLI, and floor plate secrete Shh (blue). **(D-H)** Serial coronal sections (~240 µm apart) to better show that Olig2^{Cre} mediated recombination occurs within the MGE, POA, pTH, and TH. Olig2 is also present within the LGE, although there is little to no GFP present within this region at this age. Scale bars = 200 µm.

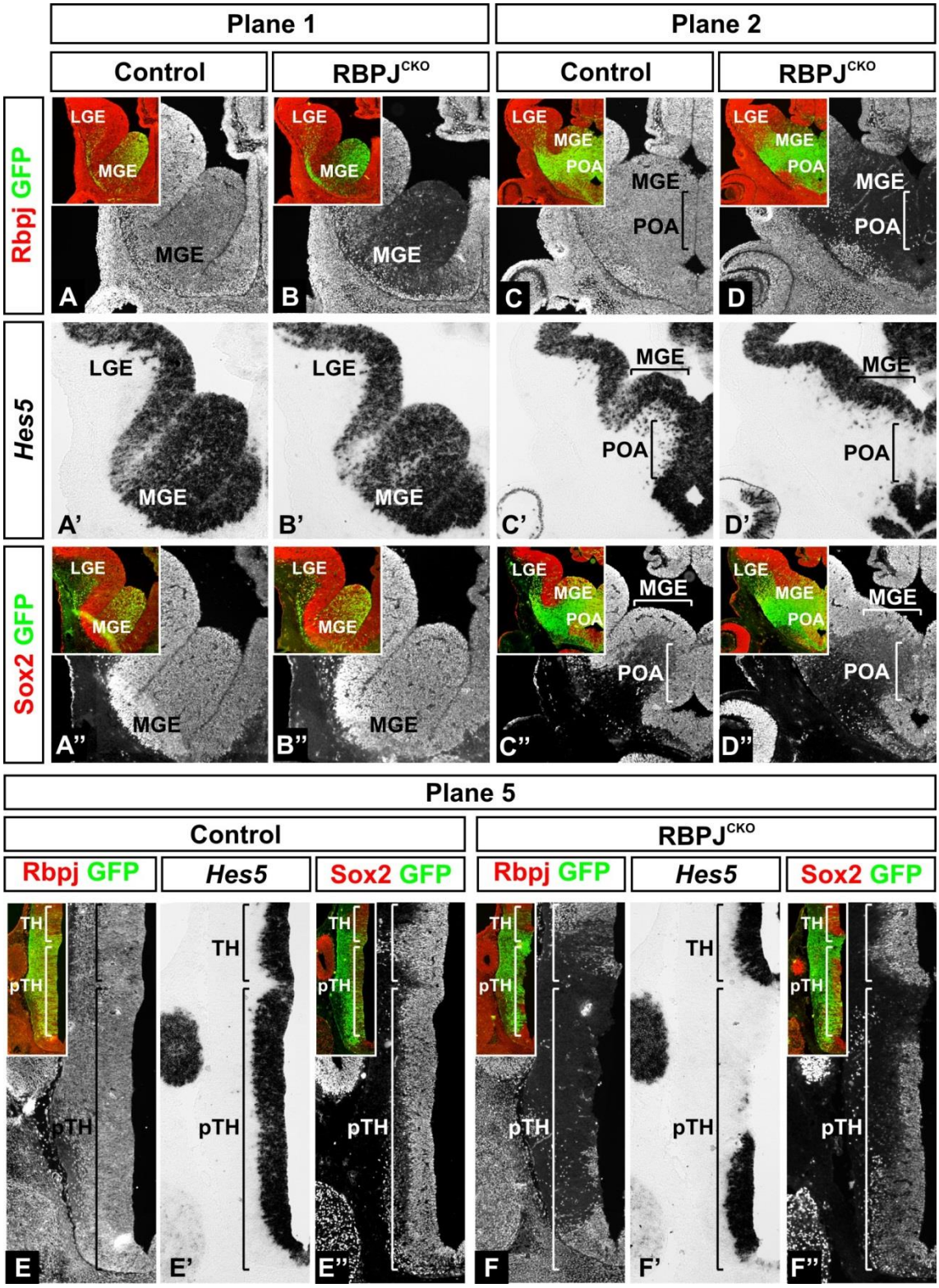
Plane 1
Plane 2
Control
RBPJ^CKO
Control
RBPJ^CKO
Rbpj GFP
Hes5
Sox2 GFP
LGE
MGE
POA
A
B
C
D
A'
B'
C'
D'
A''
B''
C''
D''
Plane 5
Control
RBPJ^CKO
Rbpj GFP
Hes5
Sox2 GFP
TH
pTH
E
E'
E''
F
F'
F''

Figure 3-2: The loss of Rbpj has a region-specific effect on the Notch signaling activity of neural progenitors

(A-F) Coronal sections of e12.5 control and $Rbpj^{CKO}$ brains collected from three regions: (A-B) telencephalon (Plane 1), (C-D) rostral diencephalon (Plane 2), and (E-F) caudal diencephalon (Plane 5). In all regions, a loss of Rbpj protein was observed in the $Rbpj^{CKO}$ tissue. However, a loss of the downstream Notch effector *Hes5* was only observed in the preoptic area (POA) and prethalamus (pTH). A thinning of the Sox2+ neural progenitors was observed in the POA; however, a complete loss of these neural progenitors was only observed in the prethalamus (pTH). The insets indicate where the GFP+ cells that have undergone Cre mediated recombination are located. Lateral ganglionic eminence (LGE), medial ganglionic eminence (MGE), and thalamus (TH).

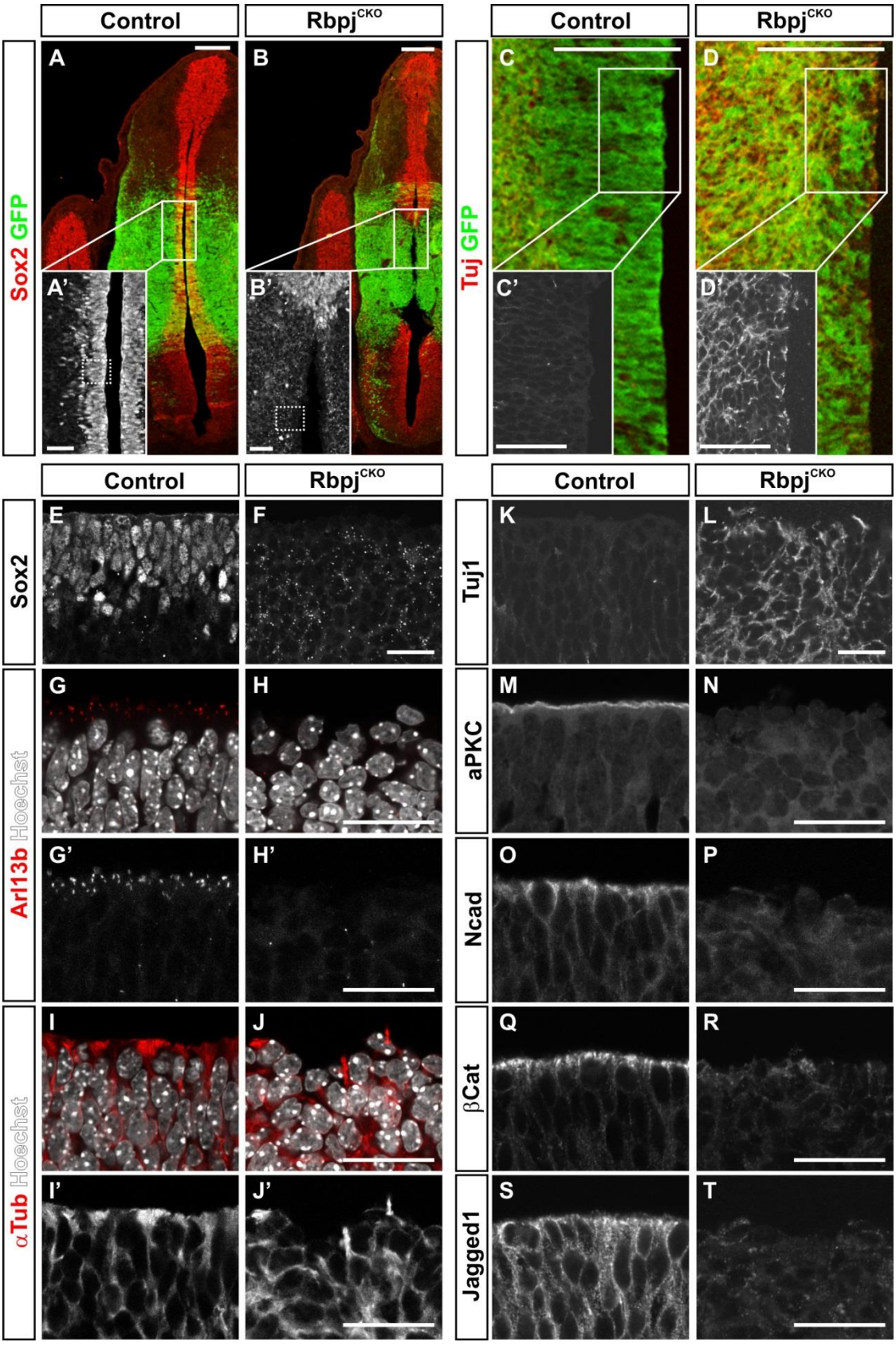
Control
Rbpj^CKO
Control
Rbpj^CKO
Sox2 GFP
A
B
C
D
A'
B'
C'
D'
Tuj GFP
Control
Rbpj^CKO
Control
Rbpj^CKO
Sox2
E
F
K
L
Tuj1
Arl13b Hoechst
G
H
M
N
aPKC
G'
H'
O
P
Ncad
αTub Hoechst
I
J
Q
R
βCat
I'
J'
S
T
Jagged1

Figure 3-3: Loss of Notch signaling activity results in a loss of neural progenitors, cell adhesion, and cell polarity within the developing diencephalon

(A-B) Low magnification coronal sections through the caudal diencephalon of e12.5 control and $Rbpj^{CKO}$ embryos. The enlarged insets (bottom left, A' and B') highlight a loss of Sox2+ progenitors within the $Rbpj^{CKO}$ brains. The dotted box in the inset illustrates the approximate region captured in images E-T. **(C, D)** The presence of Tuj1+ neurons present within the developing diencephalon. The enlarged insets (bottom left, C' and D') highlight an increase in Tuj1+ neurons present within the $Rbpj^{CKO}$ brains. The apical side is to the right. Scale bars, low mag = 200 µm and high mag = 50 µm. To assess for changes in cell identity, polarity, and adhesion, we used antibodies to look at the following proteins. **(E, F)** Sox2+ neural progenitors. **(G, H)** Arl13b+ primary cilia present on the apical surface of neural progenitors and extending into the ventricle. **(I, J)** Acetylated α-tubulin, labels the cytoplasmic microtubules and allows us to assess the morphology of the cells. **(K, L)** Tuj1+ neurons. **(M, N)** aPKC, an apically localized cell polarity marker and component of the Par3/Par6/aPKC complex[86]. **(O, P)** Ncad, an apically localized cell adhesion marker. **(Q, R)** βCat, an apically localized cell polarity marker. **(S, T)** Jagged1, a Notch ligand that is upregulated in this region. In all the enlarged images (E-T), the apical side is up. Scale bars = 25 µm.

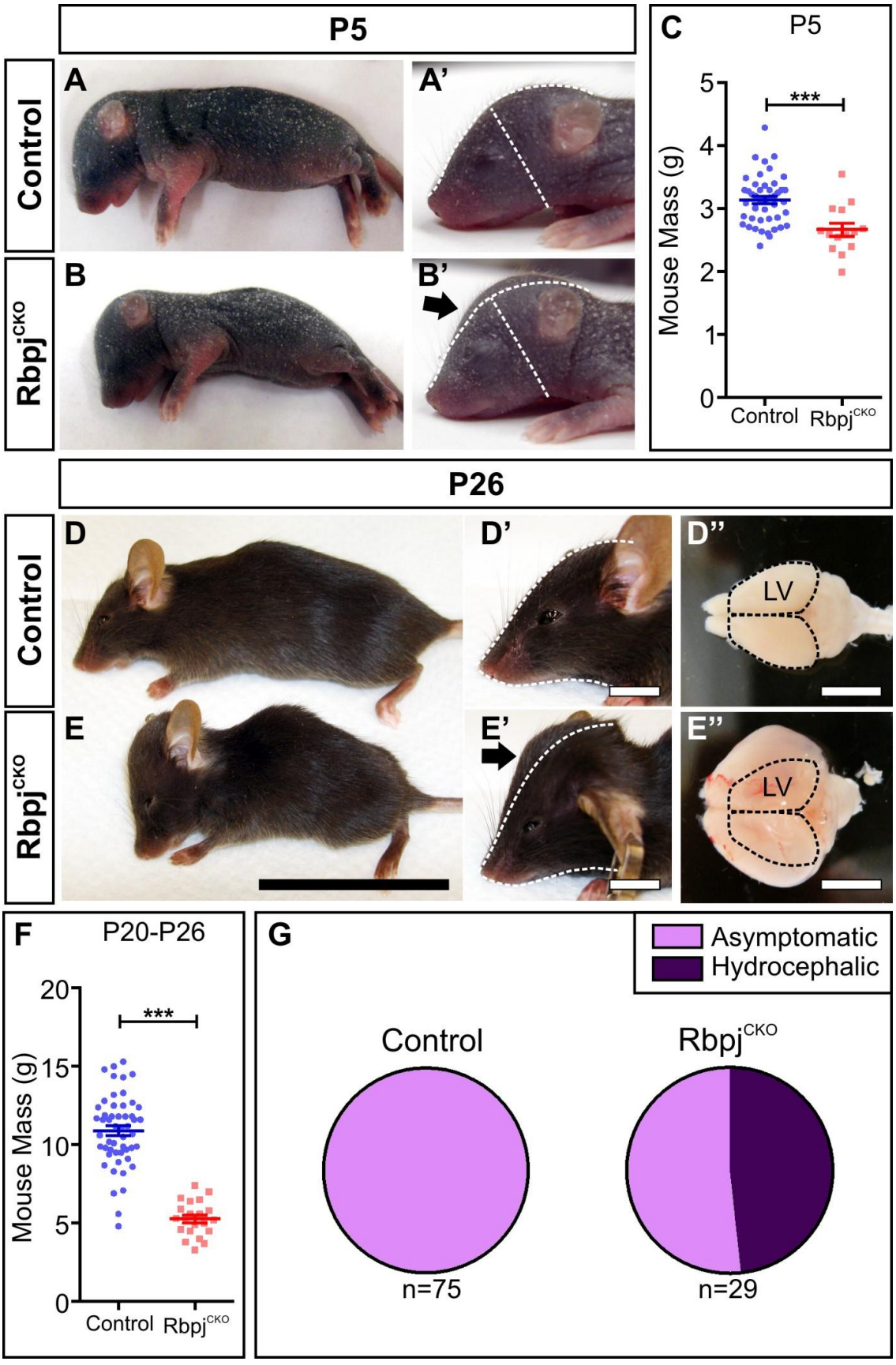
P5
Control
Rbpj^CKO
A
A'
B
B'
C
P5
Mouse Mass (g)
***
Control
Rbpj^CKO
P26
D
D'
D''
LV
E
E'
E''
F
P20-P26
G
Asymptomatic
Hydrocephalic
Control
Rbpj^CKO
n=75
n=29

Figure 3-4: Gross analysis of Rbpj^{CKO} mice

(A-B, D-E) External appearance of Rbpj^{CKO} mice and littermate controls at P5 and P26. **(A-B)** At P5, Rbpj^{CKO} mice were moderately smaller and many possessed a slightly domed head. **(C)** A box and whisker plot of P5 mouse masses. Control = 3.14 ± 0.06 grams (n = 46). Rbpj^{CKO} = 2.67 ± 0.10 grams (n = 14). ***p < 0.001. **(D-F)** At P20-26, all Rbpj^{CKO} mice were noticeably smaller than littermate controls and ~50% developed severe hydrocephalus. Scale bars (D-E) = 5 cm. Scale bars (D'-E') = 1 cm. **(D'' and E'')** Brains collected from P26 control and Rbpj^{CKO} mutants. The dotted white and black lines represent an outline of the control head and brain, which has been placed over the mutant head and brain to better illustrate the domed phenotype and enlarged lateral ventricles (LV) that are characteristic of hydrocephalus. Scale bars = 1 cm. **(F)** A box and whisker plot of P20-26 mouse masses. Control = 10.89 ± 0.32 grams (n = 52). Rbpj^{CKO} = 5.28 ± 0.24 grams (n = 21). ***p < 0.001. **(G)** Graphs to illustrate the penetrance of the hydrocephalus phenotype. Based on the absence or presence of a domed head, the mice were classified as either asymptomatic or hydrocephalic (n = 75 control and 29 Rbpj^{CKO}).

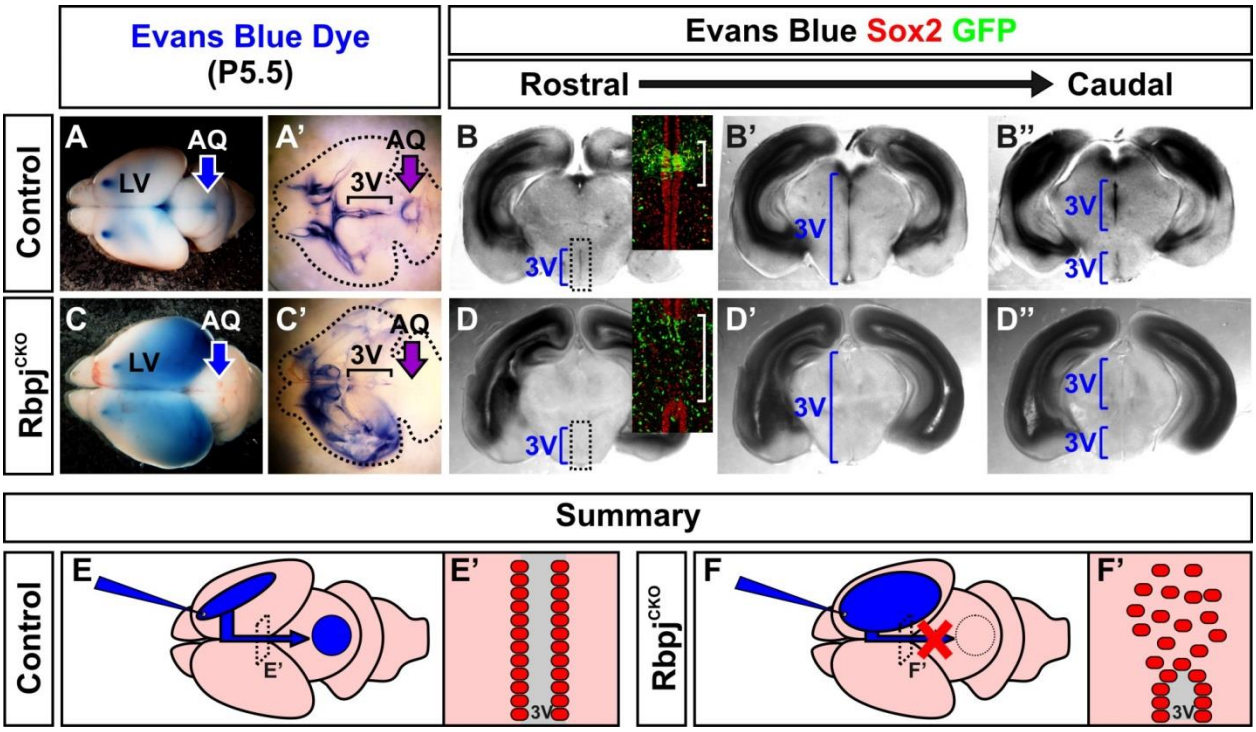

Figure 3-5: Rbpj^{CKO} mice develop obstructive hydrocephalus

(A-D) Evans blue dye injected into the lateral ventricles of P5.5 Control and Rbpj^{CKO} brains. **(A)** In control brains, Evans blue dye easily passes from the lateral ventricles (LV) into the third ventricle (3V), Sylvian aqueduct (AQ), and fourth ventricle. **(C)** In comparison, the Evans blue dye accumulates in the lateral ventricles of the Rbpj^{CKO} brains due to an obstruction of the third ventricle. Utilizing this Evans blue dye assay, the ventricular system of all the P5 Rbpj^{CKO} brains were obstructed and all the control brains were not obstructed (n = 39 control and 10 Rbpj^{CKO}). **(A, C)** External view of the Evans blue filled brains before and after clearing. **(B, D)** Serial coronal vibratome sections of control and Rbpj^{CKO} brains injected with Evans blue dye. Evans blue dye, represented by the blue brackets, is present throughout the third ventricle of the control brain, but is completely absent in the third ventricle of the mutant brain. Insert represents the lining of the third ventricle in the boxed region. The Sox2+ neuroepithelial cells lining the third ventricle are highly disorganized in the mutant brain. **(E, F)** Model of the obstructive hydrocephalus.

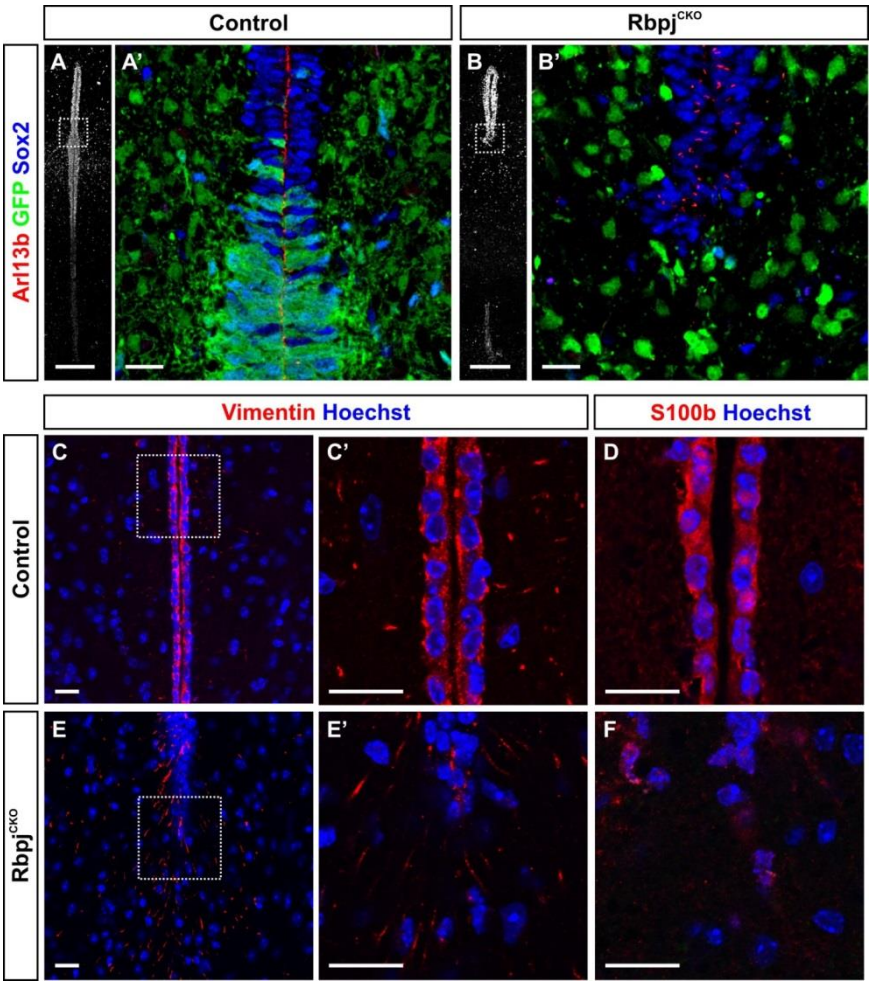

Figure 3-6: Obstructive hydrocephalus in the Rbpj^{CKO} mutants is due to a loss of ependymal cell integrity

(A-B) Horizontal sections through the diencephalon of e18.5 control and Rbpj^{CKO} embryos. The white brackets illustrate a loss of Sox2+ progenitors present along the rostrocaudal axis and the dotted box identifies the region depicted in the enlarged images (A' and B'). **(A'-B')** Arl13b+ cilia are present on the inner layer of Sox2+ progenitors lining the ventricles. Scale bars, low mag = 200 µm and high mag = 20 µm. **(C-F)** Coronal sections through the third ventricle of 2 month old control and asymptomatic Rbpj^{CKO} adults. The dotted box identifies the region depicted in the enlarged images (C', D, E', F). The Vimentin+ and S100β+ ependymal cells lining the third ventricles are disorganized and largely absent in the mutant brain. Scale bars = 20 µm.

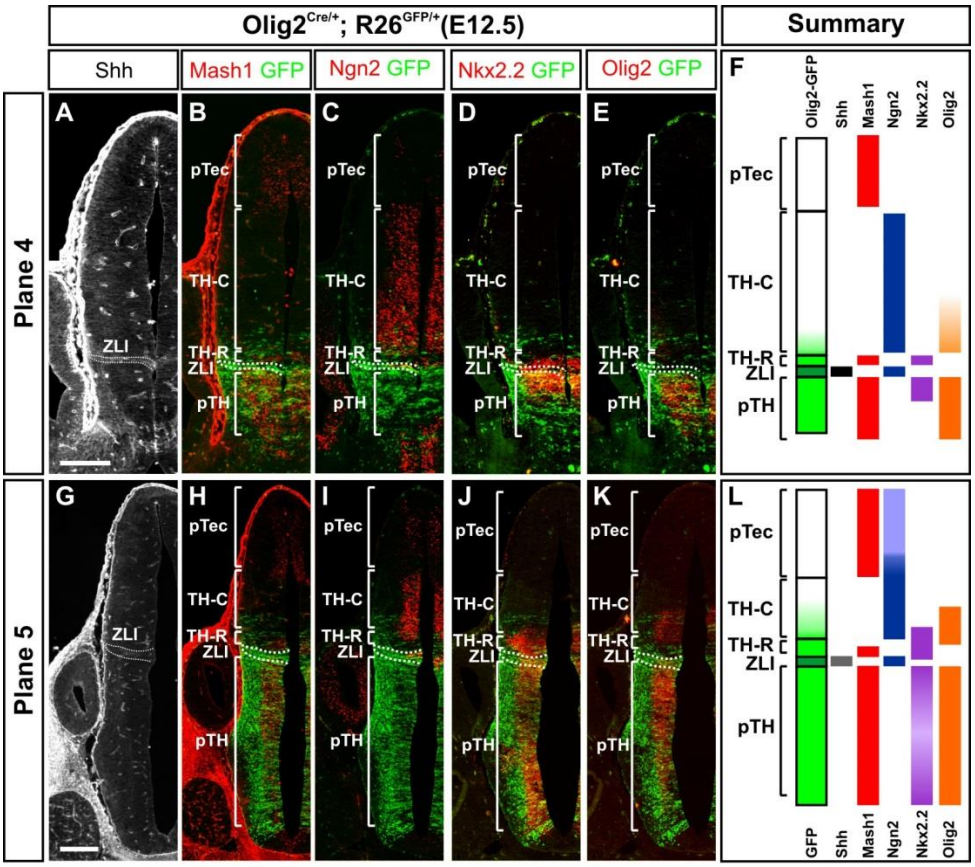

Supplementary Figure 3-S1. Detailed analysis of Olig2^{Cre} mediated recombination in the developing diencephalon

(A-L) Expression of various transcription factors (Mash1, Ngn2, Nkx2.2, and Olig2) within the developing diencephalon. Different thalamic progenitor populations can be identified by the combinatorial expression of these transcription factors[53,54]. Olig2^{Cre}-mediated recombination occurs within the rostral/ventral thalamus (TH-R), zona limitans intrathalamica (ZLI), prethalamus (pTH), and a small portion of the caudal/dorsal thalamus (TH-C). Planes 4 and 5 refer to the rostrocaudal positions depicted in Figures 3-1A and 3-1C, these two coronal planes are separated by roughly 240 µm. Scale bars = 200 µm.

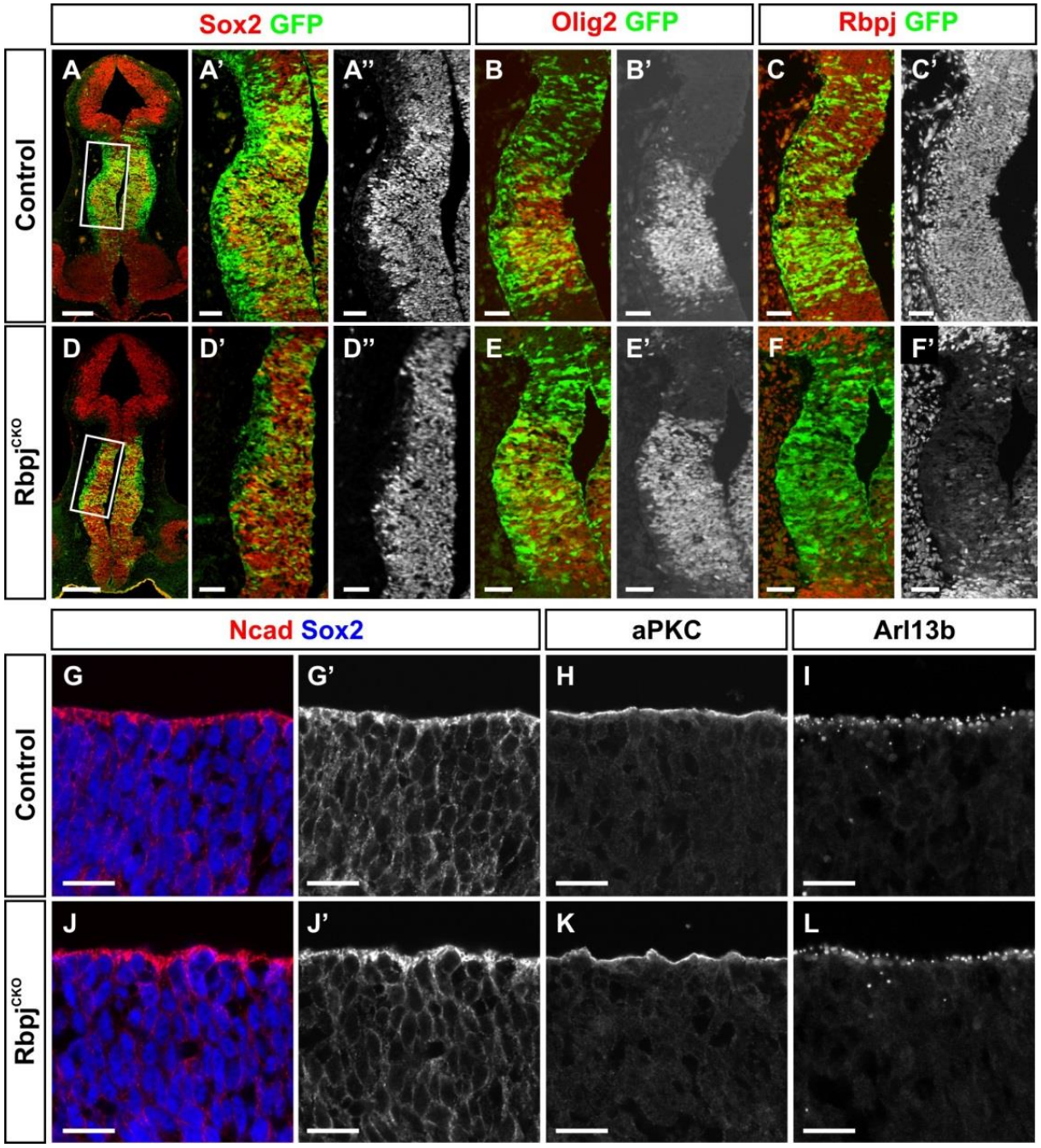
Sox2 GFP
Olig2 GFP
Rbpj GFP
Control
Rbpj^CKO
A
A'
A''
B
B'
C
C'
D
D'
D''
E
E'
F
F'
Ncad Sox2
aPKC
Arl13b
G
G'
H
I
J
J'
K
L

Supplementary Figure 3-S2. Notch signaling activity is essential for the maintenance of cell polarity and cell adhesion within the developing diencephalon.

(A-F) Coronal sections through the caudal diencephalon of e10.5 control and $Rbpj^{CKO}$ embryos. (B, E) At e10.5, GFP is present and overlaps with Olig2. (C, F) In addition, there is a loss of Rbpj protein present within the $Rbpj^{CKO}$ embryos. (A, D) However, there was no reduction in Sox2+ neural progenitors. Scale bars, low mag = 200 µm and high mag = 50 µm. **(G-L)** To assess for any disruptions in the neuroepithelial cell layer, we used antibodies to look at the distribution of the cell polarity market aPKC (G, J), the cell adhesion marker Ncad (H, K), and the cilia marker Arl13b. In all assays, we observed no loss in cell polarity or adhesion. In all the enlarged images (G-L), the apical side is up. Scale bars = 20 µm.

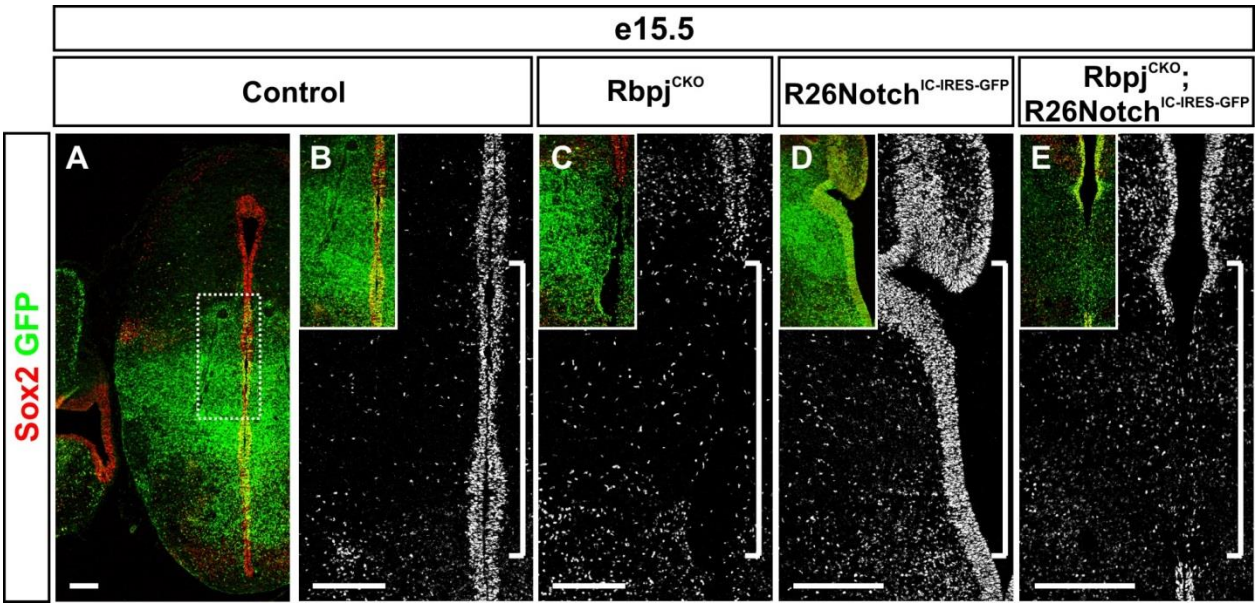

Supplementary Figure 3-S3. The loss of neuroepithelial integrity is due to a loss of Notch signaling activity

(A-E) Coronal sections through the diencephalon of e15.5 control, Rbpj^{CKO}, R26Notch$^{IC\text{-}IRES\text{-}GFP}$, and Rbpj^{CKO} + R26Notch$^{IC\text{-}IRES\text{-}GFP}$ embryos. **(A-B)** In control embryos, Sox2+ progenitors line the ventricles. **(C)** In Rbpj^{CKO} embryos, the Sox2+ progenitors that line the diencephalon are depleted. **(D)** In R26Notch$^{IC\text{-}IRES\text{-}GFP}$ embryos, misexpression of NICD results in a generally thicker Sox2+ population lining the ventricles and pockets of massive progenitor growth. **(E)** RbpjCKO; R26Notch$^{IC\text{-}IRES\text{-}GFP}$ embryos are double mutants in which a loss of Rbpj accompanies the misexpression of NICD. In these embryos there is a depletion of Sox2+ progenitors.

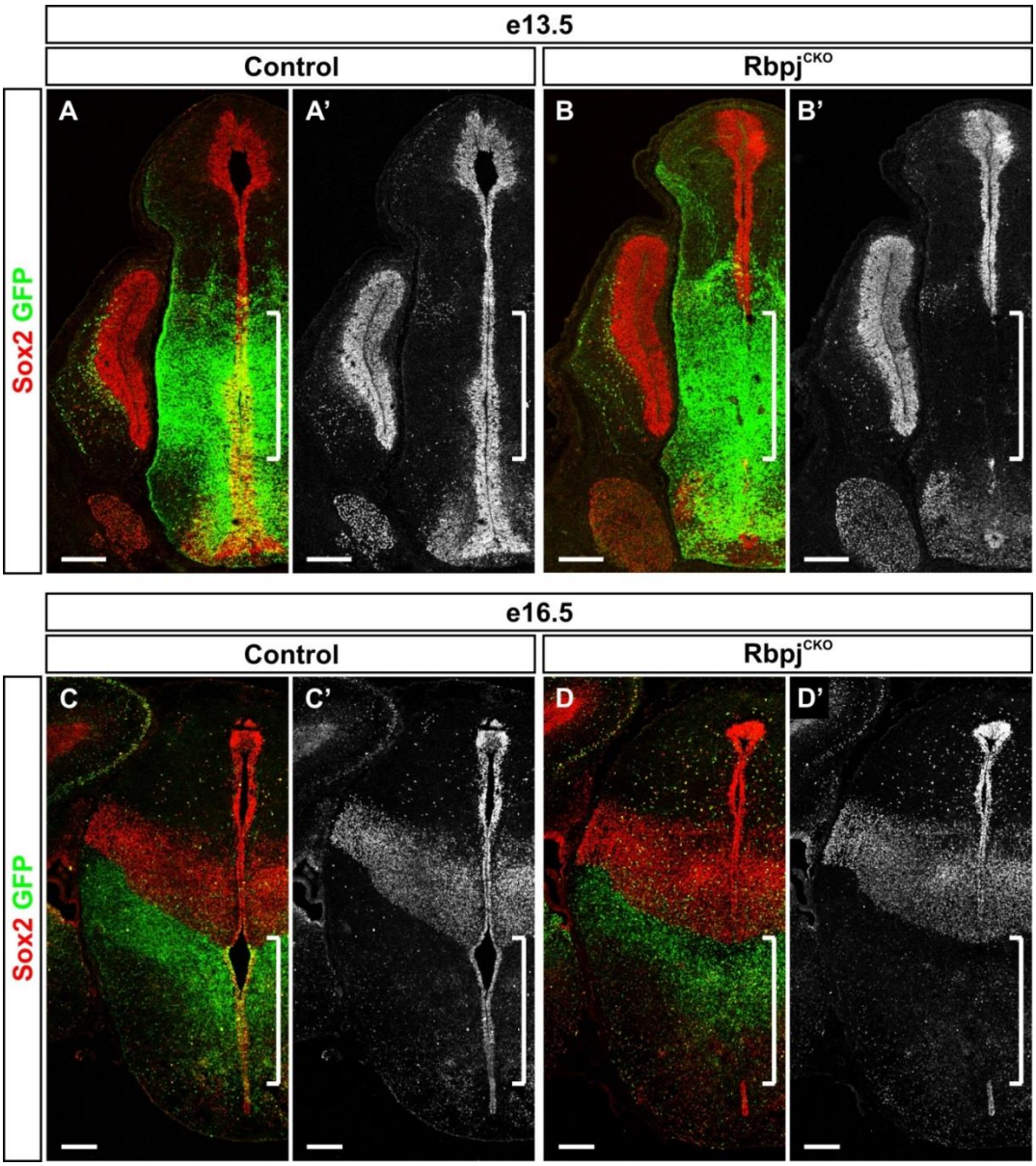

Supplementary Figure 3-S4. Over time, the disruption to the neuroepithelial cell layer grows in the Rbpj^{CKO} mutants.

(A-D) Coronal sections through the diencephalon of e13.5 (A-B) and e16.5 (C-D) control and Rbpj^{CKO} embryos. The white brackets illustrate where Sox2+ neuroepithelial progenitors are absent along the dorsoventral axis of the mutant brain. This loss of progenitors overlaps heavily with GFP, an indicator of where the Olig2^{Cre} mediated recombination occurred. Scale bars = 200 µm.

Table 3-1. Genetic mouse models of hydrocephalus

Gene	Gene Name	Mutation	Cause of the hydrocephalus	References
4930444A02 Rik	4930444A02 Rik	KO: Rik4930444A02$^{-/-}$	Unknown	[87]
Dscam	Down syndrome cell adhesion molecule	KO: *Dscam*$^{del17/\ del17}$	Unknown	[88]
Fzd3	Frizzled homolog 3	Humanized *FZD3* knock-in mice and Hypermethylated *FZD3*	Unknown	[87,89]
Mboat7	Membrane bound O-acyltransferase domain containing 7	KO: *Mboat7*$^{-/-}$	Unknown	[87]

Gene	Gene Name	Mutation	Cause of the hydrocephalus	References
Dlg5	Discs, large homolog 5	KO: *Dlg5*$^{-/-}$	Cell Adhesion Defects	[82]
L1cam	L1 cell adhesion moledule	L1-6D (L1cam with a deleted sixth Ig domain) and *L1cam*$^{-/-}$ KO	Cell Adhesion Defects	[83,90]
Llgl1	Lethal giant larvae homolog 2	KO: *Lgl1*$^{-/-}$	Cell Adhesion Defects	[84]
Myh10	Myosin, heavy polypeptide 10, non-muscle	NMHC II-B R709C mutant mice (reduced Myh10 expression)	Cell Adhesion Defects	[85]
Napa	N-ethylmaleimide sensitive fusion protein attachment protein alpha	KO: *hyh* (hydrocephalus with hop gait) mutant	Cell Adhesion Defects	[91-93]
Srgap3	Slit-Robo Rho GTPase activating protein 3	KO: *Wrp*$^{-/-}$ and CKO: *Nestin*^{Cre}	Cell Adhesion Defects	[39]

Gene	Gene Name	Mutation	Cause of the hydrocephalus	References
Ctnnb1	Catenin, beta 1	CKO: *Dmbx1*^{Cre}; *Nestin*^{Cre}	Developmental Defects (Abnormal midbrain)	[94,95]
Foxc1	Forkhead box C1	KO: *Mf1*$^{lacZ/lacZ}$	Developmental Defects (Abnormal skull)	[96,97]
Pten	Phosphatase and tensin homolog	CKO: *Dmbx1*^{Cre};*Gfap*^{Cre}	Developmental Defects (Enlarged brain regions that obstructs CSF flow)	[94,98]

Gene	Gene Name	Mutation	Cause of the hydrocephalus	References
4931429I11 Rik	4931429I11 Rik	KO: *Jhy*$^{LacZ/LacZ}$	Ciliary Defects	99
Ak7	Adenylate kinase 7	KO: *Ak7*$^{-/-}$	Ciliary Defects	87
Ak8	Adenylate kinase 8	KO: *Ak8*$^{-/-}$	Ciliary Defects	87
Bbs1	Bardet-Biedl syndrome 1	KO: *Bbs1*$^{M390R/\ M390R}$	Ciliary Defects	38
Bbs2	Bardet-Biedl syndrome 2	KO: *Bbs2*$^{-/-}$	Ciliary Defects	38
Bbs4	Bardet-Biedl syndrome 4	KO: *Bbs4*$^{-/-}$	Ciliary Defects	38
Bbs6	Bardet-Biedl syndrome 6	KO: *Bbs6*$^{-/-}$	Ciliary Defects	38
Celsr2	Cadherin, EGF LAG seven-pass G-type receptor 2	KO: *Celsr2*$^{-/-}$ and *Celsr2*$^{LacZ/LacZ}$	Ciliary Defects	87,100
Cfap221	Cilia and flagella associated protein 221	KO: *nm1054* mutant	Ciliary Defects	101
Dpcd	Deleted in primary ciliary dyskinesia	KO: *Dpcd*$^{-/-}$	Ciliary Defects	87
Dnah5	Dynein, axonemal, heavy chain 5	KO: *Mdnah5*$^{-/-}$	Ciliary Defects	102,103
Foxj1	Forkhead box J1	KO: *hfh4*$^{-/-}$	Ciliary Defects	104
Hydin	Hydin, axonemal central pair apparatus protein	KO: autosomal-recessive mutation hydrocephalus 3	Ciliary Defects	105,106
Ift88	Intraflagellar transport 88	KO: *Tg737*$^{orpk/\ orpk}$	Ciliary Defects	107
Kif27	Kinesin family member 27	KO: *Kif27*$^{-/-}$	Ciliary Defects	87
Mns1	Meiosis-specific nuclear structural protein 1	KO: *Mns1*$^{-/-}$	Ciliary Defects	108
Nme5	NME/NM23 family member 5	KO: *Nme5*$^{-/-}$	Ciliary Defects	87
Nme7	NME/NM23 family member 5	KO: *Nme7*$^{-/-}$	Ciliary Defects	87
Pkd1	Polycystic kidney disease 1 homolog	KO and CKO: *Nestin*^{Cre}	Ciliary Defects	109
Poll	Polymerase (DNA directed), lambda	KO: Pol λ$^{-/-}$	Ciliary Defects	110
Spag6	Sperm associated antigen 6	KO: *Spag6*$^{-/-}$	Ciliary Defects	111
Spef2	Sperm flagellar 2	KO: *bgh* (big giant head) mutant	Ciliary Defects	112
Stk36	Serine/threonine kinase 36	KO: *Stk36*$^{-/-}$	Ciliary Defects	87
Tmem67	Transmembrane protein 67 (meckelin)	KO: *bpck/bpck* mutant	Ciliary Defects	113,114
Ulk4	Unc-51-like kinase 4	KO: *Ulk4*$^{-/-}$	Ciliary Defects	87

Gene	Gene Name	Mutation	Cause of the hydrocephalus	References
Aqp4	Aquaporin 4	KO: *Aqp4*$^{-/-}$	Choroid plexus and/or CSF Defects	[115]
Col18a1	Collagen, type XVIII, alpha 1	KO: *Col18a1*$^{-/-}$	Choroid plexus and/or CSF Defects	[116]
E2f5	E2F transcription factor 5	KO: *E2f5*$^{-/-}$	Choroid plexus and/or CSF Defects	[117]
Htt	Huntingtin	CKO: Wnt1^{Cre}	Choroid plexus and/or CSF Defects	[118]
Otx2	Orthodenticle homolog 2	*Otx2*$^{+/-}$ mutant	Choroid plexus and/or CSF Defects	[119]

Gene	Gene Name	Mutation	Cause of the hydrocephalus	References
En1	Engrailed 1	Ectopic *En1* in the dorsal midline: *WEXPZ.En1*	Subcommissural Organ Defects	[120]
Msx1	Msh homeobox 1	KO: *Msx1*$^{nlacZ/nlacZ}$	Subcommissural Organ Defects	[121]
Pax6	Paired box 6	KO: *Pax6*$^{Sey/Sey}$	Subcommissural Organ Defects	[122,123]
Rfx3	Regulatory factor X, 3	KO: Rfx3$^{-/-}$	Subcommissural Organ Defects (may also be a Ciliary Defects)	[124]
Rfx4	Regulatory factor X, 4	KO: loss of a variant transcript of *Rfx4*	Subcommissural Organ Defects	[125]
Socs7	Suppressor of cytokine signaling 7	KO: *Socs7*$^{-/-}$	Subcommissural Organ Defects	[126]
Sox3	SRY-box3	*Sox3* transgenic mice (2-3 fold higher SOX3 protein levels)	Subcommissural Organ Defects	[127]
Wnt1	Wingless-type MMTV integration site family, member 1	KO: *Wnt1*$^{sw/sw}$	Subcommissural Organ Defects	[120,128]

Age	e10.5	e11.5	e12.5	e13.5	e14.5-e18.5	Postnatal
Control	0 / 3	0 / 12	0 / 8	0 / 4	0 / 6	0 / 8
Rbpj^{CKO}	0 / 3	8 / 8	5 / 5	3 / 3	6 / 6	8 / 8

Table 3-2. The presence of a disrupted neuroepithelial cell layer at various ages in the Rbpj^{CKO} mice

Neuroepithelial integrity was evaluated in sectioned brain tissue by looking for the continuous presence of Sox2+ progenitors and apical cell adhesion proteins. The ratios in the table represent the number of animals with a disrupted neuroepithelium / total number of animals assessed. In the Rbpj^{CKO} mice, a disruption of the neuroepithelium was first observed at e11.5 and this disruption was observed into the postnatal ages.

ACKNOWLEDGEMENTS

This work was supported by the UCLA Broad Center for Regenerative Medicine and Stem Cell Research, the Rose Hills Foundation, and grants to BGN from the March of Dimes Foundation (6-FY10-296) and the NINDS (NS053976 and NS072804). JHK was also supported by a UCLA Dissertation Year Fellowship.

REFERENCES

1 Gilmore, E. C. & Walsh, C. A. Genetic causes of microcephaly and lessons for neuronal development. *Wiley interdisciplinary reviews. Developmental biology* **2**, 461-478, doi:10.1002/wdev.89 (2013).

2 Lasky, J. L. & Wu, H. Notch signaling, brain development, and human disease. *Pediatric research* **57**, 104R-109R, doi:10.1203/01.PDR.0000159632.70510.3D (2005).

3 Barkovich, A. J., Guerrini, R., Kuzniecky, R. I., Jackson, G. D. & Dobyns, W. B. A developmental and genetic classification for malformations of cortical development: update 2012. *Brain : a journal of neurology* **135**, 1348-1369, doi:10.1093/brain/aws019 (2012).

4 Chenn, A., Zhang, Y. A., Chang, B. T. & McConnell, S. K. Intrinsic polarity of mammalian neuroepithelial cells. *Mol Cell Neurosci* **11**, 183-193, doi:10.1006/mcne.1998.0680 (1998).

5 Imai, F. *et al.* Inactivation of aPKClambda results in the loss of adherens junctions in neuroepithelial cells without affecting neurogenesis in mouse neocortex. *Development* **133**, 1735-1744, doi:10.1242/dev.02330 (2006).

6 Kadowaki, M. *et al.* N-cadherin mediates cortical organization in the mouse brain. *Developmental biology* **304**, 22-33, doi:10.1016/j.ydbio.2006.12.014 (2007).

7 Willardsen, M. I. & Link, B. A. Cell biological regulation of division fate in vertebrate neuroepithelial cells. *Developmental dynamics : an official publication of the American Association of Anatomists* **240**, 1865-1879, doi:10.1002/dvdy.22684 (2011).

8 Baye, L. M. & Link, B. A. Interkinetic nuclear migration and the selection of neurogenic cell divisions during vertebrate retinogenesis. *J Neurosci* **27**, 10143-10152, doi:10.1523/JNEUROSCI.2754-07.2007 (2007).

9 Chenn, A. & McConnell, S. K. Cleavage orientation and the asymmetric inheritance of Notch1 immunoreactivity in mammalian neurogenesis. *Cell* **82**, 631-641 (1995).

10 Martin, A. H. Significance of mitotic spindle fibre orientation in the neural tube. *Nature* **216**, 1133-1134 (1967).

11 Gotz, M. & Huttner, W. B. The cell biology of neurogenesis. *Nature reviews. Molecular cell biology* **6**, 777-788, doi:10.1038/nrm1739 (2005).

12 Zhong, W., Feder, J. N., Jiang, M. M., Jan, L. Y. & Jan, Y. N. Asymmetric localization of a mammalian numb homolog during mouse cortical neurogenesis. *Neuron* **17**, 43-53 (1996).

13 Cayouette, M., Whitmore, A. V., Jeffery, G. & Raff, M. Asymmetric segregation of Numb in retinal development and the influence of the pigmented epithelium. *J Neurosci* **21**, 5643-5651 (2001).

14 Hitoshi, S. *et al.* Notch pathway molecules are essential for the maintenance, but not the generation, of mammalian neural stem cells. *Genes & development* **16**, 846-858, doi:10.1101/gad.975202 (2002).

15 de la Pompa, J. L. *et al.* Conservation of the Notch signalling pathway in mammalian neurogenesis. *Development* **124**, 1139-1148 (1997).

16 Yoon, K. & Gaiano, N. Notch signaling in the mammalian central nervous system: insights from mouse mutants. *Nature neuroscience* **8**, 709-715, doi:10.1038/nn1475 (2005).

17 Lutolf, S., Radtke, F., Aguet, M., Suter, U. & Taylor, V. Notch1 is required for neuronal and glial differentiation in the cerebellum. *Development* **129**, 373-385 (2002).

18 Irvin, D. K., Zurcher, S. D., Nguyen, T., Weinmaster, G. & Kornblum, H. I. Expression patterns of Notch1, Notch2, and Notch3 suggest multiple functional roles for the Notch-DSL signaling system during brain development. *J Comp Neurol* **436**, 167-181 (2001).

19 Stump, G. *et al.* Notch1 and its ligands Delta-like and Jagged are expressed and active in distinct cell populations in the postnatal mouse brain. *Mechanisms of development* **114**, 153-159 (2002).

20 Lindsell, C. E., Boulter, J., diSibio, G., Gossler, A. & Weinmaster, G. Expression patterns of Jagged, Delta1, Notch1, Notch2, and Notch3 genes identify ligand-receptor pairs that may function in neural development. *Mol Cell Neurosci* **8**, 14-27, doi:10.1006/mcne.1996.0040 (1996).

21 Louvi, A. & Artavanis-Tsakonas, S. Notch signalling in vertebrate neural development. *Nature reviews. Neuroscience* **7**, 93-102, doi:10.1038/nrn1847 (2006).

22 Williams, S. E., Beronja, S., Pasolli, H. A. & Fuchs, E. Asymmetric cell divisions promote Notch-dependent epidermal differentiation. *Nature* **470**, 353-358, doi:10.1038/nature09793 (2011).

23 Bultje, R. S. *et al.* Mammalian Par3 regulates progenitor cell asymmetric division via notch signaling in the developing neocortex. *Neuron* **63**, 189-202, doi:10.1016/j.neuron.2009.07.004 (2009).

24 Bao, S. Notch controls cell adhesion in the Drosophila eye. *PLoS genetics* **10**, e1004087, doi:10.1371/journal.pgen.1004087 (2014).

25 Wang, W. *et al.* Notch signaling regulates neuroepithelial stem cell maintenance and neuroblast formation in Drosophila optic lobe development. *Developmental biology* **350**, 414-428, doi:10.1016/j.ydbio.2010.12.002 (2011).

26 Main, H., Radenkovic, J., Jin, S. B., Lendahl, U. & Andersson, E. R. Notch signaling maintains neural rosette polarity. *PloS one* **8**, e62959, doi:10.1371/journal.pone.0062959 (2013).

27 Dessaud, E. *et al.* Interpretation of the sonic hedgehog morphogen gradient by a temporal adaptation mechanism. *Nature* **450**, 717-720, doi:10.1038/nature06347 (2007).

28 Bielle, F. *et al.* Multiple origins of Cajal-Retzius cells at the borders of the developing pallium. *Nature neuroscience* **8**, 1002-1012, doi:10.1038/nn1511 (2005).

29 Mao, X., Fujiwara, Y., Chapdelaine, A., Yang, H. & Orkin, S. H. Activation of EGFP expression by Cre-mediated excision in a new ROSA26 reporter mouse strain. *Blood* **97**, 324-326 (2001).

30 Han, H. *et al.* Inducible gene knockout of transcription factor recombination signal binding protein-J reveals its essential role in T versus B lineage decision. *International immunology* **14**, 637-645 (2002).

31 Novitch, B. G., Chen, A. I. & Jessell, T. M. Coordinate regulation of motor neuron subtype identity and pan-neuronal properties by the bHLH repressor Olig2. *Neuron* **31**, 773-789 (2001).

32 Pearson, C. A. *et al.* FGF-dependent midline-derived progenitor cells in hypothalamic infundibular development. *Development* **138**, 2613-2624, doi:10.1242/dev.062794 (2011).

33 Rousso, D. L. *et al.* Foxp-mediated suppression of N-cadherin regulates neuroepithelial character and progenitor maintenance in the CNS. *Neuron* **74**, 314-330, doi:10.1016/j.neuron.2012.02.024 (2012).

34 Ito, T. *et al.* Basic helix-loop-helix transcription factors regulate the neuroendocrine differentiation of fetal mouse pulmonary epithelium. *Development* **127**, 3913-3921 (2000).

35 Jacob, J. *et al.* Retinoid acid specifies neuronal identity through graded expression of Ascl1. *Current biology : CB* **23**, 412-418, doi:10.1016/j.cub.2013.01.046 (2013).

36 Briscoe, J. *et al.* Homeobox gene Nkx2.2 and specification of neuronal identity by graded Sonic hedgehog signalling. *Nature* **398**, 622-627, doi:10.1038/19315 (1999).

37 Novitch, B. G., Wichterle, H., Jessell, T. M. & Sockanathan, S. A requirement for retinoic acid-mediated transcriptional activation in ventral neural patterning and motor neuron specification. *Neuron* **40**, 81-95 (2003).

38 Swiderski, R. E. *et al.* Structural defects in cilia of the choroid plexus, subfornical organ and ventricular ependyma are associated with ventriculomegaly. *Fluids and barriers of the CNS* **9**, 22, doi:10.1186/2045-8118-9-22 (2012).

39 Kim, I. H., Carlson, B. R., Heindel, C. C., Kim, H. & Soderling, S. H. Disruption of wave-associated Rac GTPase-activating protein (Wrp) leads to abnormal adult neural progenitor migration associated with hydrocephalus. *The Journal of biological chemistry* **287**, 39263-39274, doi:10.1074/jbc.M112.398834 (2012).

40 Alanentalo, T. *et al.* Tomographic molecular imaging and 3D quantification within adult mouse organs. *Nature methods* **4**, 31-33, doi:10.1038/nmeth985 (2007).

41 de la Pompa, J. L. & Epstein, J. A. Coordinating tissue interactions: Notch signaling in cardiac development and disease. *Developmental cell* **22**, 244-254, doi:10.1016/j.devcel.2012.01.014 (2012).

42 Apelqvist, A. *et al.* Notch signalling controls pancreatic cell differentiation. *Nature* **400**, 877-881, doi:10.1038/23716 (1999).

43 Lammert, E., Brown, J. & Melton, D. A. Notch gene expression during pancreatic organogenesis. *Mechanisms of development* **94**, 199-203 (2000).

44 Fre, S. *et al.* Notch signals control the fate of immature progenitor cells in the intestine. *Nature* **435**, 964-968, doi:10.1038/nature03589 (2005).

45 Zanotti, S. & Canalis, E. Notch regulation of bone development and remodeling and related skeletal disorders. *Calcified tissue international* **90**, 69-75, doi:10.1007/s00223-011-9541-x (2012).

46 Hilton, M. J. *et al.* Notch signaling maintains bone marrow mesenchymal progenitors by suppressing osteoblast differentiation. *Nature medicine* **14**, 306-314, doi:10.1038/nm1716 (2008).

47 Jiang, Y. J. *et al.* Notch signalling and the synchronization of the somite segmentation clock. *Nature* **408**, 475-479, doi:10.1038/35044091 (2000).

48 Oka, C. *et al.* Disruption of the mouse RBP-J kappa gene results in early embryonic death. *Development* **121**, 3291-3301 (1995).

49 Ono, K. *et al.* Regional- and temporal-dependent changes in the differentiation of Olig2 progenitors in the forebrain, and the impact on astrocyte development in the dorsal pallium. *Developmental biology* **320**, 456-468, doi:10.1016/j.ydbio.2008.06.001 (2008).

50 Furusho, M. *et al.* Involvement of the Olig2 transcription factor in cholinergic neuron development of the basal forebrain. *Developmental biology* **293**, 348-357, doi:10.1016/j.ydbio.2006.01.031 (2006).

51 Takebayashi, H. *et al.* Dynamic expression of basic helix-loop-helix Olig family members: implication of Olig2 in neuron and oligodendrocyte differentiation and identification of a new member, Olig3. *Mechanisms of development* **99**, 143-148 (2000).

52 Takebayashi, H. *et al.* Non-overlapping expression of Olig3 and Olig2 in the embryonic neural tube. *Mechanisms of development* **113**, 169-174 (2002).

53 Vue, T. Y. *et al.* Characterization of progenitor domains in the developing mouse thalamus. *J Comp Neurol* **505**, 73-91, doi:10.1002/cne.21467 (2007).

54 Vue, T. Y. *et al.* Sonic hedgehog signaling controls thalamic progenitor identity and nuclei specification in mice. *J Neurosci* **29**, 4484-4497, doi:10.1523/JNEUROSCI.0656-09.2009 (2009).

55 Ohtsuka, T. *et al.* Hes1 and Hes5 as notch effectors in mammalian neuronal differentiation. *The EMBO journal* **18**, 2196-2207, doi:10.1093/emboj/18.8.2196 (1999).

56 Kageyama, R., Ohtsuka, T. & Kobayashi, T. The Hes gene family: repressors and oscillators that orchestrate embryogenesis. *Development* **134**, 1243-1251, doi:10.1242/dev.000786 (2007).

57 Ingram, W. J., McCue, K. I., Tran, T. H., Hallahan, A. R. & Wainwright, B. J. Sonic Hedgehog regulates Hes1 through a novel mechanism that is independent of canonical Notch pathway signalling. *Oncogene* **27**, 1489-1500, doi:10.1038/sj.onc.1210767 (2008).

58 Wall, D. S. *et al.* Progenitor cell proliferation in the retina is dependent on Notch-independent Sonic hedgehog/Hes1 activity. *The Journal of cell biology* **184**, 101-112 (2009).

59 Kong, J. H., Yang, L., Dessaud, E., Chuang, K., Moore, D.M., Rohatgi, R., Briscoe, J., Novitch, B.G. Notch activity modulates the responsiveness of neural progenitors to Sonic hedgehog signaling. *Developmental cell* **33**, 1-15 (2015).

60 Nery, S., Wichterle, H. & Fishell, G. Sonic hedgehog contributes to oligodendrocyte specification in the mammalian forebrain. *Development* **128**, 527-540 (2001).

61 Barth, A. I., Nathke, I. S. & Nelson, W. J. Cadherins, catenins and APC protein: interplay between cytoskeletal complexes and signaling pathways. *Current opinion in cell biology* **9**, 683-690 (1997).

62 Higginbotham, H. *et al.* Arl13b-regulated cilia activities are essential for polarized radial glial scaffold formation. *Nature neuroscience* **16**, 1000-1007, doi:10.1038/nn.3451 (2013).

63 Svoboda, K. K. & O'Shea, K. S. An analysis of cell shape and the neuroepithelial basal lamina during optic vesicle formation in the mouse embryo. *Development* **100**, 185-200 (1987).

64 Del Bigio, M. R. The ependyma: a protective barrier between brain and cerebrospinal fluid. *Glia* **14**, 1-13, doi:10.1002/glia.440140102 (1995).

65 Tait, M. J., Saadoun, S., Bell, B. A. & Papadopoulos, M. C. Water movements in the brain: role of aquaporins. *Trends in neurosciences* **31**, 37-43, doi:10.1016/j.tins.2007.11.003 (2008).

66 Jimenez, A. J., Dominguez-Pinos, M. D., Guerra, M. M., Fernandez-Llebrez, P. & Perez-Figares, J. M. Structure and function of the ependymal barrier and diseases associated with ependyma disruption. *Tissue barriers* **2**, e28426, doi:10.4161/tisb.28426 (2014).

67 Bruni, J. E. Ependymal development, proliferation, and functions: a review. *Microscopy research and technique* **41**, 2-13, doi:10.1002/(SICI)1097-0029(19980401)41:1<2::AID-JEMT2>3.0.CO;2-Z (1998).

68 Spassky, N. *et al.* Adult ependymal cells are postmitotic and are derived from radial glial cells during embryogenesis. *J Neurosci* **25**, 10-18, doi:10.1523/JNEUROSCI.1108-04.2005 (2005).

69 Weller, R. O., Mitchell, J., Griffin, R. L. & Gardner, M. J. The effects of hydrocephalus upon the developing brain. Histological and quantitative studies of the ependyma and subependyma in hydrocephalic rats. *Journal of the neurological sciences* **36**, 383-402 (1978).

70 Mirzadeh, Z., Merkle, F. T., Soriano-Navarro, M., Garcia-Verdugo, J. M. & Alvarez-Buylla, A. Neural stem cells confer unique pinwheel architecture to the ventricular surface in neurogenic regions of the adult brain. *Cell stem cell* **3**, 265-278, doi:10.1016/j.stem.2008.07.004 (2008).

71 Hatakeyama, J. & Kageyama, R. Notch1 expression is spatiotemporally correlated with neurogenesis and negatively regulated by Notch1-independent Hes genes in the developing nervous system. *Cerebral cortex* **16 Suppl 1**, i132-137, doi:10.1093/cercor/bhj166 (2006).

72 Doetzlhofer, A. *et al.* Hey2 regulation by FGF provides a Notch-independent mechanism for maintaining pillar cell fate in the organ of Corti. *Developmental cell* **16**, 58-69, doi:10.1016/j.devcel.2008.11.008 (2009).

73 Shi, M. *et al.* Notch-Rbpj signaling is required for the development of noradrenergic neurons in the mouse locus coeruleus. *Journal of cell science* **125**, 4320-4332, doi:10.1242/jcs.102152 (2012).

74 Zheng, M. H. *et al.* The transcription factor RBP-J is essential for retinal cell differentiation and lamination. *Molecular brain* **2**, 38, doi:10.1186/1756-6606-2-38 (2009).

75 Gelman, D. M. *et al.* The embryonic preoptic area is a novel source of cortical GABAergic interneurons. *J Neurosci* **29**, 9380-9389, doi:10.1523/JNEUROSCI.0604-09.2009 (2009).

76 Alvarez-Bolado, G., Paul, F. A. & Blaess, S. Sonic hedgehog lineage in the mouse hypothalamus: from progenitor domains to hypothalamic regions. *Neural development* **7**, 4, doi:10.1186/1749-8104-7-4 (2012).

77 Hatakeyama, J. *et al.* Hes genes regulate size, shape and histogenesis of the nervous system by control of the timing of neural stem cell differentiation. *Development* **131**, 5539-5550 (2004).

78 Li, Y., Hibbs, M. A., Gard, A. L., Shylo, N. A. & Yun, K. Genome-wide analysis of N1ICD/RBPJ targets in vivo reveals direct transcriptional regulation of Wnt, SHH, and hippo pathway effectors by Notch1. *Stem cells* **30**, 741-752, doi:10.1002/stem.1030 (2012).

79 Hamidi, H., Gustafason, D., Pellegrini, M. & Gasson, J. Identification of novel targets of CSL-dependent Notch signaling in hematopoiesis. *PloS one* **6**, e20022, doi:10.1371/journal.pone.0020022 (2011).

80 Castel, D. *et al.* Dynamic binding of RBPJ is determined by Notch signaling status. *Genes & development* **27**, 1059-1071, doi:10.1101/gad.211912.112 (2013).

81 Zhang, J., Williams, M. A. & Rigamonti, D. Genetics of human hydrocephalus. *Journal of neurology* **253**, 1255-1266, doi:10.1007/s00415-006-0245-5 (2006).

82 Nechiporuk, T., Fernandez, T. E. & Vasioukhin, V. Failure of epithelial tube maintenance causes hydrocephalus and renal cysts in Dlg5-/- mice. *Developmental cell* **13**, 338-350, doi:10.1016/j.devcel.2007.07.017 (2007).

83 Dahme, M. *et al.* Disruption of the mouse L1 gene leads to malformations of the nervous system. *Nature genetics* **17**, 346-349, doi:10.1038/ng1197-346 (1997).

84 Klezovitch, O., Fernandez, T. E., Tapscott, S. J. & Vasioukhin, V. Loss of cell polarity causes severe brain dysplasia in Lgl1 knockout mice. *Genes & development* **18**, 559-571, doi:10.1101/gad.1178004 (2004).

85 Ma, X., Bao, J. & Adelstein, R. S. Loss of cell adhesion causes hydrocephalus in nonmuscle myosin II-B-ablated and mutated mice. *Molecular biology of the cell* **18**, 2305-2312, doi:10.1091/mbc.E07-01-0073 (2007).

86 Chen, J. & Zhang, M. The Par3/Par6/aPKC complex and epithelial cell polarity. *Experimental cell research* **319**, 1357-1364, doi:10.1016/j.yexcr.2013.03.021 (2013).

87 Vogel, P. *et al.* Congenital hydrocephalus in genetically engineered mice. *Veterinary pathology* **49**, 166-181, doi:10.1177/0300985811415708 (2012).

88 Xu, Y. *et al.* Dscam mutation leads to hydrocephalus and decreased motor function. *Protein & cell* **2**, 647-655, doi:10.1007/s13238-011-1072-8 (2011).

89 Wang, L. *et al.* Impaired methylation modifications of FZD3 alter chromatin accessibility and are involved in congenital hydrocephalus pathogenesis. *Brain research* **1569**, 48-56, doi:10.1016/j.brainres.2014.04.010 (2014).

90 Itoh, K. *et al.* Brain development in mice lacking L1-L1 homophilic adhesion. *The Journal of cell biology* **165**, 145-154, doi:10.1083/jcb.200312107 (2004).

91 Bronson, R. T. & Lane, P. W. Hydrocephalus with hop gait (hyh): a new mutation on chromosome 7 in the mouse. *Brain research. Developmental brain research* **54**, 131-136 (1990).

92 Paez, P. *et al.* Patterned neuropathologic events occurring in hyh congenital hydrocephalic mutant mice. *Journal of neuropathology and experimental neurology* **66**, 1082-1092, doi:10.1097/nen.0b013e31815c1952 (2007).

93 Chae, T. H., Kim, S., Marz, K. E., Hanson, P. I. & Walsh, C. A. The hyh mutation uncovers roles for alpha Snap in apical protein localization and control of neural cell fate. *Nature genetics* **36**, 264-270, doi:10.1038/ng1302 (2004).

94 Ohtoshi, A. Hydrocephalus caused by conditional ablation of the Pten or beta-catenin gene. *Cerebrospinal fluid research* **5**, 16, doi:10.1186/1743-8454-5-16 (2008).

95 Schuller, U. & Rowitch, D. H. Beta-catenin function is required for cerebellar morphogenesis. *Brain research* **1140**, 161-169, doi:10.1016/j.brainres.2006.05.105 (2007).

96 Kume, T. *et al.* The forkhead/winged helix gene Mf1 is disrupted in the pleiotropic mouse mutation congenital hydrocephalus. *Cell* **93**, 985-996 (1998).

97 Hong, H. K., Lass, J. H. & Chakravarti, A. Pleiotropic skeletal and ocular phenotypes of the mouse mutation congenital hydrocephalus (ch/Mf1) arise from a winged helix/forkhead transcriptionfactor gene. *Human molecular genetics* **8**, 625-637 (1999).

98 Kwon, C. H. *et al.* Pten regulates neuronal soma size: a mouse model of Lhermitte-Duclos disease. *Nature genetics* **29**, 404-411, doi:10.1038/ng781 (2001).

99 Appelbe, O. K. *et al.* Disruption of the mouse Jhy gene causes abnormal ciliary microtubule patterning and juvenile hydrocephalus. *Developmental biology* **382**, 172-185, doi:10.1016/j.ydbio.2013.07.003 (2013).

100 Tissir, F. *et al.* Lack of cadherins Celsr2 and Celsr3 impairs ependymal ciliogenesis, leading to fatal hydrocephalus. *Nature neuroscience* **13**, 700-707, doi:10.1038/nn.2555 (2010).

101 Lee, L. *et al.* Primary ciliary dyskinesia in mice lacking the novel ciliary protein Pcdp1. *Molecular and cellular biology* **28**, 949-957, doi:10.1128/MCB.00354-07 (2008).

102 Ibanez-Tallon, I., Gorokhova, S. & Heintz, N. Loss of function of axonemal dynein Mdnah5 causes primary ciliary dyskinesia and hydrocephalus. *Human molecular genetics* **11**, 715-721 (2002).

103 Ibanez-Tallon, I. *et al.* Dysfunction of axonemal dynein heavy chain Mdnah5 inhibits ependymal flow and reveals a novel mechanism for hydrocephalus formation. *Human molecular genetics* **13**, 2133-2141, doi:10.1093/hmg/ddh219 (2004).

104 Chen, J., Knowles, H. J., Hebert, J. L. & Hackett, B. P. Mutation of the mouse hepatocyte nuclear factor/forkhead homologue 4 gene results in an absence of cilia and random left-right asymmetry. *The Journal of clinical investigation* **102**, 1077-1082, doi:10.1172/JCI4786 (1998).

105 Davy, B. E. & Robinson, M. L. Congenital hydrocephalus in hy3 mice is caused by a frameshift mutation in Hydin, a large novel gene. *Human molecular genetics* **12**, 1163-1170 (2003).

106 Dawe, H. R., Shaw, M. K., Farr, H. & Gull, K. The hydrocephalus inducing gene product, Hydin, positions axonemal central pair microtubules. *BMC biology* **5**, 33, doi:10.1186/1741-7007-5-33 (2007).

107 Banizs, B. *et al.* Dysfunctional cilia lead to altered ependyma and choroid plexus function, and result in the formation of hydrocephalus. *Development* **132**, 5329-5339, doi:10.1242/dev.02153 (2005).

108 Zhou, J., Yang, F., Leu, N. A. & Wang, P. J. MNS1 is essential for spermiogenesis and motile ciliary functions in mice. *PLoS genetics* **8**, e1002516, doi:10.1371/journal.pgen.1002516 (2012).

109 Wodarczyk, C. *et al.* A novel mouse model reveals that polycystin-1 deficiency in ependyma and choroid plexus results in dysfunctional cilia and hydrocephalus. *PloS one* **4**, e7137, doi:10.1371/journal.pone.0007137 (2009).

110 Kobayashi, Y. *et al.* Hydrocephalus, situs inversus, chronic sinusitis, and male infertility in DNA polymerase lambda-deficient mice: possible implication for the pathogenesis of immotile cilia syndrome. *Molecular and cellular biology* **22**, 2769-2776 (2002).

111 Sapiro, R. *et al.* Male infertility, impaired sperm motility, and hydrocephalus in mice deficient in sperm-associated antigen 6. *Molecular and cellular biology* **22**, 6298-6305 (2002).

112 Sironen, A. *et al.* Loss of SPEF2 function in mice results in spermatogenesis defects and primary ciliary dyskinesia. *Biology of reproduction* **85**, 690-701, doi:10.1095/biolreprod.111.091132 (2011).

113 Cook, S. A. *et al.* A mouse model for Meckel syndrome type 3. *Journal of the American Society of Nephrology : JASN* **20**, 753-764, doi:10.1681/ASN.2008040412 (2009).

114 Leightner, A. C. *et al.* The Meckel syndrome protein meckelin (TMEM67) is a key regulator of cilia function but is not required for tissue planar polarity. *Human molecular genetics* **22**, 2024-2040, doi:10.1093/hmg/ddt054 (2013).

115 Feng, X. *et al.* Sporadic obstructive hydrocephalus in Aqp4 null mice. *Journal of neuroscience research* **87**, 1150-1155, doi:10.1002/jnr.21927 (2009).

116 Utriainen, A. *et al.* Structurally altered basement membranes and hydrocephalus in a type XVIII collagen deficient mouse line. *Human molecular genetics* **13**, 2089-2099, doi:10.1093/hmg/ddh213 (2004).

117 Lindeman, G. J. *et al.* A specific, nonproliferative role for E2F-5 in choroid plexus function revealed by gene targeting. *Genes & development* **12**, 1092-1098 (1998).

118 Dietrich, P., Shanmugasundaram, R., Shuyu, E. & Dragatsis, I. Congenital hydrocephalus associated with abnormal subcommissural organ in mice lacking huntingtin in Wnt1 cell lineages. *Human molecular genetics* **18**, 142-150, doi:10.1093/hmg/ddn324 (2009).

119 Makiyama, Y., Shoji, S. & Mizusawa, H. Hydrocephalus in the Otx2+/- mutant mouse. *Experimental neurology* **148**, 215-221, doi:10.1006/exnr.1997.6638 (1997).

120 Louvi, A. & Wassef, M. Ectopic engrailed 1 expression in the dorsal midline causes cell death, abnormal differentiation of circumventricular organs and errors in axonal pathfinding. *Development* **127**, 4061-4071 (2000).

121 Ramos, C., Fernandez-Llebrez, P., Bach, A., Robert, B. & Soriano, E. Msx1 disruption leads to diencephalon defects and hydrocephalus. *Developmental dynamics : an official publication of the American Association of Anatomists* **230**, 446-460, doi:10.1002/dvdy.20070 (2004).

122 Estivill-Torrus, G., Vitalis, T., Fernandez-Llebrez, P. & Price, D. J. The transcription factor Pax6 is required for development of the diencephalic dorsal midline secretory radial glia that form the subcommissural organ. *Mechanisms of development* **109**, 215-224 (2001).

123 Huh, M. S., Todd, M. A. & Picketts, D. J. SCO-ping out the mechanisms underlying the etiology of hydrocephalus. *Physiology* **24**, 117-126, doi:10.1152/physiol.00039.2008 (2009).

124 Baas, D. *et al.* A deficiency in RFX3 causes hydrocephalus associated with abnormal differentiation of ependymal cells. *The European journal of neuroscience* **24**, 1020-1030, doi:10.1111/j.1460-9568.2006.05002.x (2006).

125 Blackshear, P. J. *et al.* Graded phenotypic response to partial and complete deficiency of a brain-specific transcript variant of the winged helix transcription factor RFX4. *Development* **130**, 4539-4552, doi:10.1242/dev.00661 (2003).

126 Krebs, D. L. *et al.* Development of hydrocephalus in mice lacking SOCS7. *Proc Natl Acad Sci U S A* **101**, 15446-15451, doi:10.1073/pnas.0406870101 (2004).

127 Lee, K. *et al.* Congenital hydrocephalus and abnormal subcommissural organ development in Sox3 transgenic mice. *PloS one* **7**, e29041, doi:10.1371/journal.pone.0029041 (2012).

128 Thomas, K. R. & Capecchi, M. R. Targeted disruption of the murine int-1 proto-oncogene resulting in severe abnormalities in midbrain and cerebellar development. *Nature* **346**, 847-850, doi:10.1038/346847a0 (1990).

CHAPTER 4 – Retinoic Acid Specifies Neuronal Identity through Graded Expression of Ascl1

ABSTRACT

Cell diversity and organization in the neural tube depend on the integration of extrinsic signals acting along orthogonal axes. These are believed to specify distinct cellular identities by triggering all-or-none changes in the expression of combinations of transcription factors[1]. Under the influence of dorsoventral and anterior-posterior (A-P) inductive signals[2,3], two topographically related progenitor pools that share a common transcriptional code produce serotonergic and V3 neurons in the hindbrain and spinal cord, respectively[4-7]. These neurons have different physiological properties, functions, and connectivity[8,9]. Serotonergic involvement in neuropsychiatric diseases has prompted greater characterization of their postmitotic repertoire of fate determinants, which include Gata2, Lmx1b, and Pet1[10], whereas V3 neurons express Sim1[4]. How distinct serotonergic and V3 neuronal identities emerge from progenitors that share a common transcriptional code is not understood. Here, we show that changes in retinoid activity in these two progenitor pools determine their fates. Retinoids, via Notch signaling, control the expression level of the transcription factor Ascl1 in progenitors, which selects serotonergic and V3 neuronal identities in a dose-dependent manner. Therefore, quantitative differences in the expression of a single component of a transcriptional code can select distinct cell fates.

This chapter is modified from:

Jacob J, Kong J, Moore S, Milton C, Sasai N, Gonzalez-Quevedo R, Terriente J, Imayoshi I, Kageyama R, Wilkinson DG, Novitch BG, and Briscoe J. (2013). Retinoid Acid specifies neuronal identity through graded expression of Ascl1. *Current Biology 23*: 412-418. DOI: 10.1016/j.cub.2013.01.046

JJ performed a majority of the experiments and wrote the manuscript. JK analyzed the $Rbpj^{CKO}$ tissue, quantified the results, and generated a summary figure. JJ, JK, SM, CM, NS, RGQ, JT, II, RK, DGW, BGN, and JB edited the manuscript, designed experiments, and provided vital reagents.

INTRODUCTION

The broad range of distinct neuronal subtypes that comprise the central nervous system (CNS) arise, in large part, as a consequence of molecular differences in their antecedent neural progenitors[1]. Initially naive progenitors acquire molecular heterogeneity through their exposure to different types or amounts of patterning signals. Within cells, the interpretation of these signals is manifested as the combinatorial expression of a relatively small number of transcriptional determinants that autonomously direct progenitor fate. The combinatorial nature of transcriptional coding of cell fate is thought to explain the diversity of neuronal subtypes in the CNS. In certain instances however, neural progenitors that express a common set of fate determinants produce different neuronal subtypes. Two topographically related neural progenitor pools comprise the p3 progenitor domain and are located in the ventral hindbrain and spinal cord of vertebrates (**Figure 4-5A**). In the hindbrain, p3 progenitors are, in general, bipotent and sequentially produce visceral motor (VM) and serotonergic (5HT) neurons, whereas unipotent spinal cord p3 progenitors produce V3 interneurons (**Figure 4-S1A and**

Figure 4-5A)[4-6]. 5HT and V3 neurons follow divergent differentiation pathways characterized by post-mitotic expression of the transcription factors Gata2/3[11], Lmx1b[12,13], and Pet1[14] in 5HT neurons and Sim1[4] in V3 interneurons. Consistent with their different ontogeny, 5HT and V3 neurons have distinct physiological properties, functions, and connectivity[9,15]. However, their progenitors share a common genetic identity marked by the expression of the homeodomain protein, Nkx2.2[4,16], the bHLH protein, Ascl1[17-19] and the forkhead box factor, Foxa2 (**Figures 4-S1A-C**)[5,20]. All three factors are involved in the specification of both neuronal subtypes, and Ascl1 additionally has a common proneural function[4,5,17,18] (**Figures 4-S1C**). Here we show that quantitative differences in Ascl1 expression discriminate between 5HT and V3 progenitors and that the level of Ascl1 instructs corresponding changes in the identity of p3 progenitors. In turn, the level of Ascl1 expression is regulated by retinoid signaling acting via the Notch pathway (**Figure 4-5B**). Therefore, both qualitative and quantitative differences in the expression of transcription factors contribute to the range of neuronal subtypes in the CNS.

MATERIALS AND METHODS

Expression constructs and in ovo electroporation: *zCyp26B1* cDNA[21] was cloned into the EcoRV and Sal1 restriction sites of a *miniTol2 HSP-UAS*-α-*crystallin RFP* plasmid in frame with 3' *myc* tag sequences using the In-Fusion PCR Cloning System (Clontech). To drive the expression of *zCyp26B1* in ovo, a *pCS2* vector containing *GAL4* (KalTA4)[22] was co-electroporated together with a *UAS-GFP* reporter plasmid. *UAS-GFP* was obtained by replacing the *CMV* promoter in *pCS2 GFP* with five tandem *UAS* sequences (gift from Dr. Q. Xu). To construct the *Hes1* expression vector, chicken *Hes1* was amplified by RT-PCR and an approximately 900 bp fragment was subcloned into the *pCAGGS* vector at Nhe1/Xho1 restriction sites upstream of *IRES GFP* using the following pair of primers: 5'-tatagctagcatgcccgccgacacgggcatggaaaaaccc-3' and 5'-tatactcgagtcaccacggcctccagacggactccctgcg-3'[23]. Expression vectors for *Fkh*^{A2}*-EnR*[5],

Nkx2.2-VP16[24], *Olig2-VP16*[25], *Olig2*[26], *RAR403*[27], *VP16RAR*[28], *Ascl1* and *Neurog2*[29], *Foxa2*[5] and *Nkx2.2*[24] have been described. An N-terminal *eYFP*-tagged *Pet1* expression vector was obtained through the ORFeome Collaboration[30]. *cAscl1-shRNA* was constructed using the following pair of primers:

5'-gagaggtgctgctgagcgagagtcaagctggtgaacctttagtgaagccacagatgta-3';

5'-attcaccaccactaggcacgagtcaagctggtgaacctttacatctgtggcttcact-3' and subcloned into Nhe1/Mlu1 restriction sites in the *pRFP-RNAiC* expression vector[31].

cAscl1-shRNA SCR was constructed using the primer pair:

5'-gagaggtgctgctgagcgatcgaacgtsgtcggacttaatagtgaagccacagatgta-3' and

5'-attcaccaccactaggcagtcgaacgtcgtcggacttaatacatctgtggcttcact-3' and subcloned into *pRFP-RNAiC*. In ovo electroporation was performed as described at Hamburger-Hamilton stages 10-12[23] and harvested from E3–5 of development. For each condition, observations were based on analysis of at least 4 or 5 embryos. Cell counts were derived from at least 2 sections per embryo from a minimum of 3 embryos.

Immunohistochemistry and in situ hybridization: Localization of proteins and mRNA was performed using antibodies or riboprobes as described[4,5,19,21,23,24,32-34]. Rabbit polyclonal antibodies were used to detect β-galactosidase (Biogenesis, Poole UK). Images were obtained as described[23]. The Ascl1 expression level was assayed in p3 progenitor cells by determining the mean pixel intensity (ImageJ) within a traced outline of individual nuclei on one or both sides of the neural tube at the developmental stages and axial levels described. For each measurement the mean background intensity was determined by measuring the mean pixel intensity in an area of tissue not expressing Ascl1, a region outside of the p3 domain. The mean background intensity per pixel was calculated by dividing the mean intensity in the defined area by the number of pixels in that area. The mean background intensity/pixel was multiplied by the number of pixels in the region of interest (p3 domain progenitor) to derive the mean background intensity for each p3 progenitor. This value was subtracted from the mean intensity of Ascl1

expression in the region of interest to obtain the background corrected mean intensity per cell. These calculations were iterated across the population of p3 progenitor cells in each experimental condition to obtain an overall mean intensity. Cells that failed to express GFP/RFP on the electroporated side were excluded from the analysis. For any given experiment, all sections were processed under the same conditions and imaged during the same session using identical microscope settings. The statistical significance of the differences in neuronal counts in the various experimental conditions was tested using an unpaired Student's t-test. In all graphs the "average" refers to the mean and error range is represented by the standard deviation (SD).

Mouse lines: The *RARE-LacZ*[35], *Rbpjf*$^{lox/+}$[36], *Hes5*[37] and *Olig2*$^{Cre/+,}$ *ROSA26*[38,39] mouse lines were generated as described.

RESULTS

Retinoids regulate p3 progenitor identity

Through the inductive effects of signaling molecules such as Sonic hedgehog (Shh)[4] and fibroblast growth factors (FGFs)[3], hindbrain serotonergic (5HT) progenitors acquire a Foxa2$^+$/Nkx2.2$^+$/Ascl1$^+$ transcriptional code. Topographically related V3 neural progenitors in the spinal cord express the same three factors (**Figures 4-S1A-C**). All three factors are necessary for the generation of 5HT neurons, and Nkx2.2 and Ascl1 are critical for V3 neurogenesis[4,5,17,18]. Consistent with its expression in spinal cord p3 progenitors, Foxa2 is also required for the generation of V3 interneurons (**Figures 4-S1B and 4-S1D-E**)[20]. This raises the question of how hindbrain and spinal p3 progenitors, designated p3/5HT and p3/V3 respectively, generate different cell types.

To identify the expression of retinoic acid (RA) signaling activity in the developing hindbrain and spinal cord, we analyzed β-galactosidase (β-gal) expression in *RARE-LacZ* mice, a transgenic mouse line that drives β-gal gene expression (*LacZ*) under the control of a retinoic acid responsive element (RARE)[35]. The hindbrain has a segmental organization and is

composed of eight compartments termed rhombomeres (r1-r8)[40]. β-gal immunostaining revealed low or absent RA signaling in p3/5HT progenitors at multiple rhombomeric levels, but high levels of activity in p3/V3 cells in the spinal cord (**Figure 4-S2A and Figure 4-5A**). This is consistent with other assays of retinoid signaling in amniotes[41,42] and suggested that retinoid signaling could be involved in p3 progenitor fate determination. To test this, we took advantage of a constitutively active retinoid receptor α derivative, *VP16RAR*, which has previously been shown to activate retinoic acid receptor target genes independently of RA[28]. Forced expression of *VP16RAR* by in ovo electroporation reduced 5HT neuronal differentiation by 40%–50% throughout the A-P extent of the hindbrain (**Figures 4-1A-C**). Concomitantly, occasional ectopic V3 neurons, marked by expression of the postmitotically expressed transcription factor *Sim1*, were produced in the caudal hindbrain (data not shown)[4]. Conversely, blockade of retinoid signaling in p3/V3 progenitors, either by misexpression of *Cyp26B1*, a member of the cytochrome P450 class of enzymes that degrades retinoic acid, or *RAR403*, a dominant negative version of the human RA receptor α[27], resulted in ectopic 5HT neuronal generation (**Figure 4-1D**). These neurons expressed the postmitotic serotonergic determinants Gata2[11] and Lmx1b[12,13], but not Pet1[14], and they also expressed the terminal differentiation marker Tph2[43] (**Figure 4-1E**). Therefore, ectopic spinal 5HT neurons share the same differentiation pathway as hindbrain 5HT neurons, of which approximately one-third do not depend on Pet1 for their generation[44,45].

The ventral restriction of ectopic spinal 5HT neurons suggested their derivation from presumptive p3/V3 progenitors, and blockade of Nkx2.2 or Foxa2 activity using a dominant interfering derivative of Nkx2.2 (*Nkx2.2-VP16*)[24] or Foxa2 (*Fkh^{A2}-EnR*)[5], respectively, prevented *RAR403* induction of ectopic 5HT neurons (**Figure 4-S2B**). Consistent with these data, forced expression of *Foxa2*, *Nkx2.2*, and *RAR403* in the dorsal neural tube led to extensive ectopic generation of 5HT neurons, whereas the omission of *RAR403* led to a failure to induce ectopic 5HT neurons (**Figure 4-1F**). This result also suggested that the small number of ectopic 5HT

neurons generated by p3/V3 in ovo electroporation with *RAR403* is likely to be a consequence of the restricted overlap of endogenous Foxa2 and Nkx2.2 expression and mosaic misexpression of *RAR403*. Furthermore, at brachial level the p3 domain normally only generates relatively small numbers of V3 neurons, suggesting that low neurogenic potential might further limit ectopic 5HT neurogenesis.

V3 neuronal differentiation was suppressed by 60% upon *RAR403* misexpression (average V3 neurons in control = 10.7 ± 4.1; V3 neurons following *RAR403* misexpression = 4.7 ± 2.2; $p = 7.18 \times 10^{-9}$, unpaired Student's t-test) (**Figure 4-1E**). This was not due to cell death or to a fate transformation to other ventral neuronal subtypes (**Figure 4-S2C**). Furthermore, ectopic visceral motor (VM) neurons that precede the generation of 5HT neurons in the hindbrain from p3 progenitors[6] (**Figure 4-S1A**) were not detected (**Figure 4-S2C**). Altogether, these data indicate that high-level versus low-level/absent retinoid signaling in p3/V3 and p3/5HT, respectively, determines the corresponding neuronal identities.

Retinoids regulate Ascl1 expression in p3 progenitors via the Notch pathway

The profile of RA signaling in the ventral neural tube correlates with the longitudinal expression of Ascl1 in p3 progenitors (**Figure 4-S1C and 4-S2A**). The significance of this observation lies in the critical subtype specification function of *Ascl1* in p3/5HT and p3/V3 progenitors, which is separable from its neurogenic properties[17,18]. In the p3/5HT domain where RA signaling is weak or absent, the expression level of chick *Ascl1* appeared markedly higher than in the p3/V3 domain where RA signaling is strong (**Figure 4-S1C**). This observation prompted closer scrutiny of the expression of Ascl1 in p3 progenitors in the hindbrain and spinal cord (**Figures 4-2A-B**). Indeed, the mean level of Ascl1 expression was consistently greater in p3/5HT than in p3/V3 progenitors between E9.5 and E11.5 (**Figure 4-5A**). Moreover, Ascl1 expression level was enhanced in hindbrain p3 progenitors after E9.5, corresponding to the time 5HT neurogenesis commences[5].

The Notch pathway is known to inhibit proneural gene expression, and, consistent with this regulatory relationship, in chick p3 progenitors the *Hes* family of Notch target genes showed reciprocal patterns of expression to *Ascl1* (**Figures 4-S2D-E**). Moreover, the Notch pathway lies downstream of retinoid signaling. Misexpression of *RAR403* in the p3/V3 domain led to the downregulation of the Notch pathway by E4 (**Figure 4-2C**). Conversely, forced expression of *VP16RAR* in the hindbrain p3/5HT domain upregulated Notch activity (**Figure 4-2D**). Retinoid regulation of the Notch pathway suggested Notch signaling might serve to link the A-P pattern of retinoid activity and Ascl1 expression in p3 progenitors.

To test whether the expression level of Ascl1 in p3/5HT and p3/V3 is regulated by retinoid signaling, we analyzed *Ascl1* expression in chick p3 progenitors following cell-autonomous blockade or activation of RA signaling. *RAR403* markedly upregulated *Ascl1* expression in the p3/V3 domain by E5 24 hr after the downregulation of the Notch pathway (average intensity of *Ascl1* in p3/V3 progenitors = 126 ± 19.3 arbitrary units (AU); *RAR403* p3/V3 expression = 221.6 ± 7.8; control p3/5HT expression = 223.1 ± 26.3) (**Figures 4-2E, 4-2H, and 4-S2F**). Moreover, the upregulation of *Ascl1* could be prevented by the co-misexpression of a short hairpin RNA against chick *Ascl1* (*cAscl1-shRNA*) (average intensity of *Ascl1* in p3/V3 progenitors = 110.9 ± 19.4; *RAR403* + *cAscl1-shRNA* p3/V3 expression = 107.1 ± 11.2; control p3/5HT expression = 208.4 ± 27.5) (**Figures 4-2E and 4-2H**). By contrast, misexpression of *VP16RAR* in p3/5HT progenitors downregulated *Ascl1* by E4 one day after the upregulation of the Notch pathway in these progenitors (average intensity of *Ascl1* in p3/5HT progenitors = 193.1 ± 27.1 arbitrary units (AU); *VP16RAR* p3/5HT expression = 94.4 ± 16.9; control p3/V3 expression = 105.1 ± 16.9) (**Figure 4-2F**). In neither condition were there detectable changes in expression of other proneural genes (*Neurog1* and *Neurog2*), other ventral progenitor markers (Pax6, Arx, Nkx2.2, and Foxa2), or Shh. Moreover, there was no increase in cell death (**Figures 4-S2F-H**).

To determine whether Notch signaling regulates Ascl1 expression in p3 progenitors, we conditionally deleted *Rbpj* (recombination signal binding protein for immunoglobulin kappa J), the principle effector of the Notch pathway[46], using *Olig2*^{cre38}. At E10.5, mice conditionally lacking *Rbpj* (*Rbpj*^{CKO}) expressed higher levels of Ascl1 in the spinal cord p3 domain, compared to either mice that have only one conditional allele or mice that lacked *Cre* (average Ascl1 expression in WT p3/V3 progenitors = 50.5 ± 28.0 arbitrary units (AU); *Rbpj*$^{flox/+}$ p3/V3 = 49.3 ± 29.0; *Rbpj*^{CKO} p3/V3 = 78.1 ± 50.4; WT p3/5HT = 90.3 ± 56.8) (**Figure 4-2G**). Conversely, misexpression of *Hes1*, a gene that is activated downstream of the Notch pathway, in the caudal hindbrain of the chick lowered the expression of *Ascl1* in p3/5HT progenitors to levels comparable to the expression of *Ascl1* in spinal cord p3 progenitors (average Ascl1 expression in control p3/5HT progenitors = 221.9 ± 20.9 arbitrary units (AU); *Hes1* electroporation p3/5HT = 123.4 ± 8.7; control p3/V3 = 119.8 ± 22.1) (**Figure 4-2I**). The expression of Foxa2 and Nkx2.2 were unaffected (**Figure 4-S2I**). Together, these gain- and loss-of-function data suggested that differential expression of Ascl1 in the two p3 progenitor pools is determined by retinoid signaling acting via the Notch pathway (**Figure 4-5**). Furthermore, our findings raise the possibility that differences in the expression level of Ascl1 might determine p3 progenitor fate.

Ascl1 expression level discriminates p3/V3 from p3/5HT progenitors

We exploited the regulatory relationship between Notch signaling and proneural gene expression to test the effect of boosting Ascl1 expression in the spinal cord on p3 progenitor fate. Strikingly, although 5HT neurons are normally never found in this region of the neural tube, ectopic spinal 5HT^{+}/GFP^{+} neuronal cell bodies were observed in the cervical cords of nine out of nine *Rbpj*^{CKO} mice and two out of five Olig2$^{Cre/+}$; *Rbpj*$^{flox/+}$ mice (**Figure 4-3A**). Moreover, analysis of embryos lacking *Hes5,* which is a target of Notch signaling broadly expressed in the spinal cord[47] (**Figure 4-3B**), revealed ectopic 5HT neurons in the ventral spinal cord at forelimb levels in three out of four *Hes5*$^{+/-}$ embryos and four out of four *Hes5* null

embryos. 5HT neurons were more abundant in the *Hes5* null mutants than in the *Rbpj*^{CKO} mutants, this may be due to the later deletion of *Rbpj* in neural cells by *Olig2*^{Cre} (~E9.5).

To further explore the role of Ascl1 expression level in regulating p3 progenitor fate, we first increased *Ascl1* levels in the p3/V3 domain by direct overexpression in ovo (**Figure 4-3C**). Boosting the level of Ascl1 in the p3/V3 domain was sufficient to generate ectopic 5HT neurons cell autonomously and suppress V3 neuronal differentiation (the average number of *Sim1*$^{+}$ cells on the electroporated side = 1.59 ± 1.6, the control side = 8.12 ± 2.3; $p = 2.80 \times 10^{-10}$), indicating that upregulation of Ascl1 reprograms the p3/V3 domain to a p3/5HT identity. Moreover, there was no evidence that cell death, as revealed by activated Caspase3 immunostaining, could account for the reduced number of V3 neurons (**Figure 4-3C**). Next, we misexpressed the three p3-defining transcription factors, *Nkx2.2*, *Foxa2*, and *Ascl1*, in the dorsal spinal cord. The widespread and cell-autonomous generation of ectopic 5HT neurons that resulted shows that *Ascl1* can substitute for *RAR403* and supports the view that high-level Ascl1 expression is sufficient to select a p3/5HT identity over a p3/V3 identity (**Figure 4-3C**). Ectopic 5HT neurons expressed postmitotic markers of hindbrain 5HT neurons Lmx1b and Gata2, but not *Pet1* (**Figure 4-3D** and data not shown), suggesting that the differentiation of these neurons largely recapitulates the serotonergic differentiation pathway. Importantly, neither overexpression of *Foxa2* and *Nkx2.2* alone nor replacement of *Ascl1* by another bHLH gene, *Neurog2*, led to ectopic 5HT neuronal generation (**Figures 4-1F and 4-3C**). Therefore, increasing the expression of *Ascl1* converts p3/V3 to a p3/5HT identity.

We then asked whether reducing the expression of *Ascl1* in presumptive p3/5HT progenitors would cause a reciprocal switch to a p3/V3 identity. Following *Hes1* in ovo electroporation into presumptive p3/5HT progenitors, significant reductions in 5HT neuronal differentiation were observed, using Lmx1b and *Pet1* as markers (average 5HT neurons on the control side = 8.2 ± 2.8; *Hes1*-electroporated side = 2.5 ± 2.1; $p = 8.2 \times 10^{-8}$), and small numbers of *Sim1* expressing ectopic V3 neurons were consistently detected in the caudal

hindbrain (**Figure 4-3E**). This is consistent with the low neurogenic potential of the caudal hindbrain p3/5HT domain. The block in generation of ectopic V3 neurons by co-misexpression of *Nkx2.2-VP16* confirmed the derivation of these *Hes1*-induced ectopic V3 neurons from the presumptive p3/5HT domain (**Figure 4-S3A**). To further test the idea that Ascl1 expression level is important for p3/5HT identity, we measured the expression of Ascl1 in *Ascl1* heterozygote mice, in which 5HT neuronal differentiation is intact[17]. No significant change in Ascl1 expression was detected (average Ascl1 intensity in WT p3/5HT progenitors = 151.1 ± 53.2 arbitrary units (AU); *Ascl1*$^{+/-}$ p3/5HT = 149.3 ± 39.7), which implies that allele number is not the main determinant of the level of Ascl1 expression (**Figure 4-S3B**). Together, these data support the case for the critical role of Ascl1 expression level in the selection of 5HT over V3 neuronal fate.

Finally, to test directly whether the level of Ascl1 determines p3 progenitor fate, we used *cAscl1-shRNA*. Forced expression of *cAscl1-shRNA* in the ventral region of the caudal hindbrain reduced the expression of*Ascl1* in hindbrain p3 progenitors (average *Ascl1* expression in control p3/5HT = 213.6 ± 22.8 arbitrary units (AU); *cAscl1-shRNA* p3/5HT = 123.9 ± 13.3; control p3/V3 = 119.5 ± 19.5), and this was accompanied by a ~40% reduction in 5HT neuronal differentiation (**Figures 4-4A and 4-4D**). Consistent with the retinoid and Notch pathway gain-of-function experiments in the caudal hindbrain in ovo, occasional ectopic V3 neurons were also detected (**Figure 4-S3C**). We then attempted to rescue these neural patterning defects by co-misexpression of rat *Ascl1* (*rAscl1*), which is resistant to this *cAscl1-shRNA*. *rAscl1* restored serotonergic neurogenesis and prevented the ectopic generation of any V3 neurons by *cAscl1-shRNA* (**Figures 4-4B, 4-4E, and 4-S3D**). Transfection of a scrambled version of the chick *Ascl1* shRNA (*cAscl1-shRNA-SCR*) did not alter the expression of *Ascl1* in p3/5HT progenitors (average *Ascl1* expression in control p3/5HT = 185.9 ± 30.1 arbitrary units (AU); *cAscl1-shRNA-SCR* p3/5HT = 176.0 ± 38.5), nor did it alter 5HT neurogenesis or induce any ectopic V3 neurons (**Figures 4-S3E and 4-S3F**). Furthermore, when the increased expression of *Ascl1* in p3/V3 progenitors elicited by *RAR403* was prevented by co-

misexpression of *cAscl1-shRNA* (**Figure 4-2E**), V3 neuronal differentiation was rescued (average V3 neurons in control = 11 ± 4.6; V3 neurons following *RAR403* + *cAscl1-shRNA* misexpression = 10.8 ± 5.1; p = 0.92, not significant), and ectopic 5HT neuronal generation was blocked (**Figure 4-4C**). Taken together, these data indicate that Ascl1 recapitulates the effect of retinoids on p3 progenitor identity and that retinoids regulate the neuronal fates of p3 progenitors in an *Ascl1*-dependent manner (**Figure 4-5B**).

DISCUSSION

We have shown how different profiles of retinoid signaling in p3 progenitors that share a common transcriptional code generate distinct neuronal identities at spinal cord and hindbrain levels. Binary differences in retinoid activity result in graded shifts in expression of a pivotal transcription factor, Ascl1, which is critical for the selection of alternate progenitor identities (**Figure 4-5**). This mechanism of progenitor fate specification is distinct from the conventional combinatorial model, because allocation to V3 or 5HT neuronal identity is determined not by qualitative but by quantitative differences in the transcriptional code[1]. Moreover, this model does not exclude the possibility that other, as yet uncharacterized, intrinsic determinants function in the same pathway as Ascl1 and could discriminate p3/5HT from p3/V3.

In invertebrates, graded activity of transcription factors has been shown to control differential gene expression and thereby diversify cell fates[48]. By contrast in vertebrates, in general, transcription factor gradients appear to refine neural identity rather than instruct distinct cell identities in a dose-dependent manner[49-53]. Consistent with their closely similar genetic identities, the manipulations of retinoid signaling and Ascl1 expression demonstrate that spinal p3 progenitors possess a cryptic bipotency. The induction of ectopic V3 neurons in the hindbrain is less robust, which implies that hindbrain p3 progenitors are not fully interconvertible by graded Ascl1 expression alone. Nevertheless, it is clear that *Ascl1* expression must be tightly

regulated to regionally constrain 5HT neurogenesis. Importantly, failure to appropriately regulate the number of 5HT neurons is associated with neuropsychiatric disease states, for example Smith-Lemli-Opitz syndrome, in which hypermorphic serotonergic differentiation occurs[54].

FIGURES

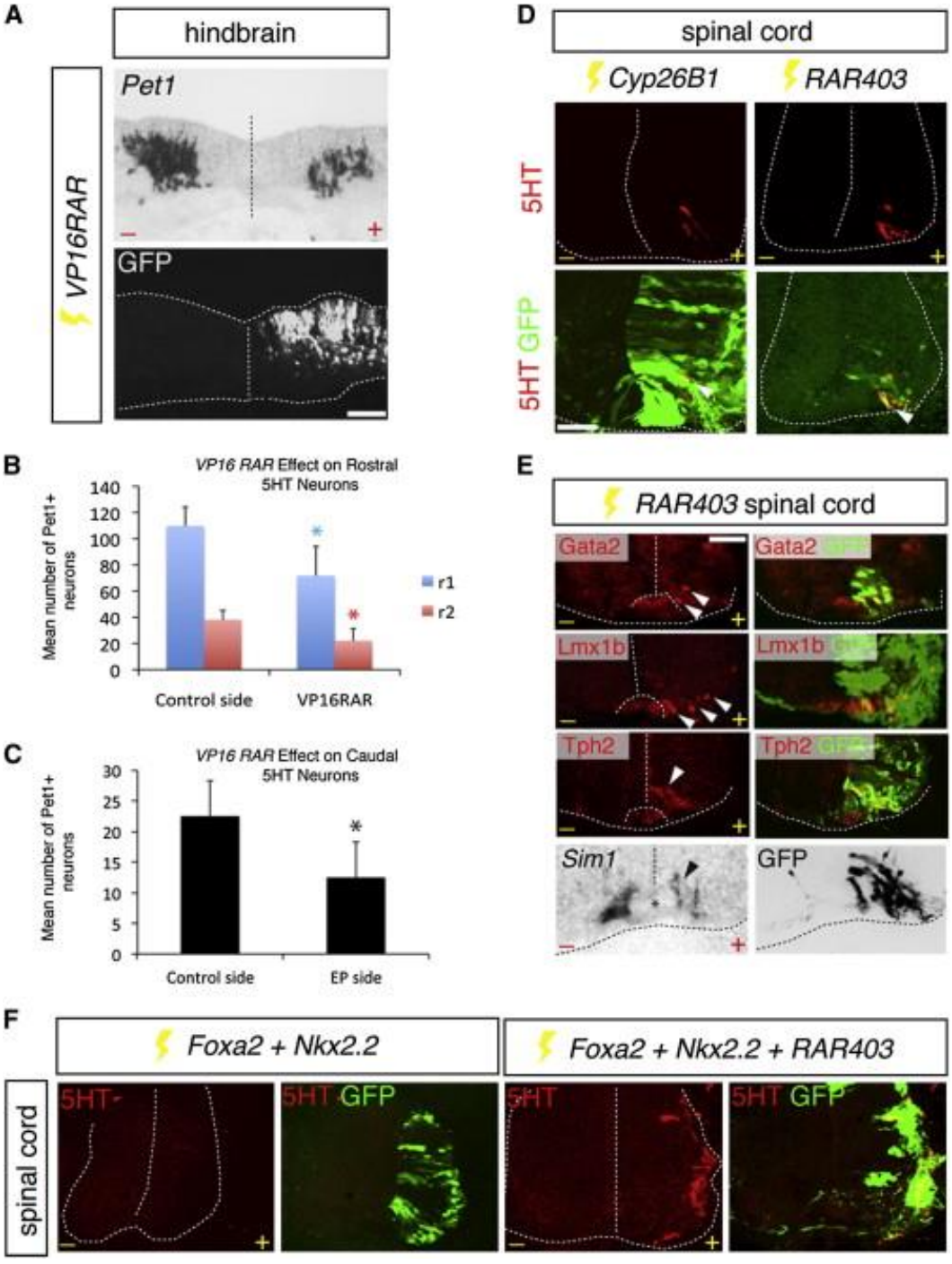
A
hindbrain
VP16RAR
Pet1
GFP
D
spinal cord
Cyp26B1
RAR403
5HT
5HT GFP
B
VP16 RAR Effect on Rostral 5HT Neurons
Mean number of Pet1+ neurons
140
120
100
80
60
40
20
0
r1
r2
Control side
VP16RAR
C
VP16 RAR Effect on Caudal 5HT Neurons
Mean number of Pet1+ neurons
30
25
20
15
10
5
0
Control side
EP side
E
RAR403 spinal cord
Gata2
Lmx1b
Tph2
Sim1
GFP
F
Foxa2 + Nkx2.2
Foxa2 + Nkx2.2 + RAR403
spinal cord
5HT
5HT GFP

Figure 4-1: Retinoid signaling determines p3 progenitor fate

(A) Upregulation of RA signaling in hindbrain p3/5HT progenitors by misexpression of *VP16RAR-IRES GFP* reduces *Pet1* expression. Scale bar = 25 µm.

(B-C) Effect of *VP16RAR* misexpression on *Pet1*$^{+}$ neurons in the rostral (B) or caudal (C) hindbrain at E5. $^{*}p = 0.025$ (B, blue bar), $^{*}p = 0.026$ (B, red bar), $^{*}p = 8.11 \times 10^{-6}$ (C, black bar) (Unpaired Student's t tests). Error bars represent SD in all graphs. r, rhombomere.

(D) Forced expression of *Cyp26B1* or *RAR403* in p3/V3 generates ectopic 5HT neurons (arrowheads) by E5. Scale bar = 14 µm.

(E) Ectopic spinal 5HT neurons express the indicated markers (arrowheads), and *Sim1* expression is reduced. Asterisk marks the floor plate. Scale bar = 16 µm.

(F) *Nkx2.2* and *Foxa2* misexpression only induce ectopic spinal 5HT neurons when RA signaling is blocked by *RAR403*. –, control side; +, electroporated side.

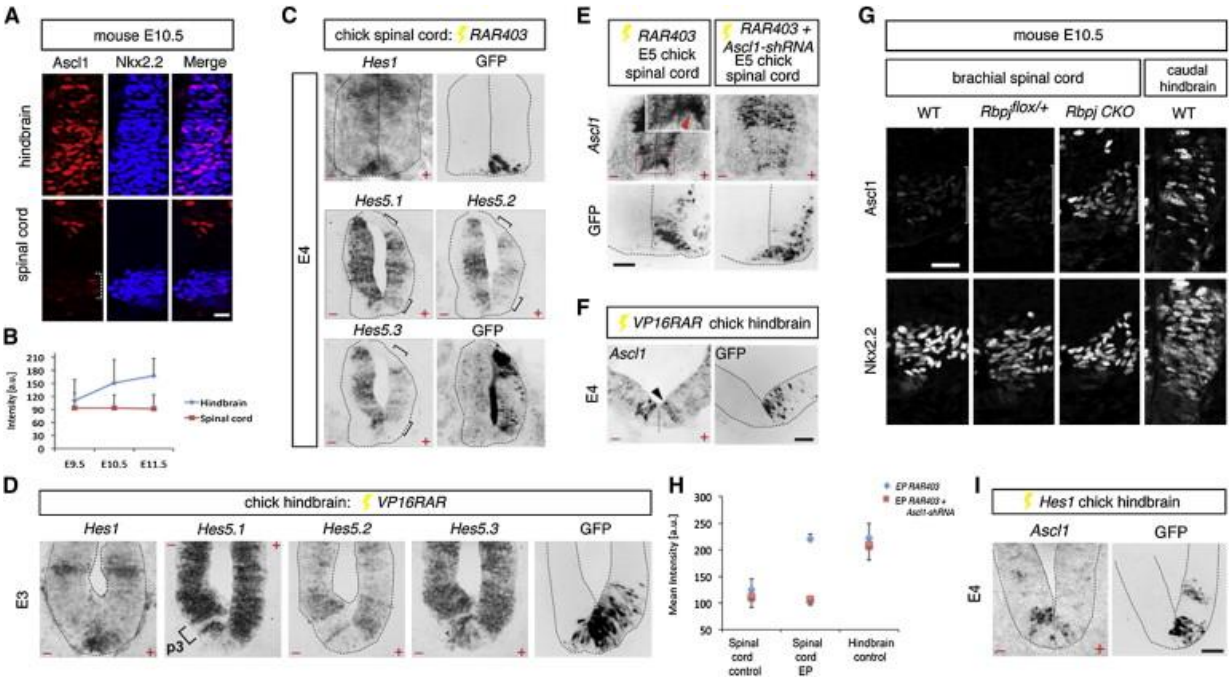

Figure 4-2: Ascl1 expression level in p3 progenitors is negatively correlated with Notch activity, which in turn is regulated by Retinoids

(A-B) Ascl1 expression in mouse Nkx2.2^{+} p3 progenitors (A), with quantification (mean ± SD) shown in (B). Scale bar = 9 µm. a.u., arbitrary units. n = 3 sections from each of three embryos per developmental stage.

(C) Spinal *RAR403* misexpression, marked by anti-GFP immunofluorescence, downregulates *Hes* gene expression (bracketed).

(D) Misexpression of *VP16RAR* upregulates hindbrain p3 *Hes* gene expression.

(E) Misexpression of *RAR403* in p3/V3 progenitors upregulates *Ascl1* expression (arrowhead, inset) at E5, and this is prevented by *cAscl1-shRNA*. Inset shows a high-power image of the boxed region. Scale bar = 18 µm.

(F) *VP16RAR* misexpression attenuates *Ascl1* expression (arrowhead) in p3/5HT progenitors. Scale bar = 18 µm. **(G)** Increased Ascl1 expression in brachial Nkx2.2^{+} p3/V3 cells (white brackets) of *Rbpj^{CKO}* mouse embryos is similar to Ascl1 expression in WT p3/5HT cells. Scale bar = 14 µm.

(H) Quantification of *Ascl1* expression in presumptive p3/V3 cells misexpressing *RAR403* or *RAR403* and *cAscl1-shRNA*.

(I) Misexpression of *Hes1-IRES GFP* in caudal hindbrain p3/5HT reduces *Ascl1* expression. Scale bar = 18 µm.

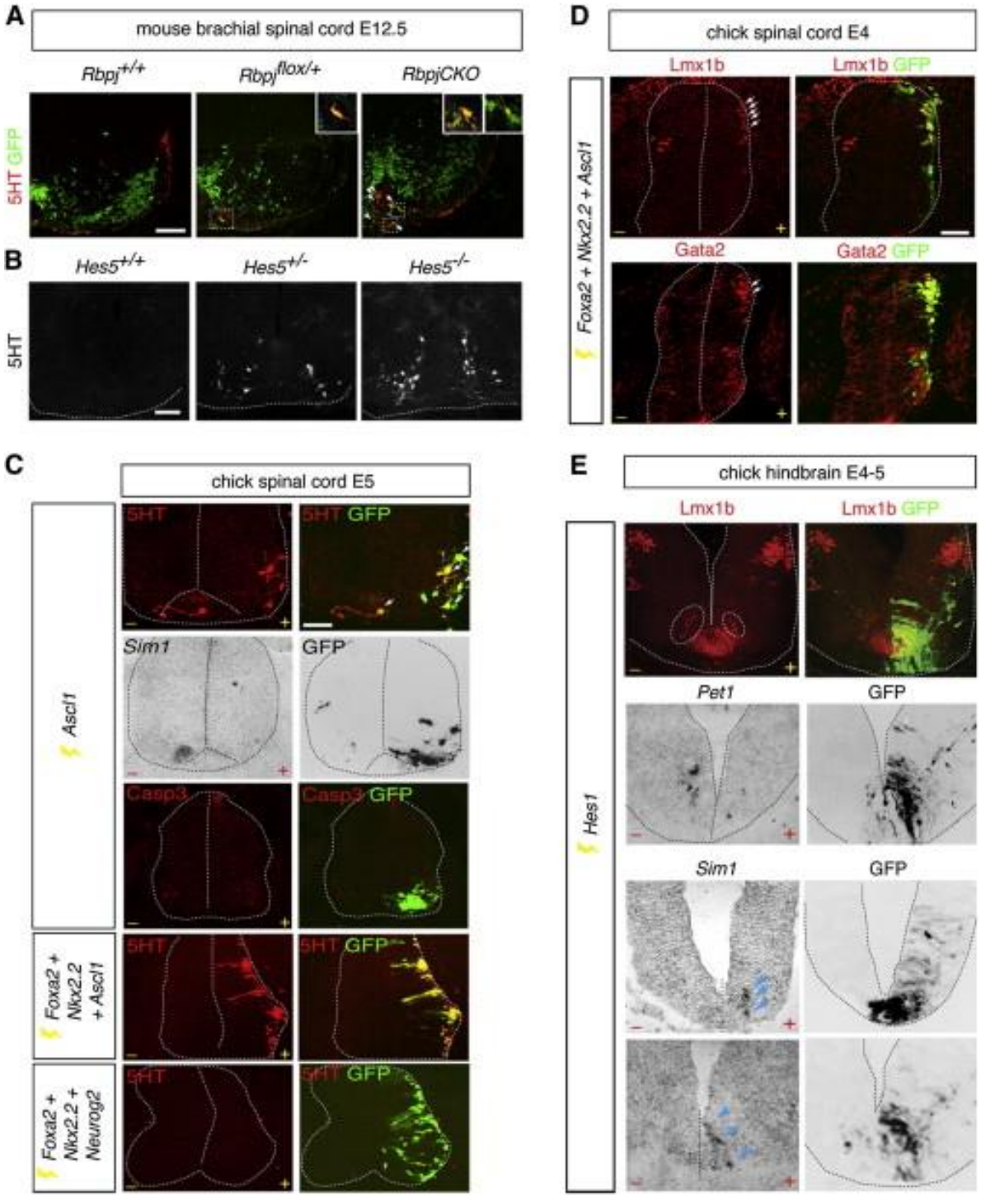
A
mouse brachial spinal cord E12.5
Rbpj+/+
Rbpjflox/+
RbpjCKO
5HT GFP
B
Hes5+/+
Hes5+/-
Hes5-/-
5HT
C
chick spinal cord E5
Ascl1
5HT
5HT GFP
Sim1
GFP
Casp3
Casp3 GFP
Foxa2 + Nkx2.2 + Ascl1
Foxa2 + Nkx2.2 + Neurog2
D
chick spinal cord E4
Foxa2 + Nkx2.2 + Ascl1
Lmx1b
Lmx1b GFP
Gata2
Gata2 GFP
E
chick hindbrain E4-5
Hes1
Lmx1b
Lmx1b GFP
Pet1
GFP
Sim1
GFP

Figure 4-3: Altering Ascl1 expression level in p3 progenitors produces corresponding changes in p3 progenitor identity

(A-B) Ectopic $5HT^+/GFP^+$ neurons (yellow cells, arrowheads) in the cervical cord of *Rbpj*^{CKO} mutants (A) and $5HT^+$ cells in the brachial cord of *Hes5* mutants (B). Insets show high-power images of $5HT^+/GFP^+$ neurons in boxed regions. Scale bar = 25 µm (A), 13 µm (B).

(C) Forced *Ascl1* expression in cervicobrachial p3/V3 cells induces ectopic 5HT neurons (arrows) and reduces V3 differentiation. Cell death, assayed by activated Caspase3 expression, is not detected in the ventral spinal cord. *Ascl1*, but not *Neurog2*, substitutes for *RAR403* in combined electroporation with *Foxa2* and *Nkx2.2* to induce ectopic spinal 5HT neurons. Scale bar = 13 µm.

(D) Ectopic Lmx1b and Gata2 expression (arrows) upon combined *Foxa2*, *Nkx2.2*, and *Ascl1* electroporation at brachial level. Scale bar = 14 µm.

(E) *Hes1-IRES GFP* misexpression in caudal p3/5HT cells reduces 5HT neuronal differentiation marked by Lmx1b (circled) and*Pet1* and induces ectopic V3 neurons (arrowheads).

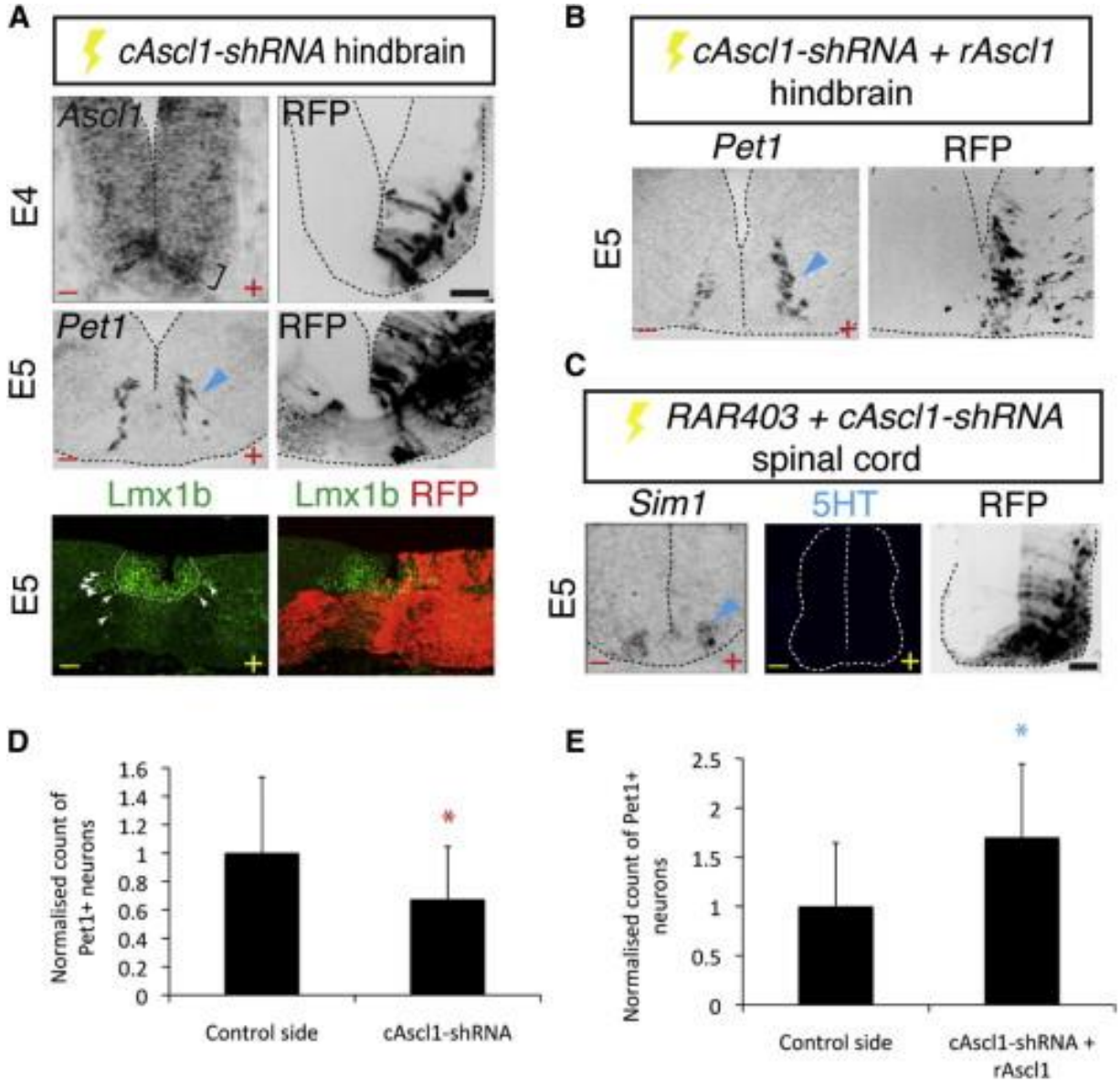
A
cAscl1-shRNA hindbrain
Ascl1
RFP
E4
Pet1
RFP
E5
Lmx1b
Lmx1b RFP
E5
B
cAscl1-shRNA + rAscl1
hindbrain
Pet1
RFP
E5
C
RAR403 + cAscl1-shRNA
spinal cord
Sim1
5HT
RFP
E5
D
Normalised count of Pet1+ neurons
1.6
1.4
1.2
1
0.8
0.6
0.4
0.2
0
*
Control side
cAscl1-shRNA
E
Normalised count of Pet1+ neurons
2.5
2
1.5
1
0.5
0
*
Control side
cAscl1-shRNA + rAscl1

Figure 4-4: Knockdown of chick *Ascl1* alters p3 progenitor identity

(A) Misexpression of *cAscl1-shRNA IRES RFP* decreases *Ascl1* expression in hindbrain p3 progenitors (bracket) and reduces*Pet1* (arrowhead) and Lmx1b expression (short arrows). Dotted white line demarcates Lmx1b expression corresponding to the floor plate. RFP expression on the control side is confined to decussating axons. Scale bar represents 18 μm.

(B) Co-electroporation of *cAscl1-shRNA* and *rAscl1* rescues *Pet1* expression (arrowhead).

(C) *cAscl1-shRNA* restores *Sim1*+ V3 neurons (arrowhead) and blocks ectopic spinal 5HT expression induced by *RAR403*. Scale bar represents 13 μm.

(D-E) Quantification of *Pet1*+ neurons in the caudal hindbrain at E5 following forced expression of *cAscl1-shRNA* (D) or *cAscl1-shRNA* and *rAscl1* (E). Red asterisk, $p = 0.028$; blue asterisk, $p = 0.002$.

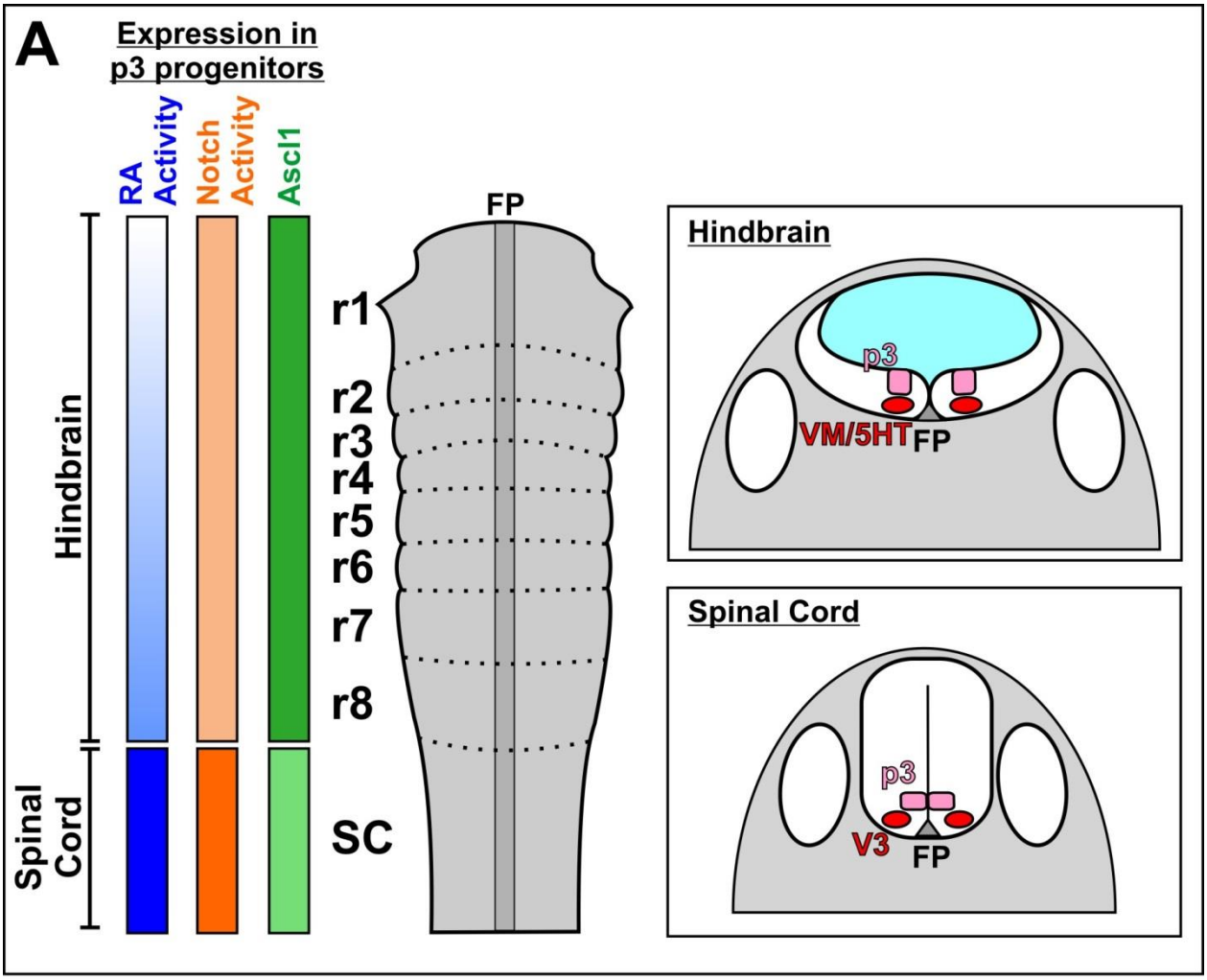
A
Expression in
p3 progenitors
RA Activity
Notch Activity
Ascl1
Hindbrain
Spinal Cord
r1
r2
r3
r4
r5
r6
r7
r8
SC
FP
Hindbrain
p3
VM/5HT
FP
Spinal Cord
p3
V3
FP

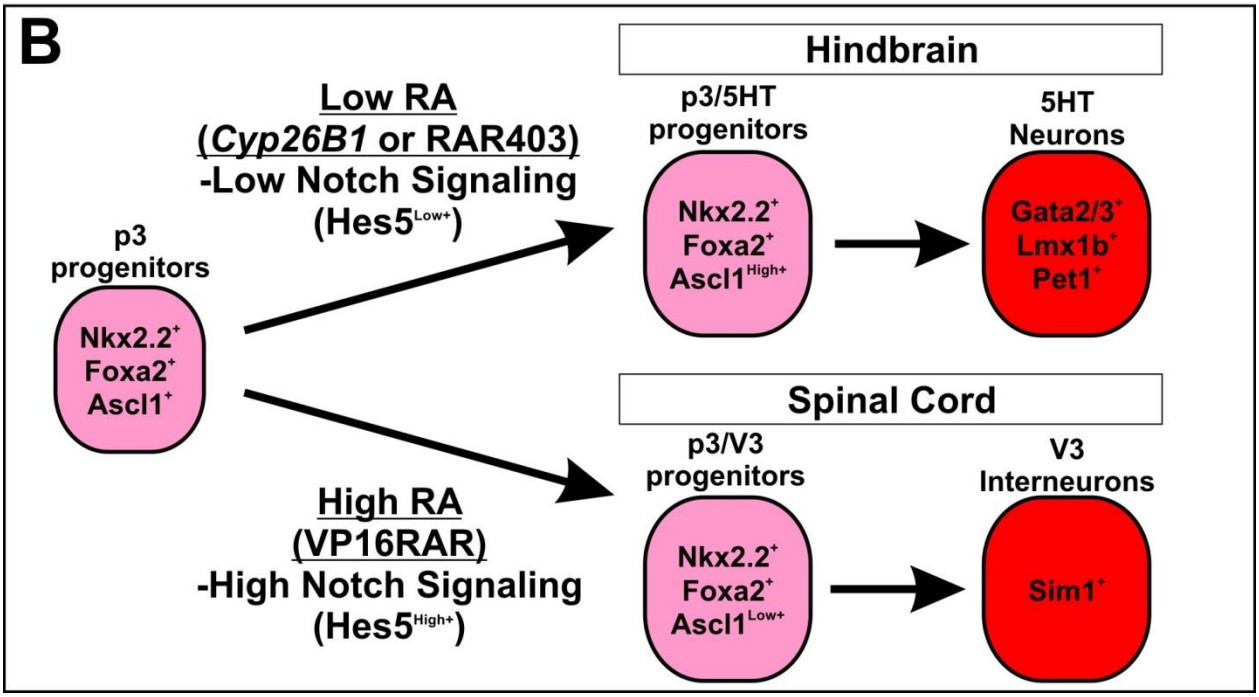
B
Low RA
(Cyp26B1 or RAR403)
-Low Notch Signaling
(Hes5Low+)
p3
progenitors
Nkx2.2+
Foxa2+
Ascl1+
Hindbrain
p3/5HT
progenitors
Nkx2.2+
Foxa2+
Ascl1High+
5HT
Neurons
Gata2/3+
Lmx1b+
Pet1+
High RA
(VP16RAR)
-High Notch Signaling
(Hes5High+)
Spinal Cord
p3/V3
progenitors
Nkx2.2+
Foxa2+
Ascl1Low+
V3
Interneurons
Sim1+

Figure 4-5: Model for how retinoic acid specifies neuronal identity by regulating Ascl1 expression in p3 progenitors via a modulation of Notch pathway activity

(A-B) An illustration of the hindbrain and rostral spinal cord[55]. RA signaling activity is low in p3/5HT hindbrain progenitors, resulting in a downregulation of Notch signaling and increased expression of Ascl1. Conversely, RA signaling activity is high is p3/V3 spinal cord progenitors, resulting in an upregulation of Notch signaling and decreased expression of Ascl1. Ultimately, it is this quantitative difference in Ascl1 that distinguishes between the p3/5HT and p3/V3 progenitors. The p3/5HT progenitors produce 5HT neurons in the hindbrain, which may express Gata2/3, Lmx1b, and Pet1. On the other hand, the p3/V3 progenitors produce V3 interneurons in the spinal cord which express Sim1.

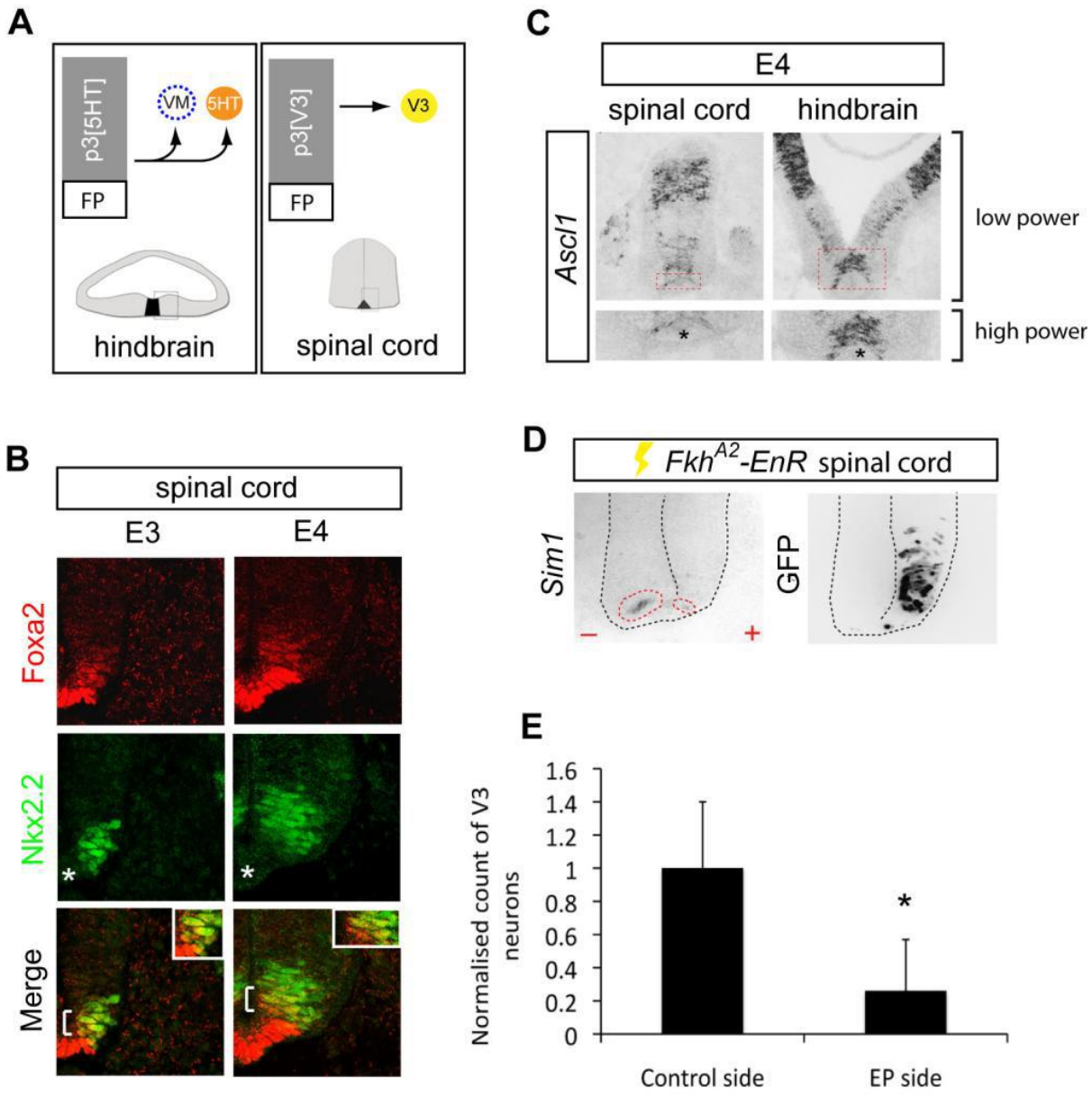
A
p3[5HT]
VM
5HT
FP
hindbrain
p3[V3]
V3
FP
spinal cord
B
spinal cord
E3
E4
Foxa2
Nkx2.2
Merge
C
E4
spinal cord
hindbrain
Ascl1
low power
high power
D
Fkh^A2-EnR spinal cord
Sim1
GFP
E
Normalised count of V3 neurons
1.6
1.4
1.2
1
0.8
0.6
0.4
0.2
0
Control side
EP side

Supplementary Figure 4-S1: Fate determinants that specify the p3 domain of the spinal cord

(A) Schematic showing the different neuronal progeny derived from p3 progenitors in the hindbrain and spinal cord. VM, visceral motor.

(B) Horizontal sections of the rostral spinal cord of the chick showing co-expression of Foxa2 (red) and Nkx2.2 (green) by immunofluorescence. The region of overlap is indicated by a square bracket, and is shown at high power in the insets.

(C) *Ascl1* expression detected by in-situ hybridization in the p3 domain (boxed) of the rostral spinal cord (left) and caudal hindbrain (right) of the chick. Lower panels show high power views of *Ascl1* expression in the boxed regions. In (B and C) the asterisk marks the floor plate.

(D) Forced expression of a dominant negative version of Foxa2, *FkhA2-EnR,* in chick p3/V3 progenitors markedly reduces the expression of *Sim1*$^{+}$ V3 interneurons.

(E) Quantification of *Sim1*$^{+}$ V3 interneurons at E5 following in ovo electroporation of *FkhA2-EnR*. * $p = 2.05 \times 10^{-11}$. Error bars represent SD.

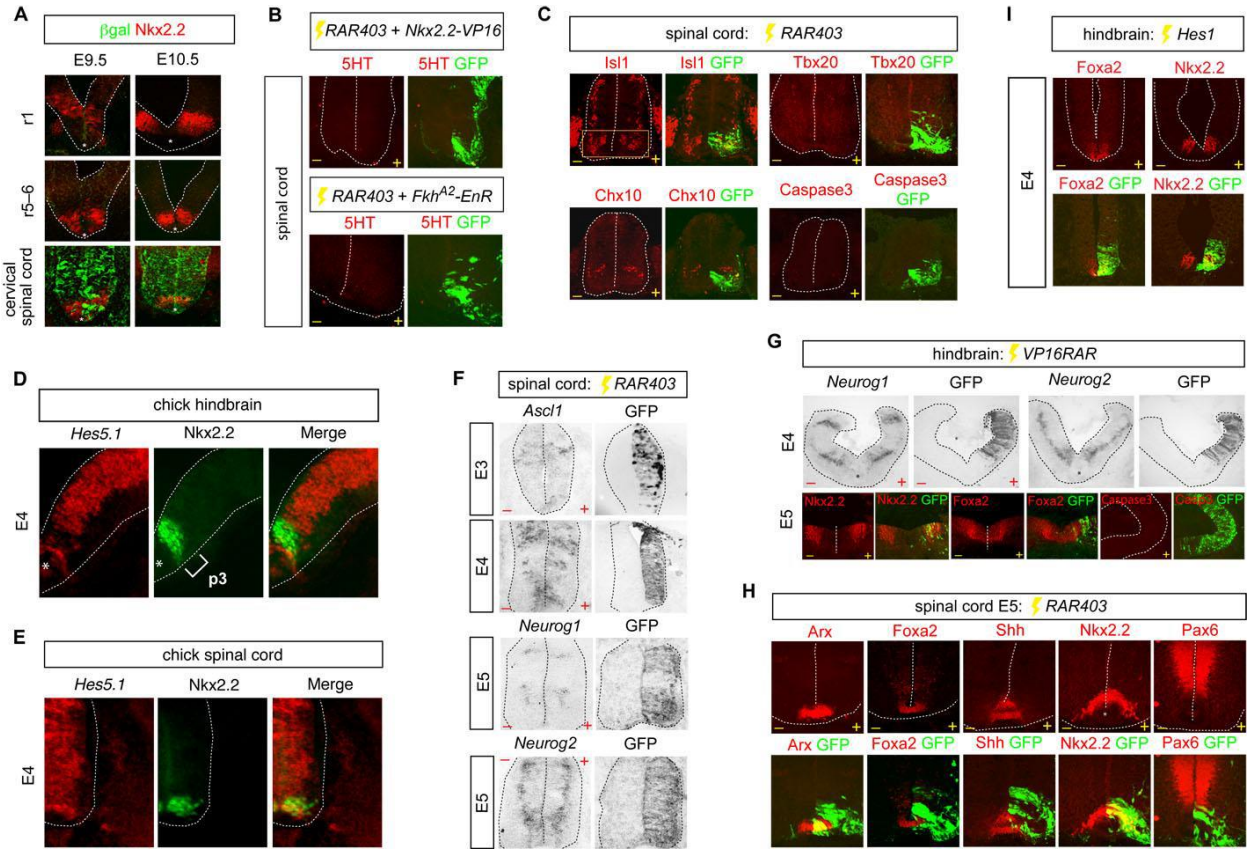

Supplementary Figure 4-S2: Effect of Retinoid signaling on ventral neural progenitor identities in developing mouse and chick embryos

(A) In a transgenic mouse line harboring a retinoic acid response element fused to the β-galactosidase gene (*RARE-LacZ*), β-gal (green) detection by immunofluorescence reports the spatial distribution of retinoid signaling. The p3 domain in the hindbrain and spinal cord is marked by immunostaining for Nkx2.2 (red). Representative sections are shown at the indicated axial levels. r, rhombomere.

(B) Ectopic spinal cord 5HT neurons are derived from p3 progenitors. In ovo electroporation of *RAR403* and either a dominant negative version of Nkx2.2, *Nkx2.2-VP16* (upper panels) or Foxa2, *FkhA2-EnR* (lower panels) prevents ectopic 5HT neuronal generation in the brachial level spinal cord as shown by the absence of 5HT immunostaining.

(C) Blockade of retinoid signalling in the chick by *RAR403* misexpression in p3/V3 progenitors does not affect patterning of other neuronal subtypes, the $Isl1^+$ somatic motor neurons and $Chx10^+$ V2 interneurons in the ventral spinal cord. Moreover, ectopic VM neurons, marked by Tbx20 expression are not induced. *RAR403* misexpression does not result in increased cell death in the ventral spinal cord as indicated by the absence of activated Caspase3 immunostaining.

(D-E) Expression of the Notch pathway gene *Hes5.1* in $Nkx2.2^+$ p3/5HT (D) and p3/V3 progentiors (E).

(F) In-situ hybridization for *Ascl1* at E3 and E4 and the classic proneural genes, *Neurog1* and *Neurog2* at E5, following *RAR403 IRES GFP* misexpression in the spinal cord.

(G) Following in ovo *VP16RAR* misexpression in the caudal hindbrain no change in *Neurog1* or *Neurog2* expression is detected. Expression of the p3/5HT progenitor markers, Nkx2.2 and Foxa2 is not altered by *VP16RAR* misexpression. Assay for cell death by immunostaining for activated Caspase3 shows that *VP16RAR* misexpression does not induce cell death in the hindbrain.

(H) Immunofluorescence images of the floor plate markers, Arx and Shh and the ventral progenitor markers Foxa2, Nkx2.2 and Pax6 following *RAR403* misexpression in the p3/V3 domain.

(I) Expression of progenitor markers FoxA2 and Nkx2.2 in the caudal hindbrain at E4 following forced expression of *Hes1-IRES GFP.*

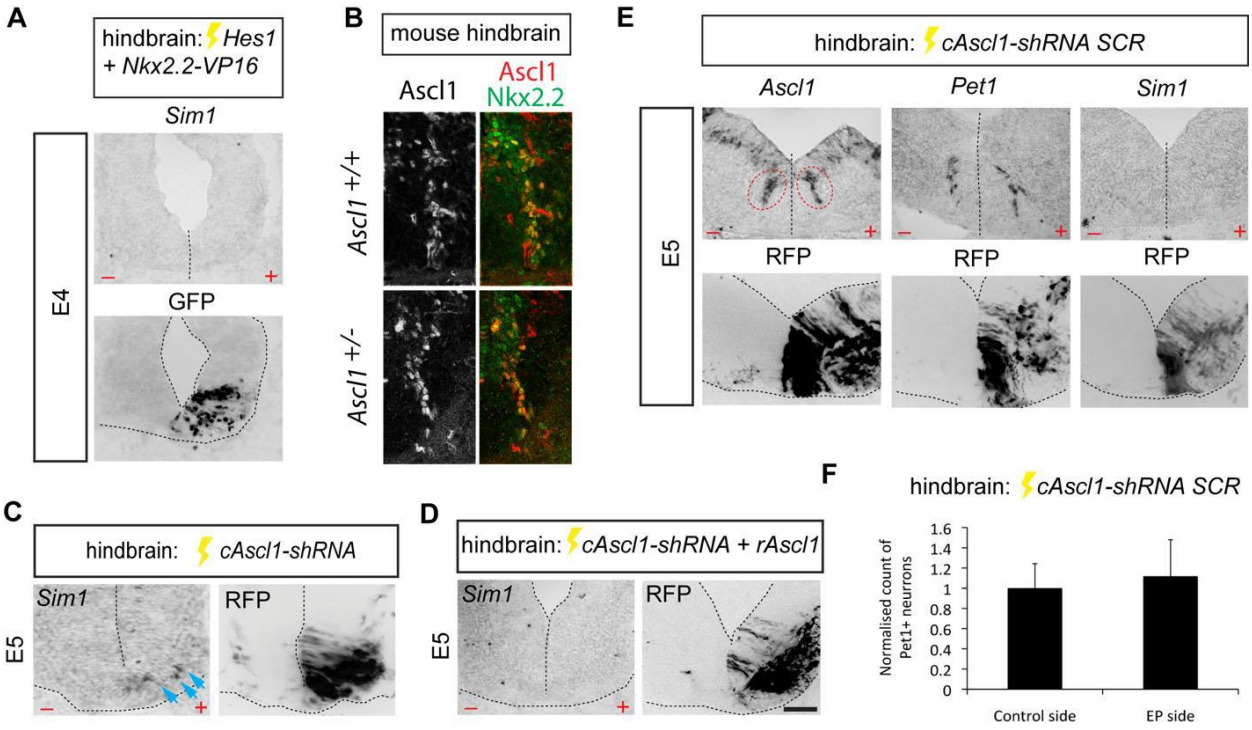

Supplementary Figure 4-S3: Effect on neural patterning of lowering *Ascl1* expression in p3/5HT progenitors in the chick, by *Hes1* in ovo electroporation, or directly by *Ascl1* knockdown in ovo

(A) Absence of ectopic expression of *Sim1*, the V3 neuronal marker in the caudal hindbrain at E4 following co-electroporation of *Hes1* and *Nkx2.2-VP16*.

(B) Horizontal sections through the caudal hindbrain of E11.5 WT (*Ascl1*$^{+/+}$) and Ascl1 heterozygous (*Ascl1*$^{+/-}$) mouse embryos showing Ascl1 expression in hindbrain p3 progenitors (marked by Nkx2.2 expression in green). Embryos were imaged using identical settings in the same confocal session.

(C) Misexpression of *cAscl1-shRNA IRES RFP* induces occasional ectopic *Sim1*$^{+}$ V3 neurons (arrows) in the ventral region of the caudal hindbrain.

(D) Following co-misexpression of *cAscl1-shRNA* and *rAscl1* in ovo, ectopic V3 neurons are never detected in the caudal hindbrain.

(E) Lack of effect of control scrambled *cAscl1-shRNA* (*cAscl1-shRNA SCR*) on *Ascl1,* 5HT neuronal differentiation, marked by *Pet1* expression, and V3 differentiation, marked by *Sim1*, at E5 in the caudal hindbrain of chick. *Ascl1* expression corresponding to the p3/5HT domain is circled.

(F) Quantification of 5HT neuronal differentiation, using *Pet1* as a marker, in the caudal hindbrain of the chick following forced expression of *cAscl1-shRNA SCR*. p = 0.38, N.S.

ACKNOWLEDGEMENTS

We thank F. Guillemot for comments on the manuscript and P. Dollé and V. Ribes for *RARE-LacZ* mice. This work was funded by the Medical Research Council (UK).

REFERENCES

1 Jessell, T. M. Neuronal specification in the spinal cord: inductive signals and transcriptional codes. *Nature reviews. Genetics* **1**, 20-29, doi:10.1038/35049541 (2000).

2 Briscoe, J. & Ericson, J. Specification of neuronal fates in the ventral neural tube. *Current opinion in neurobiology* **11**, 43-49 (2001).

3 Ye, W., Shimamura, K., Rubenstein, J. L., Hynes, M. A. & Rosenthal, A. FGF and Shh signals control dopaminergic and serotonergic cell fate in the anterior neural plate. *Cell* **93**, 755-766 (1998).

4 Briscoe, J. *et al.* Homeobox gene Nkx2.2 and specification of neuronal identity by graded Sonic hedgehog signalling. *Nature* **398**, 622-627, doi:10.1038/19315 (1999).

5 Jacob, J. *et al.* Transcriptional repression coordinates the temporal switch from motor to serotonergic neurogenesis. *Nature neuroscience* **10**, 1433-1439, doi:10.1038/nn1985 (2007).

6 Pattyn, A. *et al.* Coordinated temporal and spatial control of motor neuron and serotonergic neuron generation from a common pool of CNS progenitors. *Genes & development* **17**, 729-737, doi:10.1101/gad.255803 (2003).

7 Cordes, S. P. Molecular genetics of cranial nerve development in mouse. *Nature reviews. Neuroscience* **2**, 611-623, doi:10.1038/35090039 (2001).

8 Ray, R. S. *et al.* Impaired respiratory and body temperature control upon acute serotonergic neuron inhibition. *Science* **333**, 637-642, doi:10.1126/science.1205295 (2011).

9 Zhang, Y. *et al.* V3 spinal neurons establish a robust and balanced locomotor rhythm during walking. *Neuron* **60**, 84-96, doi:10.1016/j.neuron.2008.09.027 (2008).

10 Deneris, E. S. & Wyler, S. C. Serotonergic transcriptional networks and potential importance to mental health. *Nature neuroscience* **15**, 519-527, doi:10.1038/nn.3039 (2012).

11 Craven, S. E. *et al.* Gata2 specifies serotonergic neurons downstream of sonic hedgehog. *Development* **131**, 1165-1173, doi:10.1242/dev.01024 (2004).

12 Cheng, L. *et al.* Lmx1b, Pet-1, and Nkx2.2 coordinately specify serotonergic neurotransmitter phenotype. *J Neurosci* **23**, 9961-9967 (2003).

13 Ding, Y. Q. *et al.* Lmx1b is essential for the development of serotonergic neurons. *Nature neuroscience* **6**, 933-938, doi:10.1038/nn1104 (2003).

14 Hendricks, T., Francis, N., Fyodorov, D. & Deneris, E. S. The ETS domain factor Pet-1 is an early and precise marker of central serotonin neurons and interacts with a conserved element in serotonergic genes. *J Neurosci* **19**, 10348-10356 (1999).

15 Jacobs, B. L. & Azmitia, E. C. Structure and function of the brain serotonin system. *Physiological reviews* **72**, 165-229 (1992).

16 Briscoe, J., Pierani, A., Jessell, T. M. & Ericson, J. A homeodomain protein code specifies progenitor cell identity and neuronal fate in the ventral neural tube. *Cell* **101**, 435-445 (2000).

17 Pattyn, A. *et al.* Ascl1/Mash1 is required for the development of central serotonergic neurons. *Nature neuroscience* **7**, 589-595, doi:10.1038/nn1247 (2004).

18 Sugimori, M. *et al.* Combinatorial actions of patterning and HLH transcription factors in the spatiotemporal control of neurogenesis and gliogenesis in the developing spinal cord. *Development* **134**, 1617-1629, doi:10.1242/dev.001255 (2007).

19 Jacob, J. *et al.* Insm1 (IA-1) is an essential component of the regulatory network that specifies monoaminergic neuronal phenotypes in the vertebrate hindbrain. *Development* **136**, 2477-2485, doi:10.1242/dev.034546 (2009).

20 Ribes, V. *et al.* Distinct Sonic Hedgehog signaling dynamics specify floor plate and ventral neuronal progenitors in the vertebrate neural tube. *Genes & development* **24**, 1186-1200, doi:10.1101/gad.559910 (2010).

21 Hernandez, R. E., Putzke, A. P., Myers, J. P., Margaretha, L. & Moens, C. B. Cyp26 enzymes generate the retinoic acid response pattern necessary for hindbrain development. *Development* **134**, 177-187, doi:10.1242/dev.02706 (2007).

22 Distel, M., Wullimann, M. F. & Koster, R. W. Optimized Gal4 genetics for permanent gene expression mapping in zebrafish. *Proc Natl Acad Sci U S A* **106**, 13365-13370, doi:10.1073/pnas.0903060106 (2009).

23 Stamataki, D., Ulloa, F., Tsoni, S. V., Mynett, A. & Briscoe, J. A gradient of Gli activity mediates graded Sonic Hedgehog signaling in the neural tube. *Genes & development* **19**, 626-641, doi:10.1101/gad.325905 (2005).

24 Muhr, J., Andersson, E., Persson, M., Jessell, T. M. & Ericson, J. Groucho-mediated transcriptional repression establishes progenitor cell pattern and neuronal fate in the ventral neural tube. *Cell* **104**, 861-873 (2001).

25 Novitch, B. G., Chen, A. I. & Jessell, T. M. Coordinate regulation of motor neuron subtype identity and pan-neuronal properties by the bHLH repressor Olig2. *Neuron* **31**, 773-789 (2001).

26 Zhou, Q., Choi, G. & Anderson, D. J. The bHLH transcription factor Olig2 promotes oligodendrocyte differentiation in collaboration with Nkx2.2. *Neuron* **31**, 791-807 (2001).

27 Damm, K., Heyman, R. A., Umesono, K. & Evans, R. M. Functional inhibition of retinoic acid response by dominant negative retinoic acid receptor mutants. *Proc Natl Acad Sci U S A* **90**, 2989-2993 (1993).

28 Castro, D. S., Arvidsson, M., Bondesson Bolin, M. & Perlmann, T. Activity of the Nurr1 carboxyl-terminal domain depends on cell type and integrity of the activation function 2. *The Journal of biological chemistry* **274**, 37483-37490 (1999).

29 Castro, D. S. *et al.* Proneural bHLH and Brn proteins coregulate a neurogenic program through cooperative binding to a conserved DNA motif. *Developmental cell* **11**, 831-844, doi:10.1016/j.devcel.2006.10.006 (2006).

30 Temple, G. *et al.* From genome to proteome: developing expression clone resources for the human genome. *Human molecular genetics* **15 Spec No 1**, R31-43, doi:10.1093/hmg/ddl048 (2006).

31 Das, R. M. *et al.* A robust system for RNA interference in the chicken using a modified microRNA operon. *Developmental biology* **294**, 554-563, doi:10.1016/j.ydbio.2006.02.020 (2006).

32 Teraoka, H. *et al.* Hedgehog and Fgf signaling pathways regulate the development of tphR-expressing serotonergic raphe neurons in zebrafish embryos. *J Neurobiol* **60**, 275-288, doi:10.1002/neu.20023 (2004).

33 Jasoni, C. L., Walker, M. B., Morris, M. D. & Reh, T. A. A chicken achaete-scute homolog (CASH-1) is expressed in a temporally and spatially discrete manner in the developing nervous system. *Development* **120**, 769-783 (1994).

34 Perez, S. E., Rebelo, S. & Anderson, D. J. Early specification of sensory neuron fate revealed by expression and function of neurogenins in the chick embryo. *Development* **126**, 1715-1728 (1999).

35 Rossant, J., Zirngibl, R., Cado, D., Shago, M. & Giguere, V. Expression of a retinoic acid response element-hsplacZ transgene defines specific domains of transcriptional activity during mouse embryogenesis. *Genes & development* **5**, 1333-1344 (1991).

36 Han, H. *et al.* Inducible gene knockout of transcription factor recombination signal binding protein-J reveals its essential role in T versus B lineage decision. *International immunology* **14**, 637-645 (2002).

37 Cau, E., Gradwohl, G., Casarosa, S., Kageyama, R. & Guillemot, F. Hes genes regulate sequential stages of neurogenesis in the olfactory epithelium. *Development* **127**, 2323-2332 (2000).

38 Dessaud, E. *et al.* Interpretation of the sonic hedgehog morphogen gradient by a temporal adaptation mechanism. *Nature* **450**, 717-720, doi:10.1038/nature06347 (2007).

39 Soriano, P. Generalized lacZ expression with the ROSA26 Cre reporter strain. *Nature genetics* **21**, 70-71, doi:10.1038/5007 (1999).

40 Lumsden, A. & Krumlauf, R. Patterning the vertebrate neuraxis. *Science* **274**, 1109-1115 (1996).

41 MacLean, G. *et al.* Cloning of a novel retinoic-acid metabolizing cytochrome P450, Cyp26B1, and comparative expression analysis with Cyp26A1 during early murine development. *Mechanisms of development* **107**, 195-201 (2001).

42 Wilson, L. J., Myat, A., Sharma, A., Maden, M. & Wingate, R. J. Retinoic acid is a potential dorsalising signal in the late embryonic chick hindbrain. *BMC developmental biology* **7**, 138, doi:10.1186/1471-213X-7-138 (2007).

43 Zhang, X., Beaulieu, J. M., Sotnikova, T. D., Gainetdinov, R. R. & Caron, M. G. Tryptophan hydroxylase-2 controls brain serotonin synthesis. *Science* **305**, 217, doi:10.1126/science.1097540 (2004).

44 Hendricks, T. J. *et al.* Pet-1 ETS gene plays a critical role in 5-HT neuron development and is required for normal anxiety-like and aggressive behavior. *Neuron* **37**, 233-247 (2003).

45 Kiyasova, V. *et al.* A genetically defined morphologically and functionally unique subset of 5-HT neurons in the mouse raphe nuclei. *J Neurosci* **31**, 2756-2768, doi:10.1523/JNEUROSCI.4080-10.2011 (2011).

46 Kopan, R. & Ilagan, M. X. The canonical Notch signaling pathway: unfolding the activation mechanism. *Cell* **137**, 216-233, doi:10.1016/j.cell.2009.03.045 (2009).

47 Hatakeyama, J. *et al.* Hes genes regulate size, shape and histogenesis of the nervous system by control of the timing of neural stem cell differentiation. *Development* **131**, 5539-5550 (2004).

48 Lewis, J. From signals to patterns: space, time, and mathematics in developmental biology. *Science* **322**, 399-403, doi:10.1126/science.1166154 (2008).

49 Chen, A. I., de Nooij, J. C. & Jessell, T. M. Graded activity of transcription factor Runx3 specifies the laminar termination pattern of sensory axons in the developing spinal cord. *Neuron* **49**, 395-408, doi:10.1016/j.neuron.2005.12.028 (2006).

50 Sansom, S. N. & Livesey, F. J. Gradients in the brain: the control of the development of form and function in the cerebral cortex. *Cold Spring Harbor perspectives in biology* **1**, a002519, doi:10.1101/cshperspect.a002519 (2009).

51 Hamasaki, T., Leingartner, A., Ringstedt, T. & O'Leary, D. D. EMX2 regulates sizes and positioning of the primary sensory and motor areas in neocortex by direct specification of cortical progenitors. *Neuron* **43**, 359-372, doi:10.1016/j.neuron.2004.07.016 (2004).

52 Dasen, J. S., De Camilli, A., Wang, B., Tucker, P. W. & Jessell, T. M. Hox repertoires for motor neuron diversity and connectivity gated by a single accessory factor, FoxP1. *Cell* **134**, 304-316, doi:10.1016/j.cell.2008.06.019 (2008).

53 Rousso, D. L., Gaber, Z. B., Wellik, D., Morrisey, E. E. & Novitch, B. G. Coordinated actions of the forkhead protein Foxp1 and Hox proteins in the columnar organization of spinal motor neurons. *Neuron* **59**, 226-240, doi:10.1016/j.neuron.2008.06.025 (2008).

54 Waage-Baudet, H. *et al.* Abnormal serotonergic development in a mouse model for the Smith-Lemli-Opitz syndrome: implications for autism. *International journal of developmental neuroscience : the official journal of the International Society for Developmental Neuroscience* **21**, 451-459 (2003).

55 Bravo-Ambrosio, A. & Kaprielian, Z. Crossing the border: molecular control of motor axon exit. *International journal of molecular sciences* **12**, 8539-8561, doi:10.3390/ijms12128539 (2011).

CHAPTER 5 – Gli protein activity is controlled by multisite phosphorylation in vertebrate Hedgehog signaling

ABSTRACT

Gli proteins are transcriptional effectors of the Hedgehog (Hh) pathway in both normal development and cancer. We describe a program of multisite phosphorylation that regulates the conversion of Gli proteins into transcriptional activators. In the absence of Hh ligands, Gli activity is restrained by the direct phosphorylation of six conserved serine residues by protein kinase A (PKA), a master negative regulator of the Hh pathway. Activation of signaling leads to a global remodeling of the Gli phosphorylation landscape: the PKA target sites become dephosphorylated, while a second cluster of sites undergo phosphorylation. The pattern of Gli phosphorylation can regulate Gli transcriptional activity in a graded fashion, suggesting a phosphorylation based-mechanism for how a gradient of Hh signaling in a morphogenetic field can be converted into a gradient of transcriptional activity.

This chapter is modified from:

Niewiadomski P, Kong JH, Ahrends R, Ma Y, Humke EW, Khan S, Teruel MN, Novitch BG, and Rohatgi R. (2014). Gli protein activity is controlled by multisite phosphorylation in vertebrate Hedgehog signaling. *Cell Reports* 6(1): 168-181. Doi:10.1016/j.cellrep.2013.12.003.

PN performed a majority of the experiments and wrote the manuscript. JHK performed and analyzed all the chick electroporations. PN, JHK, RA, YM, EWH, SK, MNT, BGN, and RR edited the manuscript, designed experiments, and provided vital reagents.

INTRODUCTION

The Hedgehog (Hh) pathway is an evolutionarily conserved signaling system that plays a central role in embryogenesis and adult tissue homeostasis. Its misregulation leads to developmental defects and to cancers of the skin and the brain[1,2]. The Gli (Glioblastoma) transcription factors in vertebrates control the Hh gene expression program[3]. Despite the importance of Gli proteins in development, regeneration, and cancer, the mechanism by which they acquire the ability to activate target genes has remained enigmatic.

Among the three mammalian Gli proteins, Gli2 and Gli3 are the first responders to the Hh signal. Once activated, Gli2/3 then induce the expression of Gli1, which acts as an amplifier of the response. Gli2/3 can perform two opposing functions at target promoters[3]. When the pathway is off, Gli2/3 proteins are converted into truncated repressor forms (hereafter abbreviated GliR), which inhibit target gene transcription. When the Hh ligand is received, GliR production is blocked, and Gli2/3 proteins are converted into transcriptional activators (hereafter abbreviated GliA). In the nucleus, the balance between GliR and GliA shapes the Hh response. Between these two extremes, a substantial fraction of Gli2/3 remains in the cytoplasm in a transcriptionally inactive state[4] (**Figure 1A**). Quantitative changes in the GliR/GliA ratio can lead to developmental defects in humans, underscoring the point that the precise level of Gli activity is often critical for the sophisticated patterning events regulated by Hh signaling during development[5-7].

GliR and GliA production are both controlled by the 7-transmembrane protein Smoothened (Smo; **Figure 1A**). Upon Hh ligand reception by Patched (Ptc), Smo accumulates in a microtubule-based protrusion of the cell membrane known as the primary cilium[8]. Through an unknown mechanism, ciliary Smo inhibits GliR formation and induces the transport of Gli proteins to the tips of cilia[9,10], where they dissociate from the negative regulator Suppressor of Fused (Sufu)[4,11]. Thereupon, Glis translocate into the nucleus and activate target genes. Nuclear Gli proteins are characterized by a short half-life and reduced mobility on SDS-PAGE gels caused by a distinct phosphorylation event, hereafter referred to as “hyperphosphorylation”[4].

The mechanistic details of the interaction between Smo and Gli proteins are not understood. Several lines of evidence point to protein kinase A (PKA) as a key regulator of the Hh signal downstream of Smo[12-21]. Pharmacological activation of PKA completely blocks Hh signaling, even in presence of the Hh ligand or a Smo agonist. Conversely, genetic ablation of PKA shifts the GliR/GliA balance strongly in favor of GliA. This leads to full ligand-independent activation of Hh target genes, manifesting itself as complete ventralization of the embryonic neural tube in mutant animals[13]. This data clearly identifies PKA as a negative regulator of Gli function, but on a molecular level, our understanding of how Gli proteins are affected by PKA remains incomplete.

The mechanism by which PKA promotes GliR has been elucidated in detail, guided by studies of the *Drosophila* Gli homolog *cubitus interruptus* (Ci)[22-25]. PKA can phosphorylate Gli2/3 at six conserved serine residues (P1-6) located on the carboxyterminal side of the DNA binding Zn-finger domain[6] (**Figure 5-1B**). The phosphorylation of the first four of these residues (P1-4) by PKA initiates a pathway that leads to the partial processing of full-length Glis into GliR fragments by the proteasome[22,26]; the function of the last two phosphorylation sites (P5,6) is unknown.

PKA plays an equally important but much less well-understood role in suppressing Gli2/3A. Loss of phosphorylation at sites P1-4, which regulates GliR production, does not seem to be sufficient for this activation step. Transgenic mice harboring nonphosphorylatable serine-to-alanine mutations in P1-4 of Gli2 do not show the developmental phenotypes expected if Gli2 was fully activated[26]. Importantly, the neural tube of these animals, in contrast to animals lacking PKA activity, is not strongly ventralized. Thus, PKA must inhibit Gli2 activation by phosphorylating sites other than P1-4.

Here, we elucidate the mechanism by which PKA inhibits the production of GliA. PKA uses distinct phosphorylation patterns to regulate GliR and GliA; phosphorylation of P1-4 is sufficient for GliR production, while the inhibition of GliA formation is dependent on all six sites from the P1-6 cluster. Smo activation reduces phosphorylation of P1-6, showing that Hh signaling wields direct control over phosphorylation at these sites. We also find that P1-6

*de*phosphorylation allows the phosphorylation of Gli2 at a distinct cluster of sites, which plays a positive role in Hh signaling. We propose that remodeling of the phosphorylation landscape of Gli2/3 proteins controls the transcriptional output of Hh signaling and discuss the implications of this model for the role of Hh as a morphogen in development.

MATERIALS AND METHODS

Molecular cloning and site-directed mutagenesis:

For the purpose of *in vitro* phosphorylation, short fragments of Gli2 and Gli3 were generated from full length mouse Gli2 and Gli3 clones by PCR. These fragments were then inserted into a custom pCS2 plasmid containing FseI and AscI sites downstream of the Kozak sequence followed by a sequence for the 6 Myc tags in tandem. Respective mutant constructs lacking the putative PKA target serine/threonine residues were generated by site-directed mutagenesis (see below). The amino acid boundaries for mouse Gli2/Gli3 fragments were as follows: Gli3: Pa – 145-216, Pb – 207-237, Pc-g – 259-323, Ph – 312-346, Pi,j – 379-480, P1-4 – 837-922, Pk – 915-978, P5,6 – 965-1018, Pl – 1007-1042, Pm-o – 1510-1577, Gli2 Pc-g – 201-258.

For the generation of stable cell lines and for Gli2/3 activity assays, full length Gli2 and Gli3 sequences were amplified by PCR and cloned into the pENTR2B vector (Life Technologies). Subsequently, a triple HA tag was inserted in-frame on the N-terminus of both constructs, and a FLAG tag was added to the C-terminus of the mGli3 construct. These constructs were used for PCR/DpnI-based site-directed mutagenesis (the QuikChange method). Alternatively, large fragments containing multiple mutations were created by gene synthesis (Integrated DNA Technologies) and inserted into the WT plasmid by restriction enzyme-based cloning. The WT and mutant variants of Gli protein genes were shuttled into the pEF5/FRT/V5-DEST using Gateway cloning (Life Technologies).

For *in ovo* electroporation assays, full length Gli2 constructs were subcloned using PCR from the pENTR2B-based plasmids described above into the pCIG vector[27], which

contains the IRES-GFP cassette. From these plasmids, each Gli2 sequence including the IRES-GFP cassette was cloned into the pECE vector[28].

Cell culture: 293T cells, NIH/3T3 cells, and NIH/3T3 Flp-In cells (Life Technologies), including stable clones generated based on the Flp-In cell line, $SuFu^{-/-}$ fibroblasts, and Med1 cells were cultured in media composed of DMEM (high glucose), 10% fetal bovine serum (FBS; Thermo Fisher Scientific), 1x GlutaMAX, 1x non-essential amino acids, 1x sodium pyruvate, 1x penicillin/streptomycin (all from Life Technologies). Prior to harvesting, the cells were serum-starved in the same media but containing 0.5% FBS for 24-36 hours, and treated with the indicated drugs/compounds. 24 hours starvation was only used in assays where treatment time was 18-24 hours long. For shorter treatment times (2-6 hours) a 36-hours starvation was preferred to induce a rapid response. For qPCR experiments using bortezomib, cells were serum starved for 16 hours.

Transfection: The FuGene 6 reagent (Roche) was used for transient and stable transfections of plasmids into the NIH/3T3-derived lines according to the manufacturer's instructions. Lipofectamine RNAiMAX (Life Technologies) was used for RNAi transfections. The calcium phosphate method was used for transfection of 293T cells.

In-vitro phosphorylation: Myc-tagged Gli2/3 fragments were cloned into pCS2 and overexpressed in HEK 293T cells. They were immunoprecipitated overnight from RIPA buffer lysates using Dynabeads Protein G (Life Technologies) coupled to the goat anti-Myc antibody (Bethyl). *In vitro* phosphorylation was carried out in the PKA reaction buffer (50 mM Tris pH 7.5, 10 mM $MgCl_2$, 0.1% NP-40, 1 mM DTT) in the presence of 0.5 mM ATP, 10 µCi of (γ-^{32}P) ATP, and 21 units of PKA (NEB) for 30 min at 30°C and stopped by washing the beads in ice-cold 50 mM Tris pH 7.5, 0.1% NP-40. Protein was eluted off beads using 2x SDS sample buffer and resolved on a 12% SDS-PAGE gel. The protein was transferred onto nitrocellulose and the membranes were air-dried. Radioactivity recorded on Storage Phosphor Screens was quantified using a Typhoon Imager (GE). The membranes were then re-wetted and the Myc tag was detected by western blot.

Sequence analysis: Multiple sequence alignment was carried out using Geneious Pro using the Geneious global alignment protocol with the Blosum62 cost matrix, free end gaps, gap open pentalty of 12, and gap extension penalty of 3.

Hedgehog reporter luciferase assay: NIH/3T3 Flp-In cells were seeded into 24-well plates at a density of 10^5 cells/well and co-transfected 1-2 hours later with the indicated amounts of the mGli2/mGli3 construct and two luciferase plasmids: pRL-TK containing the renilla luciferase under the constitutive thymidine kinase promoter, and a plasmid containing firefly luciferase driven by octameric Gli binding sites[29]. After reaching confluence the cells were serum-starved and treated for 18-24 hours with vehicle or 100 nM SAG. The cells were harvested and the luciferase assay was performed using the Dual Luciferase Reporter Assay System (Promega) according to the manufacturer's instructions on a BioTek H1 plate reader. All luminescence values were background-corrected using readouts from untransfected cell lysates. For each sample, to control for transfection efficiency, the firefly luciferase luminescence value (Hh-dependent) was divided by the renilla luciferase luminescence value (Hh-independent) to obtain relative luminescence units (RLU). These were then normalized to RLU values obtained from samples that were only transfected with the two luciferase plasmids and not treated with any drugs, yielding fold increase over control. In this assay, the over-expressed Gli proteins are not responsive to Hh ligands, and so their intrinsic transcriptional potential can be gauged. Each experiment was repeated at least three times with similar results.

Generation of stable cell lines: Stable cell lines expressing low levels of HA-tagged Gli2 and Gli3 variants were generated using the Flp-In method. Briefly, cells were co-transfected with pOG44 and the pEF5/FRT/V5-DEST vector containing the Gli2/3 construct of interest. After 2 days the cells were reseeded at low density and the culture media was supplemented with hygromycin for stable integrant selection. After approximately 7 days, clones of surviving cells became apparent and these were pooled and replated. Stable cell lines were reselected with hygromycin on every other passage to preserve selection pressure and prevent silencing of the transgene.

SDS-PAGE and western blotting: Cells were harvested in PBS and lysed in a RIPA buffer containing protease and phosphatase inhibitors. Protein concentration was measured using BCA and equal amounts of protein for each sample was mixed with 2x sample buffer and run on 8-12% polyacrylamide gels. The protein was transferred to nitrocellulose and the membranes were blotted with the appropriate primary antibodies followed by secondary antibodies conjugated to infrared dyes (IRDye™). Sixteen-bit images generated from these blots were used for quantification of all protein bands (ImageJ). This pipeline allowed accurate quantification of protein levels on immunoblots across a much wider dynamic range compared to the use of HRP-conjugated secondary antibodies and conventional film. The primary antibodies used for western blotting were as follows: mouse anti-Gli1 (L42B10, Cell Signaling), guinea pig anti-Gli2 (antigen made in-house[30], sera generated by Cocalico Biologicals, affinity-purified in-house), mouse anti-HA (clone 16B12, Covance), mouse anti-α-tubulin (Sigma), rabbit anti-lamin A (Abcam), goat anti-Myc (Bethyl Labs), rabbit anti-Sufu (made in-house[4]), anti-pan-14-3-3 (clone K19, Santa Cruz).

Quantitative real-time RT-PCR (qPCR): RNA was harvested from cells using the TRIzol reagent (Life Technologies) according to manufacturer's instructions. cDNA was generated using the iScript Supermix (Bio-Rad). qPCR reactions were run using the iTaq SYBR green Supermix (Bio-Rad) on the Applied Biosystems 7900HT Fast real-time PCR system. Data were analyzed using the standard curve method. The following primers were used: *GAPDH*, forward 5'-GGCCTTCCGTGTTCCTAC-3' and reverse 5'-TGTCATCATACTTGGCAGGTT-3'; *Gli1*, forward 5'-CCAAGCCAACTTTATGTCAGGG-3' and reverse 5'-AGCCCGCTTCTTTGTTAATTTGA-3'; *HA-Gli2*, forward 5'-CGCGGTACCAAGCGGAGGAA-3' and reverse 5'-TGGGTCGGGGAAGCTGCTGT-3'; *HPRT,* forward 5'-GCTGACCTGCTGGATTACAT-3' and reverse 5'-TTGGGGCTGTACTGCTTAAC-3'.

Subcellular fractionation: The method for subcellular fractionation was performed as previously described[4].

In ovo electroporation and immunohistochemistry/in situ hybridization of chick tissue:

Hamburger-Hamilton (HH) stage 10-14 chick embryos were electroporated as previously described[31] and incubated for ~48 hours to HH stages 20-22. Spinal cords were collected, fixed for 1 hour in 4% PFA at 4°C, cryoprotected in 30% sucrose overnight, mounted in OCT, cut into 12 µm thick sections, and collected directly onto slides. To observe the progenitor domains that make up the developing spinal cord the following antibodies were used: rabbit anti-Olig2 (Millipore); sheep anti-GFP (Biogenesis); rabbit anti-GFP (Invitrogen); mouse anti-HNF3β, mouse anti-Nkx2.2, mouse anti-Nkx6.1, mouse anti-Pax6, and mouse anti-Pax7 (Developmental Studies Hybridoma Bank); rabbit anti-HNF3β[32]. In addition, Alexa488-, FITC-, Cy3- and Cy5-conjugated secondary antibodies were obtained from Jackson ImmunoResearch. Fluorescence images were collected using a Zeiss LSM5 Exciter confocal imaging system and processed using ImageJ. The constructs used for electroporation alone were: pECE-Gli2-IRES-GFP, pECE-Gli2P1-4A-IRES-GFP, pECE-Gli2P1-6A-IRES-GFP. For co-electroporation with mPtc$^{\Delta loop2}$-IRES-GFP[33], the pECE plasmids were replaced with the respective pCIG plasmids. Gli2-IRES-GFP and mPtc$^{\Delta loop2}$-IRES-GFP constructs were electroporated at a final ratio of 1:4 (0.125 µg/µl Gli2 + 0.5 µg/µl mPtc$^{\Delta loop2}$).

For in situ hybridization, digoxigenin (DIG)-labeled Ptch1 antisense probes were prepared by in vitro transcription using a chick Ptch1 construct[34]. Slides were fixed in PFA, digested in Proteinase K, postfixed in PFA, acetylated, and hybridized with DIG-labeled probes overnight at 72°C. After hybridization the slides were washed, blocked, and stained with alkaline phosphatase-conjugated anti-DIG antibodies (Roche) overnight at 4°C. The signal was developed using NBT/BCIP (Roche), and the slides were dried and mounted with coverslips.

Immunoprecipitation/western blot: For HA tag immunoprecipitation the anti-HA agarose (high affinity; Roche) was used. Elution was carried out in 1x SDS sample buffer at 37°C for 30 min and the eluate was loaded directly on gel.

Data normalization: In Hh reporter assay using transient expression of Gli variants, all values for the Gliinduced firefly luciferase activity were normalized to the activity of a co-

transfected renilla luciferase enzyme expressed under a constitutive thymidine kinase promoter to account for well-to-well variability in transfection efficiencies.

For immunoblot experiments, band intensities derived from densitometry were normalized to intensities of a loading control band (tubulin or lamin) from the same lane. In addition, where appropriate, levels of Gli1 protein or mRNA, which was taken as a metric for the transcriptional activity of HA-Gli2 variants, was normalized to the band intensity of the corresponding HA-Gli2 variant to calculate the specific activity (Gli1 activation per unit of HAGli2). This normalization method accounts for differences in HA-Gli2 protein expression between the different cell lines, allowing a comparison of the intrinsic transcriptional activity of each HA-Gli2 variant.

In real-time qRT-PCR experiments, all gene expression values were corrected for variability in mRNA loading and PCR efficiency using the standard curve method with GAPDH acting as the housekeeping gene. To calculate the specific activity of each mutant HA-Gli2 protein, *Gli1* mRNA values (**Figures 5-3D and 5-3E**) obtained from the standard curve method were normalized to the corresponding HA-Gli2 protein levels from separate immunoblot experiments (**Figure 5-3C**).

Mass spectrometric results of phosphopeptide abundance were normalized both to the peak intensity of the corresponding heavy isotope-labeled standard peptide spiked into the tryptic digest at a constant concentration and to the mean of relative intensities of two non- hosphorylatable “loading control” Gli2 tryptic peptides present in the same sample. This second operation ensured that sample-to-sample variability in protein harvesting, tryptic digest, and extraction of peptides from the gel did not affect the quantification of phosphopeptide abundance.

RESULTS

PKA phosphorylates Gli2/3 at multiple sites in vitro

Previous work has implicated PKA both in GliR formation and in GliA inhibition[6,12,13,22,26], but the biochemical mechanism by which PKA blocks GliA formation was

unknown. We hypothesized that PKA suppresses the formation of GliA by direct phosphorylation of Gli2/3. In order to identify putative inhibitory PKA target sites on Gli2/3, we looked for full consensus sites (R or K present at positions -2 and -3 from the S or T) and partial consensus sites (R or K only present at either position -2 or position -3 from the S or T) that were conserved among human and mouse Gli2 and Gli3 and were located outside the DNA-binding zinc finger domain (**Figure 5-S1A**). In addition to the full consensus sites (P1-6) described previously[22,25,26], we identified 15 partial consensus sites (hereafter called Pa-o; **Figures 5-1B and 5-S1B**). Myc-tagged fragments of Gli3 containing various subsets of these sites were tested as PKA substrates using an in vitro kinase assay. Four fragments containing sites P1-4, P5,6, Pc-g, and Pm-o could be phosphorylated by PKA (**Figures 5-1C and 5-1D**). Interestingly, both the P1-6 and the Pc-g clusters are located in regions of Gli2/3 that are strongly conserved between the *Drosophila*, *Xenopus*, and mouse proteins (**Figure 5-1E**).

PKA target sites P1-6 regulate Gli3 repressor and activator functions

We first analyzed the six sites in P1-6 cluster, which had previously been identified as PKA targets[6,35] (**Figure 5-2A**). We decided to study P1-6 in the context of both Gli3 and Gli2, since Gli3 is the major repressor (Gli3R) and Gli2 the major activator (Gli2A) in most tissues. To understand the role of specific sites within the P1-6 cluster in regulating the GliR/GliA balance, we made nonphosphorylatable alanine mutants of P1-4 (P1-4A), P5 and P6 (P5,6A), or of the entire P1-6 cluster (P1-6A) in Gli2 and Gli3. Since Gli proteins fail to be regulated by Hh signaling when over-produced in cells[4], we sought to evaluate these Gli mutants under endogenous expression levels. To that end, we stably expressed hemagglutinin (HA)-tagged Gli2/3 (HA-Gli2/3) mutants in NIH/3T3 fibroblasts using the Flp-In system, in which an expression construct is introduced as a single-copy insertion into a defined locus in the genome by Flp-mediated recombination[36,37]. The Flp-In system allowed us to rapidly generate stable cell lines expressing Gli protein variants at near-endogenous (**Figure 5-S2A**) and roughly equal (**Figure 5-2B**) levels.

Starting with Gli3, we verified that a wild-type (WT) HA-Gli3 behaved like its endogenous counterpart. Indeed, HA-Gli3(WT) could be processed into a HA-GliR fragment when expressed using the Flp-In system (**Figure 5-2B**). Consistent with previous reports[26,38-40], mutation of sites P1-4 into alanine was sufficient to block Gli3R formation, as neither Gli3(P1-4A) nor Gli3(P1-6A) was converted into Gli3R. In contrast, Gli3(P5,6A) readily formed Gli3R in unstimulated cells (**Figure 5-2B**). Prior reports have implicated all six sites in the P1–6 cluster in GliR formation[6], but these studies were based on transient Gli3 overexpression and required stimulation with high doses of forskolin (a compound commonly used to activate PKA) for prolonged periods of time to produce Gli3R. Using experimental conditions that faithfully reflect endogenous Gli3 processing in untreated cells, we find that sites P5 and P6 are not involved in the PKA-dependent truncation of Gli3 into a repressor fragment.

The formation of Hh-induced Gli3A can be experimentally followed by two biochemical events: activated Gli3 translocates into the nucleus and undergoes hyperphosphorylation, which appears as a shift in the apparent molecular weight of Gli proteins on SDS-PAGE gels[4]. As we have previously described for endogenous Gli3, treatment of cells with the Smo agonist SAG led to the redistribution of HA-Gli3(WT) into the nuclear fraction; nuclear HA-Gli3 also showed the characteristic reduction in electrophoretic mobility indicative of hyperphosphorylation (**Figure 5-2C, top panel, and Figure 5-S2B**). In contrast, when all six of the P1-6 sites were simultaneously mutated to alanines, Gli3 accumulated to high levels in the nucleus even in the absence of Hh signaling (**Figure 5-2C, middle panel, and Figure 5-S2B**). Saturating concentrations of SAG did not further increase the nuclear accumulation of HA-Gli3(P1-6A), showing that the mutation of these six residues makes Gli3 unresponsive to upstream Hh signals. Alanine mutations only in sites P5 and P6 increased levels of Gli3 in the nucleus seen in the absence of signaling, but did not result in maximal nuclear accumulation; HA-Gli3(P5,6A) still moved to the nucleus in response to SAG (**Figure 52C, bottom panel, and Figure 5-S2B**).

To measure transcriptional activity of the Gli3 mutants, we transiently transfected constructs encoding each protein and measured the activation of an Hh-dependent firefly luciferase reporter gene[29]. Consistent with prior characterization of Gli3 as a weak transcriptional activator[29], both HA-Gli3(WT) and HA-Gli3(P1–4A) failed to substantially increase Hh-dependent luciferase expression. On the other hand, HA-Gli3(P1–6A) could activate the reporter gene (**Figure 5-2D**), confirming the role of P5 and P6 in limiting the ability of Gli3 to activate transcription. Neither HA-Gli3(P1–4A) nor HA-Gli3(P1–6A) could be processed to Gli3R (**Figure 5-2B**), and so differences in their ability to activate transcription cannot be attributed to differences in Gli3R levels. All six sites in the P1–6 cluster play a role in tuning Gli3 activity, since HA-Gli3(P5,6A) also demonstrated low levels of transcriptional activity, analogous to that of HA-Gli3(P1-4A) (**Figure 5-S2C**).

These results suggest that Gli3 may be regulated by graded dephosphorylation. Loss of P1-4 phosphorylation blocks Gli3R repressor formation but is insufficient for the full activation of Gli3. The additional loss of P5,6 phosphorylation is required to achieve complete transformation of Gli3 into Gli3A.

Sites P1-6 determine the transcriptional activity of Gli2

Since Gli2 is the major transcriptional activator of Hh target genes in most tissues, we made a similar series of mutations in the P1-6 sites of Gli2. While WT HA-Gli2 can activate the Hh reporter in transient overexpression assays (**Figure 5-3A**)[29], the Gli2(P1-6A) mutant was significantly more active at all doses tested. The P1-4A and P5,6A mutants of Gli2 showed an intermediate capacity to activate the reporter. Mutation of either P5 or P6 individually in combination with P1-4 also increased activity of Gli2, suggesting that P5 and P6 may be partially redundant (**Figure 5-S2D**). Conversely, mutation of both sites P5 and P6 to aspartate (P5,6D), a phospho-mimetic mutation, substantially reduced the activating potential of Gli2 (**Figure 5-S2D**). These results are consistent with an inhibitory role of P1-6 phosphorylation in the activation of Gli2.

To examine Gli2 regulation under physiological expression levels, we turned to Flp-In stable lines carrying HA-tagged Gli2 mutants (**Figure 5-S2A**). Similar to its effect on Gli3, the P1-6A mutation in HA-Gli2 caused constitutive Hh-independent accumulation in the nucleus, consistent with Gli2(P1-6A) being a fully active molecule (**Figure 5-3B**). In order to correlate nuclear accumulation with transcriptional activity, we measured the expression of endogenous *Gli1*, a Hh target gene commonly used as a metric for pathway activity, in these same stable cell lines. In the absence of Hh signaling, Gli1 levels were not elevated in the line expressing HA-Gli2(WT), confirming that this exogenous protein is properly regulated (**Figure 5-S2E**). To account for differences in expression levels of the HA-Gli2 variants (**Figure 5-3C**), we compared their specific activities, calculated as the level of Gli1 induction divided by the protein level of the corresponding HA-Gli2 variant. The specific activities of the mutants fell along a clear gradient: the HA-Gli2(P1-4A) and HA-Gli2(P5,6A) mutants demonstrated ~3-to 4-fold higher specific activity and the HA-Gli2(P1-6A) mutant displayed ~13-fold higher specific activity compared to HA-Gli2(WT) (**Figure 5-3C**). The high level of Gli1 in cells carrying Gli2(P1-6A) was resistant to inhibition by two Smo antagonists, cyclopamine and SANT-1 (**Figures 5-3D and 5-S2F**), demonstrating that the activity of this mutant protein was independent of Smo. Importantly, all the stable cell lines (which also contain endogenous Gli2) were able to produce equivalent levels of Gli1 when stimulated with SAG, showing that they did not differ in their intrinsic capacity to activate Hh targets (**Figure 5-3C**). Since the Flp-In lines also expressed endogenous Gli2, the *GLI1* induction in response to SAG (**Figure 5-3C**) could not be used to infer the Hh-responsiveness of the HA-Gli2 variants expressed in these lines.

To analyze the ability of upstream Hh signaling to regulate the HA-Gli2 mutants in our Flp-In cell lines, we selectively depleted endogenous Gli2 with a small interfering RNA (siRNA) directed against its 3'UTR (**Figures 5-3E and 5-S2G**). Under these conditions, the SAG initiated signal should be largely transduced through our HA-tagged Gli2 variants. In the absence of endogenous Gli2, SAG could significantly increase *Gli1* expression in either HA-Gli2(WT) or HA-Gli2(P1-4A) cells. In the same cell lines, PKA activation, accomplished

with the drugs isobutylmethylxanthine (IBMX) and forskolin (FSK) antagonized the effect of SAG (**Figure 5-3E**). In contrast, the high baseline expression of Gli1 in the HA-Gli2(P1-6A) line was largely insensitive to regulation by either SAG or IBMX/FSK (**Figures 5-3E and 5-S2G**). This is further evidence that Gli2(P1-6A) corresponds to a maximally active form of Gli2, which cannot be regulated by either Smo or PKA. Gli2(P1-4A) remains SAG and PKA sensitive most likely through phosphoregulation at the P5 and P6 sites. We conclude that only after losing all phosphates at sites P1-6 does Gli2 become a bona fide GliA. These data explain why the previously studied Gli2(P1-4A) mutant of Gli2 failed to fully activate Hh responses during development[26].

P1-6 mutants of Gli2 ectopically specify ventral cell types in the developing spinal cord

Encouraged by these results, we tested the ability of Gli2(P1-6A) to drive Hh-regulated cell fate decisions in vivo in a cell-autonomous manner. In the ventral neural tube, Shh acts as a graded signal that specifies the dorsal-ventral pattern of progenitor subtypes (**Figure 5-4A**). This precise spatial patterning is established by a gradient of Gli activity[41-43], making the neural tube an ideal place to test the activities of our Gli2(P1-4A) and Gli2(P1-6A) mutants. Using in ovo electroporation techniques, we expressed the Gli2 mutants under the control of a weak SV40 early promoter in one-half of the neural tube of Hamburger-Hamilton (HH) stage 10-12 chicken embryos and examined the expression of various progenitor markers 48 hours later. Ectopic expression of Gli2(WT) did not alter the spatial arrangement of progenitors (**Figures 5-4B-D, top row, and 5-S3C**) and also did not induce expression of *PTCH1*, a direct Hh target gene (**Figure 5-4E, top row**).

In contrast, overexpression of Gli2(P1–6A) at any position along the dorsoventral axis led to the ectopic specification of ventral cells, identified by the ventral-most progenitor domain (pFP/p3) marker FOXA2 and the p3 marker NKX2.2, both of which depend on the highest levels of Hh/Gli signaling (**Figures 5-4B, bottom row, and 5-S3C**). Gli2(P1–6A) could also induce NKX6.1, which labels the pFP, p3, pMN, and p2 progenitor domains.

OLIG2, a marker of motor neuron progenitors (pMN), which are specified by intermediate levels of Hh signaling, was induced mostly in cells expressing lower levels of Gli2(P1–6A) but often suppressed in strongly Gli2(P1–6A)-positive cells, most likely reflecting the cross-repressive interaction between NKX2.2 and OLIG2 in the neural tube[31]. Moreover, Gli2(P1–6A) suppressed the expression PAX6, a dorsal marker known to be negatively regulated by Hh signaling. Consistent with this ability to specify cell fates that depend on high levels of Hh ligand, Gli2(P1–6A) induced the robust expression of *PTCH1*, a direct Hh target gene, throughout the neural tube. The ability Gli2(P1–6A) to induce the ventral and suppress the dorsal markers was resistant to coexpression of a constitutively active mutant of Patched, $Ptch^{\Delta loop2}$ [33], confirming that the P1–6A mutant of Gli2 escapes regulation by the upstream elements of the Hh pathway (**Figure 5-S3A**).

Gli2(P1-4A) demonstrated intermediate activity: it induced FOXA2, NKX2.2, and NKX6.1 when expressed immediately adjacent to their normal domains but not when expressed in more dorsal regions of the neural tube (**Figures 5-4B-D, middle row, and 5-S3C**). This expansion of the ventral domains suggests that Gli2(P1-4A) sensitized cells to Shh, such that the same level of Shh exposure is translated to more ventral cell fates. Even though our Gli2 variants induced ectopic FOXA2, they did not drive SHH expression (**Figure 5-S3B**), suggesting that the effects we describe in Figure 5-4 were not due to non-cell-autonomous effects of ectopic floor plate induction in the electroporated spinal cords. These data are consistent with previous reports showing that activated Smo and Gli proteins expressed in the HH12 stage neural tube can promote ventral character while at the same time inhibiting the formation of floor-plate cells[43,44]. Neither Gli2 mutant affected the expression of Hh-independent progenitor markers SOX2 and NGN2, suggesting that the total number of neuronal progenitors is unchanged by the expression of these constructs (**Figure 5-S3B**).

Taken together, these data suggest that there is a fundamental difference between blocking phosphorylation at sites P1-4 only and blocking it throughout the P1-6 cluster. Because both the P1-4A and P1-6A mutations block repressor formation (**Figure 5-2B**) the

marked differences in the activities of Gli2(P1-4) and Gli2(P1-6), both in cultured cells and in the developing neural tube, must be attributed to the role of P5 and P6 in the formation of Gli2A. Dephosphorylation of these sites in response to Hh ligands appears to be necessary to unleash the full activation potential of Gli2. P6 phosphorylation has been previously implicated in the interaction of Glis with 14-3-3 proteins[45], but in our system, this interaction did not appear to be required for the inhibitory function of P6 in GliA formation (**Figures 5-S6B-C**).

Hh signaling reduces phosphorylation of P1-6

Our mutagenesis studies suggested that loss of phosphorylation on the serine residues at P1-6 is a regulatory step in the activation of Gli proteins. Hence, we sought to monitor changes in the phosphorylation status of these sites on endogenous Gli2 in response to signaling. We were unable to raise phospho-specific antibodies that recognized multiple sites on endogenous Gli2 in a quantitative fashion. Instead, we developed a mass spectrometry (MS)-based selected reaction monitoring (SRM) assay to quantitatively assess phosphate occupancy at P1, P2, P5, and P6[46-48]. Endogenous Gli2, isolated by immunoaffinity purification, was digested with trypsin, and the phosphorylated versions of the tryptic peptides encompassing sites P1, P2, P5 and P6 were quantified by triple-quadrupole MS (**Figure 5-5A**). To compare phospho-peptide abundances between different samples, such as those cultured with or without SAG, tryptic digests were supplemented with internal standards, synthetic phosphorylated peptides identical in sequence to the P1, P2, P5 and P6 tryptic peptides but labeled with heavy isotopes to distinguish them in the mass spectrometer from their endogenous counterparts (**Figures 5-5A and 5-5B**). The ratio of the peak area under the curve (AUC) of the endogenous peptide to the internal standard was then compared across conditions. In addition, a control, non-phosphorylatable tryptic peptide in Gli2 was also monitored to ensure equal input of total Gli2 across various conditions (**Figure 5-5A**).

Activation of Hh signaling by SAG reduced the abundance of phosphorylated peptides containing sites P1, P2, P5 and P6 (**Figures 5-5B and 5-5C**), with changes at P5 and P6 being more marked than those in sites P1 and P2. The phosphorylation of sites P5 and P6 was sensitive to both the concentration of SAG and the duration of SAG treatment (**Figures 5-5E and 5-5F**). In both cases, reduction in phosphorylation correlated with the amount of Gli in the nucleus. The changes in Gli2 phosphorylation were not due to differences in protein stability; since all measurements were conducted on cells pretreated with the proteasome inhibitor bortezomib and results obtained in the absence and presence of this drug were similar (**Figures 5-5C and 5-S4A**). In addition, no changes were observed after SAG addition in the abundance of a control, nonphosphorylatable peptide from a different region of Gli2 (**Figure 5-5A**). A caveat with measuring dephosphorylation by quantitative MS is that the observed reduction in the abundance of a phosphopeptide might reflect a change in phosphate occupancy of nearby sites rather than actual dephosphorylation of the site of interest. To address this concern, we also monitored the nonphosphorylated peptide encompassing site P6 (dephospho-P6) by SRM and observed that its abundance rose with SAG treatment and declined with IBMX and FSK (reciprocal to the pattern seen with phospho-P6; **Figure 5-S4B**), suggesting that the changes in phospho-P6 were due to bona fide dephosphorylation of the P6 site.

Stimulation of PKA activity with IBMX and FSK strongly increased phosphate occupancy at all sites within the P1-6 cluster and also prevented SAG from decreasing phosphorylation (**Figure 5-5D**). This result is consistent with the model that PKA negatively regulates Hh signaling by phosphorylating P1-6. It also suggests that even in resting cells, Gli proteins are not all fully phosphorylated at the P1-6 sites. The reason why these partially dephosphorylated Glis do not become transcriptionally active is unknown but may be related to the precise dynamics of the phosphate turnover on individual sites within the cluster. For instance, there may be some redundancy between individual sites in the P1-4 and P5,6 clusters.

A cluster of serine/threonine sites is important for Gli2/3 activation

Since phosphorylation of the P1-6 cluster seemed sufficient for the inhibition of GliA formation, we were curious to determine how the two remaining clusters of putative PKA target sites (Pc-g, Pm-o; **Figures 5-1B and 5-1C**) affected Gli function. Alanine mutations in Pm–o cluster did not have a discernable effect (**Figure 5-S5A**) in our assays, so we focused on the Pc–g cluster. To explore the role of Pc–g phosphorylation in the regulation of Gli2, we made both nonphosphorylatable and phosphomimetic mutations of this cluster in Gli2, replacing the serine and threonine residues with alanine or glutamate, hereafter called Gli2(Pc-gA) and Gli2(Pc-gE). In Hh reporter assays, HA-Gli2(Pc-gE) was significantly more active than the WT protein (**Figure 5-6A**) and Gli2(Pc-gA) was approximately 40% less active than the WT protein (**Figure 5-6B**). We also generated cell lines stably expressing HA-Gli2(Pc-gE) using the Flp-In system. Gli2(Pc-gE) protein levels were lower than Gli2 (WT), suggesting that the mutant protein was less stable (**Figure 5-S5B**). The higher specific activity of HA-Gli2(Pc-gE) (**Figure 5-6C**) supported the model that Pc-g phosphorylation, in contrast to P1–6 phosphorylation, plays a positive role in Gli2 activity. Gli2(Pc-gE) also showed other hallmarks of activation, including reduced mobility on a gel and higher levels in the nucleus (**Figure 5-6D**).

Hh signaling promotes and PKA antagonizes phosphorylation on Pg

The characterization of Pc-g phosphorylation as playing a positive role in Gli activity was inconsistent with our initial identification of these sites as *in vitro* targets for PKA (**Figure 5-1**), a kinase that has an inhibitory effect on Hh signaling in vertebrates[4,11,13,49]. To monitor Pc-g phosphorylation in the context of endogenous Gli2 in cells, we established an SRM assay to measure levels of a phosphorylated tryptic peptide that encompassed Pg, the only site in the Pc-g cluster whose phosphorylation could be easily monitored by MS. Surprisingly, in cells treated with FSK and IBMX to activate PKA, Pg phosphorylation was reduced (**Figure 5-6E**), demonstrating that the Pg site is not a bona fide PKA target in cells. Instead, we observed a 5-fold increase in the abundance of phosphorylated Pg upon SAG

treatment (**Figure 5-6E**), supporting the mutational data pointing to a positive role for Pc-g phosphorylation in Gli2 activity. As for P6, we also monitored the abundance of a nonphosphorylated tryptic peptide encompassing site Pg (dephospho-Pg; **Figure 5-S5C**). As expected, dephospho-Pg abundance dropped with SAG treatment and increased with IBMX + FSK treatment, providing further evidence for the positive regulation of Pc-g phosphorylation by the Shh signal. Experiments performed in the presence and absence of a proteasome inhibitor gave qualitatively similar results (**Figure 5-S5D**).

Interestingly, both the temporal dynamics and SAG dose-sensitivity of Pc-g phosphorylation (**Figures 5-6F and 5-6G**) mirrored those of P1–6 dephosphorylation (**Figures 5-5E and 5-5F**). PKA activation had opposite effects on the phosphorylation of the Pc-g and P1-6 clusters, suppressing the former while promoting the latter (**Figures 5-6E and 5-5D**). A parsimonious interpretation of these data is that PKA prevents Pc-g phosphorylation and Gli activation by directly phosphorylating the P1-6 sites.

To dissect the hierarchy between the Pc-gE and P1-6 sites, we combined activating (Pc-gE) and inhibitory (Pc-gA) mutations in the Pc-g sites with either inactivating (P5,6D) or activating (P1-6A) mutations in the P1-6 sites (**Figure 5-6H**). In Hh reporter assays, the activities of the Gli2(Pc-gE/P5,6D) and Gli2(Pc-gE/P1-6A) combination mutants were very similar, demonstrating that activating modifications at Pc-g make the phosphorylation status of P1-6 irrelevant. Controls confirmed that the isolated P5,6D mutation is much less active than the P1-6A mutant. Conversely, introduction of the inactivating Pc-gA mutation into Gli2(P1-6A) caused a substantial drop in its constitutive activity both in transient transfection assays (**Figure 5-6I**) and in a stable cell line (**Figure 5-6J**). These results support the model that Pc–g phosphorylation is an activating event gated by PKA-regulated phosphorylation of the P1–6 sites.

DISCUSSION

Distinct phospho-codes for Gli activator and Gli repressor regulation

We show here that phosphorylation of Gli proteins at six PKA target sites (P1-6) is a central determinant of their transcriptional activity, controlling the production of both repressor (GliR) and activator (GliA) forms. Our data are most consistent with a model involving ordered changes of phosphate occupancy at sites located in two distinct serine/threonine clusters (**Figure 5-1B**). In resting cells, PKA phosphorylates sites P1-6 on Gli2/3, triggering proteasomal processing into GliR and blocking conversion into GliA. When Hh binds to Ptc, Smo inhibits P1–6 phosphorylation, initiating a pathway that ultimately leads to the production of GliA: Gli proteins undergo phosphorylation at the Pc-g cluster, enter the nucleus, and are converted to unstable transcriptional activator proteins. We propose that the full transcriptional activation of Gli proteins requires the loss of phosphates at the P1-6 cluster followed by the gain of phosphates at the Pc-g cluster. The relative ordering of these two events is demonstrated by the fact that PKA activation enhances P1-6 phosphorylation and blocks Pc-g phosphorylation (**Figure 5-7A**). This regulatory motif, a gating dephosphorylation event coupled to nuclear translocation and an activating phosphorylation event at a distinct site, is reminiscent of the mechanism by which nuclear factor of activated T cells (NFAT) is regulated in response to T cell receptor engagement[50]. The concerted dephosphorylation of 13 phosphoserine residues by the phosphatase calcineurin triggers a conformational change in NFAT that drives nuclear localization. Like the Gli proteins, NFAT also requires an activating phosphorylation event at a separate site to acquire full transcriptional activity. Interestingly, in Gli1, which acts as a strong constitutive activator, the P1-6 cluster is poorly conserved (only sites P1, P2, and P6 show some degree of conservation). By contrast, four out of the five sites in the Pc-g cluster, including Pg, show remarkable sequence conservation among the three mammalian Gli proteins. This suggests that Pc-g phosphorylation may act as a universal activating signal for the Gli family.

Many signaling pathways, such as the NFAT pathway, regulate the conversion of a transcription factor from an inactive to an active state. The Hh pathway is different in that it controls the balance between gene repression, mediated by GliR, and gene activation, mediated by GliA. For instance, in *Drosophila*, low levels of Hh signaling suppress the

formation of CiR, but higher levels are required for the production of CiA[24,51]. Our analysis of the P1-6 cluster in Gli3 (**Figure 5-2**) suggests that repressor and activator functions of Gli proteins can be encoded by different patterns of phosphorylation: loss of phosphates at P1-4 is enough to block repressor formation, but loss of phosphates at all six P1-6 residues is needed for full nuclear translocation and transcriptional activity (**Figure 5-7B**). This provides a simple mechanism by which signaling can exert independent control over the repressor and activator functions of Gli2/3.

While repressor forms of the Gli proteins can be assayed directly due to their truncated length, a reliable biochemical mark for Gli activator formation has remained elusive. GliA formation has been inferred indirectly from changes in subcellular localization, such as nuclear translocation, or from target gene activation. This is a clinically relevant issue, since such a mark of Gli protein activity would be a valuable predictive biomarker for patients being considered for Hh antagonists, and could be used as a pharmacodynamic parameter to assess responses. Our SRM MS analysis suggests that Pg phosphorylation can serve as such a marker for Gli2 activity.

Graded control of Gli activity by multisite phosphorylation

Why might Gli proteins be regulated through such a complex phosphorylation scheme? Multisite phosphorylation is a commonly used regulatory module in diverse signaling systems[52]. It can be used to engineer an ultrasensitive ON/OFF switch or to encode a rheostat, allowing graded responses to varying signal strength. Examples of the latter include graded enhancement of p53 binding to CREB in response to genotoxic stress[53], graded binding of Ets-1 to DNA[54], and graded regulation of the gating properties of the Kv2.1 potassium channel[55]. In fact, a theoretical model has shown that multisite phosphorylation may serve to refine such a rheostat by allowing multistability, the existence of multiple discrete activity states in the target protein or signaling module[56]. A multistable rheostat would be well adapted to the function that Gli proteins serve during embryonic development. In developmental fields such as the limb, the inner ear, and the neural tube,

Hh ligands function as classical morphogens, and a central task of signaling is to translate ligand exposure into discrete outputs, such as cell fate, at the level of transcription[41,42,57,58]. Multisite phosphorylation might provide one mechanism by which differences in signal strength are converted into multiple discrete states of Gli activity (**Figure 5-7B**).

Indeed, our mutant analysis of the P1-6 cluster in Gli2 (**Figures 5-3 and 5-4**) is not consistent with a two-state model, in which Gli2 exists in either a fully inactive or fully active state. Particularly pertinent is the observation that both the P5,6A and the P1-4A mutants of Gli2 show an intermediate intrinsic capacity for transcriptional activation, which is higher than that of the WT protein, but significantly lower than that of the P1-6A mutant. Thus, Gli2 may occupy multiple states with differing activity, states that could represent different conformations of Gli2 that are stabilized by different patterns of phosphorylation in the P1-6 and Pc-g clusters. An important question going forward will be to ascertain how these changes in phosphate occupancy at the two conserved serine/threonine clusters affect the ability of Gli proteins to interact with other proteins in the cytoplasm, the cilium, and the nucleus and how these changes ultimately shape the Hh transcriptional program.

Additional support for a model involving multiple activation states of Gli2/3 comes from a recent paper[59], in which GliA was shown to be instructive in specifying ventral-most cell populations in the embryonic neural tube, but to only play a facilitating, non-instructive role in intermediate cell fate specification. In view of our data, the most plausible explanation is that progressive dephosphorylation along the Hh gradient leads to the creation of “weak” partially dephosphorylated Gli activators at moderate Hh concentrations, and favors “strong” fully dephosphorylated GliA conformations in ventral-most cells exposed to high Hh signal. “Strong” GliA can act independently of GliR to specify floor plate and V3 domains, but “weak” GliA must rely on the GliR gradient to force cell fate decisions. Consistent with this model, the “weak” GliA - Gli2(P1-4) - does not alter the expression of cell population markers in the dorsal neural tube. However, Gli2(P1-4) needs to lose only 2 additional phosphates, and thus requires lower Hh concentrations, to become the “strong” fully dephosphorylated GliA.

Hence, in areas receiving moderate Hh signal Gli2(P1-4) acts like the constitutively activated Gli2(P1-6A), promoting expression of the ventral markers HNF3β and Nkx2.2 (**Figure 5-4**).

Role of protein disorder in phospho-regulation of Gli proteins

Gli proteins are predicted to be disordered in segments that overlap the Pc-g and P1-6 phosphosites (**Figure 5-S6A**). Similar for many other intrinsically unstructured proteins, multi-site phosphorylation of Glis might therefore control their conformation by affecting the order/disorder balance in these regions[60].

Regulation of Gli proteins by phosphorylation in the morphogen gradient

Interestingly, recently published data on the role of GliA and GliR in ventral spinal cord development seem to support the notion of multiple discrete activation states of GliA[59]. In this paper, GliA was found to perform two distinct functions. In areas exposed to the highest concentrations of Hh, GliA was self-sufficient in specifying ventral-most progenitor cells. By contrast, in regions receiving intermediate to low concentrations of the morphogen, GliA was only permissive and instead GliR played the key role in cell fate determination. In view of our data, one plausible explanation is that fully dephosphorylated “strong” GliA proteins determine the boundaries of the ventral-most pFP and p3 regions, whereas partially dephosphorylated “weak” GliA proteins, most prevalent in the intermediate pMN-p0 regions, are non-instructive and subordinate to GliR in transducing the long-range Hh signal. The GliR gradient, critical for setting progenitor region boundaries in intermediate to dorsal areas of the neural tube, arises stochastically from the increasing probability of sites P1-4 being phosphorylated as the concentration of Hh goes down (**Figure 5-7B**).

Smo controls P1-6 phosphorylation

In accordance with the notion that P1-6 phosphorylation stoichiometry regulates the GliR/GliA balance, we find that these sites undergo dephosphorylation when Smo is activated by its direct agonist SAG (**Figure 5-5**). There is some evidence that Smo can act

as a G-protein coupled receptor (GPCR), activating Gαi, reducing cyclic AMP (cAMP) levels, and reducing PKA activity[35,61-64]. However, some studies have suggested that Gαi is not absolutely required for canonical Hh signaling[63,65]. An alternate mechanism has been suggested by the recent discovery that the inhibition of a ciliary Gαs-coupled receptor Gpr161 by Smo is required for Hh signal transduction[66]. It is tempting to speculate that Gpr161 maintains high baseline phosphorylation of Gli proteins by locally boosting cAMP levels and increasing PKA activity at primary cilia[19,67] and that Smo promotes Gli dephosphorylation by antagonizing Gpr161.

Mechanism of Gli activation downstream of P1-6 dephosphorylation

Our data suggests that loss of phosphorylation of the P1-6 cluster on Gli2/3 is a critical outcome of Smo activation. However, our mechanistic understanding of how the phosphorylation pattern is interpreted at the level of gene expression remains rudimentary. The most straightforward possibility is that phosphorylation simply influences the nucleocytoplasmic transport of Gli proteins, thereby regulating their availability at target promoters. In fact, the Gli nuclear localization sequence (NLS) within the fifth zinc finger domain is located adjacent to a conserved PKA target site and this site has been shown to affect Gli1 nuclear translocation[68]. However, our data suggest that sites P1-6, and not the one located near the NLS, play a decisive role in regulating Gli nuclear entry (**Figures 5-2C and 5-3B**). Since no predicted NLS has been described near the phosphosites in the P1-6 cluster, an alternate mechanism, perhaps based on conformational changes, must explain the effect of P1-6 phosphorylation on Gli nuclear accumulation. Control of the nuclear concentration of Gli proteins may not be the only mechanism by which P1-6 phosphorylation influences the expression of Hh target genes. A prior study proposed that P6 phosphorylation induces the association of Gli proteins with 14-3-3ε, which restricts their transcriptional activity in resting cells without affecting their nuclear localization[45]. In our hands, however, 14-3-3 failed to associate with Gli2 even when the signal was off (**Figure 5-S6B**), and a Gli3 mutant lacking a proline residue essential for 14-3-3 binding did not show

signs of constitutive activation (**Figure 5-S6C**). Thus, 14-3-3 binding does not appear to play a role in limiting GliA under the conditions used in our study. Other than directly regulating nuclear trafficking and activity at target promoters, dephosphorylation of P1-6 may act by priming Gli proteins for additional posttranslational modifications (PTMs). Specifically, phosphorylation of the Pc-g cluster appears to occur downstream of the loss of phosphates at the P1-6 sites, and to be an important component of GliA formation. In addition to phosphorylation, Gli proteins have been shown to undergo ubiquitination[69], acetylation[70], and SUMOylation[71], all of which alter their transcriptional potential. How these PTMs are integrated to allow Hh signaling to control gene expression in a graded fashion during morphogenesis is an important question for future studies to explore.

FIGURES

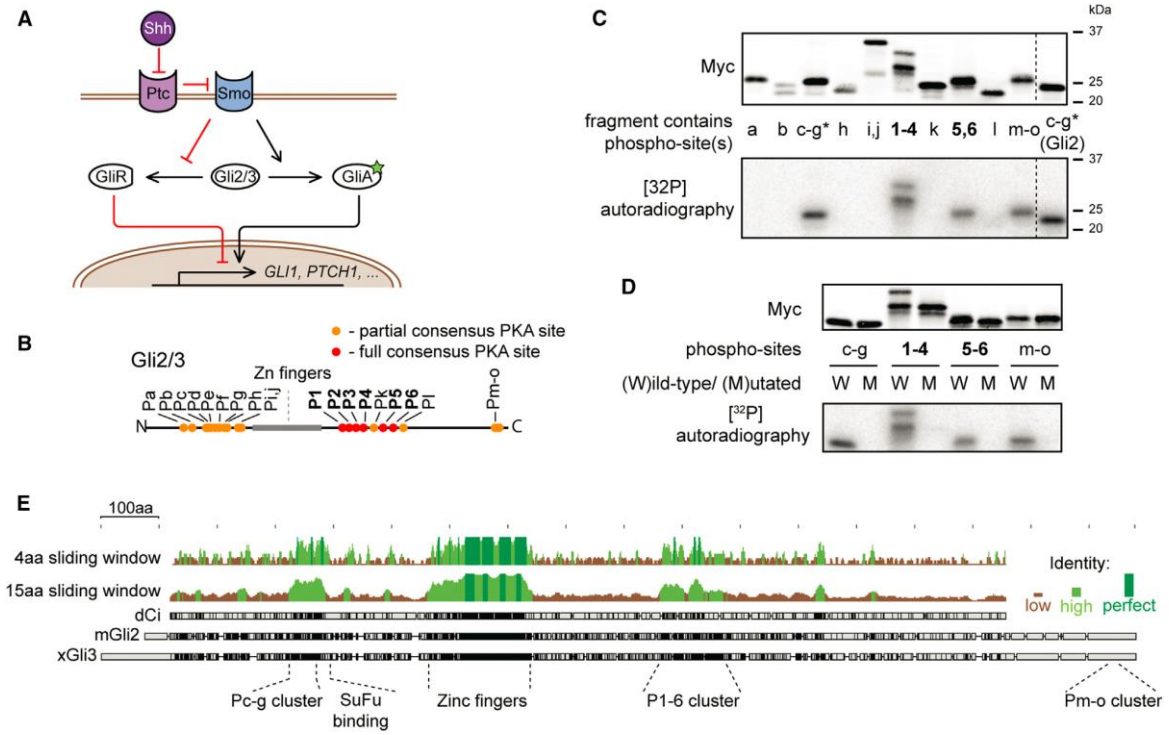

Figure 5-1: PKA phosphorylates both full and partial consensus sites on Gli2/3 *in vitro*

(A) Schematic representation of Gli2/3 regulation by Hh signaling. In the absence of signal, Smo is negatively regulated by Ptc. When the Hh ligand (Shh) binds, Smo is released from inhibition by Ptc. Active Smo induces the formation of GliA and suppresses the production of the truncated GliR form. The balance between GliA and GliR at target promoters determines signaling output.

(B) Location of the full (red dots; P1-6) and partial consensus (orange dots; Pa-o) PKA target sequences that are conserved in both mouse and human Gli2 and Gli3.

(C) In vitro PKA phosphorylation of Myc-tagged Gli3 fragments containing the indicated target sites. An anti-myc immunoblot (top) shows total protein levels of each fragment in the assay and the autoradiogram (bottom) shows ^{32}P incorporation. The Pc-g (*) fragment was tested for both Gli3 and Gli2 since only the former contains an additional PKA consensus target sequence.

(D) S/T residues presumed to be PKA targets were mutated in Gli3 fragments containing sites Pc-g, P1-4, P5,6, and Pm-o. Wild-type (W) or mutant (M) fragments were subjected to in vitro phosphorylation as in (C).

(E) Both the Pc-g cluster and the P1-6 cluster are highly conserved from the fly to mammals. Protein sequences of *Drosophila* Ci, mouse Gli2 and *Xenopus* Gli3 were aligned using the Geneious algorithm and the degree of conservation of protein sequence was plotted for either a 4-amino-acid or 15-amino-acid sliding window.

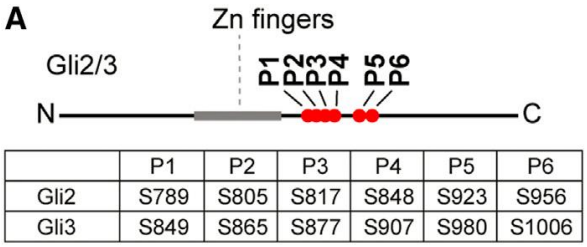

	P1	P2	P3	P4	P5	P6
Gli2	S789	S805	S817	S848	S923	S956
Gli3	S849	S865	S877	S907	S980	S1006

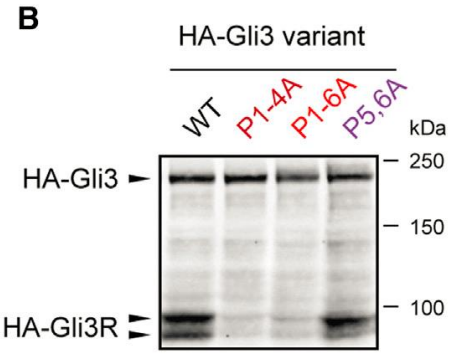

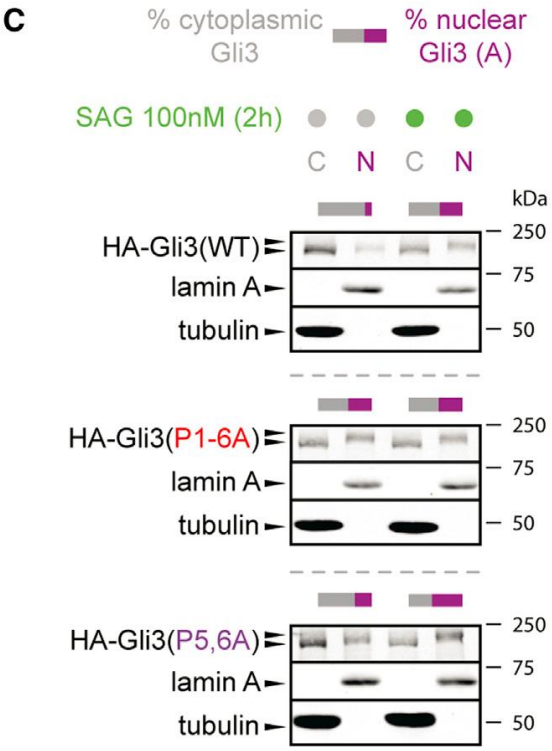

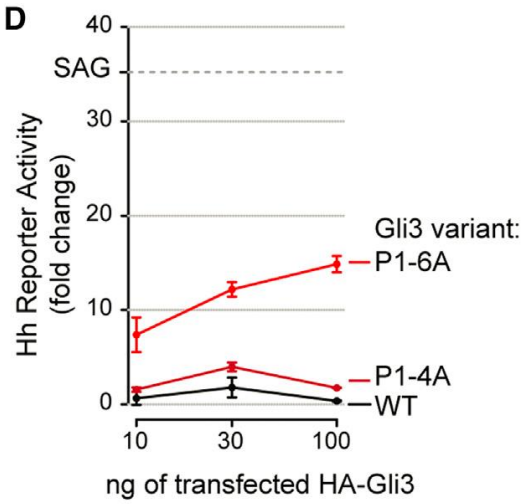

Figure 5-2: The P1-6 cluster regulates the balance between Gli3 activator and Gli3 repressor

(A) Location of sites P1-6 on Gli2 and Gli3.

(B) An anti-HA immunoblot reveals the relative levels of full-length and repressor Gli3 in whole cell extracts from NIH/3T3 Flp-In cells stably expressing HA-tagged Gli3 variants. Serine to alanine (S to A) mutation of sites P1-4 or the whole P1-6 cluster abrogates the formation of Gli3R (group of bands ~90kDa). In contrast mutation of sites P5 and P6 has no effect on Gli3R formation.

(C) Distribution of full-length HA-Gli3 variants in the nuclear (N) and cytoplasmic (C) fractions of NIH-3T3 Flp-In cells left untreated or treated with SAG (100 nM, 2 hours). In this and subsequent figures, lamin A and tubulin serve as control nuclear and cytoplasmic proteins to assess the quality of the fractionation and the bars above each blot represent the relative abundance of HA-Gli3 in the cytoplasmic (grey) and nuclear (purple) fractions as determined by quantitative immunoblotting.

(D) Activation of a luciferase-based Hh reporter gene in NIH/3T3 cells (untreated with any Hh agonists) transiently transfected with reporter construct in combination with the indicated Gli3 variants. Values were normalized to reporter induction seen with an empty plasmid (control). Dashed gray line shows the level of reporter activation seen with SAG (100 nM, 24 hours) in cells transfected with a control vector. Error bars indicate SD from three independent transfections.

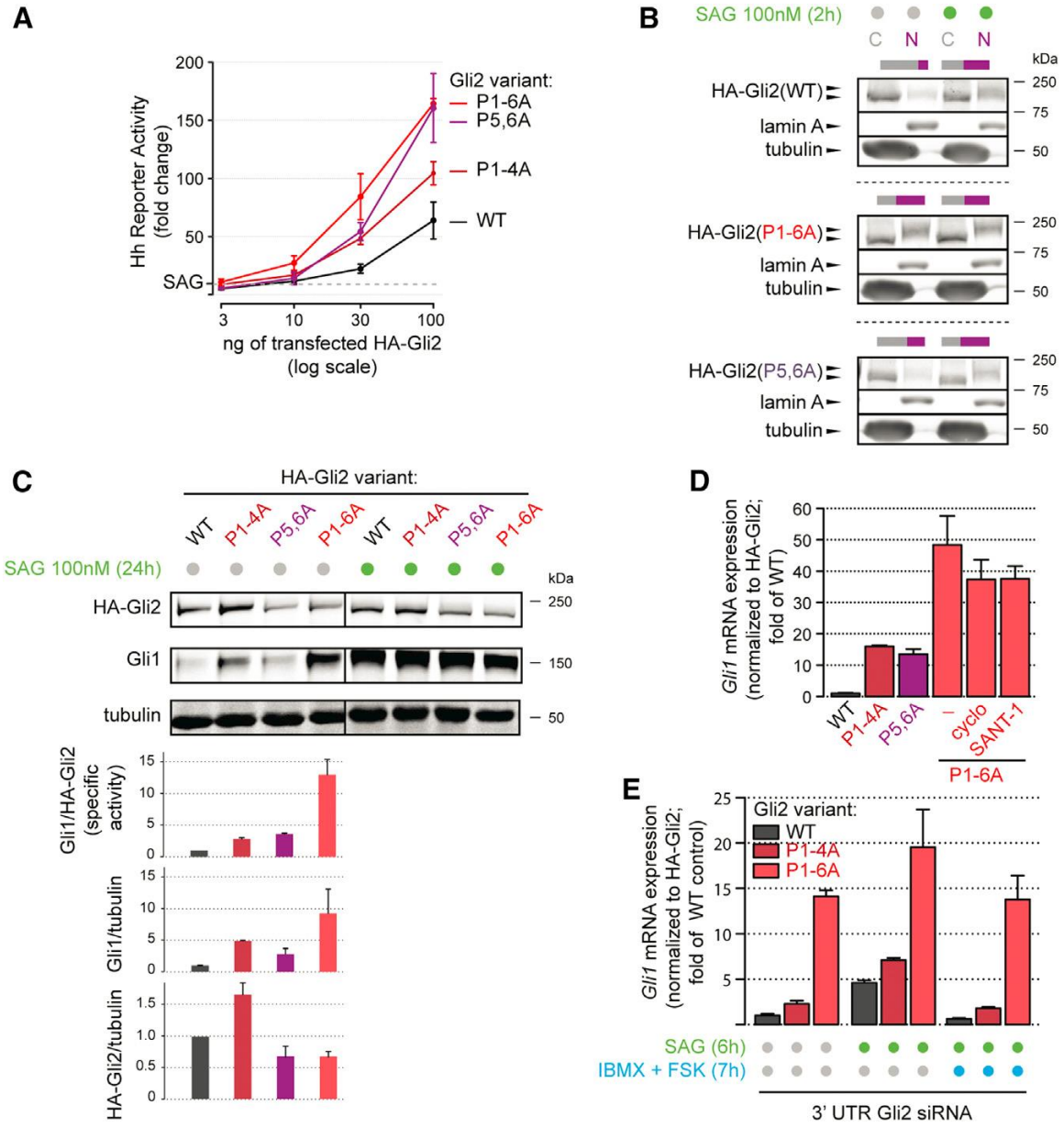
A
Hh Reporter Activity (fold change)
200
150
100
50
SAG
3
10
30
100
ng of transfected HA-Gli2 (log scale)
Gli2 variant:
P1-6A
P5,6A
P1-4A
WT
B
SAG 100nM (2h)
C
N
C
N
kDa
HA-Gli2(WT)
lamin A
tubulin
250
75
50
HA-Gli2(P1-6A)
HA-Gli2(P5,6A)
C
HA-Gli2 variant:
WT
P1-4A
P5,6A
P1-6A
SAG 100nM (24h)
HA-Gli2
Gli1
tubulin
150
Gli1/HA-Gli2 (specific activity)
Gli1/tubulin
HA-Gli2/tubulin
D
Gli1 mRNA expression (normalized to HA-Gli2; fold of WT)
60
50
40
30
20
10
0
cyclo
SANT-1
P1-6A
E
Gli1 mRNA expression (normalized to HA-Gli2; fold of WT control)
25
20
15
5
SAG (6h)
IBMX + FSK (7h)
3' UTR Gli2 siRNA

Figure 5-3: The P1-6 cluster regulates the activation of Gli2

(A) Luciferase reporter activity in NIH/3T3 cells (untreated with any Hh agonists) transiently transfected with the indicated Gli2 variants. The dashed line shows levels of reporter induction seen when cells transfected with a control vector are exposed to SAG (100 nM). Error bars denote SD from three independent transfections.

(B) Distribution of full length HA-Gli2 in NIH-3T3 cells Flp-In cells stably expressing the indicated variants.

(C) Levels of the Hh target gene Gli1 and HA-Gli2, measured using anti-Gli1 and anti-HA immunoblots respectively, in NIH/3T3 cells Flp-In stable cell lines expressing the indicated Gli2 variants. Cells were left untreated or treated with SAG (100 nM, 24 hours). Bar charts underneath show quantitation of Gli1 and HA-Gli2 proteins (normalized to tubulin) in each cell line and the specific activity of each variant (top chart), expressed as the ratio of the intensities of the Gli1 band to the HA band. Bars denote the mean (± SD) from two independent experiments.

(D) *Gli1* mRNA level, measured by quantitative RT-PCR, in Flp-In stable cell lines expressing the indicated HA-Gli2 variants. HA-Gli2(P1-6A) cells were left untreated or treated with the Smo inhibitors cyclopamine (5 µM) or SANT-1 (100 nM). The *Gli1* mRNA level was normalized to the HA-Gli2 protein level as in (C) to adjust for differences in expression level of the Gli variants. Bars denote the mean (± SD) from two independent experiments.

(E) *Gli1* mRNA level in the indicated stable cell lines treated with SAG (100 nM) in the presence or absence of PKA activators IBMX (100 µM) and FSK (0.1 µM). In all cells, expression of endogenous Gli2 was reduced by a siRNA directed against the 3' UTR to examine signaling through the HA-Gli2 variants. The *Gli1* mRNA level was normalized to HA-Gli2 protein measured as in (C) and (D); graphs depicting data without the HA-Gli2 protein normalization are shown in Figures S2F and S2G. Bars denote the mean (± SD) from two independent experiments.

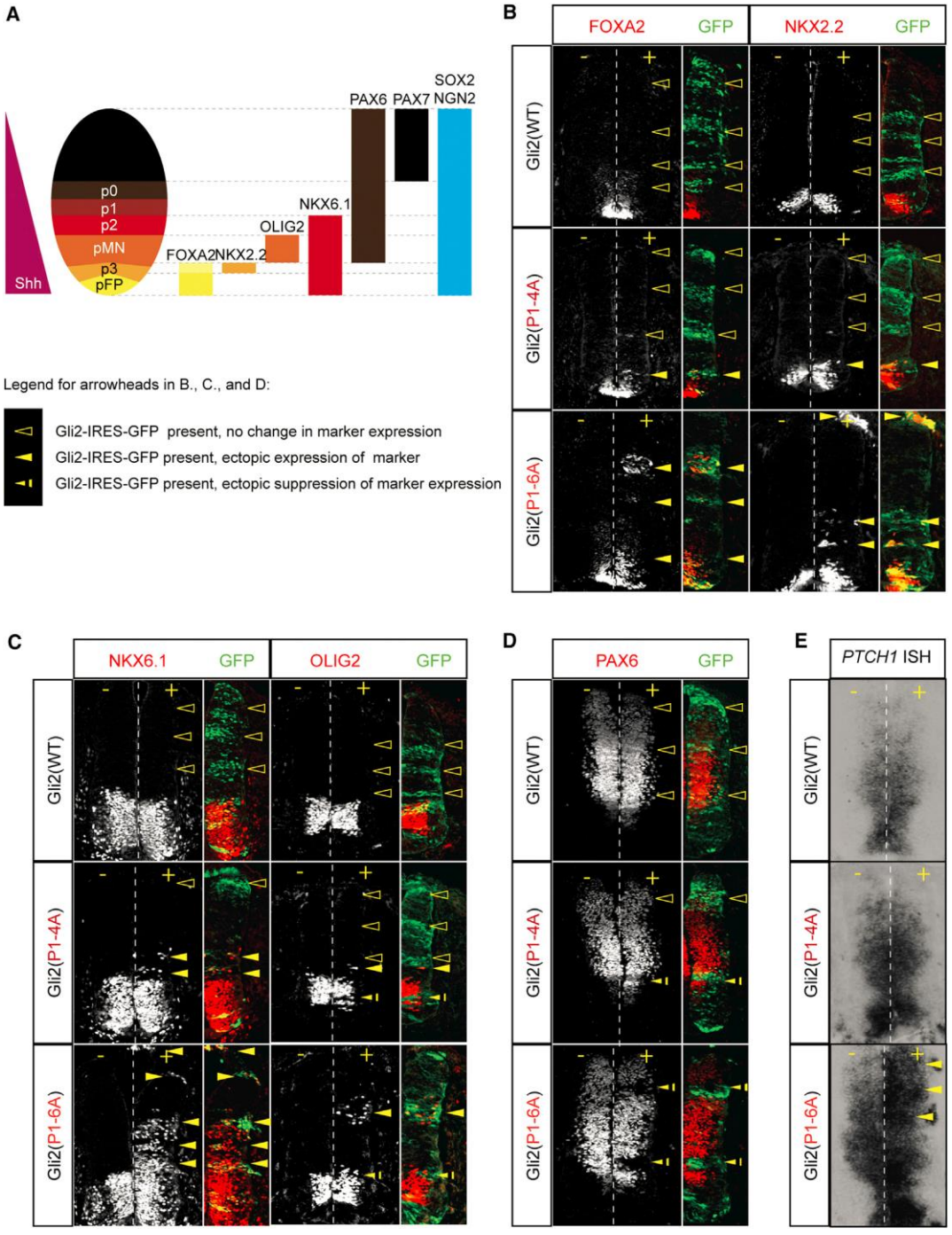
A
SOX2
NGN2
PAX6
PAX7
NKX6.1
OLIG2
FOXA2
NKX2.2
p0
p1
p2
pMN
p3
pFP
Shh
Legend for arrowheads in B., C., and D:
Gli2-IRES-GFP present, no change in marker expression
Gli2-IRES-GFP present, ectopic expression of marker
Gli2-IRES-GFP present, ectopic suppression of marker expression
B
FOXA2
GFP
NKX2.2
GFP
Gli2(WT)
Gli2(P1-4A)
Gli2(P1-6A)
C
NKX6.1
GFP
OLIG2
GFP
Gli2(WT)
Gli2(P1-4A)
Gli2(P1-6A)
D
PAX6
GFP
Gli2(WT)
Gli2(P1-4A)
Gli2(P1-6A)
E
PTCH1 ISH
Gli2(WT)
Gli2(P1-4A)
Gli2(P1-6A)

Figure 5-4: Gli2(P1-6A) can induce ventral cell fates in the developing spinal cord

(A) A schematic illustrating the relationship between marker proteins and progenitor cell populations in the embryonic neural tube[41]. pFP, floor plate progenitors; pMN, motor neurons progenitors; p0, p1, p2, p3, ventral interneuron progenitors.

(B-D) Constructs encoding Gli2 variants (green) were electroporated into developing chick spinal cords. Expression of the indicated progenitor population markers (red) was detected by immunofluorescence 48 hours after electroporation. Black and white panels show marker expression in both sides of the spinal cord ("+" indicates the electroporated side and "-" indicates the unelectroporated side). Overlay panels show the electroporated side only.

(E) In situ hybridization for *PTCH1* mRNA in sections of spinal cord electroporated with the indicated Gli2 constructs. The right side of each section was electroporated.

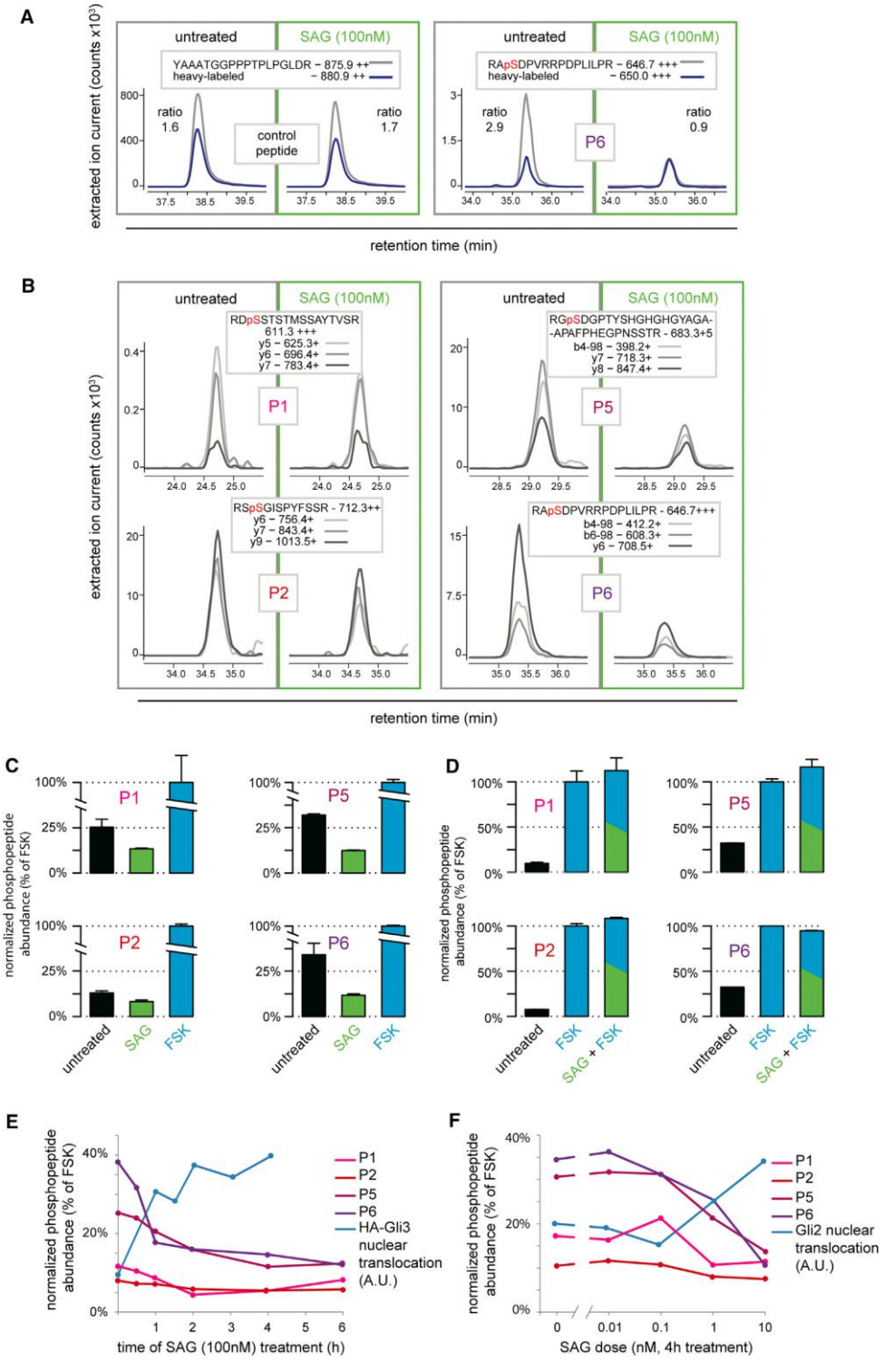
A
untreated
SAG (100nM)
YAAATGGPPPTPLPGLDR − 875.9 ++
heavy-labeled − 880.9 ++
ratio 1.6
ratio 1.7
control peptide
RApSDPVRRPDPLILPR − 646.7 +++
heavy-labeled − 650.0 +++
ratio 2.9
ratio 0.9
P6
extracted ion current (counts x10³)
retention time (min)
B
RDpSSTSTMSSAYTVSR 611.3 +++
y5 − 625.3+
y6 − 696.4+
y7 − 783.4+
P1
RSpSGISPYFSSR - 712.3++
y6 − 756.4+
y7 − 843.4+
y9 − 1013.5+
P2
RGpSDGPTYSHGHGHGYAGA--APAFPHEGPNSSTR - 683.3+5
b4-98 − 398.2+
y7 − 718.3+
y8 − 847.4+
P5
RApSDPVRRPDPLILPR - 646.7+++
b4-98 − 412.2+
b6-98 − 608.3+
y6 − 708.5+
P6
C
normalized phosphopeptide abundance (% of FSK)
untreated
SAG
FSK
D
SAG + FSK
E
HA-Gli3 nuclear translocation (A.U.)
time of SAG (100nM) treatment (h)
F
Gli2 nuclear translocation (A.U.)
SAG dose (nM, 4h treatment)

Figure 5-5: Phosphorylation of the P1-6 sites declines with Hh signaling

(A) Measurement of phosphopeptide abundance using SRM. Peptides were monitored in tryptic digests of immunoprecipitated Gli2 either in untreated NIH/3T3 Flp-In cells or in cells treated for 4 hours with 100 nM SAG, both in the presence of the proteasome inhibitor bortezomib (1 μM). The intensity of the "strongest" transition for two peptides, a nonphosphorylatable peptide used as a loading control (left) and phospho-P6-containing peptide (right), was plotted versus retention time (XIC, extracted ion current; grey trace). Blue traces are XICs of the corresponding heavy isotope-labeled standard peptide spiked into the tryptic digest before the run. For each condition, the normalized abundance of a peptide was calculated as the ratio of the area under the curve (AUC) for the light (endogenous) peptide to the AUC for the heavy peptide.

(B) XIC versus retention time plots showing three SRM transitions for each of the endogenous (light) phosphorylated peptides containing sites P1, P2, P5, and P6.

(C-D) Normalized abundance of phosphopeptides (calculated using an SRM assays of the type shown in A) containing the P1, P2, P5, and P6 sites derived from tryptic digests of immunopuffed Gli2 isolated from NIH/3T3 Flp-In cells were treated for 4 hours with SAG (100 nM) or IBMX (100 μM) + FSK (100 nM). Phosphopeptide abundance measured in cells after PKA activation with IBMX+FSK was taken as maximal (100%) phosphorylation. Bars denote means (± SD) of two or three independent MS runs.

(E-F) Phosphopeptide abundance was monitored as a function of time after SAG treatment (E) and as a function of SAG concentration (F) and compared to the levels of Gli3 (E) or Gli2 (F) in the nucleus (blue line). Percent of total Gli in the nucleaus was calculated based on subcellular fractionation experiments as shown in Figure 2C.

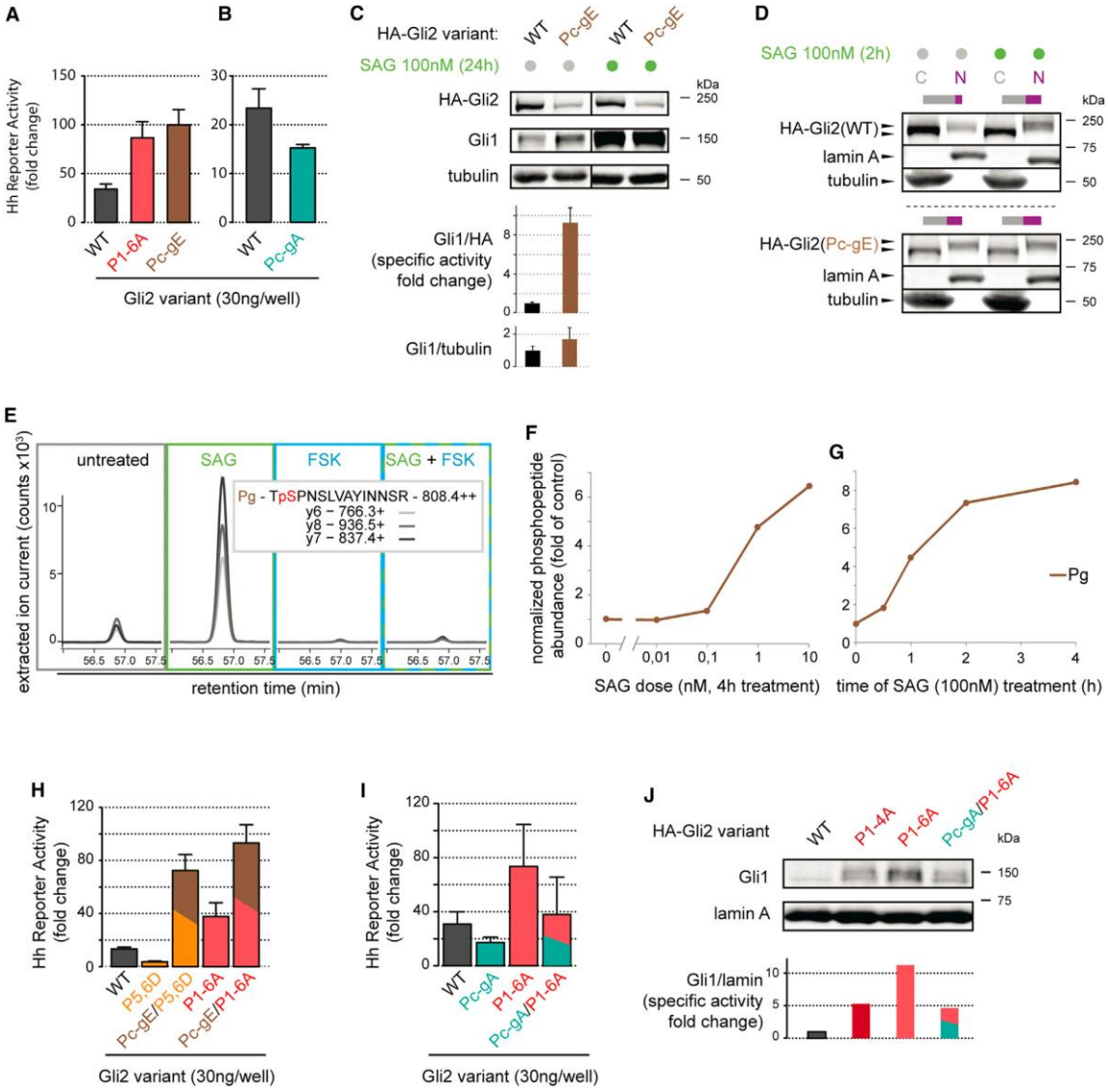
A
B
C
D
Hh Reporter Activity (fold change)
WT
P1-6A
Pc-gE
Pc-gA
Gli2 variant (30ng/well)
HA-Gli2 variant:
SAG 100nM (24h)
HA-Gli2
Gli1
tubulin
kDa
Gli1/HA (specific activity fold change)
Gli1/tubulin
SAG 100nM (2h)
C
N
HA-Gli2(WT)
HA-Gli2(Pc-gE)
lamin A
E
F
G
extracted ion current (counts x10³)
untreated
SAG
FSK
SAG + FSK
Pg - TpSPNSLVAYINNSR - 808.4++
y6 – 766.3+
y8 – 936.5+
y7 – 837.4+
retention time (min)
normalized phosphopeptide abundance (fold of control)
SAG dose (nM, 4h treatment)
time of SAG (100nM) treatment (h)
Pg
H
I
J
P5,6D
Pc-gE/P5,6D
P1-6A
Pc-gE/P1-6A
Pc-gA
Pc-gA/P1-6A
HA-Gli2 variant
P1-4A
Gli1
lamin A
Gli1/lamin (specific activity fold change)

Figure 5-6: Pc-g phosphorylation positively regulates Gli2 activity

(A-B) Hh reporter activity in NIH/3T3 cells transiently transfected with Gli2(WT), Gli2(Pc-gA), or Gli2(Pc-gE). Bars are mean ± SD of two independent transfections.

(C-D) NIH/3T3 Flp-In cell lines expressing HA-Gli2(WT) or HA-Gli2(Pc-gE) were used to elevate the specific activity (C, analyzed as in Figure 3C) and subcellular distribution (D, analyzed as in Figure 2C) of the Gli2 variants. Bars are mean ± SD of three independent transfections.

(E) XIC versus retention time traces for three SRM transitions derived from a Gli2 tryptic phosphopeptide containing the Pg residue. Phosphopeptide abundance is compared for Gli2 immunopurified from cells treated with the indicated drugs (4 hours).

(F-G) Pg phosphorylation abundance as a function of the concentration of SAG (F) or the duration of SAG exposure (G).

(H) Hh reporter activity in NIH/3T3 cells transiently transfected with Gli2(WT), Gli2(P5,6D), Gli2(P1-6A), and the combined mutants Gli2(Pc-gE/P1-6A) and Gli2(Pc-gE/P5,6D). Bars are mean ± SD of three independent transfections.

(I) Hh reporter activity in NIH/3T3 cells transiently transfected with Gli2(WT), Gli2(Pc-gA), Gli2(P1-6A), and the combined mutant Gli2(Pc-gE/P1-6A). Bars denote mean ± SD from two independent transfections.

(J) Level of the Hh target gene Gli1 measured using anti-Gli1 immunoblot in cell lines stably expressing near-endogenous levels of the indicated HA-Gli2 constructs. Bar chart shows quantitation of Gli1 protein normalized to lamin.

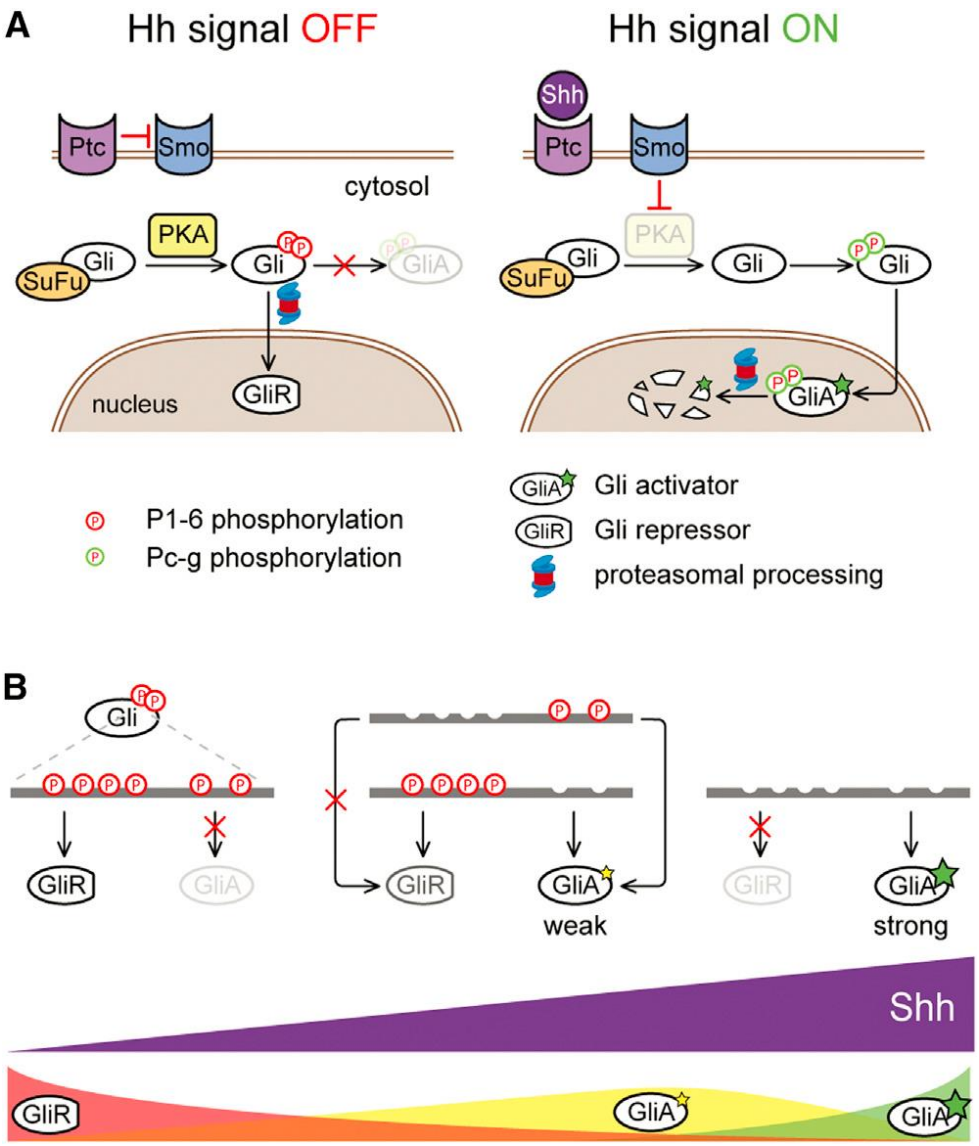

Figure 5-7: Model for the phosphoregulation of Gli proteins in Hh signaling

(A) Diagram illustrating the multisite phosphorylation model of Gli2/3 regulation.

(B) Multiple states of Gli activity can be encoded by different patterns of Gli phosphorylation at the P1–6 cluster. Full phosphorylation of P1–6 (left) drives GliR formation and blocks GliA formation. Partially dephosphorylated Gli proteins (middle) function as weak activators and may be able to form GliR, depending on the pattern of phosphorylation. Fully dephosphorylated Gli proteins (right) cannot form GliR and function as strong transcriptional activators.

A

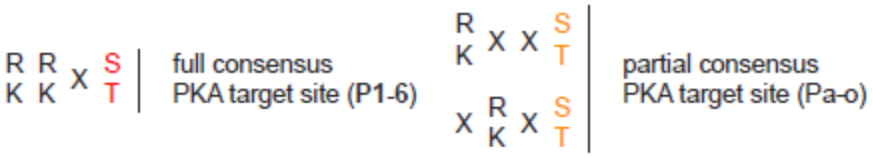

B

	Gli2	Gli3
P1	S789	S849
P2	S805	S865
P3	S817	S877
P4	S848	S907
P5	S923	S980
P6	S956	S1006

	Gli2	Gli3
Pa	S100	S177
Pb	S145	S223
Pc	S216	S281
Pd	T220	S285
Pe	S224	S289
Pf	S230	S295
Pg	S248	S313
Ph	S263	S338
Pi	S355	S419
Pj	S372	S435
Pk	S894	S952
Pl	S975	S1026
Pm	T1503	T1542
Pn	T1504	T1543
Po	S1508	S1547

Supplementary Figure 5-S1: Location of full and partial consensus PKA target sites on mouse Gli2 and Gli3

(A) Sequences of full consensus and partial consensus PKA target sites.

(B) Residue numbers of conserved partial (orange) and full (red) consensus PKA target sites in mouse Gli2 and Gli3.

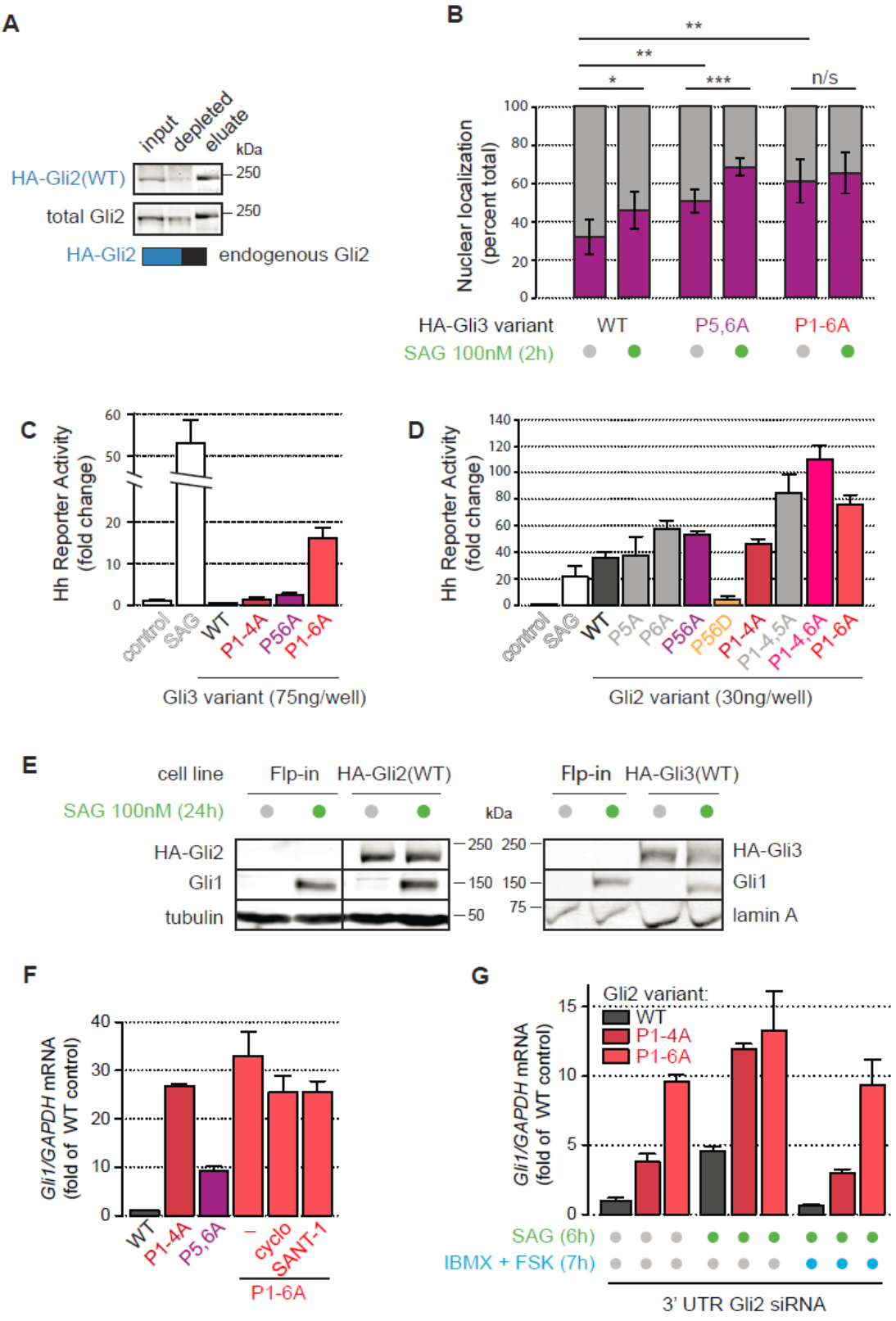
A
input
depleted
eluate
kDa
HA-Gli2(WT)
250
total Gli2
250
HA-Gli2
endogenous Gli2
B
**
**
*
***
n/s
Nuclear localization (percent total)
100
80
60
40
20
0
HA-Gli3 variant
WT
P5,6A
P1-6A
SAG 100nM (2h)
C
Hh Reporter Activity (fold change)
60
50
20
10
0
control
SAG
WT
P1-4A
P56A
P1-6A
Gli3 variant (75ng/well)
D
Hh Reporter Activity (fold change)
140
120
100
80
60
40
20
0
control
SAG
WT
P5A
P6A
P56A
P56D
P1-4A
P1-4,5A
P1-4,6A
P1-6A
Gli2 variant (30ng/well)
E
cell line
Flp-in
HA-Gli2(WT)
Flp-in
HA-Gli3(WT)
SAG 100nM (24h)
kDa
HA-Gli2
Gli1
tubulin
250
150
50
250
150
75
HA-Gli3
Gli1
lamin A
F
Gli1/GAPDH mRNA (fold of WT control)
40
30
20
10
0
WT
P1-4A
P5,6A
–
cyclo
SANT-1
P1-6A
G
Gli2 variant:
WT
P1-4A
P1-6A
Gli1/GAPDH mRNA (fold of WT control)
15
10
5
0
SAG (6h)
IBMX + FSK (7h)
3' UTR Gli2 siRNA

Supplementary Figure 5-S2: A mutation of all six PKA target sites in the P1-6 cluster results in greater Gli activity and the accumulation of more Gli2 and Gli3 in the nucleus

(A) Analysis of the levels of HA-tagged exogenous Gli2 compared to endogenous Gli2. Lysates from cells expressing wild-type HA-Gli2 were immunoprecipitated with anti-HA beads. Shown are anti-HA and anti-Gli2 immunoblots of the input (before immunoprecipitation) and the immunodepleted flow-through (after removal of the anti-HA beads). The beads deplete over 78% of HA-Gli2, and the total Gli2 (exogenous + endogenous) is depleted by 43%. The bar represents the calculated amount of exogenous and endogenous Gli2 as a fraction of the total cellular Gli2.

(B) Statistical analysis of nuclear translocation data for HA-Gli3 variants. The nuclear/cytoplasmic fractionation was performed as in Figure 5-2C. Means ± SD of percentage nuclear HA-Gli3 from 5 independent experiments are shown (purple bars).

(C) Luciferase reporter activity in NIH/3T3 cells transiently transfected with the indicated Gli3 variants. **(D)** Luciferase reporter activity in NIH/3T3 cells transiently transfected with the indicated Gli2 variants. In (C) and (D) error bars depict SD from 2-3 transfections.

(E) Levels of Gli1 and HA-Gli2, measured using anti-Gli1 and anti-HA immunoblots respectively, in NIH/3T3 Flp-In stable cell lines expressing HA-Gli2, HA-Gli3, or neither. Cells were left untreated or treated with SAG (100 nM, 24 hours).

(F) *Gli1* mRNA level, measured by qRT-PCR, in Flp-In stable cell lines expressing the indicated HA-Gli2 variants. Samples are the same as in Figure 5-3D, but the *Gli1* mRNA level was normalized to the GAPDH housekeeping gene rather than to HA-Gli2 protein. Bars denote the mean ± SD from 2 independent samples.

(G) *Gli1* mRNA level in the indicated stable cell lines transfected with Gli2 3'UTR siRNA and treated with SAG (100 nM) in the presence or absence of the PKA activators IBMX (100 µM) and FSK (0.1 µM). Samples are the same as in Figure 5-3E, but the *Gli1* mRNA level was normalized to the *GAPDH* housekeeping gene rather than to HA-Gli2 protein. Bars denote the mean ± SD from 2 independent samples.

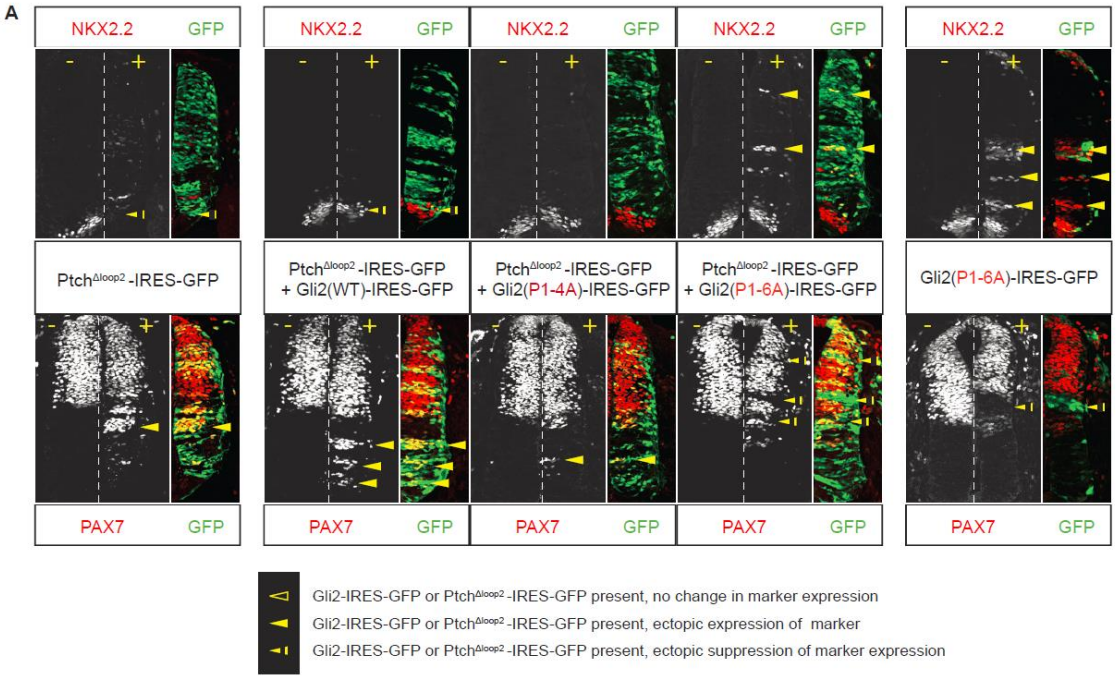
A
NKX2.2
GFP
PAX7
Ptch^Δloop2-IRES-GFP
Ptch^Δloop2-IRES-GFP + Gli2(WT)-IRES-GFP
Ptch^Δloop2-IRES-GFP + Gli2(P1-4A)-IRES-GFP
Ptch^Δloop2-IRES-GFP + Gli2(P1-6A)-IRES-GFP
Gli2(P1-6A)-IRES-GFP
Gli2-IRES-GFP or Ptch^Δloop2-IRES-GFP present, no change in marker expression
Gli2-IRES-GFP or Ptch^Δloop2-IRES-GFP present, ectopic expression of marker
Gli2-IRES-GFP or Ptch^Δloop2-IRES-GFP present, ectopic suppression of marker expression

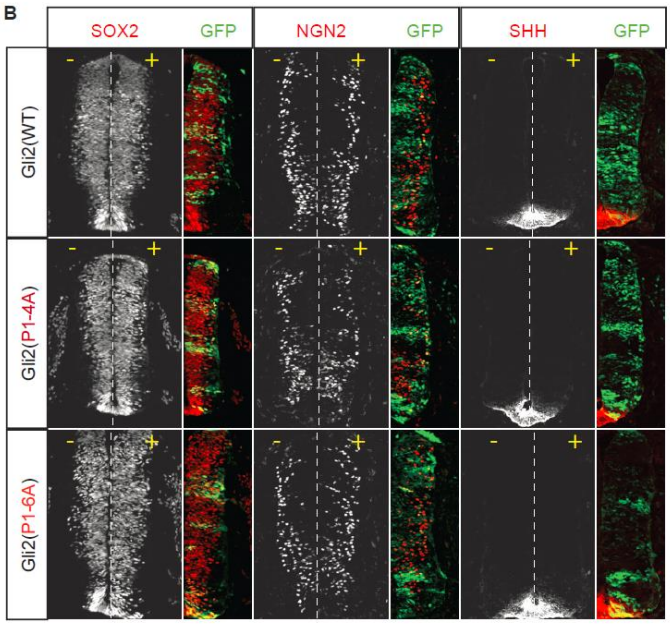
B
SOX2
GFP
NGN2
GFP
SHH
GFP
Gli2(WT)
Gli2(P1-4A)
Gli2(P1-6A)

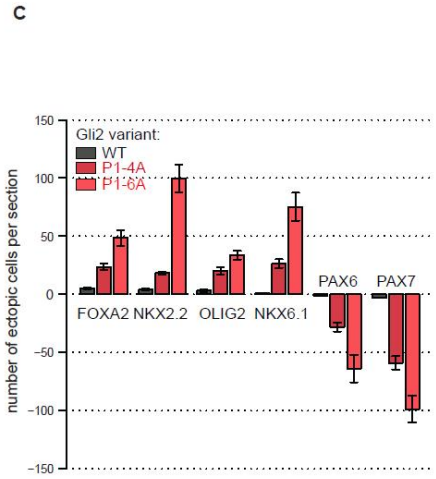
C
Gli2 variant:
WT
P1-4A
P1-6A
number of ectopic cells per section
150
100
50
0
−50
−100
−150
FOXA2
NKX2.2
OLIG2
NKX6.1
PAX6
PAX7

Supplementary Figure 5-S3: Gli2(P1-6) escapes regulation by upstream components of the Hh pathway in the developing spinal cord

(A) Expression of ventral (NKX2.2) and dorsal (PAX7) markers (both in red) in chick spinal cord co-electroporated with the indicated Gli2 constructs (green) and a constitutively active variant of Patched - PtchΔloop2 (also green). Tissue was processed as in Figure 5-4.

(B) SOX2, NGN2, and SHH expression in chick spinal cord electroporated with the indicated Gli2 constructs. Experiment was performed as in Figure 5-4.

(C) Statistical analysis of the ectopic expression of neural progenitor markers in chick spinal cords electroporated with the indicated Gli2 constructs. Bars denote mean ± SEM of GFP-positive ectopic progenitors per section from 19-32 tissue sections. Negative numbers indicate suppression of progenitor markers within their normal expression domain.

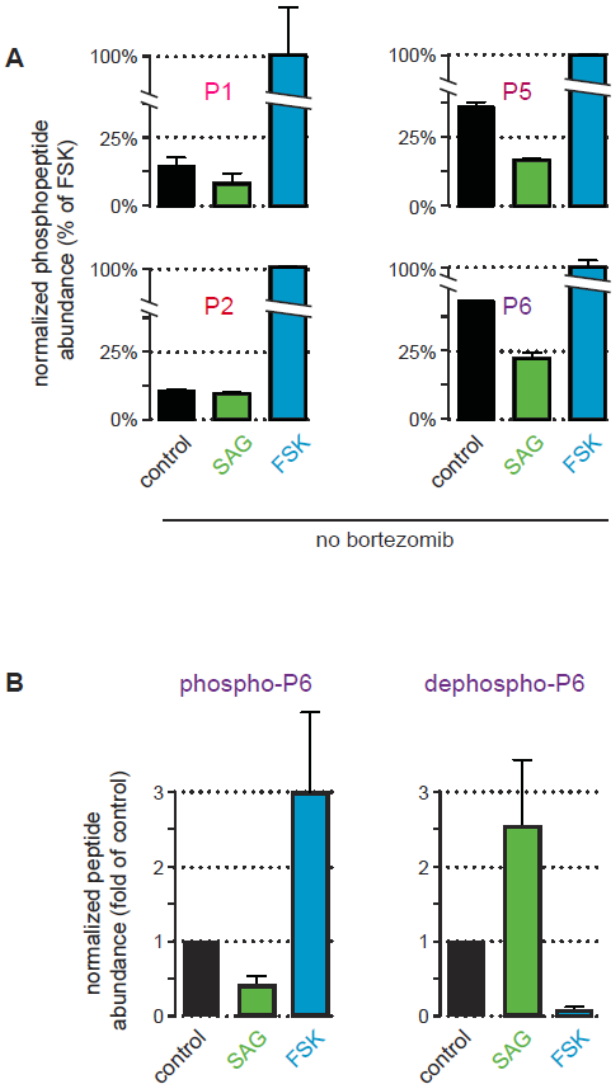

Supplementary Figure 5-S4: Activation of Hh signaling promotes the dephosphorylation of the P1-6 PKA target sites

(A) Normalized phosphopeptide abundance in tryptic digests of Gli2 isolated from NIH/3T3 cells treated with or without SAG or IBMX + FSK in the absence of bortezomib. The experiment was performed as in Figure 5-5C. Error bars are SD from 2 independent MS runs.

(B) Normalized peptide abundance in tryptic digests of Gli2 isolated from NIH/3T3 cells treated with or without SAG or IBMX + FSK in the presence of bortezomib. The experiment was performed as in Figure 5-5C. Error bars are SD from 2-3 independent MS runs.

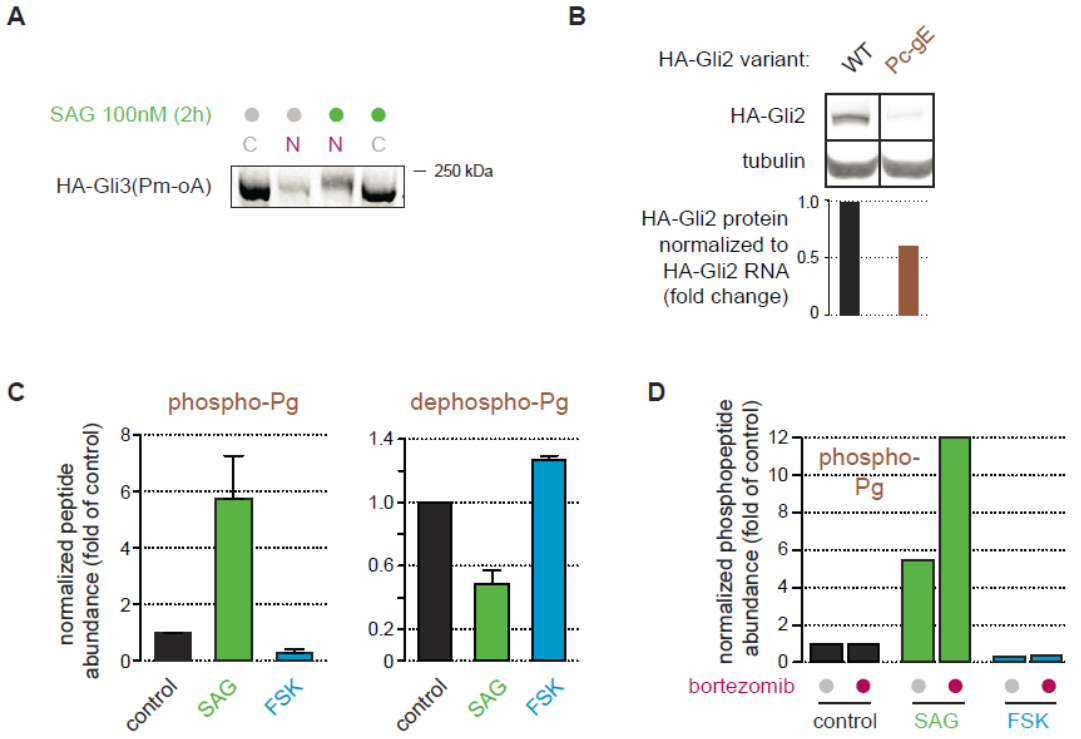

Supplementary Figure 5-S5: Activation of Hh signaling promotes the phosphorylation of the Pg partial consensus site

(A) Distribution of full-length HA-Gli3(Pm-oA) in the nuclear (N) and cytoplasmic (C) fractions of the NIH/3T3 Flp-In stable cell line left untreated or treated with SAG (100 nM, 2 hours). The experiment was performed as in Figure 5-2C.

(B) Protein levels of HA-Gli2(WT) and HA-Gli2(Pc-gE) were measured in stable NIH/3T3 Flp-in lines by anti-HA immunoblot and mRNA levels were measured by quantitative RT-PCR. Bars represent protein expression levels normalized to mRNA levels.

(C) Normalized peptide abundance in tryptic digests of Gli2 isolated from NIH/3T3 cells treated with or without SAG or IBMX + FSK in the presence of bortezomib. The experiment was performed as in Figure 5-6E. Bars denote mean ± SD from 2 independent MS runs.

(D) Normalized phosphopeptide abundance in tryptic digests of Gli2 isolated from NIH/3T3 cells treated with or without SAG or IBMX + FSK in the presence or absence of bortezomib. The experiment was performed as in Figure 5-6E.

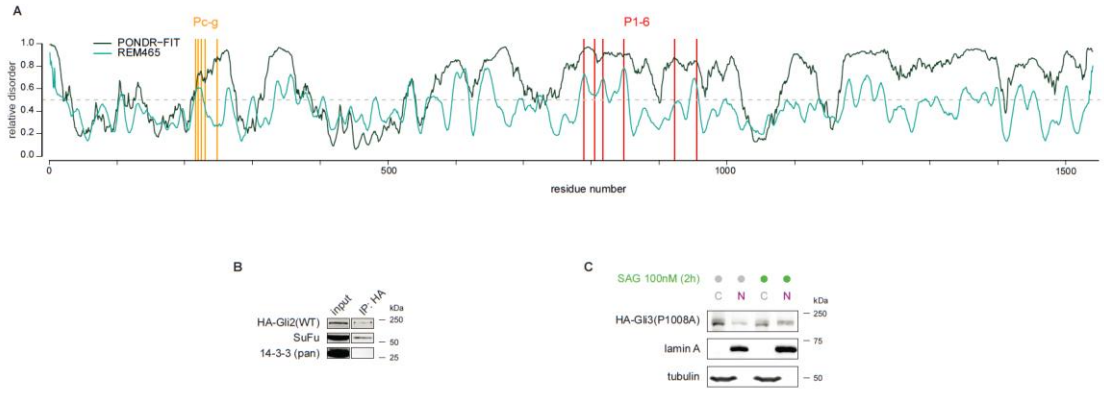

Supplementary Figure 5-S6: The P1-6 and Pc-g clusters are located in a region of the Gli2 protein predicted to be highly unstructured

(A) Clusters of phosphorylated sites in Gli2 are located in regions of high disorder. Intrinsic disorder of the mouse Gli2 sequence was calculated using two algorithms: PONDR-FIT[72] and REM465[73]. Plots show relative disorder values of regions of Gli2 centered on the indicated residue number. Values higher than 0.5 indicate protein regions that are most likely unstructured. Positions of the phosphosites belonging to the Pc-g or P1-6 clusters are indicated by vertical lines.

(B) Immunoblots showing the amount of endogenous Sufu and 14-3-3 co-immunoprecipitated with HA-Gli2 from lysates of a stable NIH/3T3 Flp-In cell line.

(C) Levels of HA-Gli3(P1008A) in the cytoplasm and nucleus of untreated cells or cells treated for 2 hours with 100 nM SAG. The P1008A mutant of Gli3 lacks the consensus proline site required for its putative interaction with 14-3-3. The experiment was performed using a stable NIH/3T3 Flp-In line as in Figure 5-2C.

ACKNOWLEDGMENTS

We would like to thank Siggy Nachtergaele, Andres Lebensohn, and Ganesh Pusapati for critical reading of the manuscript, Casey Hughes for technical assistance, and James Briscoe for insightful discussions. This work was supported by NIH grants R21NS074091 and R00CA129174 (to RR), R01NS072804 and R01NS053976 (to BGN), and P50GM107615 (to MT) and by grants from the V Foundation (to RR), the Sontag Foundation (to RR), the German Research Foundation (grant AH 220/1-1, to RA), and the March of Dimes Foundation (grant 6-FY10-296, to BGN).

REFERENCES

1 Hahn, H. *et al.* Mutations of the human homolog of Drosophila patched in the nevoid basal cell carcinoma syndrome. *Cell* **85**, 841-851 (1996).

2 Briscoe, J. & Therond, P. P. The mechanisms of Hedgehog signalling and its roles in development and disease. *Nature reviews. Molecular cell biology* **14**, 416-429, doi:10.1038/nrm3598 (2013).

3 Hui, C. C. & Angers, S. Gli proteins in development and disease. *Annu Rev Cell Dev Biol* **27**, 513-537, doi:10.1146/annurev-cellbio-092910-154048 (2011).

4 Humke, E. W., Dorn, K. V., Milenkovic, L., Scott, M. P. & Rohatgi, R. The output of Hedgehog signaling is controlled by the dynamic association between Suppressor of Fused and the Gli proteins. *Genes & development* **24**, 670-682, doi:10.1101/gad.1902910 (2010).

5 Kang, S., Graham, J. M., Jr., Olney, A. H. & Biesecker, L. G. GLI3 frameshift mutations cause autosomal dominant Pallister-Hall syndrome. *Nature genetics* **15**, 266-268, doi:10.1038/ng0397-266 (1997).

6 Wang, B., Fallon, J. F. & Beachy, P. A. Hedgehog-regulated processing of Gli3 produces an anterior/posterior repressor gradient in the developing vertebrate limb. *Cell* **100**, 423-434 (2000).

7 Hill, P., Wang, B. & Ruther, U. The molecular basis of Pallister Hall associated polydactyly. *Human molecular genetics* **16**, 2089-2096, doi:10.1093/hmg/ddm156 (2007).

8 Corbit, K. C. *et al.* Vertebrate Smoothened functions at the primary cilium. *Nature* **437**, 1018-1021, doi:10.1038/nature04117 (2005).

9 Kim, J., Kato, M. & Beachy, P. A. Gli2 trafficking links Hedgehog-dependent activation of Smoothened in the primary cilium to transcriptional activation in the nucleus. *Proc Natl Acad Sci U S A* **106**, 21666-21671, doi:10.1073/pnas.0912180106 (2009).

10 Wen, X. *et al.* Kinetics of hedgehog-dependent full-length Gli3 accumulation in primary cilia and subsequent degradation. *Molecular and cellular biology* **30**, 1910-1922, doi:10.1128/MCB.01089-09 (2010).

11 Tukachinsky, H., Lopez, L. V. & Salic, A. A mechanism for vertebrate Hedgehog signaling: recruitment to cilia and dissociation of SuFu-Gli protein complexes. *The Journal of cell biology* **191**, 415-428, doi:10.1083/jcb.201004108 (2010).

12 Hammerschmidt, M., Bitgood, M. J. & McMahon, A. P. Protein kinase A is a common negative regulator of Hedgehog signaling in the vertebrate embryo. *Genes & development* **10**, 647-658 (1996).

13 Tuson, M., He, M. & Anderson, K. V. Protein kinase A acts at the basal body of the primary cilium to prevent Gli2 activation and ventralization of the mouse neural tube. *Development* **138**, 4921-4930, doi:10.1242/dev.070805 (2011).

14 Fan, C. M. *et al.* Long-range sclerotome induction by sonic hedgehog: direct role of the amino-terminal cleavage product and modulation by the cyclic AMP signaling pathway. *Cell* **81**, 457-465 (1995).

15 Hynes, M. *et al.* Induction of midbrain dopaminergic neurons by Sonic hedgehog. *Neuron* **15**, 35-44 (1995).

16 Jiang, J. & Struhl, G. Protein kinase A and hedgehog signaling in Drosophila limb development. *Cell* **80**, 563-572 (1995).

17 Lepage, T., Cohen, S. M., Diaz-Benjumea, F. J. & Parkhurst, S. M. Signal transduction by cAMP-dependent protein kinase A in Drosophila limb patterning. *Nature* **373**, 711-715, doi:10.1038/373711a0 (1995).

18 Li, W., Ohlmeyer, J. T., Lane, M. E. & Kalderon, D. Function of protein kinase A in hedgehog signal transduction and Drosophila imaginal disc development. *Cell* **80**, 553-562 (1995).

19 Niewiadomski, P., Zhujiang, A., Youssef, M. & Waschek, J. A. Interaction of PACAP with Sonic hedgehog reveals complex regulation of the hedgehog pathway by PKA. *Cellular signalling* **25**, 2222-2230, doi:10.1016/j.cellsig.2013.07.012 (2013).

20 Pan, D. & Rubin, G. M. cAMP-dependent protein kinase and hedgehog act antagonistically in regulating decapentaplegic transcription in Drosophila imaginal discs. *Cell* **80**, 543-552 (1995).

21 Strutt, D. I., Wiersdorff, V. & Mlodzik, M. Regulation of furrow progression in the Drosophila eye by cAMP-dependent protein kinase A. *Nature* **373**, 705-709, doi:10.1038/373705a0 (1995).

22 Wang, G., Wang, B. & Jiang, J. Protein kinase A antagonizes Hedgehog signaling by regulating both the activator and repressor forms of Cubitus interruptus. *Genes & development* **13**, 2828-2837 (1999).

23 Aza-Blanc, P., Ramirez-Weber, F. A., Laget, M. P., Schwartz, C. & Kornberg, T. B. Proteolysis that is inhibited by hedgehog targets Cubitus interruptus protein to the nucleus and converts it to a repressor. *Cell* **89**, 1043-1053 (1997).

24 Methot, N. & Basler, K. An absolute requirement for Cubitus interruptus in Hedgehog signaling. *Development* **128**, 733-742 (2001).

25 Price, M. A. & Kalderon, D. Proteolysis of cubitus interruptus in Drosophila requires phosphorylation by protein kinase A. *Development* **126**, 4331-4339 (1999).

26 Pan, Y., Wang, C. & Wang, B. Phosphorylation of Gli2 by protein kinase A is required for Gli2 processing and degradation and the Sonic Hedgehog-regulated mouse

development. *Developmental biology* **326**, 177-189, doi:10.1016/j.ydbio.2008.11.009 (2009).

27 Megason, S. G. & McMahon, A. P. A mitogen gradient of dorsal midline Wnts organizes growth in the CNS. *Development* **129**, 2087-2098 (2002).

28 Ellis, L. *et al.* Replacement of insulin receptor tyrosine residues 1162 and 1163 compromises insulin-stimulated kinase activity and uptake of 2-deoxyglucose. *Cell* **45**, 721-732 (1986).

29 Sasaki, H., Hui, C., Nakafuku, M. & Kondoh, H. A binding site for Gli proteins is essential for HNF-3beta floor plate enhancer activity in transgenics and can respond to Shh in vitro. *Development* **124**, 1313-1322 (1997).

30 Cho, A., Ko, H. W. & Eggenschwiler, J. T. FKBP8 cell-autonomously controls neural tube patterning through a Gli2- and Kif3a-dependent mechanism. *Developmental biology* **321**, 27-39, doi:10.1016/j.ydbio.2008.05.558 (2008).

31 Novitch, B. G., Chen, A. I. & Jessell, T. M. Coordinate regulation of motor neuron subtype identity and pan-neuronal properties by the bHLH repressor Olig2. *Neuron* **31**, 773-789 (2001).

32 Weinstein, D. C. *et al.* The winged-helix transcription factor HNF-3 beta is required for notochord development in the mouse embryo. *Cell* **78**, 575-588 (1994).

33 Briscoe, J., Chen, Y., Jessell, T. M. & Struhl, G. A hedgehog-insensitive form of patched provides evidence for direct long-range morphogen activity of sonic hedgehog in the neural tube. *Molecular cell* **7**, 1279-1291 (2001).

34 Pearse, R. V., 2nd, Vogan, K. J. & Tabin, C. J. Ptc1 and Ptc2 transcripts provide distinct readouts of Hedgehog signaling activity during chick embryogenesis. *Developmental biology* **239**, 15-29, doi:10.1006/dbio.2001.0430 (2001).

35 Riobo, N. A., Lu, K., Ai, X., Haines, G. M. & Emerson, C. P., Jr. Phosphoinositide 3-kinase and Akt are essential for Sonic Hedgehog signaling. *Proc Natl Acad Sci U S A* **103**, 4505-4510, doi:10.1073/pnas.0504337103 (2006).

36 Torres, J. Z., Miller, J. J. & Jackson, P. K. High-throughput generation of tagged stable cell lines for proteomic analysis. *Proteomics* **9**, 2888-2891, doi:10.1002/pmic.200800873 (2009).

37 Zhou, C., Jacobsen, F. W., Cai, L., Chen, Q. & Shen, W. D. Development of a novel mammalian cell surface antibody display platform. *mAbs* **2**, 508-518, doi:10.4161/mabs.2.5.12970 (2010).

38 Pan, Y., Bai, C. B., Joyner, A. L. & Wang, B. Sonic hedgehog signaling regulates Gli2 transcriptional activity by suppressing its processing and degradation. *Molecular and cellular biology* **26**, 3365-3377, doi:10.1128/MCB.26.9.3365-3377.2006 (2006).

39 Tempe, D., Casas, M., Karaz, S., Blanchet-Tournier, M. F. & Concordet, J. P. Multisite protein kinase A and glycogen synthase kinase 3beta phosphorylation leads to Gli3 ubiquitination by SCFbetaTrCP. *Molecular and cellular biology* **26**, 4316-4326, doi:10.1128/MCB.02183-05 (2006).

40 Wang, B. & Li, Y. Evidence for the direct involvement of {beta}TrCP in Gli3 protein processing. *Proc Natl Acad Sci U S A* **103**, 33-38, doi:10.1073/pnas.0509927103 (2006).

41 Stamataki, D., Ulloa, F., Tsoni, S. V., Mynett, A. & Briscoe, J. A gradient of Gli activity mediates graded Sonic Hedgehog signaling in the neural tube. *Genes & development* **19**, 626-641, doi:10.1101/gad.325905 (2005).

42 Bai, C. B., Stephen, D. & Joyner, A. L. All mouse ventral spinal cord patterning by hedgehog is Gli dependent and involves an activator function of Gli3. *Developmental cell* **6**, 103-115 (2004).

43 Lei, Q., Zelman, A. K., Kuang, E., Li, S. & Matise, M. P. Transduction of graded Hedgehog signaling by a combination of Gli2 and Gli3 activator functions in the developing spinal cord. *Development* **131**, 3593-3604, doi:10.1242/dev.01230 (2004).

44 Ribes, V. *et al.* Distinct Sonic Hedgehog signaling dynamics specify floor plate and ventral neuronal progenitors in the vertebrate neural tube. *Genes & development* **24**, 1186-1200, doi:10.1101/gad.559910 (2010).

45 Asaoka, Y. *et al.* Identification of a suppressive mechanism for Hedgehog signaling through a novel interaction of Gli with 14-3-3. *The Journal of biological chemistry* **285**, 4185-4194, doi:10.1074/jbc.M109.038232 (2010).

46 Mayya, V., Rezual, K., Wu, L., Fong, M. B. & Han, D. K. Absolute quantification of multisite phosphorylation by selective reaction monitoring mass spectrometry: determination of inhibitory phosphorylation status of cyclin-dependent kinases. *Molecular & cellular proteomics : MCP* **5**, 1146-1157, doi:10.1074/mcp.T500029-MCP200 (2006).

47 Cox, D. M. *et al.* Multiple reaction monitoring as a method for identifying protein posttranslational modifications. *Journal of biomolecular techniques : JBT* **16**, 83-90 (2005).

48 Gerber, S. A., Rush, J., Stemman, O., Kirschner, M. W. & Gygi, S. P. Absolute quantification of proteins and phosphoproteins from cell lysates by tandem MS. *Proc Natl Acad Sci U S A* **100**, 6940-6945, doi:10.1073/pnas.0832254100 (2003).

49 Epstein, D. J., Marti, E., Scott, M. P. & McMahon, A. P. Antagonizing cAMP-dependent protein kinase A in the dorsal CNS activates a conserved Sonic hedgehog signaling pathway. *Development* **122**, 2885-2894 (1996).

50 Okamura, H. *et al.* Concerted dephosphorylation of the transcription factor NFAT1 induces a conformational switch that regulates transcriptional activity. *Molecular cell* **6**, 539-550 (2000).

51 Methot, N. & Basler, K. Hedgehog controls limb development by regulating the activities of distinct transcriptional activator and repressor forms of Cubitus interruptus. *Cell* **96**, 819-831 (1999).

52 Salazar, C. & Hofer, T. Multisite protein phosphorylation--from molecular mechanisms to kinetic models. *The FEBS journal* **276**, 3177-3198, doi:10.1111/j.1742-4658.2009.07027.x (2009).

53 Lee, C. W., Ferreon, J. C., Ferreon, A. C., Arai, M. & Wright, P. E. Graded enhancement of p53 binding to CREB-binding protein (CBP) by multisite phosphorylation. *Proc Natl Acad Sci U S A* **107**, 19290-19295, doi:10.1073/pnas.1013078107 (2010).

54 Pufall, M. A. *et al.* Variable control of Ets-1 DNA binding by multiple phosphates in an unstructured region. *Science* **309**, 142-145, doi:10.1126/science.1111915 (2005).

55 Park, K. S., Mohapatra, D. P., Misonou, H. & Trimmer, J. S. Graded regulation of the Kv2.1 potassium channel by variable phosphorylation. *Science* **313**, 976-979, doi:10.1126/science.1124254 (2006).

56 Thomson, M. & Gunawardena, J. Unlimited multistability in multisite phosphorylation systems. *Nature* **460**, 274-277, doi:10.1038/nature08102 (2009).

57 Bok, J. *et al.* Opposing gradients of Gli repressor and activators mediate Shh signaling along the dorsoventral axis of the inner ear. *Development* **134**, 1713-1722, doi:10.1242/dev.000760 (2007).

58 Fuccillo, M., Rallu, M., McMahon, A. P. & Fishell, G. Temporal requirement for hedgehog signaling in ventral telencephalic patterning. *Development* **131**, 5031-5040, doi:10.1242/dev.01349 (2004).

59 Oosterveen, T. *et al.* Mechanistic differences in the transcriptional interpretation of local and long-range Shh morphogen signaling. *Developmental cell* **23**, 1006-1019, doi:10.1016/j.devcel.2012.09.015 (2012).

60 Gsponer, J., Futschik, M. E., Teichmann, S. A. & Babu, M. M. Tight regulation of unstructured proteins: from transcript synthesis to protein degradation. *Science* **322**, 1365-1368, doi:10.1126/science.1163581 (2008).

61 Chinchilla, P., Xiao, L., Kazanietz, M. G. & Riobo, N. A. Hedgehog proteins activate pro-angiogenic responses in endothelial cells through non-canonical signaling pathways. *Cell cycle* **9**, 570-579 (2010).

62 Ogden, S. K. *et al.* G protein Galphai functions immediately downstream of Smoothened in Hedgehog signalling. *Nature* **456**, 967-970, doi:10.1038/nature07459 (2008).

63 Polizio, A. H. *et al.* Heterotrimeric Gi proteins link Hedgehog signaling to activation of Rho small GTPases to promote fibroblast migration. *The Journal of biological chemistry* **286**, 19589-19596, doi:10.1074/jbc.M110.197111 (2011).

64 Shen, F., Cheng, L., Douglas, A. E., Riobo, N. A. & Manning, D. R. Smoothened is a fully competent activator of the heterotrimeric G protein G(i). *Molecular pharmacology* **83**, 691-697, doi:10.1124/mol.112.082511 (2013).

65 Low, W. C. *et al.* The decoupling of Smoothened from Galphai proteins has little effect on Gli3 protein processing and Hedgehog-regulated chick neural tube patterning. *Developmental biology* **321**, 188-196, doi:10.1016/j.ydbio.2008.06.014 (2008).

66 Mukhopadhyay, S. *et al.* The ciliary G-protein-coupled receptor Gpr161 negatively regulates the Sonic hedgehog pathway via cAMP signaling. *Cell* **152**, 210-223, doi:10.1016/j.cell.2012.12.026 (2013).

67 Barzi, M., Berenguer, J., Menendez, A., Alvarez-Rodriguez, R. & Pons, S. Sonic-hedgehog-mediated proliferation requires the localization of PKA to the cilium base. *Journal of cell science* **123**, 62-69, doi:10.1242/jcs.060020 (2010).

68 Sheng, T., Chi, S., Zhang, X. & Xie, J. Regulation of Gli1 localization by the cAMP/protein kinase A signaling axis through a site near the nuclear localization signal. *The Journal of biological chemistry* **281**, 9-12, doi:10.1074/jbc.C500300200 (2006).

69 Di Marcotullio, L. *et al.* Multiple ubiquitin-dependent processing pathways regulate hedgehog/gli signaling: implications for cell development and tumorigenesis. *Cell cycle* **6**, 390-393 (2007).

70 Canettieri, G. *et al.* Histone deacetylase and Cullin3-REN(KCTD11) ubiquitin ligase interplay regulates Hedgehog signalling through Gli acetylation. *Nature cell biology* **12**, 132-142, doi:10.1038/ncb2013 (2010).

71 Cox, B., Briscoe, J. & Ulloa, F. SUMOylation by Pias1 regulates the activity of the Hedgehog dependent Gli transcription factors. *PloS one* **5**, e11996, doi:10.1371/journal.pone.0011996 (2010).

72 Xue, B., Dunbrack, R. L., Williams, R. W., Dunker, A. K. & Uversky, V. N. PONDR-FIT: a meta-predictor of intrinsically disordered amino acids. *Biochimica et biophysica acta* **1804**, 996-1010, doi:10.1016/j.bbapap.2010.01.011 (2010).

73 Linding, R. *et al.* Protein disorder prediction: implications for structural proteomics. *Structure* **11**, 1453-1459 (2003).

CHAPTER 6 – Conclusions and implications for cancer

Summary

In this work we focus on further understanding the roles and interactions of two major signaling pathways: Notch and Shh signaling. Notch signaling is essential for progenitor cell maintenance and as such is vital for the proper development of the CNS[1]. As a testament to its importance, a constitutive loss of the Notch effector Rbpj results in widespread premature neurogenesis and early embryonic death[2]. Although Notch signaling is most famous for its role in progenitor maintenance, Notch signaling regulates many other functions through interactions with other pathways. In Chapters 2-4, we focused on better understanding some of these additional roles of Notch signaling.

In Chapter 2, we examined the interactions between Notch and Shh signaling. Through the use of transgenic mouse models, chick neural plate explants, and cell culture systems we showed that Notch signaling is able to modulate Shh signaling activity by regulating the movement of Shh signaling components to the primary cilia (key steps in the Shh transduction pathway). By manipulating the response of progenitors to existing Shh present in the ventral spinal cord, we were able to show that Notch signaling plays an important role in progenitor patterning.

In Chapter 4 we examined interactions between Notch and RA signaling. In this study we showed that RA signaling, acting through Notch signaling, modifies the expression of the bHLH transcription factor Ascl1. In doing so, Notch signaling encourages the generation of two distinct neuronal populations (i.e. serotonergic neurons in the hindbrain and V3 interneurons in the rostral spinal cord) from a single progenitor pool (i.e. p3 progenitors). This study speaks to a larger theme of Notch signaling interacting with other signaling pathways and supports a fascinating emerging hypothesis that identifies Notch signaling as one component of a larger

integrated signaling hyper-network that collectively organizes and drives CNS development[3].

Finally, in Chapter 3 we examined a role of Notch signaling in the maintenance of progenitor cell adhesion and polarity. As a cell transitions from progenitor maintenance to neuronal differentiation, it must change its molecular composition and detach from the lumen. While much is known about how Notch signaling maintains cells as progenitors through the inhibition of proneural gene expression, significantly less is known about the role of Notch signaling in the maintenance of apical contacts that retain the cells to the progenitor rich ventricular zone. In this chapter we assessed the ability of Notch signaling to maintain adherens junctions in the developing brain. We observed that a loss of Notch signaling in the developing diencephalon not only resulted in premature neurogenesis, but also a disassembly of apical contacts and a disruption of the neuroepithelial cell layer. Ultimately, this defect resulted in hydrocephalus, which emphasizes the importance of Notch signaling in brain development.

In Chapters 2 and 5 we shift our focus to understanding the mechanisms that regulate Shh signaling activity. Shh signaling activity is a reflection of much more than the concentration of Shh ligand the cell is exposed to. An abundance of other factors influence Shh signaling activity, these include: (1) the duration of time over which the cells are exposed to Shh, (2) the ability of key Shh pathway components to enter and exit the primary cilia, and (3) the processing of Gli proteins into transcriptional activators or repressors. In Chapters 2 and 5 we focus on two of these ligand-independent factors. In Chapter 2 we demonstrate how the underlying responsiveness of progenitor cells to Shh can be adjusted by Notch signaling activity. In Chapter 5 we demonstrate how the phosphorylation of Gli proteins by PKA adjusts the potential of these Shh effectors to become transcriptional activators in a graded manner.

Collectively, this work furthers our understanding of how an abundance of cellular diversity emerges from a handful of developmental signaling cues. Although it is admittedly a small piece of very large puzzle, this work contributes significantly to the field of developmental neurobiology by drawing connections between two of the most important signaling pathways in

the developing CNS (Notch and Shh signaling), providing greater insight into the complexity of signaling networks, and identifying new mechanisms through which these signaling pathways are regulated. Through a greater understanding of how cellular diversity is generated in the developing embryo, we hope to one day use this knowledge to create new protocols that will be able to efficiently generate some of these cell types in culture. With these protocols, we would be able to better model human disease in culture and potentially even culture cells to replace ones lost due to injury and disease.

The signaling hyper-network: All roads lead to Notch

From studies conducted in an assortment of tissue types, it is becoming increasingly clear that signaling pathways do not act alone, but rather interact with other signaling pathways and exist as a part of a highly complex and integrated signaling hyper-network[3]. Although the details of the molecular circuitry of this network are still poorly understood, it is clear that Notch signaling is a major component. Various studies have shown that Notch signaling interacts with an abundance of other signaling pathways, including: Hh, Wnt[4], TGFβ[5], p53[6], vascular endothelial growth factor (VEGF)[7], Janus kinase/signal transducers and activators of transcription (Jak/STAT)[8], receptor tyrosine kinase (RTK)[9], and NF-κB[10]. This naturally leads to the question, how is it possible that a single signaling pathway can interact with so many other signaling pathways and in doing so influence so many functions in the developing embryo? The answer to this question may be the promiscuity of the Notch transcriptional effector Rbpj. Recently, multiple groups have used ChIP-seq to identify Rbpj target genes and are finding that there is much more beyond the Hes and Hey families that have become central to the study of Notch signaling. In a study conducted by Li et al., ChIP-seq was used in primary mouse neural stem cell cultures to conservatively identify 98 genes that are both direct targets of Rbpj and are activated by Notch signaling[11]. In another study conducted by Castel et al., ChIP-seq was used on C2C12 mouse myoblasts to identify 258 genes that were also both Rbpj targets and elevated

upon Notch signaling activation[12]. While many of these targets need to be studied further to verify that they are truly Notch target genes, the results show a lot of promise. Not only are many of the identified genes components of other major signaling pathways, but many of the genes are also involved in an assortment of biological processes that lie outside of the realm of progenitor maintenance. Overall, this data suggests that the multi-functional and highly interactive nature of the Notch signaling pathway is a product of the many gene targets of Rbpj.

Future directions: Notch and Hh signaling in the context of cancer

Many of the core signaling pathways that are essential for proper embryonic development are also frequently dysregulated in a variety of cancers where they are implicated in the initiation, proliferation, self-renewal, and metastasis of cancer cells[13]. With this understanding, recently a lot of effort has been directed towards designing new drugs that specifically target these dysregulated pathways. From this perspective, the field of cancer biology has the potential to learn a lot from the field of developmental biology. As we strive to understand how these fundamental signaling pathways regulate cell growth and patterning in the context of development, this information can be readily applied towards understanding how these same signaling pathways go awry in the case of cancer. Thus, new insights into pathway interactions have the potential to influence the development of new cancer therapies.

Notch and Shh signaling are two examples of signaling pathways that both play a vital role in development and are often persistently activated in many types of cancer. Notch has been associated with the pathogenesis of small-cell lung cancer[14,15], neuroblastoma[16], medulloblastoma[17], breast cancer[18], ovarian cancer[19], cervical cancer[20], prostate cancer[21], colon cancer[22-24], squamous cell carcinoma[25], and T-cell acute lymphoblastic leukemia[26]. Similarly, Shh has been associated with small-cell lung cancer[27,28], neuroblastoma[29], medulloblastoma[30,31], breast cancer[32], ovarian cancer[33,34], prostate cancer[35], colon cancer[24,36], basal cell carcinoma[37], and pancreatic cancer[38,39]. In an effort to treat these cancers, a multitude

of drugs that target and inactivate Notch and Shh signaling have been developed. There are many different types of Notch signaling inhibitors. These inhibitors can be divided into three major categories: γ-secretase inhibitors (GSIs) which block the generation of the cleaved Notch intracellular domain (NICD), anti-Dll4 and anti-Notch1 antibodies that inhibit Dll4-Notch signaling (a pathway critical for tumor angiogenesis)[40], and decoy Notch receptors that obstruct ligand-receptor interactions[41]. While there are currently many drugs that have the potential to inhibit Notch signaling, all of the drugs that currently target Hh signaling are Smo inhibitors. These drugs specifically inhibit the activation of Smo and/or the movement of Smo into the primary cilia. While none currently exist, groups are currently trying to generate drugs that inhibit the transition of Gli proteins into transcriptional activators.

Just as we see in development, the signaling pathways that drive the proliferation of cancer cells are also highly interactive[13,42,43]. In addition to our own developmental studies, there are a few other known interactions between Shh and Notch signaling. In the developing ventral spinal cord, Shh signaling drives the transient expression of the Notch ligand Jagged2. In addition, in the developing retina and cerebellum, Shh has also been shown to regulate Hes1 in a Notch independent manner[44-46]. Due to the existence of these interactions in development, it is not inconceivable that similar interactions between Notch and Shh signaling may also be present in cancer. There are reasons to suggest this could be true. First, Notch and Shh are frequently overactivated in the same cancers. And second, in many of the cancers in which Shh signaling is overactivated (i.e. medulloblastomas[47], breast cancer[48-50], and ovarian cancer[51]), an elevation of Notch signaling activity predicts a poor prognosis. While circumstantial, this evidence suggests that Notch signaling may interact with Shh signaling, or other pathways, to elevate the proliferative character of the cancer cells.

While we still do not know much about the details of the signaling interactions that exist in a variety of cancers, combination therapies that simultaneously target multiple pathways are currently in clinical trials. In these trials γ-secretase inhibitors (Notch pathway inhibitors) and

Smo inhibitors (Shh pathway inhibitors) are currently being used together to treat breast cancer and metastatic sarcomas[41]. While many of these drug therapies have proven ineffective when a single pathway is targeted, preliminary results indicate that by targeting multiple pathways, these combination therapies will be more effective.

Conclusion

In conclusion, this thesis provides important insights into signaling pathway interactions and how they give rise to greater cellular diversity and functionality. Now that new targets for Notch signaling are being identified and new pathway interactions being realized, hopefully this will lead to new discoveries that will both further out understanding of development and lead to new cancer cures.

REFERENCES

1 de la Pompa, J. L. *et al.* Conservation of the Notch signalling pathway in mammalian neurogenesis. *Development* **124**, 1139-1148 (1997).

2 Oka, C. *et al.* Disruption of the mouse RBP-J kappa gene results in early embryonic death. *Development* **121**, 3291-3301 (1995).

3 Hurlbut, G. D., Kankel, M. W., Lake, R. J. & Artavanis-Tsakonas, S. Crossing paths with Notch in the hyper-network. *Current opinion in cell biology* **19**, 166-175, doi:10.1016/j.ceb.2007.02.012 (2007).

4 Duncan, A. W. *et al.* Integration of Notch and Wnt signaling in hematopoietic stem cell maintenance. *Nature immunology* **6**, 314-322, doi:10.1038/ni1164 (2005).

5 Guo, X. & Wang, X. F. Signaling cross-talk between TGF-beta/BMP and other pathways. *Cell research* **19**, 71-88, doi:10.1038/cr.2008.302 (2009).

6 Dotto, G. P. Crosstalk of Notch with p53 and p63 in cancer growth control. *Nature reviews. Cancer* **9**, 587-595, doi:10.1038/nrc2675 (2009).

7 Phng, L. K. & Gerhardt, H. Angiogenesis: a team effort coordinated by notch. *Developmental cell* **16**, 196-208, doi:10.1016/j.devcel.2009.01.015 (2009).

8 Kamakura, S. *et al.* Hes binding to STAT3 mediates crosstalk between Notch and JAK-STAT signalling. *Nature cell biology* **6**, 547-554, doi:10.1038/ncb1138 (2004).

9 Ranganathan, P., Weaver, K. L. & Capobianco, A. J. Notch signalling in solid tumours: a little bit of everything but not all the time. *Nature reviews. Cancer* **11**, 338-351, doi:10.1038/nrc3035 (2011).

10 Maniati, E. *et al.* Crosstalk between the canonical NF-kappaB and Notch signaling pathways inhibits Ppargamma expression and promotes pancreatic cancer progression in mice. *The Journal of clinical investigation* **121**, 4685-4699, doi:10.1172/JCI45797 (2011).

11 Li, Y., Hibbs, M. A., Gard, A. L., Shylo, N. A. & Yun, K. Genome-wide analysis of N1ICD/RBPJ targets in vivo reveals direct transcriptional regulation of Wnt, SHH, and hippo pathway effectors by Notch1. *Stem cells* **30**, 741-752, doi:10.1002/stem.1030 (2012).

12 Castel, D. *et al.* Dynamic binding of RBPJ is determined by Notch signaling status. *Genes & development* **27**, 1059-1071, doi:10.1101/gad.211912.112 (2013).

13 Takebe, N., Harris, P. J., Warren, R. Q. & Ivy, S. P. Targeting cancer stem cells by inhibiting Wnt, Notch, and Hedgehog pathways. *Nature reviews. Clinical oncology* **8**, 97-106, doi:10.1038/nrclinonc.2010.196 (2011).

14 Borges, M. *et al.* An achaete-scute homologue essential for neuroendocrine differentiation in the lung. *Nature* **386**, 852-855, doi:10.1038/386852a0 (1997).

15 Sriuranpong, V. *et al.* Notch signaling induces cell cycle arrest in small cell lung cancer cells. *Cancer research* **61**, 3200-3205 (2001).

16 Pahlman, S., Stockhausen, M. T., Fredlund, E. & Axelson, H. Notch signaling in neuroblastoma. *Seminars in cancer biology* **14**, 365-373, doi:10.1016/j.semcancer.2004.04.016 (2004).

17 Manoranjan, B. *et al.* Medulloblastoma stem cells: where development and cancer cross pathways. *Pediatric research* **71**, 516-522, doi:10.1038/pr.2011.62 (2012).

18 Farnie, G. & Clarke, R. B. Mammary stem cells and breast cancer--role of Notch signalling. *Stem cell reviews* **3**, 169-175 (2007).

19 McAuliffe, S. M. *et al.* Targeting Notch, a key pathway for ovarian cancer stem cells, sensitizes tumors to platinum therapy. *Proc Natl Acad Sci U S A* **109**, E2939-2948, doi:10.1073/pnas.1206400109 (2012).

20 Maliekal, T. T., Bajaj, J., Giri, V., Subramanyam, D. & Krishna, S. The role of Notch signaling in human cervical cancer: implications for solid tumors. *Oncogene* **27**, 5110-5114, doi:10.1038/onc.2008.224 (2008).

21 Carvalho, F. L., Simons, B. W., Eberhart, C. G. & Berman, D. M. Notch signaling in prostate cancer: a moving target. *The Prostate* **74**, 933-945, doi:10.1002/pros.22811 (2014).

22 Qiao, L. & Wong, B. C. Role of Notch signaling in colorectal cancer. *Carcinogenesis* **30**, 1979-1986, doi:10.1093/carcin/bgp236 (2009).

23 Sikandar, S. S. *et al.* NOTCH signaling is required for formation and self-renewal of tumor-initiating cells and for repression of secretory cell differentiation in colon cancer. *Cancer research* **70**, 1469-1478, doi:10.1158/0008-5472.CAN-09-2557 (2010).

24 Roy, S. & Majumdar, A. P. Signaling in colon cancer stem cells. *Journal of molecular signaling* **7**, 11, doi:10.1186/1750-2187-7-11 (2012).

25 Hu, B. *et al.* Multifocal epithelial tumors and field cancerization from loss of mesenchymal CSL signaling. *Cell* **149**, 1207-1220, doi:10.1016/j.cell.2012.03.048 (2012).

26 Grabher, C., von Boehmer, H. & Look, A. T. Notch 1 activation in the molecular pathogenesis of T-cell acute lymphoblastic leukaemia. *Nature reviews. Cancer* **6**, 347-359, doi:10.1038/nrc1880 (2006).

27 Watkins, D. N. *et al.* Hedgehog signalling within airway epithelial progenitors and in small-cell lung cancer. *Nature* **422**, 313-317, doi:10.1038/nature01493 (2003).

28 Vestergaard, J. *et al.* Hedgehog signaling in small-cell lung cancer: frequent in vivo but a rare event in vitro. *Lung cancer* **52**, 281-290, doi:10.1016/j.lungcan.2005.12.014 (2006).

29 Mao, L. *et al.* A critical role of Sonic Hedgehog signaling in maintaining the tumorigenicity of neuroblastoma cells. *Cancer science* **100**, 1848-1855, doi:10.1111/j.1349-7006.2009.01262.x (2009).

30 Raffel, C. *et al.* Sporadic medulloblastomas contain PTCH mutations. *Cancer research* **57**, 842-845 (1997).

31 Goodrich, L. V., Milenkovic, L., Higgins, K. M. & Scott, M. P. Altered neural cell fates and medulloblastoma in mouse patched mutants. *Science* **277**, 1109-1113 (1997).

32 Kasper, M., Jaks, V., Fiaschi, M. & Toftgard, R. Hedgehog signalling in breast cancer. *Carcinogenesis* **30**, 903-911, doi:10.1093/carcin/bgp048 (2009).

33 Liao, X. *et al.* Aberrant activation of hedgehog signaling pathway in ovarian cancers: effect on prognosis, cell invasion and differentiation. *Carcinogenesis* **30**, 131-140, doi:10.1093/carcin/bgn230 (2009).

34 Bhattacharya, R. *et al.* Role of hedgehog signaling in ovarian cancer. *Clinical cancer research : an official journal of the American Association for Cancer Research* **14**, 7659-7666, doi:10.1158/1078-0432.CCR-08-1414 (2008).

35 Karhadkar, S. S. *et al.* Hedgehog signalling in prostate regeneration, neoplasia and metastasis. *Nature* **431**, 707-712, doi:10.1038/nature02962 (2004).

36 Varnat, F. *et al.* Human colon cancer epithelial cells harbour active HEDGEHOG-GLI signalling that is essential for tumour growth, recurrence, metastasis and stem cell survival and expansion. *EMBO molecular medicine* **1**, 338-351, doi:10.1002/emmm.200900039 (2009).

37 Oro, A. E. *et al.* Basal cell carcinomas in mice overexpressing sonic hedgehog. *Science* **276**, 817-821 (1997).

38 Bailey, J. M., Mohr, A. M. & Hollingsworth, M. A. Sonic hedgehog paracrine signaling regulates metastasis and lymphangiogenesis in pancreatic cancer. *Oncogene* **28**, 3513-3525, doi:10.1038/onc.2009.220 (2009).

39 Morton, J. P. *et al.* Sonic hedgehog acts at multiple stages during pancreatic tumorigenesis. *Proc Natl Acad Sci U S A* **104**, 5103-5108, doi:10.1073/pnas.0701158104 (2007).

40 Dufraine, J., Funahashi, Y. & Kitajewski, J. Notch signaling regulates tumor angiogenesis by diverse mechanisms. *Oncogene* **27**, 5132-5137, doi:10.1038/onc.2008.227 (2008).

41 Takebe, N. *et al.* Targeting Notch, Hedgehog, and Wnt pathways in cancer stem cells: clinical update. *Nature reviews. Clinical oncology*, doi:10.1038/nrclinonc.2015.61 (2015).

42 Bertrand, F. E., Angus, C. W., Partis, W. J. & Sigounas, G. Developmental pathways in colon cancer: crosstalk between WNT, BMP, Hedgehog and Notch. *Cell cycle* **11**, 4344-4351, doi:10.4161/cc.22134 (2012).

43 Katoh, M. Networking of WNT, FGF, Notch, BMP, and Hedgehog signaling pathways during carcinogenesis. *Stem cell reviews* **3**, 30-38 (2007).

44 Wall, D. S. *et al.* Progenitor cell proliferation in the retina is dependent on Notch-independent Sonic hedgehog/Hes1 activity. *The Journal of cell biology* **184**, 101-112 (2009).

45 Ingram, W. J., McCue, K. I., Tran, T. H., Hallahan, A. R. & Wainwright, B. J. Sonic Hedgehog regulates Hes1 through a novel mechanism that is independent of canonical Notch pathway signalling. *Oncogene* **27**, 1489-1500, doi:10.1038/sj.onc.1210767 (2008).

46 Solecki, D. J., Liu, X. L., Tomoda, T., Fang, Y. & Hatten, M. E. Activated Notch2 signaling inhibits differentiation of cerebellar granule neuron precursors by maintaining proliferation. *Neuron* **31**, 557-568 (2001).

47 Fan, X. *et al.* Notch1 and notch2 have opposite effects on embryonal brain tumor growth. *Cancer research* **64**, 7787-7793, doi:10.1158/0008-5472.CAN-04-1446 (2004).

48 Guo, S., Liu, M. & Gonzalez-Perez, R. R. Role of Notch and its oncogenic signaling crosstalk in breast cancer. *Biochimica et biophysica acta* **1815**, 197-213, doi:10.1016/j.bbcan.2010.12.002 (2011).

49 Dickson, B. C. *et al.* High-level JAG1 mRNA and protein predict poor outcome in breast cancer. *Modern pathology : an official journal of the United States and Canadian Academy of Pathology, Inc* **20**, 685-693, doi:10.1038/modpathol.3800785 (2007).

50 Reedijk, M. *et al.* High-level coexpression of JAG1 and NOTCH1 is observed in human breast cancer and is associated with poor overall survival. *Cancer research* **65**, 8530-8537, doi:10.1158/0008-5472.CAN-05-1069 (2005).

51 Groeneweg, J. W., Foster, R., Growdon, W. B., Verheijen, R. H. & Rueda, B. R. Notch signaling in serous ovarian cancer. *Journal of ovarian research* **7**, 95, doi:10.1186/s13048-014-0095-1 (2014).